Coordination of meiotic recombination in diploid and tetraploid *Arabidopsis*

By

Chris Morgan

A thesis submitted to

the University of Birmingham

for the degree of

DOCTOR OF PHILOSOPHY

School of Biosciences

University of Birmingham

September 2016

Abstract

Homologous recombination is an integral part of meiosis and is essential for generating crossovers that ensure balanced segregation of homologous chromosomes and establish genetic variation within offspring. It is therefore exceedingly important that meiotic cells employ stringent control mechanisms to safeguard crossover formation. Work in yeast has indicated that the meiotic axis, a proteinaceous structure that tethers meiotic chromosomes into looped arrays, plays a crucial role in many aspects of homologous recombination, from double strand break formation to crossover interference. It has also been suggested that increased crossover interference helps to establish meiotic stability by inhibiting multivalent formation during autopolyploid meiosis.

Using immunocytochemistry coupled with super-resolution microscopy, we have further investigated the role played by the meiotic axis protein ASY1 in stabilising meiosis in the established autotetraploid *Arabidopsis arenosa.* We have also used *Arabidopsis arenosa* as a model for studying how meiotic interference might operate within an autopolyploid context. Alongside this, experiments using transgenic lines of the model plant *Arabidopsis thaliana* have helped to shed light on how crossover formation and synapsis are affected by reduced expression of *ASY1* and *ASY3* and to determine what effect limiting meiotic crossover numbers might have on neopolyploid meiotic stabilisation.

I dedicate this thesis to my amazing wife, Louise.

Acknowledgments

First and foremost, I would like to thank my supervisor Prof. Chris Franklin for giving me the opportunity to undertake this work in his lab and for providing me with plenty of great advice and guidance whilst simultaneously granting me the trust and freedom to pursue my own research and non-research interests.

I would also like to thank other members of the Franklin lab and colleagues from the second floor for sharing their experimental and meiotic wisdom with me over the years, particularly; Eugenio Sanchez-Moran, Allan West, Kim Osman, Stefan Heckmann, Marina Martinez-Garcia, Maria Cuacos, Elaine Howell and Sue Armstrong. Expert technical support was also provided by Claire Bauckham, Lisa Burke, Steve Price, Karen Staples, Adrian Breckles and Ruth Perry.

I am also extremely grateful to our collaborators, who contributed time, advice, seeds and unrivalled access to super-resolution microscope facilities during the course of this study. Collaborators include Kirsten Bomblies, Levi Yant and Eva Wegel from the John Innes Centre, Kevin Wright from Harvard University and James Higgins from the University of Leicester. I would particularly like to thank Kirsten for giving up an enormous volume of time to perform the blind analysis of hundreds of metaphase I cells.

Thanks must also be given to Prof. Hugh Dickinson and Dr. Jose Guitierrez Marcos, and their respective labs, with whom I carried out smaller research projects before and during my PhD that equipped me with the skills and enthusiasm required to make headway during this study.

This PhD was funded by the Biotechnology and Biological Sciences Research Council (BBSRC) as part of the Midlands Integrative Biosciences Training Partnership (MIBTP).

Many other individuals and organisations have also played important roles by helping me with the non-research accomplishments that I have made during my PhD. These include; Flower Power volunteers, Jim Bell, Rachael Batchelor, Oxford Gene Technology, members of the University Graduate School and my fellow Westmere Scholars.

Finally, I would like to thank my wife Louise, my parents and all of my other friends and family for their support and kindness during the course of my PhD.

List of Contents

List of figures and tables

List of frequently used abbreviations

DSB	Double strand break
IHR	Inter-homologue recombination
SC	Synaptonemal complex
SPS	Synaptic partner switch
CO	Crossover
NCO	Non-crossover
M1	Metaphase I
EM	Electron microscopy
SIM	Structured illumination microscopy

CHAPTER 1
INTRODUCTION

1 Introduction

Meiosis is the specialised form of cell division required for the generation of haploid gametes from diploid precursor cells and is an essential stage of sexual reproduction. Meiosis consists of one round of DNA replication followed by two consecutive rounds of cellular division, generating cells with half the original chromosomal complement. The original chromosomal complement is regained when haploid gametes fuse together during sexual reproduction.

During prophase I of meiosis, DNA recombination occurs between homologous chromosomes (reviewed in Osman *et al.*, 2011). This gives rise to physical connections between the homologues, which can be cytologically visualised as chiasma. These connections are required for the correct segregation of homologues during anaphase I and create genetic diversity within offspring through the generation of crossovers (COs).

1.1 Overview of prophase I

Prophase I is typically the lengthiest stage to occur during meiosis, lasting approximately 21 hours in *Arabidopsis thaliana* (Armstrong *et al.*, 2003), and during this time homologous chromosomes must pair, synapse and carry out homologous recombination. Prophase I can be further divided into five substages; leptotene, zygotene, pachytene, diplotene and diakinesis (figure 1.1). These substages can be cytologically distinguished based upon the appearance of the chromosomes and the general level of chromatin condensation.

Following meiotic S-phase and G2, prophase I begins with the leptotene substage. During leptotene the chromosomes of unpaired homologues are visible as long thread-like structures

that are formed following the elaboration of the meiotic axis along sister chromatids. It is during this stage that meiotic recombination is initiated via the formation of programmed DNA double-strand breaks (DSBs), which can be repaired later in prophase I using the homologue, rather than the sister chromatid, as a template to generate COs.

After leptotene comes the zygotene stage, during which the axial elements of homologous chromosomes are brought into close juxtaposition via the formation of the synaptonemal complex (SC) (Reviewed in Page and Hawley, 2004). The SC is a tripartite structure consisting of a central element, transverse filaments and the axial elements, which are henceforth referred to as lateral elements. Extension of the SC between homologues is required to enable stable CO formation. Zygotene cells can be identified as cells that have some regions with thinner, unpaired chromosome axes and other regions that have thicker chromatin threads consisting of paired homologues.

The extension of the SC along paired homologues is referred to as synapsis, and synapsis continues during the zygotene stage until the pachytene substage is reached, at which point all homologues are fully synapsed along their entire lengths. This stage is characterised by cells having much thicker chromatin threads, compared to those seen in leptotene, that span the entire lengths of all the chromosomes. These first three substages can also be identified in *A. thaliana* by determining the relative abundance of the axis associated protein ASY1 and the SC lateral element protein ZYP1 using fluorescent immunolocalisation microscopy (Armstrong *et al,* 2002, Higgins *et al.*, 2005).

Following on from pachytene, meiotic cells enter the diplotene stage during which the synaptonemal complex dissociates and homologues begin to separate from one another at regions not joined by a CO. The chromosomes then condense until diakinesis, when the five pairs of homologous chromosomes in *A. thaliana* can be individually identified and the sites of crossovers are visible as chiasma linking the two homologues.

Other stages that can be easily identified cytologically in *A. thaliana* also include metaphase I, anaphase I, dyad and tetrad stages. These stages are particularly useful for identifying the downstream effects of problems encountered during homologous recombination, which can result in a reduction in crossovers that may cause univalent formation at metaphase I or homologue missegregation at anaphase I, generating dyads and tetrads with unbalanced chromosome numbers.

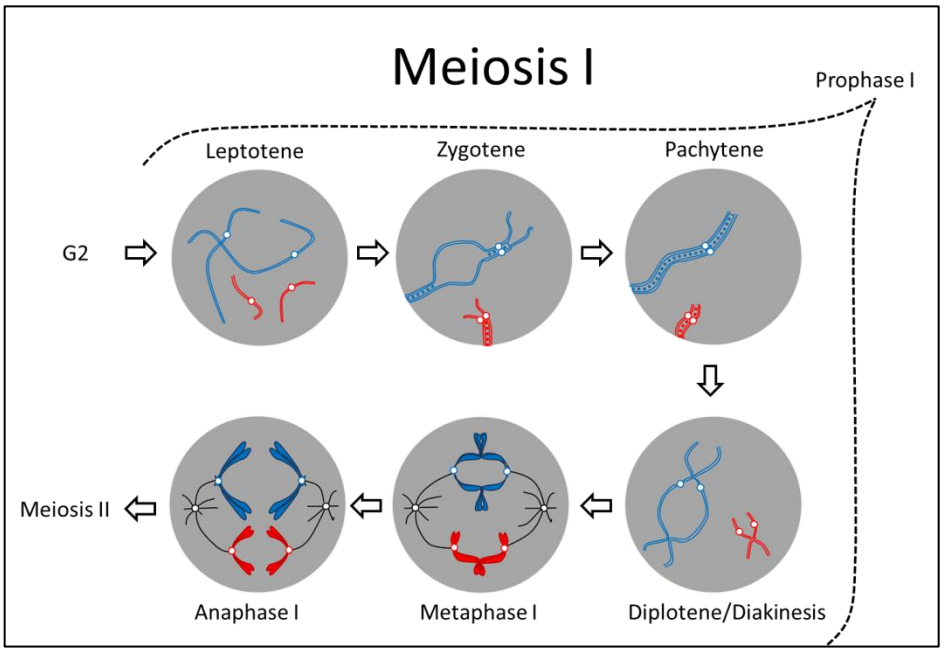

Figure 1.1. Substages of meiosis I. The meiotic axis elaborates along sister chromatids during leptotene to form long thread-like structures (2 pairs of homologous chromosomes shown). The axial elements of homologous chromosomes are brought into close juxtaposition via the formation of the synaptonemal complex (SC) during zygotene until full synapsis is achieved at the pachytene stage. Following this, the SC dissociates during diplotene and the chromosomes condense until diakinesis when both homologues are attached at the sites of chiasma. Chiasma are essential to ensure homologues are correctly oriented during metaphase I so that homologues undergo balanced segregation at anaphase I.

1.1.1 Homologous recombination

Homologous recombination is the process required to generate COs within meiotic cells. It starts with the production of numerous DSBs throughout the genome, which can then be repaired via CO or non-crossover (NCO) pathways (figure 1.2). Homologous recombination involves numerous steps and requires many regulatory control mechanisms that will now be discussed in further detail.

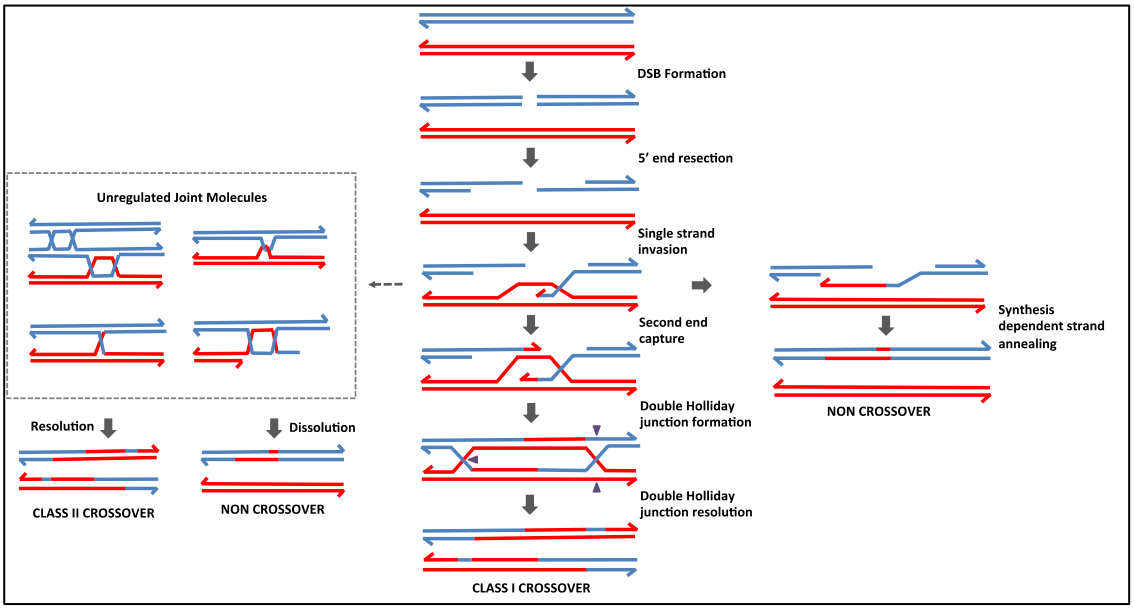

Figure 1.2. Pathways to meiotic recombination. Recombination is initiated by the formation of double strand breaks which can either be processed to generate crossover or non-crossover products via a number of different routes. 3′ ends are indicated by arrows. Modified from Osman et al., (2011).

1.2 DSB formation

The process of homologous recombination is initiated at the early leptotene stage of meiosis when the conserved topoisomerase VI-like protein Spo11 catalyses the formation of DSBs via

a transesterification reaction (Bergerat *et al.*, 1997; Keeney *et al.*, 1997). Three Spo11 homologues have been identified in *A. thaliana*, although only two, AtSPO11-1 and AtSPO11-2, are required for meiotic DSB formation and act in a non-redundant manner (Hartung *et al.*, 2000; Grelon *et al.*, 2001; Stacey *et al.*, 2006).

Spo11, however, is not capable of carrying out DSB formation on its own and requires the presence of a number of other essential accessory proteins. In *S. cerevisiae* these include; Ski8, Rec102, Rec104, Rec114, Mer2, Mei4, Rad50, Mre11 and Xrs2 (reviewed in Borde & de Massy 2013). In *A. thaliana*, alongside AtSPO11-1 and AtSPO11-2, the proteins AtMTOPVIB, AtPRD1, AtPRD2/MPS1, AtPRD3, AtDFO and AtSWI1 have all been identified, via genetic screens, as being essential for meiotic DSB formation (Vrielynck *et al.*, 2016, De Muyt *et al.*, 2007, 2009, Zhang *et al.*, 2012, Mercier *et al.*, 2001). AtMTOPVIB was recently characterised as a homologue of the archaeal topo VIB subunit. Alongside TOPOVIBL in mice, AtMTOPVIB is the first topo VIB-like protein to be identified as being required for meiotic DSB formation and it is has been demonstrated that it forms a complex with, and is required for the formation of, the SPO11-1/SPO11-2 heterodimer (Vrielynck *et al.*, 2016, Robert *et al.*, 2016). AtPRD1 and AtPRD2 are homologues of DSB proteins from other organisms. AtPRD2 is a functional orthologue of *S. cerevisiae* Mei4 (Kumar *et al.*, 2010) and AtPRD1 has low-level sequence homology with MEI1, a protein required for DSB formation in mammals. AtPRD2 has also been shown to interact with the N-terminal domain of AtSPO11-1 in a yeast-two-hybrid assay (De Muyt *et al.*, 2007). AtPRD3 shares homology with the rice protein PAIR1 (Nonomura *et al.*, 2004), but no protein homologues have been identified in other kingdoms. AtSWI1 and AtDFO also appear to have no homologues

outside the plant kingdom and T-DNA insertion mutants of both genes fail to form meiotic DSBs (Mercier *et al.,* 2001, Zhang *et al.,* 2012).

1.2.1 Control of meiotic DSBs

The formation of DSBs poses a great risk to cell and genome integrity and therefore the frequency, location and timing of meiotic DSB formation must be tightly controlled. In *A. thaliana*, meiotic DSBs are formed during the late G2/early leptotene stages of prophase I of meiosis with >100 DSBs thought to occur per meiocyte (Sanchez-Moran *et al.,* 2007). Other well studied organisms such as yeast and mammals display meiotic DSB numbers of a similar magnitude to *A. thaliana,* whilst organisms such as *C. elegans* and *D. melanogaster* experience much lower numbers of DSBs, with ~12 and ~21 DSBs per meiocyte respectively (Mets & Meyer, 2009, Janet *et al.,* 2003).

1.2.1.1 DSB location

Meiotic DSBs are not randomly distributed throughout the genome but are, instead, found with increasing likelihood in certain chromosomal regions relative to others. For instance, in *S. cerevisiae* DSBs most frequently occur within the chromosome arms and their formation is suppressed within the pericentric and subtelomeric regions (Pan *et al,* 2011). Within the chromosome arms, further layers of control are imposed to preferentially direct DSB formation to small regions roughly 200bp in length that can be found within GC-rich chromatin loop regions. These small regions are referred to as DSB hotspots (Pan *et al.,* 2011). 88% of *S. cerevisiae* DSB hotspots can be found in nucleosome-depleted regions

(NDRs) within gene promoters (Berchowitz *et al.,* 2009). The histone mark H3K4me3 is also associated with some DSB hotspots and yeast lacking the protein Set1, which is required for histone H3K4 methylation, exhibit reduced DSB numbers and an altered DSB landscape (Borde *et al.,* 2009).

In mice and humans, DSBs are targeted to transcription starts sites (TSS) by PRDM9, a zinc finger containing protein with histone H3K4 trimethyltransferase activity (Baudat *et al.,* 2010). Intriguingly, in *prdm9 -/-* mice DSBs appear to be preferentially located in promoter regions enriched in H3K4me3 in a similar manner to yeast (Brick *et al.,* 2012).

So far, no PRDM9 homologue has been identified in plants. Also, difficulties associated with isolating and purifying very large numbers of meiocytes at the same stage of meiosis have thus far prevented *A. thaliana* DSB location from being analysed at the same resolution as seen in yeast or mammals.

1.2.1.2 DSB timing

As previously mentioned, meiotic DSB formation appears to occur early during prophase I in all organisms thus far studied. In *S. cerevisiae*, DSB formation occurs 1.5-2 hours after premeiotic S-phase (Borde *et al.,* 2000) and bromo-deoxy uridine (BrdU) pulse labelling coupled with AtSPO11-1 immunolocalisation indicates that AtSPO11-1 is localised to chromatin in *A. thaliana* meiocytes 1-5 hours after DNA replication (Sanchez-Moran *et al.,* 2007).

In *S. cerevisiae*, timing of meiotic DSB formation is controlled via the tight coupling of early meiotic events with premeiotic DNA synthesis. The S-phase cyclin dependent kinases CDK-S and DDK are required for both the initiation of pre-meiotic S-phase and for the phosphorylation of Mer2 (Henderson *et al.,* 2006, Wan *et al.,* 2008), which is required for meiotic DSB formation. It is hypothesised that lower initial levels of CDK-S and DDK are sufficient to initiate premeiotic DNA replication in advance of DSB formation, for which much higher levels of CDK-S and DDK are required (Murakai & Keeney 2014). It seems likely that DNA replication and DSB formation will be linked in a similar manner in plants, although no specific cyclin or CDK complexes have yet been identified in *A. thaliana* that fulfil a similar role.

1.2.1.3 DSB numbers

The regulation of DSB numbers has been observed to occur in many species via feedback control. For instance, negative feedback mechanisms have been demonstrated to occur in both *D. melanogaster* and mice, whereby the formation of meiotic DSBs activates the DNA-damage response protein ATM which in turn inhibits further DSB formation (Lange *et al.,* 2011, Joyce *et al.,* 2011). A similar negative feedback mechanism may exist in *S. cerevisiae* involving the ATM homologue, Tel1, and the ATR homologue, Mec1, in which the proteins phosphorylate, and hence down-regulate, Rec114 (Carballo *et al.,* 2013).

Negative feedback mechanisms may also stem from meiotic processes that occur downstream of DSB formation, such as homologue synapsis. For example, in mice, it has been shown that

DSB formation is inhibited on synapsed chromosomal regions but continues to occur on unsynapsed regions during the zygotene stage of meiosis (Kauppi *et al.,* 2013).

Trans inhibition has also been shown to occur in *S. cerevisiae* chromosomes whereby the formation of a DSB at a specific region of a chromosome represses the formation of a DSB at nearby positions on the homologous chromosome. This form of inhibition is also thought to depend upon Tel1 and Mec1 (Zhang *et al.* 2011).

1.2.2 Linking the meiotic axis to DSB formation

All aspects of meiotic recombination that occur during prophase I, including DSB formation, must take place within the context of the meiotic chromosome axis. The axis is formed when sister chromatids come together during the leptotene stage of meiosis in a linear array of chromatid loops anchored at the base by a complex proteinaceous structure consisting of cohesins, condensins and other meiosis-specific proteins (reviewed in Borde & de Massy, 2013) (figure 1.3). The axial elements of homologous chromosomes are brought into close juxtaposition in order to facilitate crossing over via the formation of the SC, which extends between homologues during the zygotene stage of meiosis. Zip1 and AtZYP1 proteins come together as homodimers to form the transverse filament of the SC in *S. cerevisiae* and *A. thaliana* respectively (Meuwissen *et al.,* 1992; Higgins *et al.,* 2005).

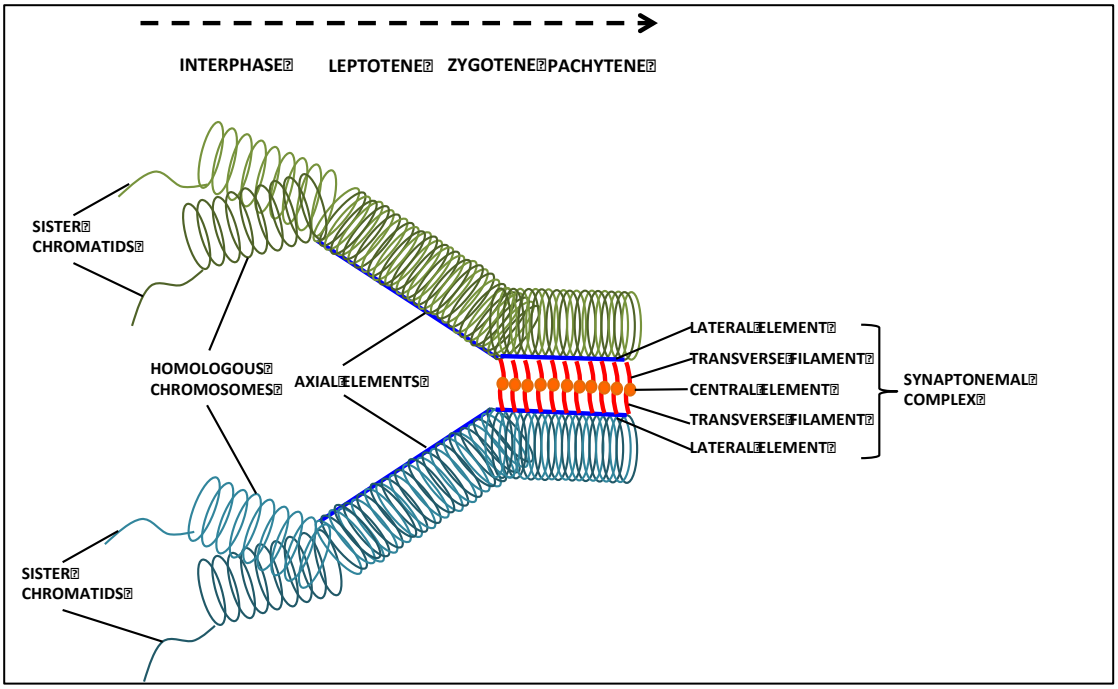

Figure 1.3. The meiotic axis and synaptonemal complex, modified from Alberts et al., (1983). The meiotic axis consists of chromatin loops anchored at their base by a complex proteinaceous structure. The axial elements of homologous chromosomes are brought into close juxtaposition via the formation of the synaptonemal complex to facilitate crossing over.

In *S. cerevisiae,* the meiosis specific axis components include the cohesin kleisin subunit Rec8 and the proteins Hop1 and Red1 (Klein *et al.*, 1999; Hollingsworth *et al.*, 1990; Smith & Roeder 1997). *red1 and hop1* mutants are completely defective in meiotic DSB formation in some *S. cerevisiae* strains, although in the SK1 strain it appears that DSBs are more reduced in the *hop1* background than the *red1* background (Woltering *et al.*, 2000). Hop1 and Red1 localise to the meiotic axis prior to DSB formation and are required for the localisation of the Spo11-acessory protein Mer2 to the axis (Panizza *et al.*, 2011). Mer2 recruits Rec114 and Mei4 to the axis to form the RMM complex (Li *et al.*, 2006). The axis bound RMM complex can then interact with Spo11 to promote DSB formation (Sasanuma *et al.*, 2007). As DSB hotspots have been shown to preferentially occur within the chromatin loops and the RMM complex instead localises to the axis, this has led to the development of the tethered-loop axis complex model, whereby loop-associated hotspots must be anchored to the axis to activate

DSB formation and promote recombination (Panizza *et al.*, 2011; Kleckner 2006) (figure 1.4). It has also been demonstrated that Spp1, a conserved subunit of the H3K4 methyltransferase Set1 complex, tethers DSB sites to the meiotic axis via an interaction with Mer2 (Sommermeyer *et al.*, 2013, Acquaviva *et al.*, 2013).

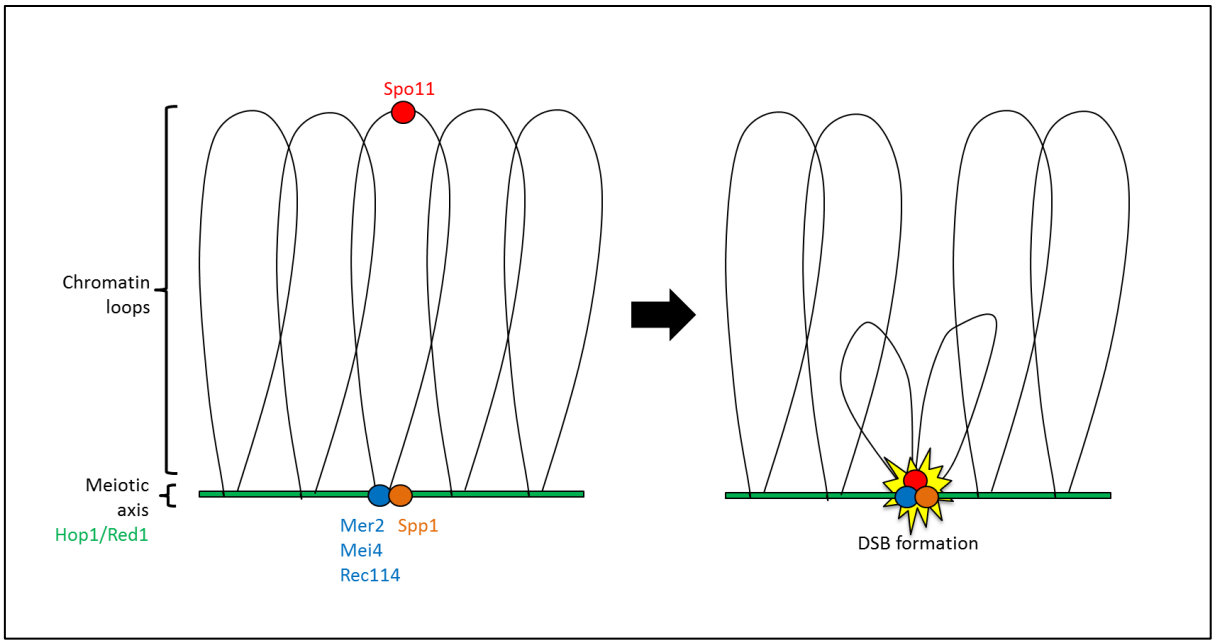

Figure 1.4. Tethered-loop/axis model for DSB formation in S. cerevisiae. Spo11 is first loaded on to the chromatin loop regions and must be tethered to the axis via the interaction of Spp1 with H3K4me3 so that the DSB accessory proteins Mer2, Mei4 and Rec114 can activate Spo11 catalysed DSB formation. Modified from Borde et al., 2013.

Recent work from Sun *et al.*, (2015) using high-resolution ChIP-seq, has also helped to determine the sites at which Hop1 and Red1 preferentially bind along *S. cerevisiae* chromosomes. The authors demonstrate that Hop1 and Red1 are both enriched at regions located between two highly transcriptionally active genes with a convergent orientation and that Rec8, Red1 and Hop1 all physically interact with each other. This leads the authors to suggest a model whereby cohesin provides a flexible anchor for the components of the meiotic axis to bind the chromosomes, allowing processes such as transcription and

recombination to occur unimpeded in an otherwise highly organised and compact chromosome structure (Sun *et al.,* 2015). The authors also note that Hop1 modulates Red1 axial recruitment by promoting the binding of Red1 to selected chromosomal regions independently of Rec8 and also by negatively regulating the accumulation of Red1 close to centromeres and on larger chromosomes (Sun *et al,.* 2015).

AtASY1 and AtASY3 have been identified in *A. thaliana* as functional homologues of Hop1 and Red1 respectively. Unlike Hop1, AtASY1 does not appear to play a role in mediating the number of AtSPO11 induced DSBs, based on AtSPO11 and γH2AX immunofluorescence, but there is a delay between the appearance of AtSPO11 and DSB formation in the *Atasy1* mutant (Sanchez-Moran *et al.,* 2007). In the *Atasy3* mutant, unlike in *Atasy1*, there is a moderate (30%) reduction in DSB number at the beginning of meiosis (Ferdous *et al.,* 2012).

1.3 Meiotic DSB processing

After Spo11 has catalysed DSB formation, Spo11 remains covalently bound to the 5′ end of the DNA at the break site via a phosphodiester bond with a tyrosine side chain (Corbett and Berger, 2004). In *S. cerevisiae,* the Mre11-Rad50-Xrs2 (MRX) complex together with Sae2/Com1 is required for the removal of Spo11 and a short covalently bound oligonucleotide fragment (Neale *et al.,* 2005). These oligonucleotide fragments have been found to occur in equal quantities at two different sizes of 7-12 nucleotides or 21-37 nucleotides in length (Neale *et al.,* 2005). The 3′ single stranded DNA (ssDNA) overhangs that remain either side of the DSB break site are then extended via the action of Sgs1-Dna2 and Exo1 (Mimitou & Symington, 2009) to produce long 3′ ssDNA tails that are hypothesised to act as probes to

identify homologous DNA sequences and are required for single-end invasion and D-loop formation.

In *A. thaliana*, the homologues AtMre11, AtRad50 and AtCom1 are all thought to fulfil similar roles to their yeast counterparts, with mutants exhibiting severe meiotic chromosome fragmentation indicative of a failure in DSB repair (Puizina *et al.*, 2004, Bleuyard *et al.*, 2004, Uanschou *et al.*, 2007). The *A. thaliana* Xrs2 homologue, AtNBS1, does not appear to have an essential role in meiosis, although it is worth noting that the T-DNA insertion mutant analysed by Waterworth *et al.,* (2007) still produced a truncated 5′ transcript that could have produced a semi-functional protein.

1.3.1 Single end invasion

Once the 3′ end resection is complete in *S. cerevisiae,* the protein Rad52 is required to load the RecA homologues Rad51 and Dmc1 on to the 3′ ssDNA to form a nucleoprotein filament capable of invading duplex homologous DNA to form a nascent D-loop (Gasior *et al.,* 1998, Paques & Haber, 1999). Rad51 is also required for mitotic homology directed DNA repair but Dmc1 is specific to meiotic DSB repair. Other yeast accessory proteins required for Rad51/Dmc1 mediated strand exchange include Rad54, Rdh54/Tid1, Rad55 and Rad57 (Osman *et al.*, 2011).

In *A. thaliana* there is a single Dmc1 paralogue and six Rad51 paralogues, although only three of these (AtRAD51, AtRAD51C and AtXRCC3) are required for meiotic DSB repair (Doutriaux *et al.,* 1998, Bleuyard *et al.,* 2005). No Rad52 homologue has been identified in *A.*

thaliana although RNAi knock-down analysis suggests that AtBRCA2 may fulfil an analogous role to promote formation of the presynaptic filament (Siaud *et al.,* 2004).

After formation of the presynaptic filament, the yeast proteins Hop2 and Mnd1, and their *A. thaliana* counterparts AtHOP2 and AtMND1, have been suggested to play a role in promoting duplex DNA capture, enabling stable strand exchange (Pezza *et al.,* 2007, Schommer *et al.,* 2003, Panoli *et al.,* 2006).

1.3.2 Linking the meiotic axis to DSB processing

Hop1 and Red1, along with the meiosis specific kinase Mek1 (Rockmill & Roeder, 1991), are also required to promote inter-homologue recombination (IHR), with *hop1, red1* and *mek1* mutants being shown to have significantly lower levels of IHR resulting in meiotic cell arrest (Hollingsworth *et al.,* 1995; Schwacha & Kleckner 1997; Niu *et al.,* 2005). Following meiotic DSB formation, the yeast ATM/ATR homologues Tel1/Mec1 promote Red1 dependent Hop1 phosphorylation at residue T318 (Carballo *et al.,* 2008). The phosphorylated form of Hop1 then goes on to activate Mek1, which in turn phosphorylates a number of target proteins responsible for meiotic progression, including Rad54, which is required for Rad51 activity (Niu *et al.,* 2009).

Pch2, a widely conserved AAA+ ATPase, ensures the correct loading of Hop1 into hyperabundant domains along the axis during pachytene and has recently been implicated in preventing Red1 independent Hop1 phosphorylation (Borner *et al.,* 2008; Lo *et al.,* 2014). Pch2 also appears to play a role in promoting IHR by inhibiting Dmc1-independent inter-

sister repair and aiding Hop1 activation by potentially remodelling chromatin structure at sites around DSBs to provide access to Tel1 (Zanders *et al.,* 2011, Ho and Burgess, 2011). In addition to this, Mek1 has recently been shown to play a role in suppressing the repair of DSBs from template DNA within close proximity and it is depleted from the SC in a Pch2 dependent manner (Subraminian *et al.,* 2016). Mutations in Pch2 have also been show to affect CO formation and localisation (Zanders *et al.,* 2009) and Pch2 also has a well characterised function in meiotic checkpoint signalling (Reviewed in Vader 2015).

Similar to its yeast counterpart, AtASY1 plays a role in ensuring IHR by stabilising the loading of AtDMC1 at DSB sites. In *Atasy1* mutants, the amount of chromatin associated AtDMC1 declines rapidly after initial loading compared to wild-type, leading to a large reduction in COs and a failure to polymerise a full SC (Sanchez-Moran *et al.,* 2007). *Atasy1, Atrad51, Atatr* triple mutants also exhibit more efficient meiotic DNA repair than an *Atrad51, Atatr* double mutant, suggesting that AtASY1 may act by inhibiting the inter-sister repair capabilities of AtDMC1, promoting IHR (Kurzbauer *et al.,* 2012). In an *Atasy3* mutant there is incomplete loading of AtASY1 on to the meiotic axis, which may also affect IHR (Ferdous *et al.,* 2012).

AtPCH2 also appears to have a key role in axis remodelling in *A. thaliana* and is required to deplete AtASY1 along the axis at areas of synapsis. Furthermore, synapsis is severely compromised in *Atpch2* mutants, which exhibit an average reduction of 68% SC polymerisation as well as a 30% reduction in CO frequency (Lambing *et al.,* 2015). In contrast to Pch2 in *S. cerevisiae*, however, *Atpch2* mutants appear to have no defects in DSB formation or repair, but time taken to progress through prophase I is delayed by 5-8 hours

(Lambing *et al.,* 2015).

1.4 CO formation

After strand exchange, a small selection of the recombination intermediates go on to form COs (~8-12 per nucleus in *A. thaliana*). The remainder of strand exchange intermediates are thought to be repaired as NCOs via the synthesis dependent strand annealing (SDSA) pathway (Higgins *et al.,* 2004), whereby the D-loop disassembles after DNA synthesis has been primed and the two DNA ends anneal without a reciprocal exchange of DNA. It is worth noting, however, that in plants there is no direct evidence for SDSA repair in meiosis and strand-exchange intermediates could also be repaired via the sister or by dissolution of joint-molecules. A current model for SDSA in *S. cerevisiae* suggests that Sgs1-Top3-Rmi1 (STR) activity is required to disassemble early strand exchange intermediates and promote SDSA (Tang *et al.,* 2015). In *A. thaliana* and *S. cerevisiae* there are two independent pathways that can result in CO formation.

1.4.1 Class I ZMM dependent COs

The class I, ZMM-dependent, pathway to CO formation is dependent upon a group of proteins referred to as the ZMM proteins (Borner *et al.,* 2004). The following ZMM proteins have been identified in *A. thaliana;* AtSHOC1/ZIP2, AtHEI10, AtZIP4, AtMSH4, AtMSH5, AtMER3/RCK (Macaisne *et al.,* 2008; Chelysheva *et al.,* 2012; Chelysheva *et al;* 2007; Higgins *et al,* 2004; Higgins *et al.,* 2008; Mercier *et al.,* 2005). Class I COs are sensitive to CO interference, non-randomly distributed and responsible for 85% of COs (Higgins *et al.,*

2004). CO interference is the mechanism by which the formation of one CO represses the formation of another CO in close proximity on the same chromosome.

AtMSH4 and AtMSH5 are homologues of the bacterial mismatch repair protein MutS. *In vitro* studies using hMSH4/MSH5 suggest that the protein forms a sliding clamp that binds to duplex DNA, promoting and stabilising the formation of a double Holliday-junction (dHj) (Snowden, *et al.,* 2004). *Atmsh4* and *Atmsh5* mutants exhibit a severe (85%) reduction in CO number that is consistent with them having a role in Class I CO formation (Higgins *et al.,* 2004). Mer3, the yeast homologue of AtMER3, is a 3′ to 5′ DNA helicase that stabilises nascent D-loops by extension of the heteroduplex DNA (Mazina *et al.,* 2004). Similar to *Atmsh4/5*, *Atmer3/rck* also exhibits a severe reduction in COs, with remaining crossovers appearing to be interference insensitive (Mercier *et al.,* 2005). AtSHOC1/ZIP2 has been shown to interact with the protein AtPTD and could also play a role in dHj stabilisation (Macasine *et al.,* 2011). In *S. cerevisiae*, Zip4, along with Zip2 and the AtHEI10 homologue Zip3, are required for the polymerisation of the SC lateral element protein Zip1 and Class I CO formation (Tsubouchi *et al.,* 2006, Chua & Roeder 1998, Agarwal & Roeder, 2000). In *A. thaliana*, AtZIP4, AtSHOC1/ZIP2 and AtHEI10 retain their essential role in Class I CO formation but *Atzip4*, *Atshoc1/zip2* and *Athei10* mutants all undergo normal SC polymerisation and synapsis (Chelysheva *et al.,* 2007, Macaisne *et al.,* 2008, Chelysheva *et al.,* 2012). Immunolocalisation studies have shown that AtHEI10 is initially loaded early during prophase I at numerous sites that are thought to correspond to early recombination intermediates and that as meiosis progresses it is only retained at sites destined to become Class I COs (Chelysheva *et al.,* 2012).

In *S. cerevisiae,* dHj's formed via the Class I CO pathway are resolved by the endonuclease MutLγ (Mlh1-Mlh3) and Exo1 (Zakharyevich *et al.,* 2012). It is likely that a similar Class I CO resolution pathway exists in plants with MLH1 and MLH3 being extensively used in immunocytological studies as markers for Class I CO sites (Lhuissier *et al.,* 2007).

1.4.2 Class II ZMM independent COs

In both *A. thaliana* and *S. cerevisiae,* around 15% of COs occur independently of the ZMM Class I pathway and are interference insensitive. These are referred to as Class II COs and arise in occasional circumstances when strand exchange intermediates evade STR processing and form unregulated joint molecules. In *S. cerevisiae* these unregulated joint molecules are resolved by the structure selective nucleases Mus81-Mms4, Yen1 and Slx1-Slx4 to produce COs or may be disassembled with the aid of the STR complex in a process called dHj dissolution to produce NCOs (de los Santos *et al.,* 2003, Zakharyevich *et al.,* 2012, Kaur *et al.,* 2015). Flux through the class II pathway is increased in *sgs1* mutants in which early NCO formation via the SDSA pathway is abolished and stable joint-molecule formation is compromised (De Muyt *et al.,* 2012).

In an *A. thaliana Atmsh4/Atmus81* double mutant there is a significant reduction in CO number relative to the *Atmsh4* single mutant, suggesting that AtMUS81 is required for some, but not all Class II COs (Higgins *et al.,* 2004). The AAA-ATPase FIDGETIN-LIKE 1 (AtFIGL1), the helicase AtFANCM, and its associated proteins AtMHF1 and AtMHF2, Topoisomerase3α (AtTOP3α) and two BLM homologs, AtRECQ4A and AtRECQ4B, have also recently been identified as anti-CO proteins in *A. thaliana* that act by limiting class II

COs (Crismani *et al.* 2012, Girard *et al.,* 2014., Girard *et al.,* 2015, Seguela-Arnaud *et al.,* 2015). AtFANCM, AtTOP3α, AtRECQ4a and AtRECQ4B are thought to inhibit class II CO formation by unwinding joint-molecules to produce NCOs and FIGL1 limits CO formation by regulating the dynamics of single-strand invasion (Girard *et al.,* 2015, Seguela-Arnaud *et al.,* 2015).

1.4.3 Crossover control

Given the essential roles of COs in establishing connections between homologues at meiosis I and also in generating novel genetic arrangements, their location and frequency must be tightly controlled. Numerous studies have identified a number of independent mechanisms that are employed by cells to ensure COs occur at suitable numbers and locations within the genome.

1.4.3.1 CO homeostasis

COs are essential to ensure correct segregation of homologues at meiosis I and therefore at least one CO must occur between each homologue pair, referred to as the obligate CO (Jones and Franklin, 2006). The ability of meiotic cells to ensure that obligate COs are maintained, even in common scenarios where the final number of COs is as low as one per bivalent, is referred to as CO assurance. CO homeostasis is a mechanism by which CO levels are maintained at the expense of NCOs when DSB numbers are reduced and this process is thought to play a role in promoting CO assurance. Martini *et al.,* (2006) experimentally

demonstrated that CO homeostasis occurs during meiosis in *S. cerevisiae* using *spo11* hypomorphs with reduced DSB levels.

1.4.3.2 CO location

As previously mentioned, regions of the genome that are more likely to experience meiotic DSBs are referred to as DSB hotspots. In a similar fashion, regions of the genome where early recombination intermediates are more likely to progress to COs are referred to as CO hotspots. It seems a reasonable assumption that the distribution of DSB hotspots would mirror that of CO hotspots and, indeed, comparison of genome wide CO and DSB maps from mice and humans has demonstrated that there is significant correlation between DSB and CO hotspot locations (Smagulova *et al.*, 2011, Pratto *et al.*, 2014). However, other evidence from *S. cerevisiae* indicates that DSB hotspots exhibiting a greater frequency of DSBs are more likely to be repaired as NCOs relative to DSB coldspots experiencing a lower frequency of DSBs in a process described as crossover invariance (Hyppa & Smith, 2010).

Spatiotemporal repair of DSBs could also have an impact in determining which DSBs progress to form COs. Evidence from barley indicates that a preference to repair the first DSBs formed in early replicating DNA as COs may result in a subtelomeric CO preference (Higgins *et al.*, 2012). This form of spatiotemporal regulation of meiotic progression has also been described in *S. cerevisiae*, with different chromosomal regions experiencing different CO:DSB ratios (Serrentino *et al.*, 2013).

Numerous studies have indicated that CO hotspots in *A. thaliana* tend to be located within gene promoter and terminator regions (Yelina *et al.*, 2012, Choi *et al.*, 2013). These studies have also shown that hotspot locations overlap strongly with regions of histone H2A.Z deposition and DNA hypomethylation. Conversely, it has been demonstrated that COs are heavily suppressed within heterochromatic regions of the chromosomes in *A. thaliana* (Yelina *et al.*, 2012)

1.4.3.3 CO interference

CO interference was first described a century ago (Sturtevant, 1915) when it was observed that the formation of one CO suppresses the formation of other COs in nearby regions of the chromosome. Despite this, relatively little is still known about how this process is controlled and implemented in meiotic cells, although many models have been proposed that attempt to explain this phenomenon. Early hypotheses for interference suggested it could result from signals transmitted along the SC from CO sites, but it has since been shown that CO-designated synapsis initiation sites are also subject to interference, prior to SC formation (Fung *et al.*, 2004). SC central element proteins have, however, recently been shown to play a role in mediating interference in *C. elegans* but this function of the SC may be limited to *C. elegans*, in which SC formation occurs prior to DSB formation and CO designation (Libuda *et al.*, 2013).

As previously mentioned, numerous models have been proposed to explain how interference is transmitted throughout chromosomes. These include the ‘polymerisation model’ of King and Mortimer, the ‘counting model’ of Stahl and colleagues and, more recently, the ‘beam-

film model' by Kleckner and colleagues (King *et al*, 1990, Foss *et al.*, 1993, Kleckner *et al.*, 2004, Zhang *et al.*, 2014a) (figure 1.5). All three models are based on the assumption that there are a number of precursor interactions, presumably early recombination intermediates, of which only a subset are eventually fated to become CO-designated sites (reviewed in Zickler and Kleckner, 2016).

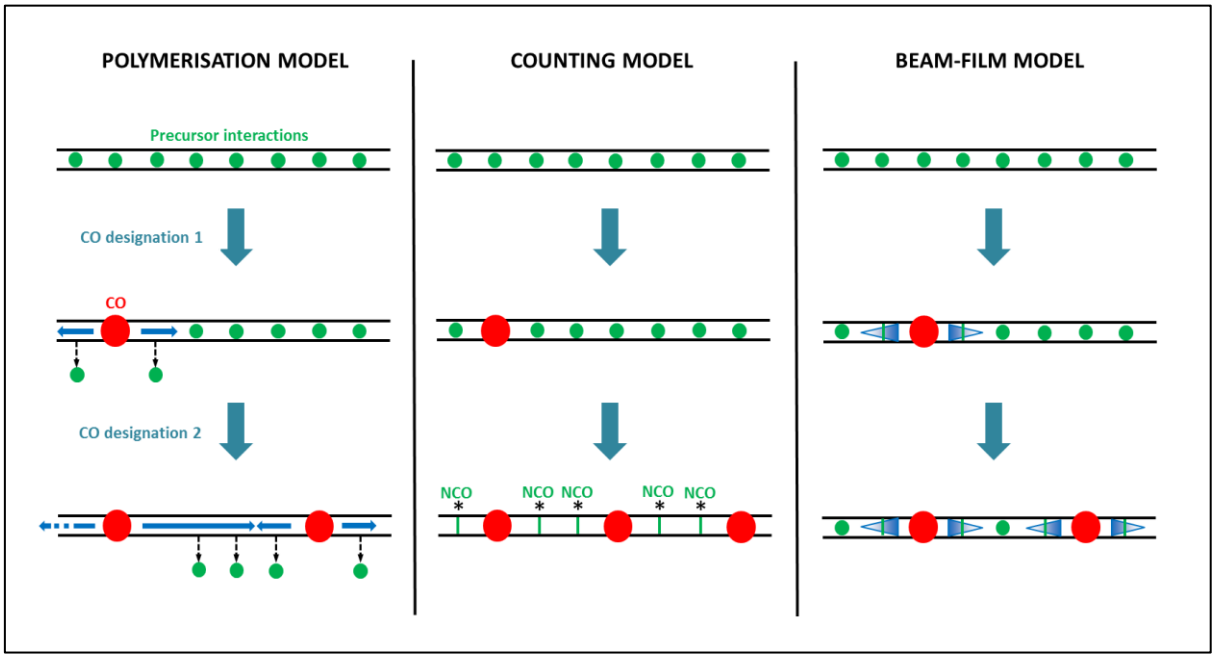

Figure 1.5. Models of CO interference. In the polymerisation model, interference spreads from CO designated sites via an unknown polymer, ejecting precursor machinery from the chromosomes as it spreads. The interference signal is terminated when it meets an opposing signal approaching from the other direction. In the counting model the initial CO site is designated at random and then a fixed number of NCOs occur between sequential CO sites. In the beam film model the interference signal spreads from CO designated sites but dissipates with increasing distance, so that the second CO designated site is likely to occur far away from the first. If more CO sites are then designated they will 'fill the gaps'.

In the polymerisation model, it is suggested that the interference signal is transmitted via the polymerisation of an unknown element which spreads bidirectionally from a CO-designated site (King and Mortimer, 1990). Precursor interactions that have yet to become CO-designated sites have the opportunity to do so until they are ejected by the advancing polymer. Once ejected, the precursor machinery is either degraded or reattaches at another unoccupied

site. The reattachment of the precursor machinery onto chromosomes that were initially void of precursor interactions is suggested by this model as a mechanism that ensures crossover assurance, however it is worth noting that the release and rebinding of early recombination intermediates has yet to be experimentally observed.

Using recombination data from *D. melanogaster,* the counting model was proposed and suggests that a fixed number of precursor interactions occur between CO-designated sites following the initial selection of one-precursor site at random to progress to become a CO-designated site (Foss *et al.,* 1993). This model fits well with experimentally determined recombination data from both *Neurospora* and *Drosophila*, however it does not fit with observations of CO homeostasis (Martini *et al.,* 2006) which have demonstrated that a reduction in precursor density does not necessarily result in a reduced number of CO-designated sites.

The beam-film model is based on an earlier 'stress-relief' model that suggests that CO designation is promoted by mechanical stress along the chromosomes and that CO designation results in a local relief of mechanical stress that dissipates with distance and supresses CO formation nearby (Kleckner *et al.,* 2004, Zhang *et al.,* 2014a, reviewed in Zickler and Kleckner 2016). In this model CO designation sites are designated sequentially, with the second CO designation site being found far away from the initial site, with any further designation events filling in the gaps. It is also suggested in this model that the initial CO-designation process is always sufficiently strong enough, for instance by ensuring an initially high enough level of 'stress', to promote designation such that the obligate CO is always formed. The beam-film mathematical model also allows outcomes to be simulated in

situations in which the number or distribution of precursor interactions is varied (Zhang *et al.*, 2014a). It is also suggested that one possible conduit for conveying stress in this system is the meiotic axis; such that when the DNA/protein axial meshwork is compressed, stress is introduced into the system. This axial stress could then be alleviated at CO designated sites and the associated local stress relief would spread along the axis. Consistent with this, electron microscopic analysis of *Sordaria* recombination nodules indicates that there are regions of axis destabilisation associated with late recombination nodules (Storlazzi *et al.*, 2008). CO designation also results in a local expansion of axis length in *C. elegans* (Libuda *et al.*, 2013).

Further evidence for the role of the meiotic axis in CO interference includes observations that the metric by which interference is transmitted is physical chromosome length, rather than genetic distance, as shown by analysis of Zip3 foci distribution on *S. cerevisiae* pachytene chromosomes (Zhang *et al.*, 2014b). Also, Topoisomerase II (TopoII) plays a role in mediating interference in *S. cerevisiae*. TopoII is axis associated and functions to alleviate topological stress along chromosomes. The TopoII pathway for interference also involves SUMOylation of the meiotic axis protein Red1 (Zhang *et al.*, 2014b).

Why interference has evolved, and why it appears to be such an evolutionarily conserved process, are both intriguing and challenging questions. It is possible that, from a genetic perspective, interference helps to promote the co-segregation of linked genes located near one another on the same chromosome, balancing the opposite but also potentially advantageous effects of recombination (Zickler and Kleckner, 2016). Interference has also recently been suggested to play a mechanistic role in stabilising meiosis in autopolyploid species by

preventing multiple COs from occurring between different combinations of homologues that could result in multivalent formation and, hence, missegregation (Bomblies *et al.*, 2016).

1.5 Polyploid meiosis

Polyploid species contain three or more complete sets of each chromosome and have been found to occur in almost every major eukaryotic taxon. It is within the plant kingdom, however, that polyploidy appears most predominant, with estimates of between 47-70% of angiosperms thought to be polyploid (Ramsey and Schemske, 1998). The abundance of polyploids is likely due to polyploid species possessing adaptive advantages relative to their diploid counterparts due to increases in effective population size and decreases in inbreeding depression (Crow and Wagner 2005). Despite their initial and long-term adaptive advantages, newly formed polyploids (neopolyploids) often encounter problems in meiosis following whole genome duplication (WGD) (reviewed in Bomblies and Madlung, 2014). Polyploids broadly fall into two categories, 'autopolyploids' and 'allopolyploids'. These two types of polyploidy arise following different types of WGD events and they each face their own meiotic challenges (figure 1.6).

Figure 1.6. Pathways to polyploid formation and associated meiotic challenges. Autopolyploids arise from WGD from within a single species. This can occur via an initial somatic doubling, via the fusion of unreduced gametes or via a triploid bridge. During meiosis, homologous chromosomes in autopolyploids can form multivalents that can lead to missegregation and aneuploid formation. By increasing the strength of interference, autopolyploids can reduce the total CO number per chromosome to one which will prevent multivalent formation and promote stable, balanced homologue segregation. Allopolyploids arise from hybridisation and WGD from within two related species. This can occur via the fusion of unreduced gametes or via a hybrid intermediate. During meiosis, the formation of COs between homoeologous chromosomes can result in aneuploidy and genomic rearrangements. By increasing pairing partner preferences such that COs only form between homologous chromosomes, rather than homoeologous chromosomes this can promote stable, balanced homologue segregation. Modified from Bomblies and Madlung, 2014.

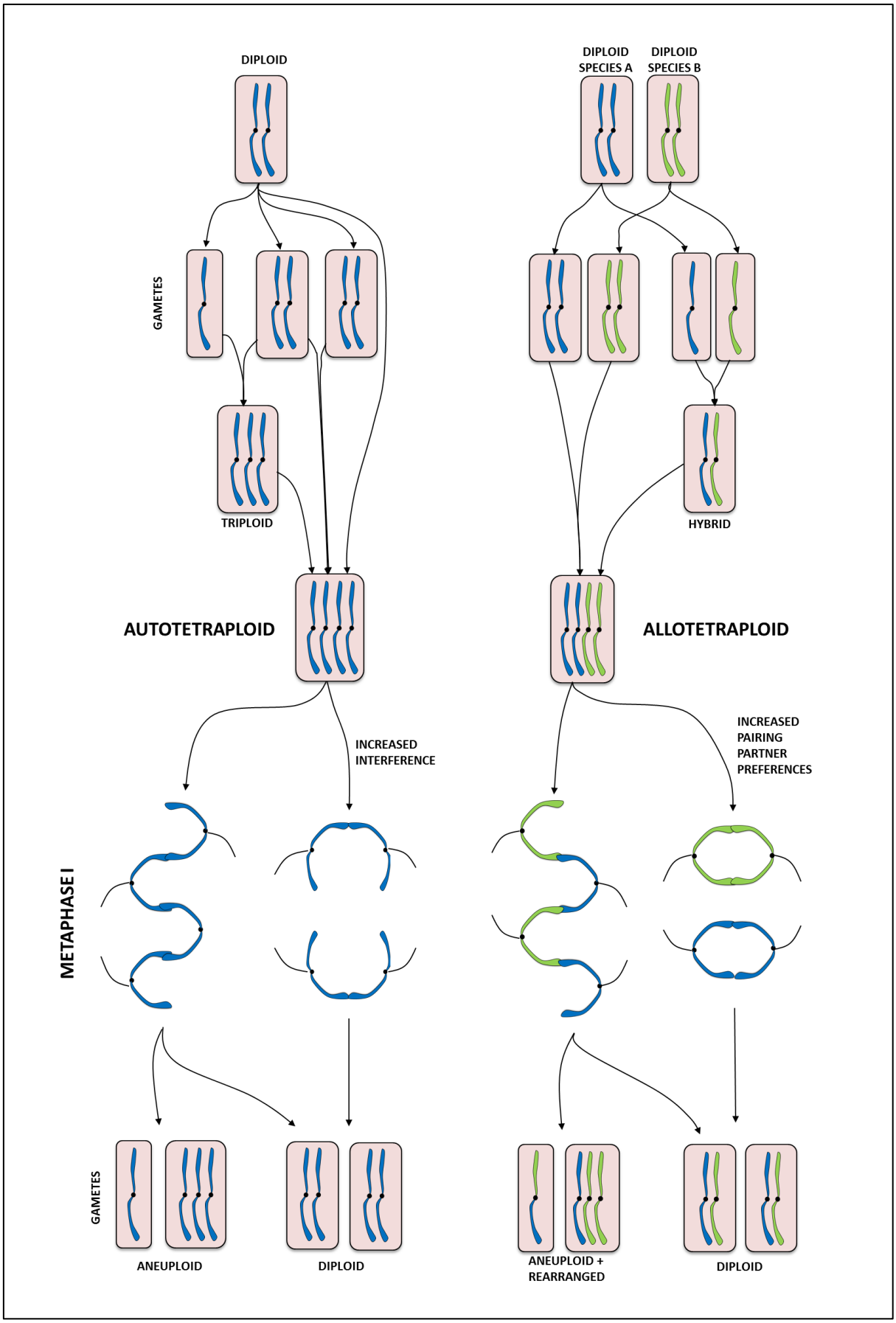
DIPLOID
GAMETES
TRIPLOID
AUTOTETRAPLOID
INCREASED
INTERFERENCE
METAPHASE I
GAMETES
ANEUPLOID
DIPLOID
DIPLOID
SPECIES A
DIPLOID
SPECIES B
HYBRID
ALLOTETRAPLOID
INCREASED
PAIRING
PARTNER
PREFERENCES
ANEUPLOID +
REARRANGED
DIPLOID

1.5.1 Adaptation of allopolyploid meiosis

Allopolyploids arise from hybridization events between closely related species, which occur alongside WGD. Allopolyploids thus have two or more distinct genomes, referred to as homoeologous genomes, that are contained within the same nucleus. Interhomoeologue recombination events that can occur during meiosis in allopolyploids can lead to gene loss, genomic rearrangements or homologue missegregation. Therefore, evolved allopolyploids must prevent promiscuous pairing and recombination from occurring between homoeologues by restricting CO formation such that it occurs exclusively between homologues in a 'diploid like' fashion (reviewed in Cifuentes *et al.,* 2009).

The ability of allopolyploids to restrict pairing to homologues over homoeologues appears, at least in part, to have a genetic basis. This has been most extensively studied in the agriculturally significant allohexaploid *Triticum aestivum* (bread wheat), whose full genome contains three related diploid subgenomes. The diploid like behaviour of wheat meiosis is ensured via a multigenic system, which includes contributions from the *P*airing *h*omoeologous 1 (*Ph1*) locus. The role played by the *Ph1* locus in ensuring diploid like meiosis was initially described in 1958 (Riley, 1958) when it was demonstrated that in the absence of this locus, situated on the long arm of chromosome 5B, extensive homoeologous pairing and an increased number of COs were observed. The *Ph1* locus has since been defined as a region containing a cluster of cyclin dependent kinase (Cdk) genes (Griffiths *et al*., 2006) and is thought to play a role in promoting homologous synapsis and inhibiting the maturation of homoeologous COs (Greer *et al.*, 2012, Martin *et al.,* 2014). It has also been shown that in the absence of *Ph1,* transcription is dramatically increased of the wheat homologue of *AtASY1, TaASY1,* (Boden *et al.,* 2009). Significantly, *Taasy1* RNAi lines also exhibit a

reduction in synapsis and increase in homoeologous pairing at metaphase I suggesting that *TaASY1* is involved in the *Ph1* mediated inhibition of homoeologous pairing in wheat. Another locus, *PrBn*, has been identified as playing a role in the suppression of homoeologous recombination in the allotetraploid *Brassica napus* (Jenczewski *et al.*, 2003).

The progression of synapsis during allopolyploid meiosis has also been extensively studied in wheat, where it has been demonstrated that during the zygotene stage of meiosis SC can polymerise between the axial elements of both homologous and homoeologous chromosomes (Holm 1986) to generate synaptic multivalents. The regions at which a chromosome swaps its synaptic partner from a homologue to a homoeologue are referred to as synaptic partner switches (SPS). Although these structures have also commonly been referred to as pairing partner switches (PPS), it has recently been suggested by Lloyd and Bomblies (2016) that the term PPS should be reserved for regions swapping pre-synaptic alignment between separate homologues / homoeologues, with SPS sites instead referring to exchanges between regions of synapsis. In wheat, the number of SPS sites is gradually reduced as meiosis progresses through late zygotene and pachytene until diplotene, by which stage almost no SPS sites can be detected and all chromosomes are synapsed as bivalents (Holm 1986). This indicates that a system is in place by which SPS sites can be resolved by reorganising regions of synapsis and remodelling the SC to prevent non-homologous synapsis. Early recombination nodules have also been found to occur on either side of SPS sites, indicating that the early stages of recombination do occur between homoeologous chromosomes at regions of non-homologous synapsis (Hobolth 1981).

Naturally evolved allotetraploids can also be found in the *Arabidopsis* genus, with both *A. suecica* and *A. kamchatica* appearing to possess diploid like bivalent pairing at meiosis (Comai *et al.*, 2003, Shimizu *et al.*, 2005). Again, a genetic locus has also been identified in *A. suecica* that appears to contribute towards allotetraploid meiotic stability (Henry *et al.*, 2014). This indicates that, even though the diploid progenitors of the *A. suecica*, *A. thaliana* and *A. arenosa*, are reasonably diverged there is still a genetic contribution to allopolyploid meiotic stabilisation.

1.5.2 Adaptation of autopolyploid meiosis

Autopolyploids arise from whole genome duplication events that occur within a single species. This can occur either through the fusion of two unreduced gametes, via a triploid intermediate or by somatic chromosome doubling (reviewed in Bomblies & Madlung, 2014). This means that each cell contains more than two homologous copies of each chromosome and, during meiosis, each of these homologues is equally capable of pairing and recombining with any of the other homologues. This results in a polysomic inheritance pattern in autopolyploids. This is unlike the situation in allopolyploids which exhibit disomic inheritance due to their restricted pairing partner preferences (Le Comber *et al.*, 2010). As all homologues can pair and recombine with each other, this means that multivalent chromosomal associations can form at metaphase I when one chromosome forms COs with two different homologues at different positions along its length. Multivalents at metaphase I can often lead to missegregation of homologues at anaphase I (Reviewed in Lloyd and Bomblies, 2016), which results in a lowering of fertility in newly formed autopolyploid plants (Yant *et al.*, 2013). In order to prevent gametic aneuploidy, established autopolyploid species

often show diploid-like pairing between random bivalents, most likely as a result of reduced crossover (CO) frequency or increased CO interference (Reviewed in Bomblies *et al.* 2016).

Autotetraploids can be artificially induced in *A. thaliana* via treatment of plants with the microtubule poison colchicine (Maluszynska *et al,* 1990). Analysis of meiosis in artificially induced *A. thaliana* autotetraploids demonstrates that polyploidisation has varying effects on meiosis in different ecotypes. Weiss and Malusynska (2000) observed that homologous chromosomes mostly underwent diploid like pairing following tetraploidisation in the Wilna ecotype, but Santos *et al* (2003) showed that high multivalent frequency was observed in first generation autotetraploids in a Columbia background. Both studies gauged multivalent formation frequency using fluorescence *in situ* hybridisation (FISH) to distinguish DAPI stained metaphase I chromosomes, with Weiss and Malusynska noting that this method could be misleading due to the possibility of identifying overlapping bivalent chromosomes as multivalents. Santos *et al.*, (2003) found that established autotetraploid lines that had been selfed over several generations had lower multivalent frequencies than new autotetraploid lines suggesting rapid adaptation to genome doubling by cytological diploidisation. The authors suggest that the speed of this adaptation could point to a possible epigenetic explanation for this adaptation.

Unlike *A. thaliana, Arabidopsis arenosa* possesses naturally established diploid (2n=16) and autotetraploid (4n=32) populations (Hollister *et al.,* 2012). Hence, *A. arenosa* is rapidly emerging as a valuable model organism for the study of autotetraploidy in plants. Cytological studies in *A. arenosa* have demonstrated that the majority of homologous chromosomes in naturally established autotetraploids undergo diploid-like bivalent pairing. Contrastingly,

extensive multivalent formation and very low pollen viability is observed in new autotetraploids derived from colchicine treated diploids (Yant *et al.*, 2013).

Genome scans in *A. arenosa* have also demonstrated that meiotic genes, in particular, have undergone strong ploidy specific selection (Hollister *et al.,* 2012, Yant *et al.,* 2013). These genes are involved in sister chromatid cohesion, meiotic axis formation and homologue synapsis and include; *ASY1, ASY3, PDS5, PRD3, SMC3, SYN1, ZYP1a* and *ZYP1b*. For *ASY1*, a derived SNP that results in a single amino-acid change at a highly conserved site within the protein's HORMA domain was found at a high frequency within the tetraploid population (~90%), but only at a very low frequency (~4%) in the diploids and is unrepresented in any other sequenced vascular plant species (Hollister *et al.,* 2012).

Cytological comparison of diploid and autotetraploid *A. arenosa* also revealed that the diploid lines experience a higher frequency of COs per pair of homologues as indicated by a higher frequency of ring bivalents relative to rod bivalents at metaphase I in the diploid line compared to the established autotetraploid (Yant *et al.,* 2013). This lends support to the theory that stabilisation of autotetraploid meiosis could result from a decrease in CO numbers or an increase in CO interference that would inhibit multivalent formation by preventing multiple crossovers occurring between more than two homologues.

Indeed, a lowering of CO frequency to ~1 CO per pair of chromosomes has also been noted in other established autotetraploid species including *Physaria vitulifera* and *Lotus corniculatus* (Mulligan 1967, Davies *et al.,* 1990). However, not all established autotetraploids appear to adopt this behaviour, with autotetraploid *Dactylis glomerata* experiencing a higher CO

frequency than the diploid (McCollum 1958). Chromosomal configurations at M1 that favour balanced homologue segregation also appear to be more common in naturally evolved autotetraploids, For instance, trivalent-univalent combinations, where three homologues are linked by COs whilst one homologue is absent of COs, are rare with most established autotetraploids exhibiting only bivalent or quadrivalent configurations that are more likely to result in balanced segregation (Bomblies *et al.*, 2016).

SPS sites have also commonly been found to occur is zygotene and pachytene cells of autopolyploid species. Electron microscopic analysis of silver stained prophase I spreads from the autotetraploid silkworm *Bombyx mori* have shown that, similar to wheat, a greater frequency of SPS sites are observed in zygotene cells compared to late pachytene cells suggesting that some SPS sites are resolved (Rasmussen 1987). Unlike in wheat, however, a much greater proportion of SPS sites persist until diplotene in the autotetraploid *B. mori* spermatocytes. This also differs from the situation in *B. mori* oocytes, which lack COs and where almost all SPS sites are resolved by late pachytene. This has led to the suggestion that the presence of COs in autotetraploids could prevent the resolution of SPS sites and increase the frequency of synaptic multivalents that persist into late pachytene (Rasmussen 1987).

1.5.3 The possible role of interference in stabilising autopolyploid meiosis

Bomblies *et al.,* (2016) proposed that a critical step in the evolution of autopolyploidy is to increase the CO interference distance/strength relative to diploids. By increasing the interference signal to a length greater than or equal to the length of the whole chromosome this should encourage only one CO to form per pair of homologues, thus preventing

multivalent formation. This could be achieved by increasing the distance over which the interference signal can extend or by reducing the physical length of the chromosome axis (and increasing chromatin loop size or density) such that the same level of interference will extend to a further genetic distance along the chromosomes (Bomblies *et al.*, 2016). In support of the latter suggestion, electron microscopic analysis in *B. mori* has shown that the mean SC length in pachytene cells is reduced by up to 27% in tetraploid spermatocytes compared to diploid spermatocytes (Rasmussen 1987). As previously mentioned, the meiotic axis is also hypothesised to play a significant role in CO interference and the high degree of selection for axis proteins and axis-associated proteins in *A. arenosa* tetraploids also lends support to CO interference playing a substantial role in the stabilisation of autopolyploid meiosis (Yant *et al.*, 2013). This proposal of interference based stabilisation would also ensure that the efficiency of CO designation would be strong enough to establish CO assurance and prevent the occurrence of unpaired chromosomes.

It is worth noting that CO number could be reduced in ways other than by increasing interference, for instance by reducing the total number of precursor recombination interactions, by reducing the efficiency of CO designation or by impeding CO maturation (Bomblies *et al.*, 2016). It is unlikely that reducing the number or precursor interactions would be effective as CO homeostasis would counteract this to maintain the same number of COs. Similarly, simply inhibiting CO designation or maturation could fail to ensure that the obligate CO is formed and would increase the frequency of univalents.

1.6 Aims of the project

During this study, we have investigated how the interplay between meiotic recombination and axis proteins regulates recombination and CO formation from late G2 through prophase I in *Arabidopsis thaliana* and the model tetraploid species *Arabidopsis arenosa*.

As *A. arenosa* has only recently become established as a model organism for investigating polyploid meiosis (Hollister *et al.,* 2012), many of the basic features of meiosis in *A. arenosa* have yet to be characterised or observed cytologically. Therefore, we have built upon prior work (Higgins *et al.,* 2014) to dissect the fundamental meiotic behaviour of *A. arenosa*, particularly with respect to how DSB formation, pairing and CO formation progress during meiosis I and how these processes have adapted or changed to cope with the extra levels of chromosomal complexity associated with polyploidisation.

We have also examined how meiotic behaviour differs in tetraploid *A. arenosa* lines expressing diploid or tetraploid alleles of the meiotic axis protein ASY1. To accomplish this we investigated whether there are any differences in DSB number, CO number or CO localisation in lines homozygous for either allele. As the diploid and tetraploid accessions of *A. arenosa* are often found at different altitudes in the wild (Wright *et al.,* 2014) we also set out to test whether tetraploid *A. arenosa* lines with different *ASY1* genotypes appeared to possess differing levels of meiotic thermotolerance.

As well as investigating the behaviour of ASY1 in *A. arenosa*, we also further examined the role played by ASY1 in *A. thaliana* meiosis by generating RNAi knockdown lines with reduced *ASY1* expression. We also generated RNAi knockdown lines targeting another axis-

associated protein *ASY3.* Again, using a combination of cytology and immunocytochemistry we determined what meiotic defects were associated with reduced expression of both of these axis proteins. We also generated neopolyploids of some of these lines via colchicine treatment to find out what effect, if any, slight reductions in CO number can have on the stabilisation of polyploid meiosis and fertility.

By investigating the modes by which axis organisation and CO formation is coordinated in *Arabidopsis* it is hoped that this will lead to the development of novel strategies for manipulating crossover distribution within plants. This could have a profound influence upon current plant breeding strategies, especially for many cereals in which 30-50% of genes rarely recombine (Higgins *et al.*, 2012), enabling plant breeders to generate plants with novel allelic combinations and potentially beneficial characteristics. It has also often been observed that polyploid plants exhibit increased vigour relative to their diploid counterparts (Sattler *et al.*, 2015). However, the disruptive effects of polyploidy on meiosis often results in a severe reduction in fertility (Sattler *et al.*, 2015), preventing normal seed set from being achieved and therefore lowering the obtainable yield of neopolyploid cereal crops. Finding a way of stabilising meiosis in new, artificially induced, autopolyploids could promote the use of neopolyploids in agriculture by ensuring that beneficial increases in vigour are not accompanied by a loss of fertility.

CHAPTER 2

MATERIALS AND METHODS

2. Materials and Methods

2.1 Plant material

Seeds of the *Arabidopsis thaliana* ecotype Columbia [0] (Col-0) and *Arabidopsis arenosa* accessions Triberg (TBG) (4n) and Strecno 29 (SN29) (2n) (Yant *et al.*, 2013) were sown on soil based compost and grown in a glasshouse with supplementary lighting (400W high pressure sodium lamps) under 16 hours light, 8 hours dark cycles. Transgenic *A. thaliana* seeds obtained following *Agrobacterium tumefaciens* mediated transformation underwent selection on 0.8% Agar Murashige and Skoog (1962) medium containing 50 μg/mL Kanamycin. Seedlings were transferred to soil based compost two to three weeks after germination. The T-DNA insertion lines SALK_143676, SALK_144182 and SAIL_1187_CO6 were obtained from the European *Arabidopsis* stock centre in Nottingham (NASC).

2.2 DAPI staining of acid-fixed meiocytes

For epifluorescence microscopy of DAPI-stained meiotic spreads, inflorescences were first fixed in 3:1 ethanol:glacial acetic acid. Where possible, slides were made on the day following fixation to prevent degradation of the material. Inflorescences were washed 3 x 5 minutes in 10 mM citrate buffer at pH 4.5 and buds of the desired size were dissected and subsequently incubated in 300 μL of enzyme mixture (0.3% cellulase, 0.3% pectolyase in 10 mM citrate buffer) in a moist chamber at 37^{o}C for 90 minutes. The enzyme mixture was removed and replaced with cold deionized water to stop digestion, with 1-2 buds being used per slide. For *A. thaliana*, buds were transferred to ~2 μL of 60% acetic acid on a slide and macerated with a mounted needle and brass-rod. 7 μL of 60% acetic acid was then added to

the slide and the slide was placed on a hot block for 30 seconds, before adding another 7 μL of 60% acetic acid and leaving the slide on the hot-block for another 30 seconds. 2 x 200 μL of 3:1 fixative was then added to the slide, before drying the back of the slide with a hairdryer. For *A. arenosa,* buds were transferred to ~2 μL of 80% acetic acid on a slide and macerated with a mounted needle and brass-rod. 10 μL of 80% acetic acid was then added to the slide and the slide was placed on a hot block for 60 seconds, before adding another 10 μL of 80% acetic acid and leaving the slide on the hot-block for another 60 seconds. 2 x 200 μL of 3:1 fixative was then added to the slide, before drying the back of the slide with a hairdryer. Slides were then mounted in 7 μL 1 μg/mL 4',6-diamidino-2-phenylindole (DAPI) in Vectashield mounting medium (Vector laboratories).

2.3 Immunolocalisation of acid-fixed DAPI slides

For immunolocalisation of AtASY1 and AtZYP1 on 3:1 fixed spreads, slides were prepared as previously described for acid-fixed DAPI spreads. To remove the coverslips and dissolve the mounting medium, DAPI stained slides were immersed in 100% ethanol in a coplin jar for 10 minutes. Slides were then submerged in boiling pH 7 citrate buffer for 45 seconds before being transferred to room temperature 1% phosphate buffered saline (PBS), 0.1% triton X-100 solution for 10 minutes. 50 μL of rat anti-ASY1 and rabbit anti-ZYP1c antibody, diluted 1/5000 and 1/500 respectively in blocking buffer (1% PBS, 0.1% triton X-100, 1% bovine serum albumin), was then added to the slide on a parafilm coverslip and incubated in a moist chamber overnight at 4^{o}C. Slides were then washed 3 x 5 minutes in 1% PBS, 0.1% triton X-100 before adding 50 μL FITC anti-rabbit and Texas-red anti-rat secondary antibody, diluted 1/50 and 1/100 respectively in blocking buffer, to the slide on a parafilm coverslip and incubating the slides in a moist chamber at 37^{o}C for 30 minutes. Slides were then washed

again 3 x 5 minutes in 1% PBS, 0.1% triton X-100 and mounted in 7 µL 1 µg/mL DAPI in Vectashield mounting medium.

2.4 Fluorescence *in situ* hybridisation of acid fixed DAPI slides

For fluorescence *in situ* hybridisation (FISH) analysis of 3:1 fixed spreads, slides were prepared as previously described for acid-fixed DAPI spreads. To remove the coverslips and dissolve the mounting medium, DAPI stained slides were immersed in 100% ethanol in a coplin jar for 10 minutes. Slides were then washed in 4x SSC buffer (0.3 M NaCl, 0.03 M sodium citrate, pH 7.0), 0.05% Tween 20 solution for 1 hour. Slides were then washed in 2x SSC buffer for 10 minutes and then for exactly 90 seconds in 0.01% pepsin, 0.01 HCl solution that had been pre-warmed to 37^{o}C. Following this, slides were washed again in 2x SSC for 10 minutes. Slides were then washed for 10 minutes in 4% paraformaldehyde (pH 8) and material was dehydrated by washing in an alcohol series of 70%, 90% and finally 100% ethanol for 2 minutes at each concentration. Slides were then air-dried for at least 15 minutes.

20 µL of FISH probe was prepared for each slide. To prepare the FISH probes 14 µL of master mix (5 mL deionised formamide, 1 mL 20x SSC, 1 g dextran sulphate) was mixed with 3 µL biotin tagged 5S probe (2 ng/µL) and 3 µL digoxygenin tagged 45S probe (2 ng/µL). Probes were tagged using the nick labelling kit (Roche) to incorporate biotin-16-dUTP or digoxygenin -11-dUTP conjugates following the manufacturer's instructions. The 20 µL probe mix was then incubated at 94^{o}C for 10 minutes to denature the probes and then immediately placed on ice. 20 µL of the probe mix was added to each slide on a hotplate at 75^{o}C. Coverslips were then applied to the slides and sealed with vulcanising rubber solution and incubated on the hotplate at 75^{o}C for a total of four minutes. Slides were then placed in a

humid chamber overnight at 37°C. The following day, coverslips were removed and the slides were washed for 3 x 5 minutes in 50% formamide, 2x SSC solution that had been pre-warmed to 45°C and then for exactly 4 minutes in 2x SSC pre-warmed to 45°C. After this, slides were washed in 4X SSC buffer, 0.05% Tween 20 solution prewarmed to 45°C for 5 minutes and then in 4X SSC buffer, 0.05% Tween 20 solution at room temperature for 5 minutes. Slides were then incubated in 80 µL anti-biotin Cy3 antibody which had been diluted 1/200 in milk block (100 mL 4 x SSC, 0.05% Tween 20 and 5 g dried skim milk) on a parafilm coverslip at 37°C for 30 minutes. Slides were then washed 3 x 5 minutes in 4 x SSC, 0.05% Tween 20 solution before being incubated in 80 µL anti-digoxygenin FITC antibody which had been diluted 1/50 in digoxygenin blocking solution (100 mL 4 x SSC, 0.05% Tween 20 and 0.5% Roche digoxygenin blocking reagent) on a parafilm coverslip at 37°C for 30 minutes. Slides were then washed 3 x 5 minutes in 4 x SSC, 0.05% Tween 20 solution and mounted in 7 µL 1 µg/mL DAPI in Vectashield mounting medium.

2.5 Immunolocalisation using fresh material

For immunolocalisation using fresh material from *A. thaliana* and *A. arenosa,* anthers were dissected from fresh buds on moist filter paper. To determine the meiotic stage of meiocytes within the bud, a single anther from each bud was squashed in a drop of aceto-orcein stain on a slide under a coverslip and viewed using a compound microscope. The anthers from several (~5) *A. thaliana* buds or a single *A. arenosa* bud were added to a clean slide with 5 µL digestion mix (0.4 % cytohelicase, 1.5% sucrose , and 1% polyvinylpyrollidone) and gently tapped with a brass rod for 1 minute. An extra 5 µL of digestion mix was added to the slide and the slide was incubated in a moist chamber at 37°C for 2 minutes. 10 µL of 1.5% lipsol (*A. thaliana*) or 1.8% lipsol (*A. arenosa*) was added to the slide and spread with a mounted

needle. 20 µL of 4% paraformaldehyde was immediately added to the slide and the slide was left to dry in the fume hood for 3 hours. After drying, the slide was incubated for 5 minutes with 50 µL blocking solution (0.1 x phosphate buffered saline (PBS), 0.01% Triton X-100, 0.1% Bovine Serum Albumin (BSA)) before adding 50µL of primary antibody diluted in blocking solution on a parafilm coverslip. Slides were then incubated in a moist chamber overnight at 4^{o}C. The following primary antibody dilutions were used; rat anti-ASY1 1/5000, rat/rabbit anti-ZYP1 1/500, rabbit anti-RAD51 1/500, rabbit anti-DMC1 1/500, rabbit anti-SMC3 1/500, rabbit/rat anti-MLH1 1/200, rabbit anti-HEI10 1/200. Following overnight incubation, slides were washed 3 times in washing solution (1 x PBS, 0.1% Triton X-100) for 5 minutes each time. 50 µL of secondary antibody diluted in blocking buffer was then added to the slide using a parafilm coverslip and the slide was incubated in a moist chamber at 37^{o}C for 30 minutes. The following secondary antibody concentrations were used; FITC anti-rat/rabbit 1/50, CY3 anti-rat/rabbit 1/100, Alexa-fluor 350 anti-rabbit 1/50 (ThermoFisher). After incubation, slides were washed 3 times in washing solution for 5 minutes and then mounted in 7 µL 1 µg/mL DAPI in Vectashield mounting medium.

The following modifications were made for slides being used for structured illumination microscopy (SIM). Material was spread, fixed and stained on high-precision No. 1.5 coverslips (Marienfeld). Alexa-fluor 488 anti-rat and Alexa-fluor 594 anti-rabbit secondary antibodies (ThermoFisher) were used, both at 1/200 dilution. After secondary antibody incubation, coverslips were incubated in 50 µL 1 µg/mL DAPI for 10 minutes at room temperature. Coverslips were then washed 3 times in washing solution and once in deionised water before being mounted on a slide in 7 µL Vectashield mounting medium.

2.6 Microscopy and image analysis

Epifluorescence microscopy was performed using a Nikon *90i* microscope and image analysis was carried out using Nikon NIS-Elements software and ImageJ. SIM was performed using a Zeiss ELYRA PS1 microscope and image reconstruction and analysis was carried out using the Zeiss Eclipse software and ImageJ.

2.7 Measuring Synaptonemal Complex (SC) lengths and interference analysis

SC length measurements were made using Nikon NIS-Elements software by tracing individual SCs from maximum intensity projections of well spread pachytene chromosomes. For gamma-distribution interference analysis, inter-MLH1-foci distances either across SPS sites or from SC segments without SPS sites were measured and this distance was normalized as a percentage of total SC length. Measured distances were then binned into five intervals (each 20% total SC length) and used to generate a histogram of inter-foci distance frequencies. Gamma distributions were fitted to the histograms using the maximum likelihood estimation with XLSTAT software.

To determine the distance between MLH1 foci on the same side of a synaptic multivalent with a B conformation, the distance of both MLH1 foci from the chromosome ends was measured and then normalized as a proportion of the SC length from the chromosome end to the SPS site. This length was used for normalization, rather than total SC length, as synaptic multivalent conformations with MLH1 foci on both sides of the SPS has already been excluded and therefore it would have been inappropriate to use total SC length as a relative measure of MLH1 distribution. The two normalized values were then subtracted to generate absolute values for the distance between both foci. These distances were binned into 10

intervals (each 10% normalized SC length) and the frequencies were presented on a histogram. For comparison, the relative frequencies of distances between randomly paired foci were also calculated and used to generate a histogram. To calculate the expected frequency of distances between randomly paired MLH1 foci, all 11236 possible absolute values were calculated by subtracting each of the 106 MLH1 distances (as a proportion from chromosome end to SPS site) from one another. Again, the frequency of each inter-foci distance was binned into 10 intervals (each 10% normalized SC length) and the frequencies were presented on a histogram alongside the experimentally determined inter-foci distances. Cumulative frequency plots were also generated for the continuous data from the experimentally determined inter-foci distances and the randomly paired inter-foci distances and used to calculate the one-tailed Kolmogrov-Smirnov shift in distribution between the two samples.

MLH1 foci distances were also measured from *ASY1 TTTT* and *ASY1 DDDD* pachytene cells by measuring the SC distance from the MLH1 focus to either end of the chromosome on chromosomes experiencing a single MLH1 focus. Both of these distances were converted to proportions of total SC length and then subtracted from one another to generate an absolute figure that represented the relative distance of the MLH1 focus from the middle of the chromosome (0 = middle of chromosome, 1 = very end of the chromosome). The data from all chromosomes was then binned into five intervals of equal size and used to generate frequency histograms of MLH1 position for both *ASY1 TTTT* and *ASY1 DDDD* plants. Continuous data was also used to generate a cumulative frequency distribution for a Kolmogrov-Smirnov test.

2.8 Alexander pollen staining

Alexander staining was used to check for pollen viability in *A. arenosa* (Alexander 1969). Anthers containing mature pollen were dissected from *A. arenosa* buds and placed on a slide in a drop of Alexander stain (10 ml 96% EtOH, 10 mg Malachite green, 50 ml distilled H_2O, 25 ml glycerol, 5 g phenol, 5 g chloral hydrate, 50 mg acid fuchsin, 5 mg Orange G). A coverslip was then applied and firmly pressed down onto the anther to extrude the pollen before sealing with rubber solution. Slides were then placed on a hot block at 50^{o}C for 1 hour and then viewed using a compound microscope. Viable pollen grains appear red and non-viable pollen appears blue/green.

2.9 Plant DNA extraction

Discs of leaf tissue ~5 mm in diameter were collected on ice and gently macerated in 40μL extraction buffer (100 mM Tris-HCl pH 9.5, 10 mM EDTA, 250 mM KCl). Macerated tissue was then incubated at 95^{o}C for 10 minutes before adding 40 μL of dilution buffer (3% BSA). The mixture was centrifuged for 60 seconds and the supernatant containing extracted DNA was aliquoted into a fresh tube.

2.10 *A. arenosa ASY1* Genotyping

A. arenosa plants were genotyped for diploid or tetraploid *ASY1* alleles by first amplifying a ~300bp fragment of the *ASY1* gene from extracted plant DNA using Reddymix PCR Master Mix (ThermoFisher), the primers ASY1 arenosa F1 (5'-TTTGGTTTTCGTTTTGCTGA-3'), ASY1 arenosa R1 (5'-GAGATTCAGCGTCCATAGGC-3') and the following conditions:

initial denaturation 93°C 1 minute, subsequent steps 93°C 1 minute, annealing at 50°C 1 minute, extension 72°C 30 seconds, 35 cycles total. 8 μL of PCR product was digested with *XmnI* restriction enzyme (N.E.B) for 90 minutes at 37°C. The diploid allele contains an *XmnI* restriction site and should give digestion products at sizes 200bp and 100bp. The tetraploid allele does not contain an XmnI restriction site and should, therefore, give a post-digest product of 300bp.

2.11 *A. thaliana HO* and SN *ASY1* transgene genotyping

To indicate the absence of the endogenous *ASY1* gene in the HO and SN *ASY1* transgenic *A. thaliana* lines the primers A1_At_F (TCAGCATATGTGAAACTGTTGATGG) and A1_At_R (AAGGTTTAAACAACAGCTGTCAGT) and the following PCR conditions were used: initial denaturation 95°C 2 minutes, subsequent steps 95°C 1 minute, annealing at 59°C 30 seconds, extension 74°C 1 minute 15 seconds, 30 cycles total. This reaction should only amplify the endogenous *ASY1* and not the competing transgene. To confirm the presence of the HO and SN *ASY1* alleles the same genotyping method from section 2.9 was used.

2.12 *A. thaliana* bud cDNA synthesis

~500 μL of *A. thaliana* buds were collected in diethylpyrocarbonate (DEPC) treated 1.5 mL microfuge tubes and snap frozen in liquid nitrogen. RNA was extracted from the frozen material using the Qiagen RNeasy kit following the manufacturer's instructions. DNA contamination was removed from the RNA sample by treatment with DNaseI (Invitrogen) for 15 minutes. Following DNaseI treatment, RNA was purified by phenol chloroform extraction.

Superscript II RNase reverse transcriptase (Invitrogen) and an Oligo-dT (16) primer were used to generate cDNA from DNase treated RNA.

2.13 Construction of RNA interference cassettes

DNA fragments of ~700bp were amplified from bud cDNA using the primers listed in Table 1. Pfu DNA Polymerase (Promega) and the following PCR conditions were used: initial denaturation 95^{o}C 2 minutes, subsequent steps 95^{o}C 1 minute, annealing at 55^{o}C 30 seconds, extension 74^{o}C 2 minutes, 34 cycles total.

Primer Name	Primer sequence 5' – 3'	Amplicon size (bp)
ASY1 SF	CTCGAGTCAACTCCCGTCACCTTGAT	703
ASY1 SR	GGTACCTGTGCCTTGTTGCTAATGGG	
ASY1 AF	GGATCCTCAACTCCCGTCACCTTGAT	703
ASY1 AR	ATCGATTGTGCCTTGTTGCTAATGGG	
ASY3 SF	ACTCGAGTGTGCCAGATAAGGATGATGGA	714
ASY3 SR	AGGTACCTCTGGTTACTGGCCTTCTGG	
ASY3 AF	AGGATCCTGTGCCAGATAAGGATGATGGA	714
ASY3 AR	AATCGATTCTGGTTACTGGCCTTCTGG	

Table 2.1. Primers for RNAi sense and antisense strand amplification

Amplicons were separated by gel electrophoresis and purified using the QIAquick Gel Extraction Kit (Qiagen) following the manufacturer's instructions. Purified amplicons were

ligated into the plasmid pCR-BLUNT using the Zero Blunt® PCR Cloning Kit (Invitrogen), following the manufacturer's instructions. Sense-pCR-BLUNT plasmids were digested with *KpnI* (N.E.B) and *XhoI* (N.E.B) and antisense-pCR-BLUNT plasmids were digested with *BamHI* (N.E.B) and *ClaI* (N.E.B). Digestion products (~700bp) were purified by gel electrophoresis and ligated into pHannibal that had been digested with similar restriction enzymes, using T4 DNA Ligase (N.E.B). *ASY1* and *ASY3* sense-intron-antisense cassettes were removed from pHannibal by digestion with *NotI* and ligated into the binary vector pART27 using T4 DNA ligase. During cloning, plasmids were amplified by heat-shock transformation into DH5α *E.coli* cells and plasmid isolation was performed using the Promega Wizard-prep kit.

2.14 Plant transformation

2 µl of miniprep DNA of pART27 binary vectors containing sense-antisense RNAi cassettes were transformed into *Agrobacterium tumefaciens* (GV3101) by electroporation. The *Agrobacterium* was then used to transform Col-0 *A. thaliana* plants via floral dipping (Clough & Bent, 1998).

2.15 Homozygous T3 plant identification

Transformed T1 plants were selected based on Kanamycin resistance. T2 seeds were collected from T1 transformants and again sown on 50 µg/mL Kanamycin 0.8% agar MS media. Mendelian segregation was used to confirm the presence of a single transgene in the T2 plants, with a germination rate of 75% being expected for plants that contained a single transgene. T3 seeds were again collected from T2 transformants and sown on 50 µg/mL

Kanamycin 0.8% agar MS media. A 100% germination rate of the T3 seeds indicated that the T2 plant was very likely to be homozygous for the transgene.

2.16 Seed counts

Seed counts were performed by removing 10 siliques from a selection of plants at approximately the same height from the primary stem. Siliques were then dissected under a stereo-microscope and the number of immature seeds contained per silique was counted.

2.17 Colchicine treatment of *A. thaliana*

3 weeks after sowing, when plants were at the rosette stage of growth, 20 μL of 0.25% colchicine solution was pipetted into the centre of the rosette. The flowering stems that emerged from treated plants were screened cytologically for polyploidisation.

2.18 Cytological screening of colchicine treated plants

Inflorescences from colchicine treated plants were fixed in 3:1 ethanol:acetic acid. Fixed buds were used to make DAPI spreads as previously described. Ploidy number was determined by counting chromosomes of mitotically dividing cells and analysing M1 chromosomes.

2.19 Statistical analysis

Statistical tests were performed as appropriate for the relevant data sets, ensuring all assumptions were met, and all *p*-values are reported in the main text. Analyses were performed and charts were constructed using Microsoft Excel with the XLStat statistical analysis add-on.

CHAPTER 3

INVESTIGATING POLYPLOID MEIOSIS IN *ARABIDOPSIS ARENOSA*

3. Investigating polyploid meiosis in *Arabidopsis arenosa*

3.1 Introduction

Arabidopsis arenosa is becoming rapidly established as a model organism for investigating the evolutionary causes and cellular mechanisms that lead to the stabilisation of autotetraploid meiosis. The majority of work investigating the molecular mechanisms underpinning meiosis in plants has, until now, mostly been performed using the closely related model organism *Arabidopsis thaliana* (reviewed in Osman *et al.*, 2011). However, there are no known naturally established autotetraploid *A. thaliana* populations. This has prevented *A. thaliana* from being used to investigate the evolution and long-term adaptive consequences of autopolyploidisation in plants. *A. arenosa*, on the other hand, has extant diploid ($2n = 2x = 16$) and tetraploid ($2n = 4x = 32$) populations (figure 3.1) scattered throughout central and eastern Europe (Schmickl *et al.*, 2012). All populations are obligate outcrossers and it is likely that most autotetraploid *A. arenosa* populations arose from a single ancestral diploid population that underwent whole genome duplication (WGD) 11,000-30,000 generations ago in the Northern Carpathian Mountains (Arnold *et al.*, 2015). Some recent studies have begun to investigate the behaviour of meiosis in this model plant (e.g. Yant *et al.*, 2013), but there is still a wealth of information to be gleaned about how meiosis is stabilised in the tetraploid, relative to the diploid plants, and what contributions different derived meiotic alleles could have on this.

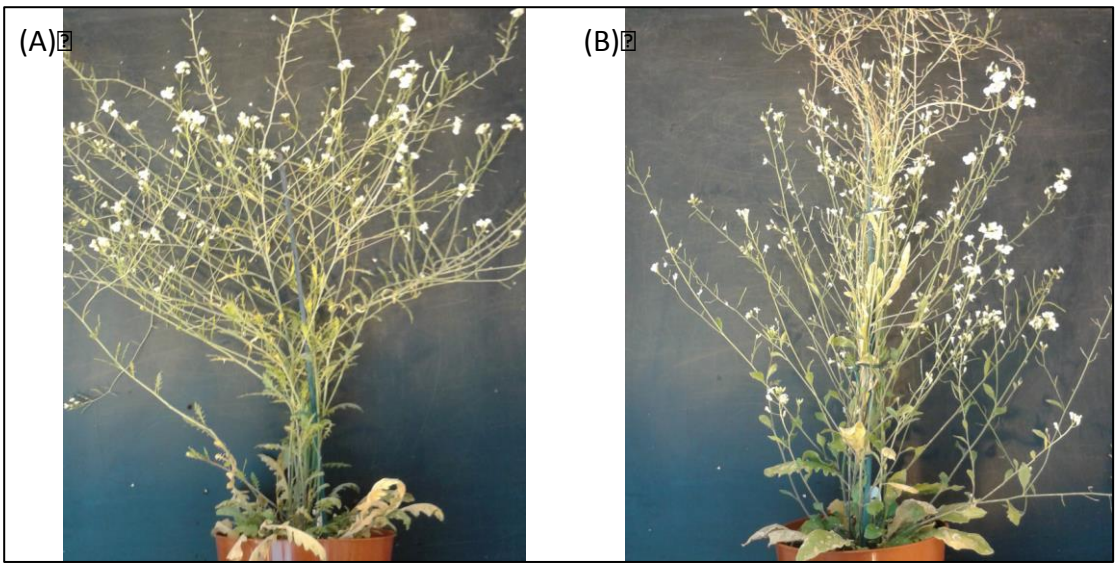

Figure 3.1. Diploid SN29 (A) and tetraploid TBG (B) Arabidopsis arenosa

Carvalho *et al.,* (2009) presented the first detailed cytological analysis of meiotic chromosome behaviour in tetraploid *A. arenosa* using fixed material from the Care-1 accession. They demonstrated that, at metaphase I, tetraploid *A. arenosa* chromosomes undergo diploid like pairing, exclusively forming 16 bivalents. It was also observed that the majority of paired bivalents exhibited a 'rod' conformation, indicating the existence of a single CO, which contrasts with the situation in *A. thaliana* in which a large portion of bivalents tend to exhibit a 'ring' structure indicating the existence of two or more COs between homologues (Sanchez-Moran *et al.,* 2001). This observation was supported by Yant *et al.,* (2013) who showed that bivalent 'rod-like' pairing is also observed in the Triberg (TBG) accession of autotetraploid *A. arenosa*. Yant *et al.,* (2013) also demonstrated that the chiasma frequency per bivalent was significantly higher in the diploid Strecno (SN) accession compared to the tetraploid, with an average of 1.36 and 1.09 chiasmata per pair being observed in the diploid and tetraploid, respectively. This observation lends support to the theory that one pathway to meiotic stability in autopolyploids is via a reduction in CO

frequency that can inhibit multivalent formation and, hence, homologue missegregation. In *A. arenosa* neotetraploids, generated via colchicine treatment, extensive multivalent formation is observed at metaphase I further indicating that derived tetraploid alleles play an important role in promoting stable bivalent pairing (Yant *et al.,* 2013).

Meiotic pairing during prophase I has also been studied in other autotetraploid species using transmission electron microscopy (TEM) of silver stained chromosomes. For instance, TEM analysis of autotetraploid *Crepis capillaris* (Jones and Vincent, 1994) showed that synaptic partner switching (SPS) sites can persist until the pachytene stage of prophase I in autotetraploids. Until recently, however, there have been very few studies analysing prophase I behaviour in autotetraploids using fluorescent immunolocalisation of proteins in freshly fixed material. This contrasts sharply with research in the model diploid *A. thaliana*, in which fluorescent immunolocalisation has been widely used for over a decade to dissect many aspects of meiotic behaviour in this species. For instance, immunolocalisation of the proteins ASY1 and ZYP1 can be used to accurately distinguish between synapsed and unsynapsed regions in zygotene (Armstrong *et al.,* 2002, Higgins *et al.,* 2005). Other notable examples include immunolocalisation of RAD51 and DMC1 (Sanchez-Moran *et al*, 2007) to indirectly quantify meiotic DSB numbers and MLH1 (Lhuissier *et al.*, 2007) to indicate the number and location of class I COs.

Recently, it was demonstrated using fluorescent immunolocalisation microscopy that ASY1 and ZYP1 also localise to unsynapsed and synapsed regions of the meiotic axis, respectively, in both diploid and tetraploid *A. arenosa* (Higgins *et al.,* 2014). Here, we have built upon these initial observations and used immunocytochemistry to determine if any other major meiotic differences can be detected between diploid and tetraploid *A. arenosa.* We have also

used advanced microscopic techniques including structured illumination microscopy (SIM) (Gustafsson, 2000) and triple-labelling of prophase I cells to provide novel insights into the mechanisms of pairing and CO formation in autotetraploids.

3.2 Results

3.2.1 Antibodies targeting ASY1, ZYP1, MLH1, HEI10, RAD51, DMC1 and γH2AX are functional in *A. arenosa*

Immunofluorescence microscopy has been widely applied to the study of meiosis in *A. thaliana* (reviewed in Sanchez-Moran & Armstrong, 2014). To use this technique for similar purposes in *A. arenosa*, it was first important to ensure that antibodies commonly used in *A. thaliana* were functional in *A. arenosa* and localized to expected regions. In *A. thaliana* the functionality of antibodies can also be confirmed by observing an absence of signal in T-DNA insertional mutants, however the lack of such mutants in *A. arenosa* meant that this further analysis could not be performed in this instance.

In *A. thaliana*, antibodies targeting γH2AX, DMC1 and RAD51 have often been used to determine the number of meiotic DSBs occurring in early prophase I (Sanchez-Moran *et al.*, 2007, Kurzbauer *et al.*, 2012). In *A. arenosa*, in both the tetraploid and diploid populations, all three of these proteins can be detected as numerous (>100) foci in early prophase I (figure 3.2 and figure 3.3). This is consistent with how the proteins localize in *A. thaliana*, demonstrating the functionality of the antibodies to also detect these proteins in *A. arenosa*. RAD51 foci counts were performed as a proxy to deduce the number of meiotic DSBs formed in both diploid and tetraploid *A. arenosa*. A mean value of 196 RAD51 foci (n = 10, S.D = 28.6) were counted in diploid SN plants and 383 RAD51 foci (n = 10, S.D = 53.0) in tetraploid TBG

plants (figure 3.4). Both these numbers are slightly larger than previously reported figures for *A. thaliana,* in which around 180 RAD51 foci are observed in mid prophase I (Kurzbauer *et al*, 2012). This observed increase in RAD51 foci in *A. arenosa* could be explained by its increased genome size (203 Mbp) relative to *A. thaliana* (157 Mbp) (Johnston *et al.,* 2004), with frequencies of roughly one DSB per Mbp being found in both species. Also, when the RAD51 foci counts from SN are doubled (393 foci, n = 10, S.D = 57.2) they match closely the values observed in TBG, indicating that DSB frequency per Mbp is maintained between ploidies. This observation also indicates that the previously observed difference in CO frequencies between ploidies (Yant *et al.,* 2013) is unlikely to be caused by a reduction in the frequency of CO-precursor interactions in the tetraploid relative to the diploid, strengthening the support for an interference driven model of CO frequency reduction.

Antibodies targeting HEI10 have been used in *A. thaliana* to detect sites of CO designation (Chelysheva *et al.*, 2012) and MLH1 has also extensively been used as a late marker of Class I CO sites (Higgins *et al.,* 2005). Both proteins form distinct foci that co-localise at late-pachytene with the SC (figure 3.2 & figure 3.3). Although HEI10 does appear as discreet foci, there is a reasonable degree of background signal that does not co-localise with the SC. It may be the case, therefore, that the dilutions and incubation time for the HEI10 antibody may need to be further optimized for *A. arenosa.* As would be expected for MLH1, there appear to be more foci in the tetraploid nuclei (~16 MLH1 foci) compared to the diploid nuclei (~9 MLH1 foci). These numbers of foci also correlate closely with the numbers of COs determined to occur in both diploid and tetraploid *A. arenosa* by Yant *et al.,* (2013) using M1 chiasma counts. In figure 3.3 it can be seen that in the tetraploid MLH1-ZYP1 pachytene nuclei that one MLH1 foci appears to occur per individual bivalent. This is also consistent with the hypothesis that CO numbers are limited to one per pair of chromosomes in tetraploid *A.*

arenosa.

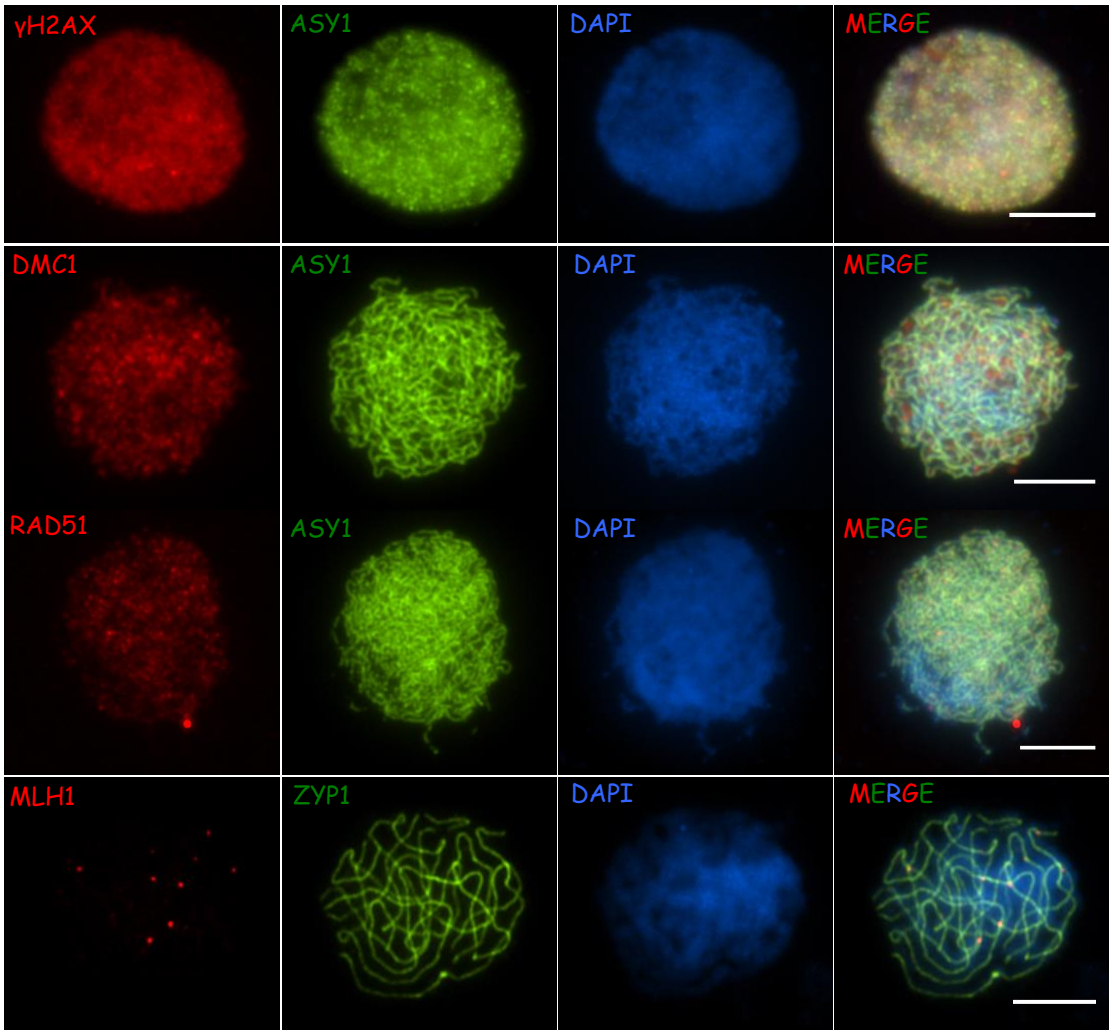

Figure 3.2. Immunolocalisation of γH2AX, DMC1, RAD51 and MLH1 (red) and ASY1 and ZYP1 (green) in diploid SN A. arenosa. DNA is stained with DAPI (blue). Scale bar = 5 μm.

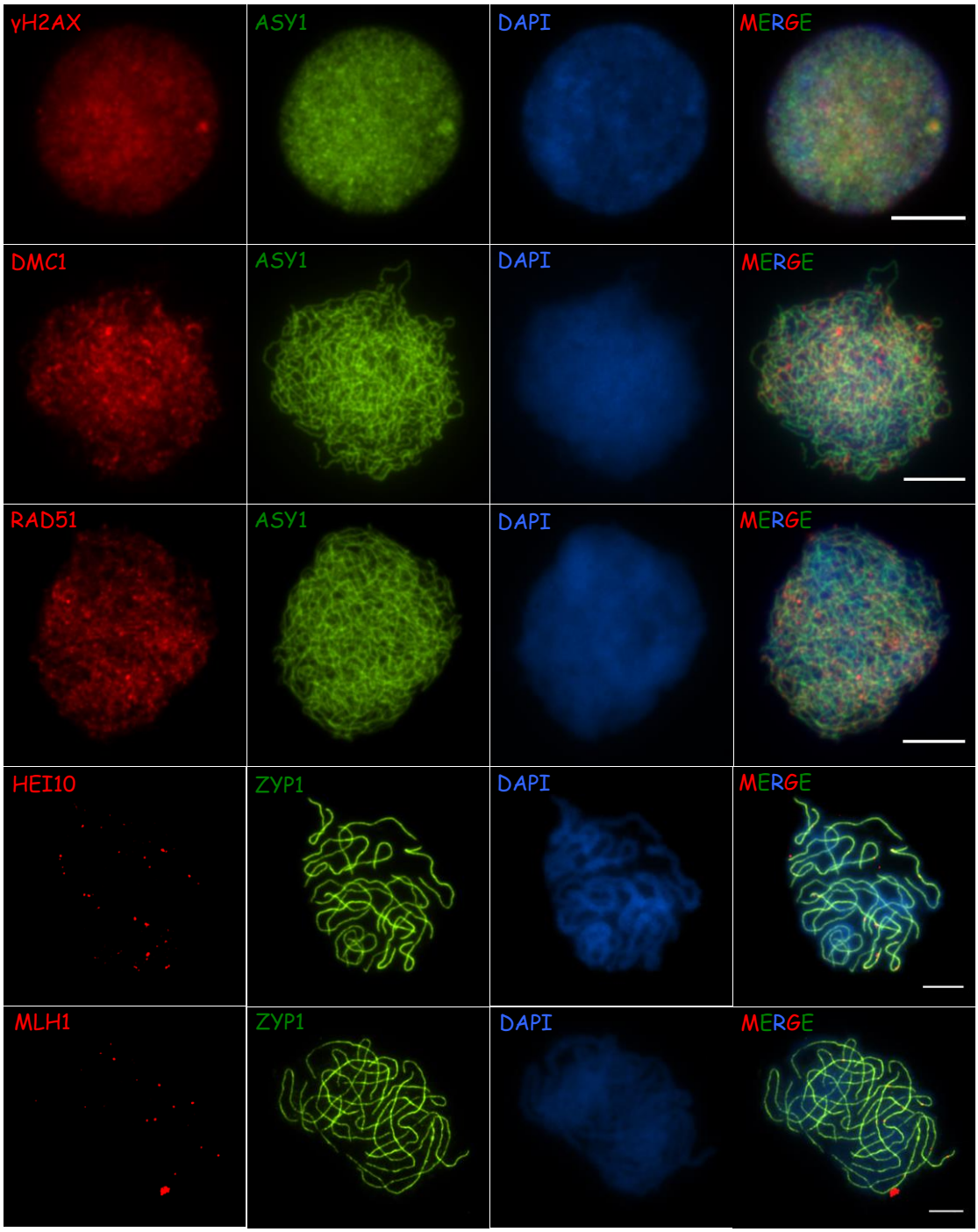

Figure 3.3. Immunolocalisation of γH2AX, DMC1, RAD51, HEI10 and MLH1 (red) and ASY1 and ZYP1 (green) in tetraploid TBG A. arenosa. DNA is stained with DAPI (blue). Scale bar = 5 µm.

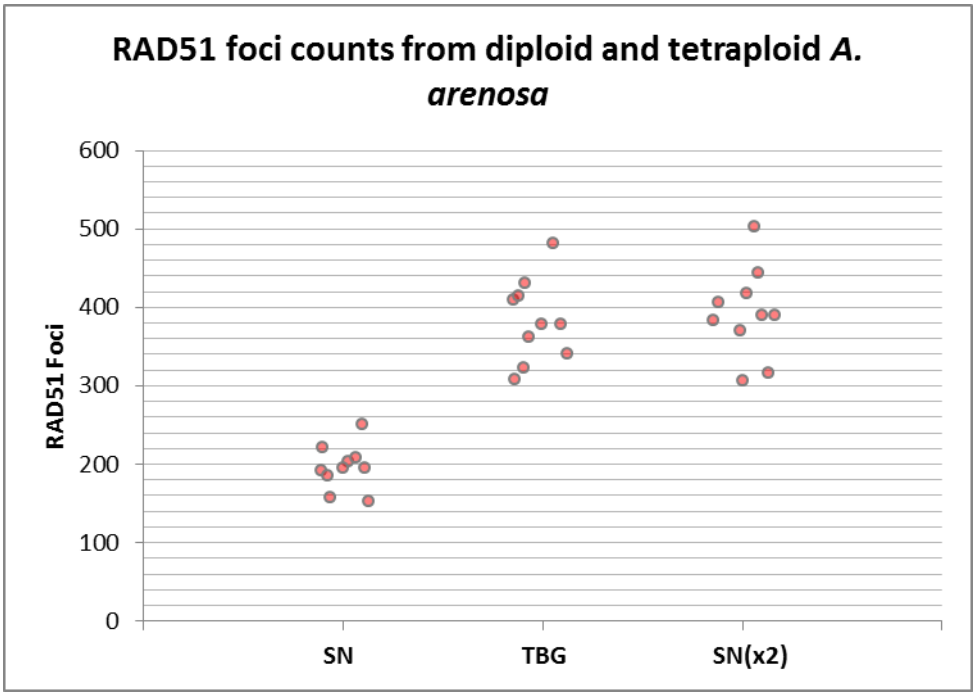

Figure 3.4. Scatter plot showing RAD51 foci counts from diploid (SN) and tetraploid (TBG) A. arenosa prophase I cells. Doubled counts from the diploid accession are also shown for comparison.

3.2.2 Multivalent and univalent chromosomes are still regularly observed in established tetraploid *A. arenosa*

One meiotic problem often encountered by autotetraploids is the formation of multivalents at metaphase I, which can lead to chromosome missegregation (reviewed in Lloyd and Bomblies, 2016). Similarly, univalents can occur in situations where no COs form between homologues and these are highly likely to missegregate at anaphase I. To determine the frequency at which multivalents and univalents occur in the naturally established tetraploid TBG *A. arenosa*, large numbers of DAPI stained metaphase I cells were cytologically examined. It was demonstrated that in 11% of M1 cells (38/353) ring-quadrivalents were observed, where all four homologues are joined by COs. Ring-quadrivalents were counted due to their highly distinguishable square shape (figure 3.5A). Other multivalent

conformations are possible based on different patterns of CO formation between >2 homologues (e.g chain quadrivalents. Reviewed in Bomblies *et al.*, 2016), however it can often be difficult to distinguish between these conformations and other 'overlapping' bivalents and therefore these were not included in this analysis. Because of this, it is likely that the frequency of total multivalents is even higher than the 11% observed. FISH analysis of metaphase I chromosomes using 45S and 5S rDNA probes was also performed to ensure that the ring quadrivalents were, indeed, formed between homologous chromosomes and not due to non-homologous interactions. All ring quadrivalents analysed using FISH (n = 14) appeared to consist of four homologues as indicated by matching 45S/5S FISH signals being present on all four interacting chromosomes.

Pairs of univalent chromosomes were also observed in 8% of cells (28/353) (figure 3.5B). These are formed when the obligate crossover fails to form between two homologues and they are highly likely to missegregate during anaphase I to generate unbalanced gametes. Again, FISH analysis also indicated that both univalents were likely to be homologous chromosomes (n = 3).

For comparison, multivalent and univalent frequencies were also analysed in acid-fixed DAPI spreads from diploid SN29 *A. arenosa*. No multivalent chromosomes were detected in diploid metaphase 1 cells (0/126), however two univalent chromosomes were observed in 4% of cells (5/126) (figure 3.5C). As the diploid has half as many chromosomes as the tetraploid, the frequency of univalent formation per chromosome is, in fact, identical between ploidies (0.5% of total metaphase I chromosomes). It is therefore only meiotic defects associated with multivalent formation that are specific to the tetraploid population.

These results demonstrate that, even though tetraploid *A. arenosa* is considered to be an

established autotetraploid that arose between 11,000 – 30,000 generations ago (Arnold *et al.*, 2015), this species still encounters some meiotic problems with a significant degree of regularity. These meiotic problems are also borne out by the fact that a number of supposed tetraploid *A. arenosa* plants were discovered to be aneuploid during cytological analysis (figure 3.6), and likely arose following fertilisation with unbalanced gametes. These aneuploid plants appeared phenotypically to be indistinguishable from the tetraploids, indicating that the tetraploid *A. arenosa* can happily withstand the loss of some single chromosomes without any dramatic effects on growth and development.

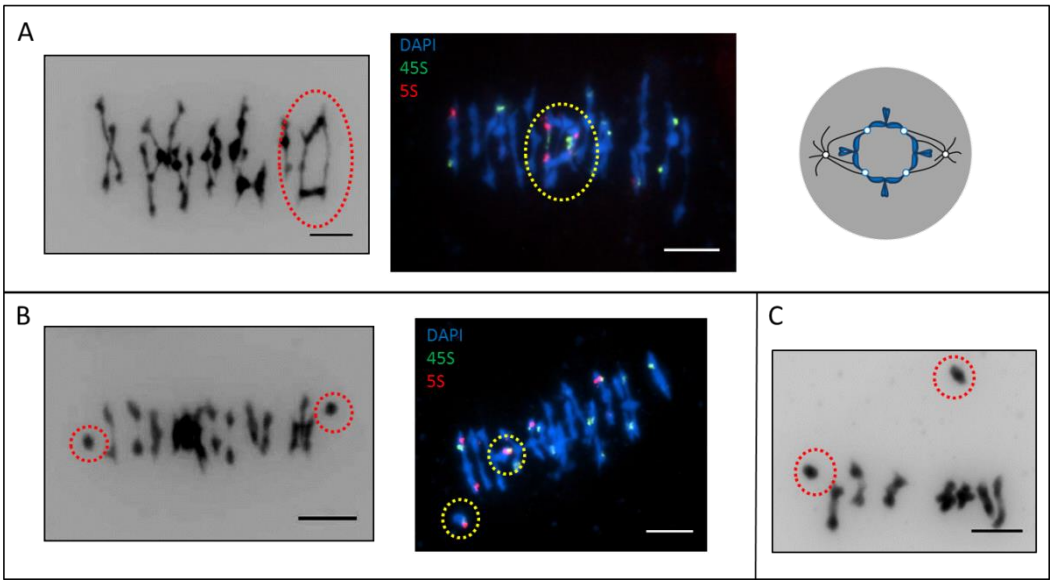

Figure 3.5. Ring quadrivalent and unpaired univalent chromosomes are still observed with a degree of regularity in tetraploid TBG A. arenosa. (A) Ring quadrivalent chromosomes are circled in a DAPI stained TBG metaphase I spread and a DAPI stained spread with 45S (green) and 5S (red) rDNA probes. The FISH probes show that all four chromosomes joined in the ring quadrivalent possess 45S and 5S rDNA loci, indicating they are probable homologues. A cartoon representation showing how four homologous chromosomes form COs with one another in a ring quadrivalent is also shown. (B) Two univalent are circled in a DAPI stained TBG metaphase I spread and a DAPI stained spread with 45S (green) and 5S (red) rDNA probes. The FISH probes show that both univalents possess 45S and 5S rDNA loci, indicating they are probable homologues. (C) A DAPI stained metaphase I spread from diploid SN A. arenosa. Two univalent chromosomes are circled. Scales bars = 5 µm.

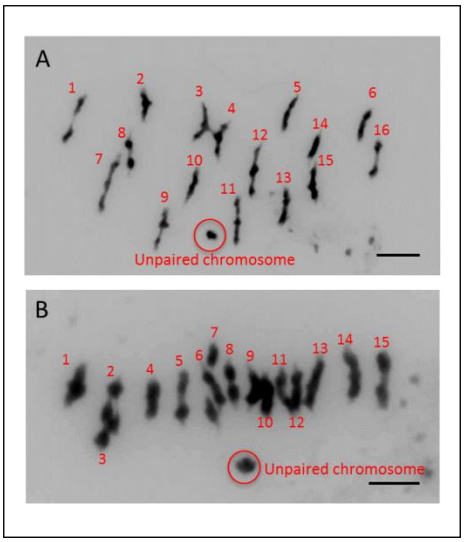

Figure 3.6. DAPI stained metaphase I spreads from aneuploid TBG A. arenosa plants. Some plants had an extra chromosome (n=33) (A), whilst others were lacking a chromosome (n=31) (B). Scale bar = 5 µm.

3.2.3 Synaptic partner switch sites are observed in tetraploid *A. arenosa*

Synaptic partner switching (SPS) during prophase I must occur as a prerequisite for multivalent formation between homologues during metaphase I. SPS sites have been observed many times before in polyploid species using EM but never with immunofluorescence microscopy. Pachytene cells from tetraploid TBG *A. arenosa* were therefore stained for ZYP1 and ASY1 in order to determine if SPS sites could be visualised with epifluorescence microscopy. ASY1 localises with greater intensity to asynaptic regions of the chromosome whilst ZYP1 localises solely to synapsed regions (Lambing *et al.*, 2015, Higgins *et al.*, 2005). It was hypothesised that, if SPS sites were to persist until pachytene in tetraploid *A. arenosa* meiocytes, then they would represent small regions of asynapsis that should exhibit greater ASY1 intensity and no ZYP1 staining relative to the rest of the synapsed chromosomes. Figure 3.7A shows a ZYP1/ASY1 stained pachytene cell from *A. arenosa*. There are four regions on this cell that appear to have brighter ASY1 intensity and these all occur at positions where two paired bivalents are crossing one another. Contrastingly, pachytene cells from diploid *A. arenosa* stained with the same antibodies do not exhibit these regions of increased ASY1 intensity (figure 3.7C) indicating they are fully synapsed along their entire length. Aside from SPS sites, another explanation for these small areas of asynapsis is that they could represent unresolved interlocks, also known as synaptic bubbles, which have been observed many times before using immunofluorescence microscopy (*e.g.* Higgins *et al.*, 2014). The resolution limit of the epifluorescence microscope meant that it was difficult to conclusively confirm that these structures were, indeed, SPS sites rather than unresolved interlocks.

To visualise the putative SPS sites with increased resolution, structured illumination

microscopy (SIM) was adopted. SIM bypasses the Abbe diffraction limit for light microscopy by using finely striped, patterned light to illuminate a sample at a number of rotations. The interaction of the stripes with high frequency sample information generates low frequency Moiré interference patterns from which sub-diffraction information can be computationally reconstructed to generate images with a resolution limit approaching 100 nm (Gustafsson, 2000). Figure 3.7B shows same cell from figure 3.7A imaged using SIM. It can clearly be seen that the SIM image is much sharper than the epifluorescence image and that a greater degree of detail and information can be gained from the SIM image. Figure 3.7E shows a magnified section of the SIM image which exhibits a greater ASY1 intensity relative to the rest of the cell. This image clearly shows that it is an SPS site, as opposed to an unresolved interlock, that is present at this area of greater ASY1 intensity with four ASY1 stained axial elements exchanging partners across a small region of asynapsis. Similar investigation of the other three sites with greater ASY1 intensity within this cell indicates that they are all SPS sites rather than unresolved interlocks, indicating that 50% of all the chromosomes in this cell have a SPS site somewhere along their length. Stretches of SC joined by SPS sites in this manner are henceforth referred to as synaptic multivalents. They differ from the multivalents observed at metaphase I as, depending on the position of COs relative to the SPS site, synaptic multivalents will not necessarily go on to form metaphase I multivalents.

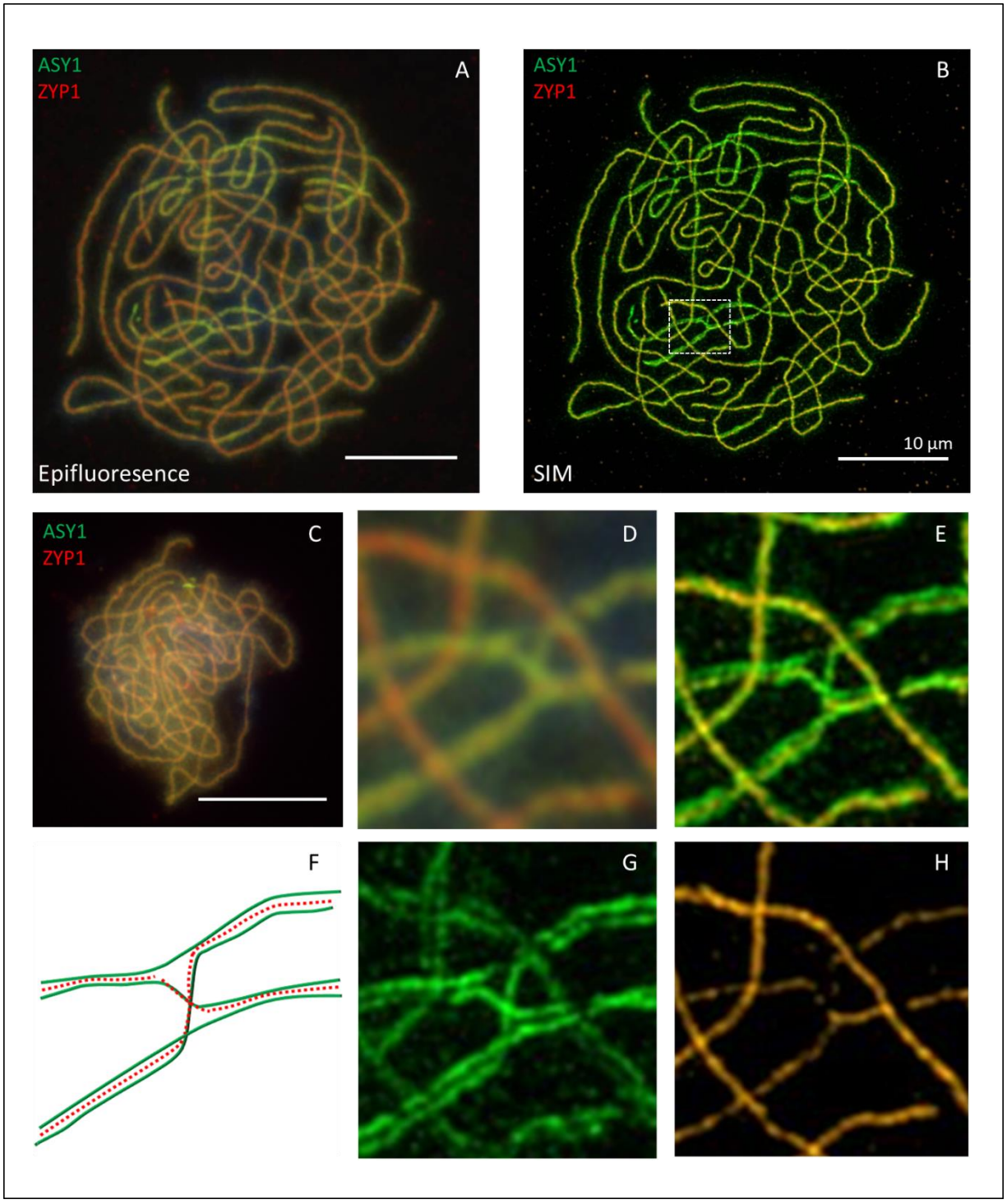

Figure 3.7. A pachytene cell from tetraploid TBG A. arenosa stained with ZYP1 (red), ASY1 (green) and DAPI (blue). The same cell was imaged using both epifluorescence (A), and structured illumination microscopy (SIM) (B). (C) Epifluorescence image showing a pachytene cell stained for ASY1 (green) and ZYP1 (red) from diploid SN29 A. arenosa. A magnified region (indicated by the white box in image B) is shown from both the epifluorescence (D) and SIM images (E). (F) A schematic representation of the SPS site showing the exchanging axial elements (green) and SC (red). Magnified SPS region showing individual colour channels for ASY1 (G) and ZYP1 (H). Scale bar = 10 µm.

3.2.4 The synaptonemal complex protein ZYP1 exhibits novel behaviour at synaptic partner switch sites

As SPS sites have only previously been analysed using EM of silver stained chromosomes, the dynamics of SC formation across these sites have only been inferred by analysing relative proximity of paired chromosomes (e.g. Rasmussen, 1987). To further elucidate the behaviour of the SC at both synapsed regions and across SPS sites, pachytene cells from TBG *A. arenosa* were stained with SMC3 and ZYP1 (figure 3.8) and imaged used SIM. SMC3 is a cohesin subunit that localises with equal intensity to both synapsed and unsynapsed regions of the meiotic axis.

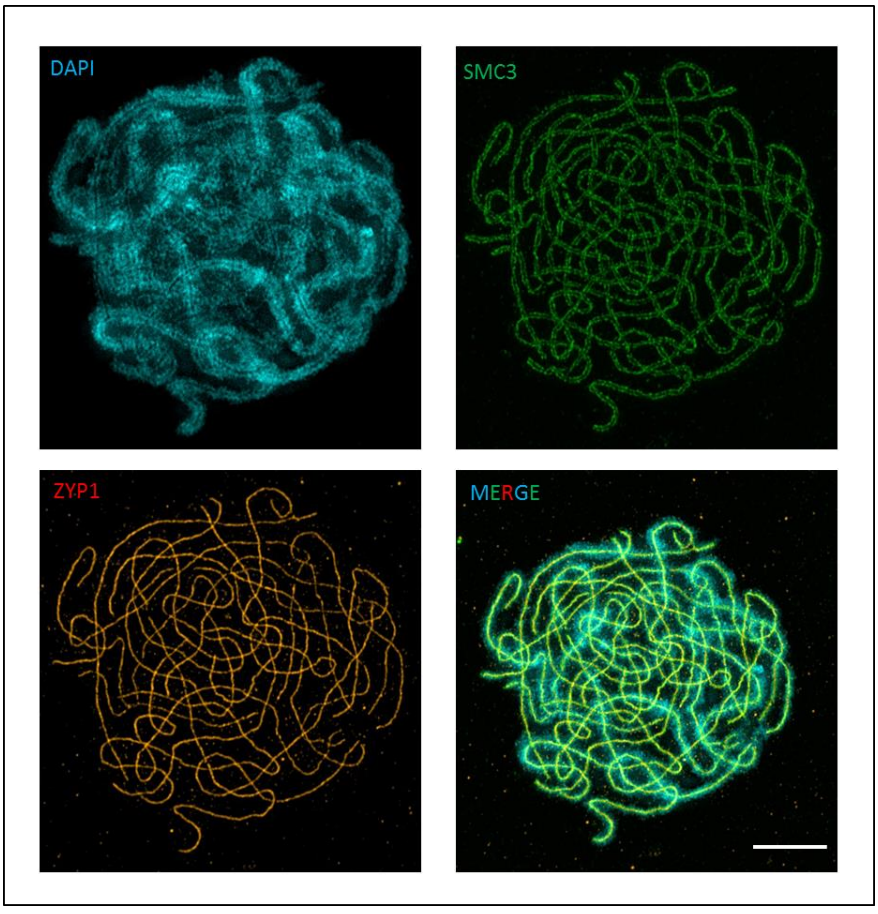

Figure 3.8. Pachytene cell from tetraploid TBG A. arenosa stained for DAPI (blue), SMC3 (green) and ZYP1 (orange) captured using SIM. Scale bar = 5 µm

Firstly, SC behaviour at normally synapsed regions was analysed in tetraploid TBG *A. arenosa*. To determine the distances across the SC, line plot intensity profiles running perpendicularly across the SC were examined for ZYP1, SMC3 and DAPI (figure 3.9). The ZYP1 antibody used for this study was raised against the N terminus of the protein, which has previously been shown to orient towards the centre of the SC (Schucker *et al.*, 2015). Therefore, a single linear signal was detected for ZYP1 at synapsed regions. The linear ZYP1 signal was also sandwiched between two parallel SMC3 signals at synapsed regions. SMC3 localises to the lateral elements of the SC. An orthogonal view also reveals that the *A. arenosa* SC exhibits a classical tripartite structure, with a single focus being found between two SMC3 foci (figure 3.9F). The distance between the intensity peaks of parallel SMC3 signals was consistently between 200-250 nm, which is in close agreement with SC widths from other organisms including barley and mice (Phillips *et al.*, 2012, Schucker *et al.*, 2015). DAPI signal from homologous chromosomes was present as two diffuse but discernibly linear structures that were separated by a similar ~250nm gap, indicating that chromatin is excluded from the transverse filaments and central element of the SC but may be intimately associated with the lateral elements.

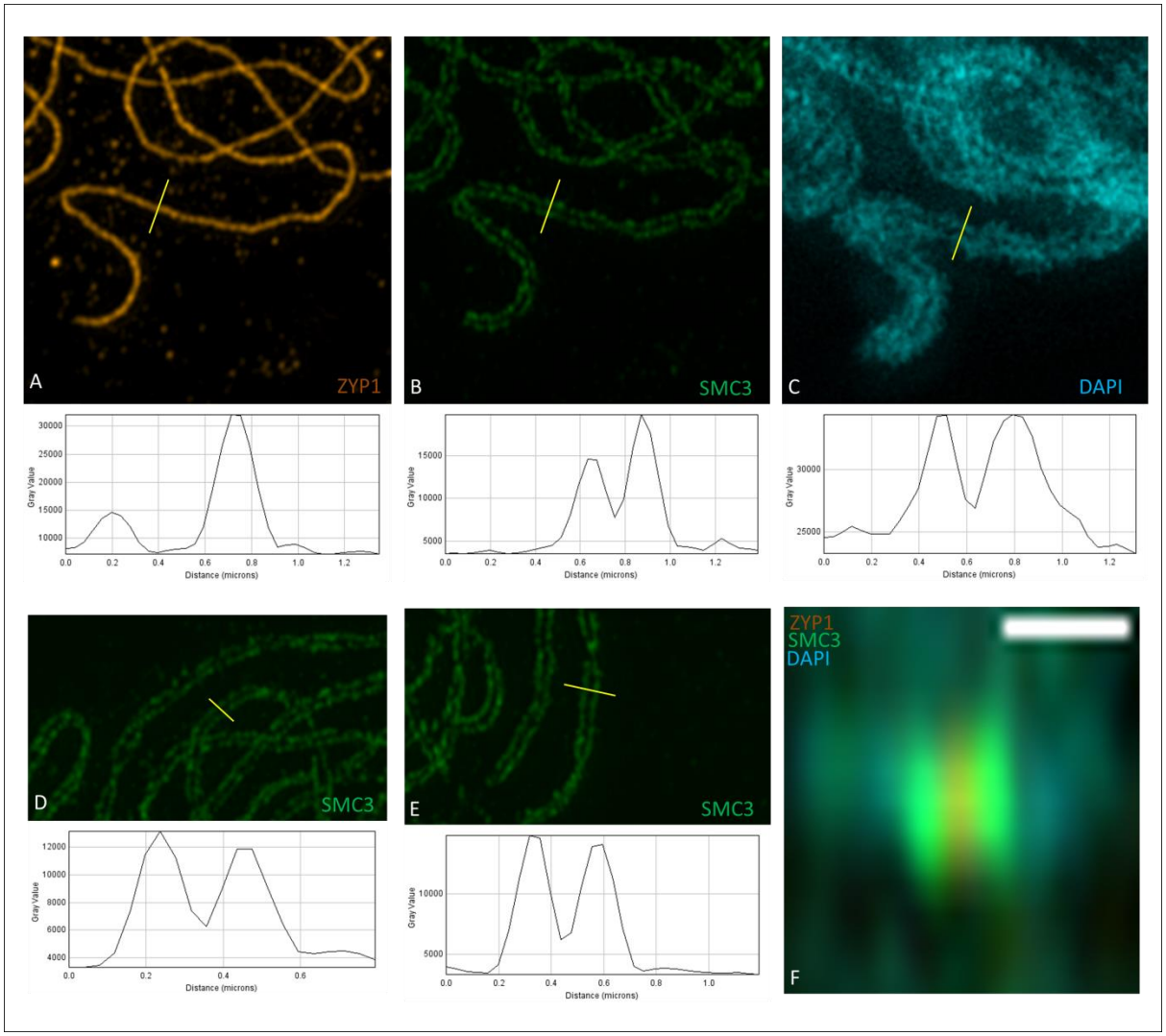

Figure 3.9. Super-resolution analysis of SC structure in tetraploid A. arenosa. A synapsed region of the SC is stained for ZYP1 (A), SMC3 (B) and DAPI (C). Linear cross-sections (yellow lines) and their accompanying intensity plot profiles are shown to demonstrate the distance between intensity peaks of proteins or chromatin across the SC. Two more sections of SC stained with SMC3 and accompanying intensity profiles are also shown (D, E). (F) An orthogonal view of the synaptonemal complex, scale bar = 500 nm.

Closer inspection of SPS sites in these cells demonstrated that the synaptonemal complex protein ZYP1 appears to undergo novel behaviour at these sites (figure 3.10). ZYP1 is only usually detected as a linear signal when it is 'sandwiched' between two lateral elements which are generally considered to be essential for construction of a functional synaptonemal complex (Page and Hawley, 2004, Higgins *et al.*, 2005). We would therefore expect to detect

no linear ZYP1 signal running across the SPS sites, where small regions of asynapsis are present as indicated by the increased intensity of ASY1 staining and the disruption in pairwise alignment of axial elements. However, linear ZYP1 signal is detected across the SPS sites. It also appears that the ZYP1 linear signals remain closely associated with only one lateral element at the asynaptic regions whilst the second lateral element has no ZYP1 associated with it.

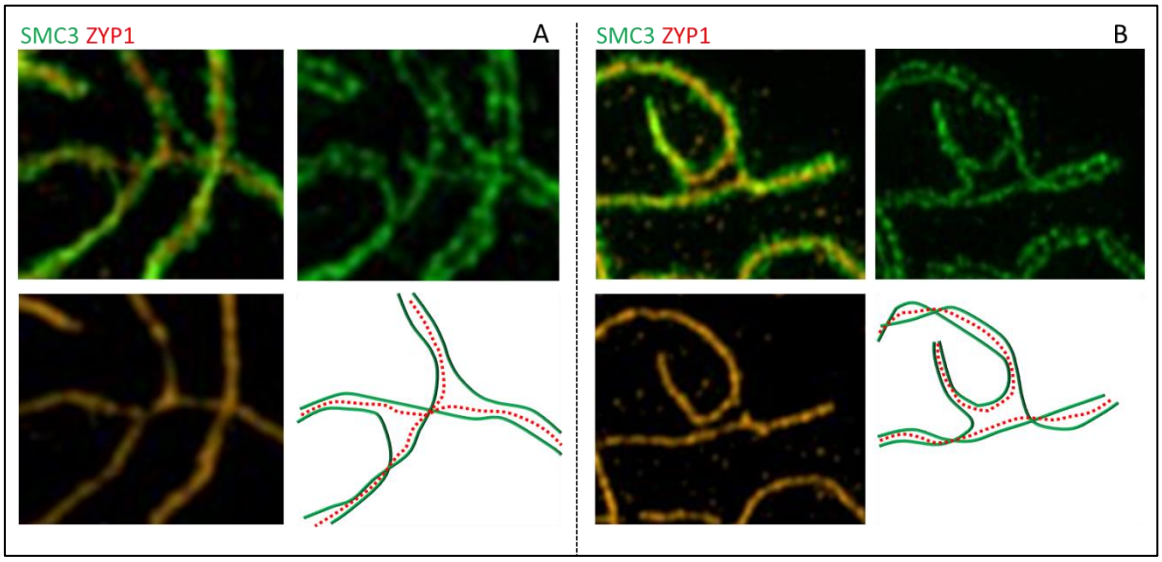

Figure 3.10. SPS sites in tetraploid TBG A. arenosa stained for SMC3 (green) and ZYP1 (orange). A cartoon representation of each structure is also shown. ZYP1 exhibits novel behaviour across SPS sites by only associating with a single lateral element.

It is unclear whether the ZYP1 traversing the SPS site is present as a dimeric structure consisting of two filaments positioned with their N-termini 'head-to-head', as we would expect to find at an ordinarily synapsed region, or whether the ZYP1 is present as only a single filament. In order to test this, SPS sites were imaged again using the same primary antibodies but with different secondary antibodies. By using secondary antibodies that emit fluorescent light at a shorter wavelength, this allows increased resolution to be obtained. Therefore, alexa-fluor 350 secondary antibody was used to detect ZYP1 rather than alexa-

fluor 594 in an effort to provide increased resolution.

Figure 3.11B shows that, at synapsed regions, ZYP1 is detected as two very closely associated linear signals when the alexa-fluor 350 secondary antibody is used, as opposed to the single linear signal observed with an alexa-fluor 594 secondary antibody. Bimodal intensity plot profiles running perpendicularly across the SC also demonstrate that two distinct ZYP1 peaks can be detected and are separated by a distance of 100 – 120 nm. This indicates that, although the N-termini of the ZYP1 proteins are closely associated, there is still a small degree of separation between them. This contrasts with previous super-resolution analysis of SC structure performed using dSTORM microscopy in mice, which demonstrated that the N-termini of the mouse ZYP1 homologue SYCP1 overlap in the centre of the SC (Schucker *et al.*, 2015). This difference may, however, be due to the size of the recombinant protein fragment used to raise the primary antibody. Here, the N-terminal ZYP1 antibody is a polyclonal antibody raised against amino-acids 1-415 of ZYP1a, which accounts for the first 48% of the entire protein length whereas the antibody used by Schucker *et al.,* was raised against a smaller region of the protein (amino acids 1-125) and therefore may be more specific to the true N-terminus of the protein.

An intensity plot profile was also measured for ZYP1 signal running across an SPS site. Again, a bimodal plot with a separation of ~120 nm between intensity peaks was observed, suggesting that the ZYP1 signal that polymerises across asynaptic SPS regions is still composed of two parallel filaments, as we would expect to find in a normally synapsed region, but without the presence of a second lateral element. One explanation for this novel ZYP1 behaviour is that SPS sites are dynamic structures which can move through previously synapsed regions, stripping the SC from one lateral element and leaving it attached to the

other. The SC would then reform on the other side of the SPS site between two different homologues. However, if indeed SPS sites are dynamic structures which can be resolved by being pushed off the chromosome ends, this does not explain why some persist until pachytene.

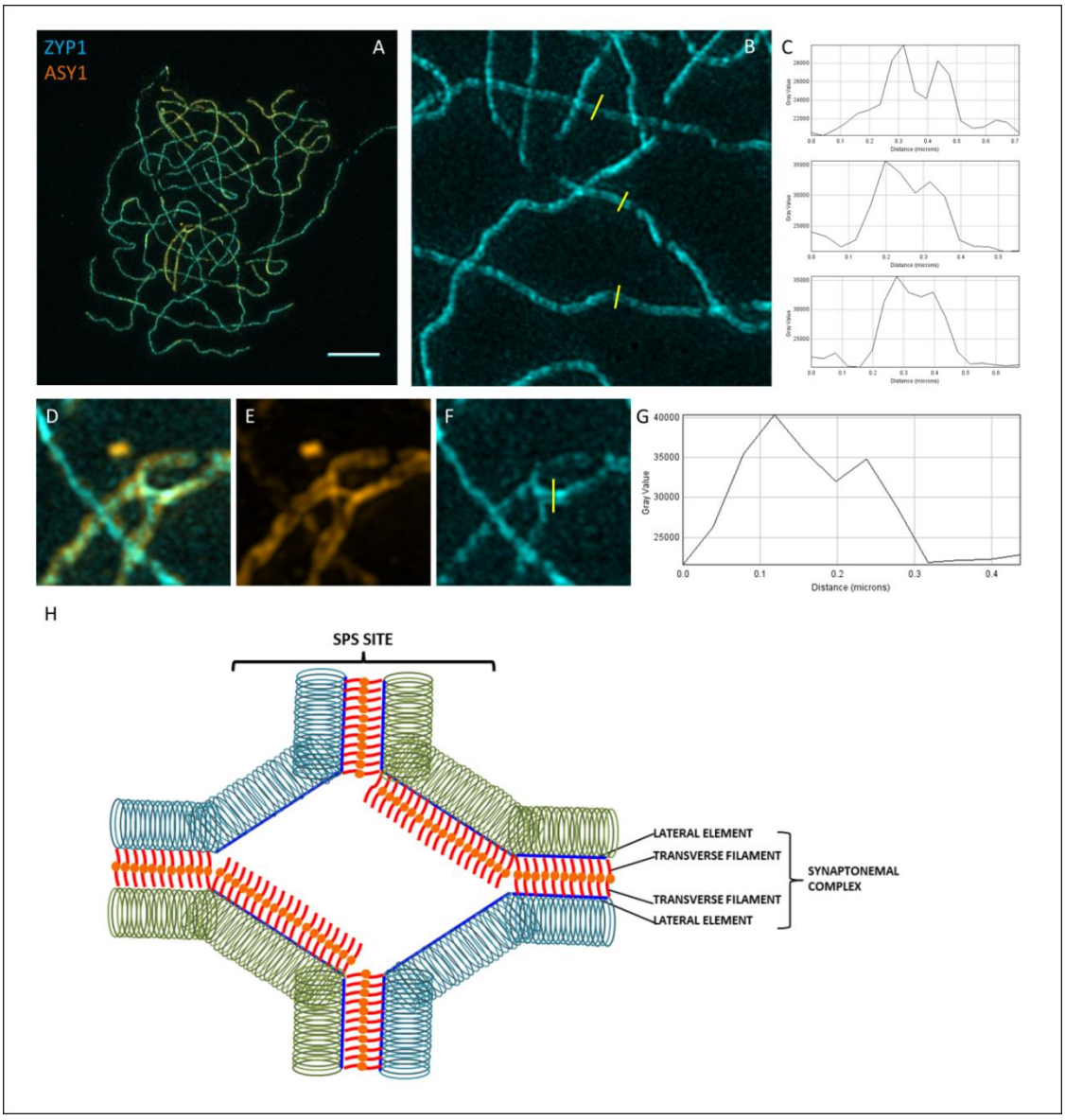

Figure 3.11. ZYP1 behaviour at asynaptic SPS sites. (A) A pachytene cell from tetraploid TBG A. arenosa stained for ZYP1 with alexa-fluor 350 (blue) and ASY1 (red). (B) Magnified region showing synapsed regions with closely associated parallel linear ZYP1 signals. Yellow lines show the regions selected for intensity plot profiles that are shown in (C). (D, E, F) Magnified region showing an SPS site. Yellow line shows the region selected for the intensity profile plot in (G). (H) Diagram showing the novel behaviour of the SC across SPS sites. Scale bar = 5 µm.

3.2.5 Examining the relationship between synaptic partner switch sites and CO location in tetraploid *A. arenosa*

Immunolocalisation of the dHj resolvase protein MLH1 has been widely used to identify sites of class I COs in a variety of model organisms (*e.g.* Lhuisser *et al.*, 2007). Again, as pairing in autotetraploid species has almost exclusively been analysed using EM, rather than by immunolocalisation, the positions of class I COs have yet to be cytologically examined in an autopolyploid context. As indicated in section 3.5.1, MLH1 forms discreet foci that co-localise with the SC in both diploid and tetraploid *A. arenosa.* Given the strong evidence for the existence of SPS sites in tetraploid *A. arenosa* presented thus far, we set out to determine what relationship, if any, SPS sites might have with regard to class I CO position.

To accomplish this, it was necessary to generate triple labelled pachytene spreads such that regions of synapsis, asynapsis and class I COs could all be observed on a single pachytene cell. Pachytene cells from tetraploid TBG *A. arenosa* were therefore simultaneously labelled with anti-ASY1, ZYP1 and MLH1 antibodies (figure 3.12). As previously shown, SPS sites can be distinguished by their regions of asynapsis associated with increased ASY1 intensity. SC length measurements of synaptic multivalents were also taken to confirm that SC stretches either side of the SPS sites were of a comparable length, as would be expected if exchanges were occurring between homologous chromosomes. In figure 3.12B, a synaptic multivalent is shown and two MLH1 foci are present, both on separate pairs of homologues on the same side of the SPS site. Providing no class II COs are present, which would not be detected using this method but are comparatively rare compared to class I COs, this CO/SPS conformation would result in the production of two stable bivalents at metaphase I.

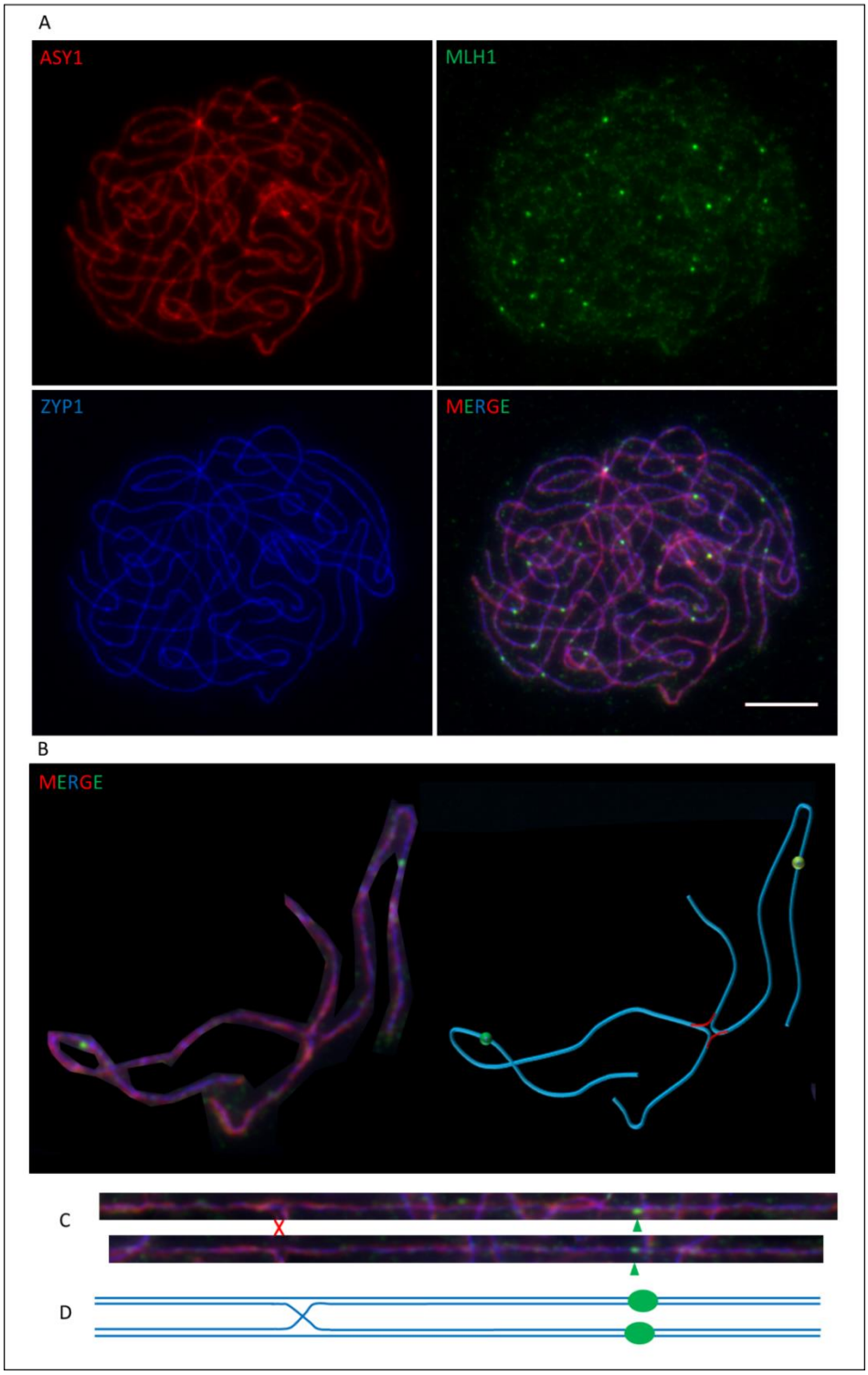

Figure 3.12. (A) Pachytene cell from tetraploid TBG A. arenosa triple labelled for ASY1 (red), MLH1 (green) and ZYP1 (blue). (B) A synaptic multivalent from the same cell showing two stretches of SC joined by a single SPS site. A cartoon representation is also shown for clarity. (C) A straightened version of the same SC stretches. The red cross signifies the position of the SPS site and the green arrowheads indicate the positions of the MLH1 Foci. (D) Cartoon representation showing how the four homologous chromosomes are pairing across the SPS site and the location of the MLH1 foci (green circles). Scale bar = 5 µm.

To further elucidate the relationship between SPS sites and COs, a further 89 synaptic multivalents were analysed using the same triple labelling method. The frequency of different SPS/CO conformations was then noted (figure 3.13). From the 89 synaptic multivalents analysed, 13 different CO/SPS conformations were observed. Each of these conformations differed based upon either the number of COs, the number of SPS sites or the position of COs relative to the SPS sites. The maximum number of COs and the maximum number of SPS sites found to occur along a single synaptic multivalent was four and two, respectively. Assuming no undetectable class II COs were present, the only synaptic multivalent conformations that were observed which would transition to metaphase I multivalents or univalents would be conformations A (bivalent + 2 univalents), C (trivalent + univalent), E (chain quadrivalent), G (ring quadrivalent), H (bivalent + 2 univalents), K (trivalent + univalent), L (chain quadrivalent) and M (ring quadrivalent). These conformations account for only 28% of synaptic multivalents suggesting that, in the majority of instances, synaptic multivalents are unlikely to transition into metaphase I multivalents. Conformation B, which is the same conformation described in figure 3.12, is by far the most frequently observed conformation and accounts for 60% of synaptic multivalents. This helps to demonstrate that SPS sites can persist until late pachytene even in situations where they are not ‘locked’ in place by two COs occurring either side of the SPS site. This also helps to show that synaptic multivalents *per se* are not sufficient to generate metaphase I multivalents.

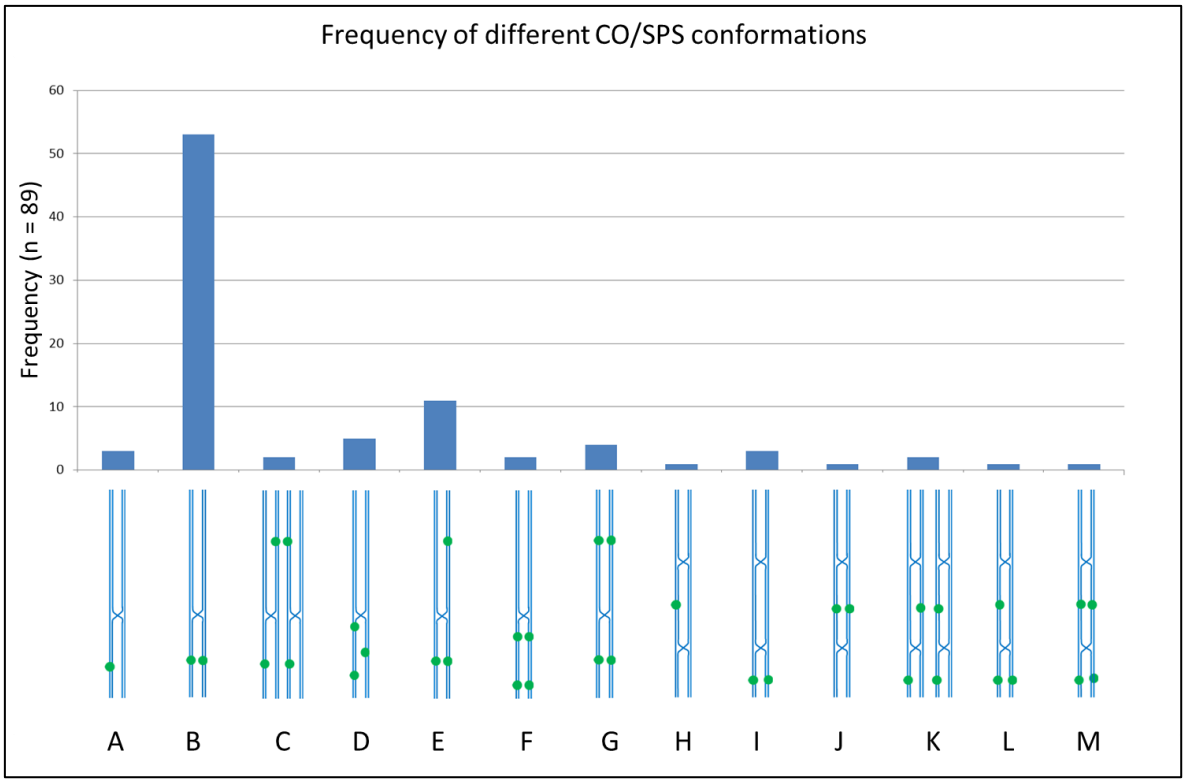

Figure 3.13. Histogram showing the frequency of different CO/SPS conformations as determined from ZYP1, ASY1, MLH1 immunolocalisation studies of pachytene cells of A. arenosa. Conformations differ based on the number of SPS sites occurring between homologues (blue lines) and the number and position of MLH1 foci (green circles).

This high prevalence of synaptic multivalents with conformation B goes some way to supporting the suggestion that CO interference can be transmitted across SPS sites, with the formation of a CO on one side of the SPS site inhibiting the formation of COs on the other side. This is of particular interest as CO interference has only previously been assessed cytologically in the context of diploid pairing, where the same homologues interact along their entire length and therefore the interference signal would be equally transmitted by both homologues. How interference would spread across a SPS site to affect CO formation on >2 homologues is explained in figure 3.14. If CO interference wasn't operating across SPS sites it may be more likely that we would see a greater number of synaptic multivalents with conformations such as C, E and G where COs are seen on both sides of the SPS site. This supports the model whereby CO interference is established prior to synapsis with the meiotic

axis being a potential conduit for transmission of the interference signal (reviewed in Zickler and Kleckner, 2016).

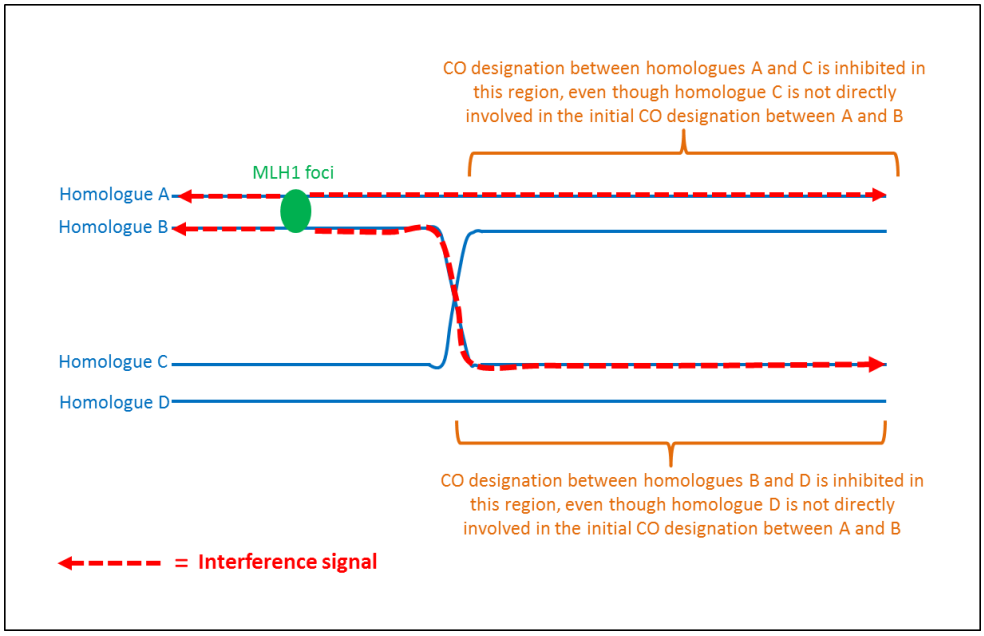

Figure 3.14. Diagram showing how CO interference can be transmitted across an SPS site through the action of single axial elements to affect the distribution of COs between multiple homologues. Interference spreads from the initial MLH1 focus position along the axes and across the SPS site to regions where both homologues are synapsed with a separate homologue, preventing CO designation at these regions.

As well as examining their general conformation, a number of precise distance measurements could be recorded for each synaptic multivalent (table S1). Examples of the type of measurement recorded are summarized in figure 3.15A. Also, as the triple stained pachytene spreads contained a mixture of paired bivalents and synaptic multivalents, similar MLH1 distance measurements could also be made for bivalent chromosomes that did not contain an SPS site (table S2). For instance, total SC length was measured for chromosomes with SPS sites and compared to total SC length of those without (figure 3.15B). A two-tailed independent T-test indicated that the mean SC length for chromosomes with an SPS site (mean = 25.5 µm, S.D = 4.88) was significantly greater than the mean SC length for

chromosomes without an SPS site (mean = 22.6 µm, S.D = 4.58), t(335) = 5.608, $p < 0.00001$. This is perhaps not surprising as it is likely that longer chromosomes will possess more synapsis initiation sites during zygotene which, if they occur between >2 homologues would result in synaptic exchange. Another explanation is that, if SPS sites are resolved during pachytene, it might take longer to achieve this with longer chromosomes and therefore SPS sites on these chromosomes are likely to persist later into pachytene.

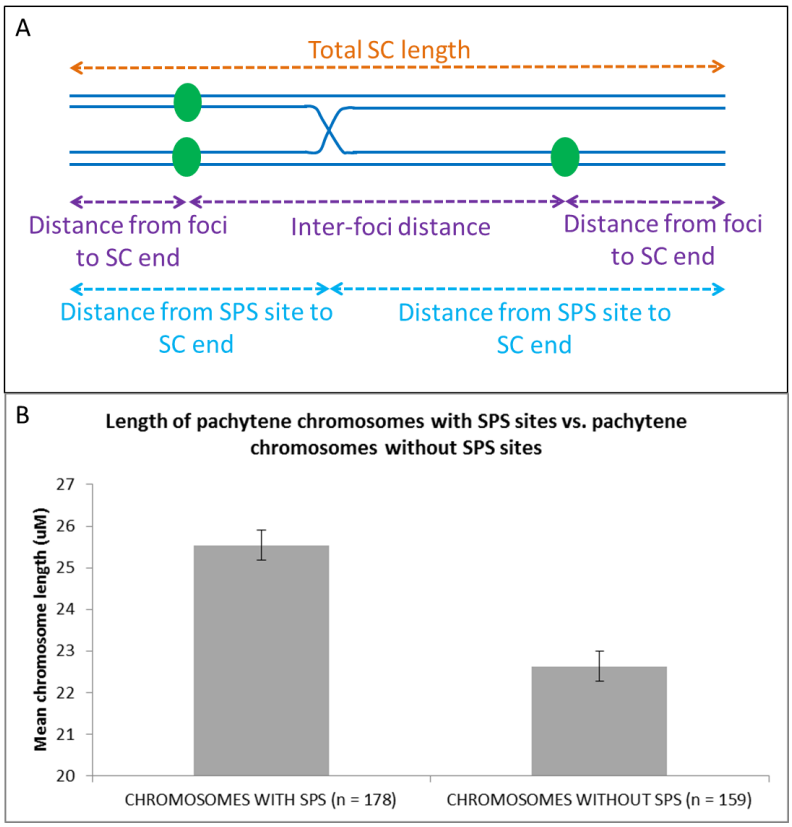

Figure 3.15. (A) Diagram showing examples of the distance measurements taken from triple labelled synaptic multivalent chromosomes. Dark blue lines represent homologous chromosomes and green circles MLH1 foci. (B) Bar chart showing the mean SC length (+/- standard error) of pachytene chromosomes with and without an SPS sites along their length.

Inter-foci distance measurements were also recorded for MLH1 foci on chromosomes with and without SPS sites (figure 3.16, table S3) and that possessed more than one MLH1 focus. An independent T-test indicated that the mean SC length for inter-foci distances across an SPS site (mean = 17.9 µm, S.D = 7.41) was not significantly greater than the mean SC length

for inter-foci distances not across an SPS site (mean = 14.4μm, S.D = 5.00), t(47) = 1.95, p = 0.0573. There does, however, appear to be a general trend that the MLH1-foci distances across SPS sites are slightly longer than those not across SPS sites, but this can be explained by the previous observation that total SC length of chromosomes with SPS sites are significantly longer and therefore there is greater potential in these cells to have a larger inter-MLH1-foci distance. In support of this, the distribution of measurements in figure 3.16A at the shorter distances appears similar for both categories.

Previous studies have used gamma distributions fitted to inter-foci distance measurements to determine the relative strength of interference (de Boer *et al.*, 2006, Libuda *et al.*, 2013), with higher values for the shape parameter, k, indicating higher strengths of interference and $k = 1$ indicating no interference. Therefore, gamma distributions were fitted to histograms of inter-MLH1 foci distances that had been normalised to a percentage of total SC length (figure 3.16B, table S4). This was done for inter-foci distances going across SPS sites and for inter-foci distances not going across SPS sites. For the gamma distribution of inter-foci distances across SPS sites k = 8.514 (S.E = 2.455) and for the gamma distribution of inter-foci distances not going across an SPS site k = 6.987 (S.E = 1.976). This indicates that CO interference still operates across SPS sites and also shows that, as the standard errors of the both distributions strongly overlap, there is unlikely to be a significant difference between the two interference strengths.

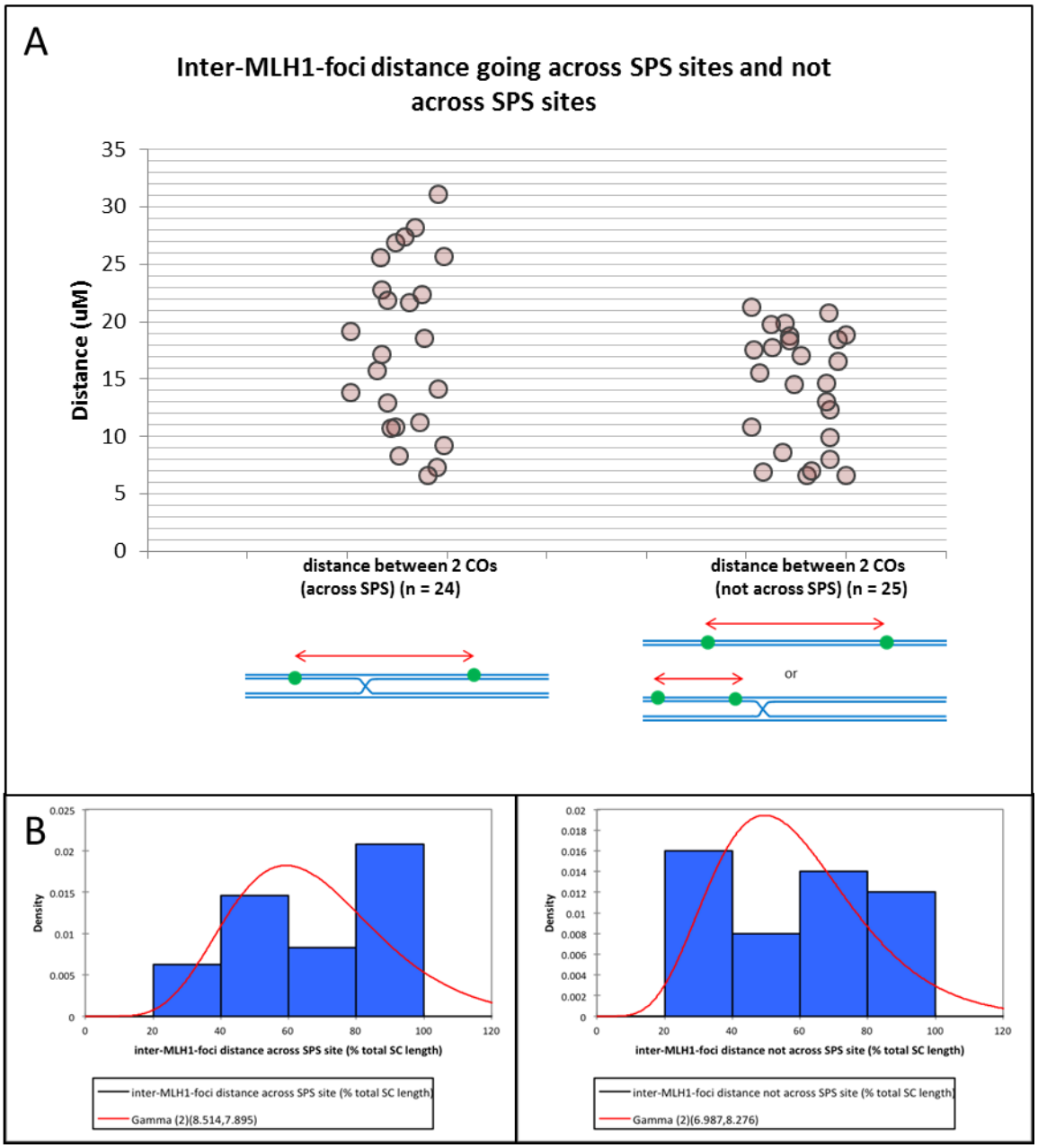

Figure 3.16.(A) Dot plot showing the inter-MLH1 foci SC distances either going across an SPS site or not going across an SPS site. (B) Histograms showing relative frequencies of inter-foci distances at 20% intervals as a percentage of total SC length. Gamma distributions have been fitted to both histograms.

As well as examining the distances between COs, it was also possible to determine if there were any differences in CO frequencies between chromosomes with a SPS site and chromosomes without a SPS site (figure 3.17). A Yates' corrected chi-squared test

demonstrated that there was a significant difference in the frequency of the number of COs between chromosomes with a SPS site and those without, χ^2 (1, N = 337) = 6.59, p = 0.037. Chromosomes with a SPS site appeared more likely to have 0 or 2 COs than chromosomes without a SPS, which were more likely to have a single CO. Previous studies have demonstrated that longer chromosomes in *A. thaliana* tend to experience a higher number of COs (Giraut *et al.*, 2011) so this could explain why the chromosomes with SPS sites have a greater frequency of double COs. It is less clear why these chromosomes may also experience a higher frequency of 0 COs, although this could be a consequence of crossover interference acting between all four homologues, such that if one homologue receives 2 COs another homologue that is connected by an SPS may be more likely to receive none.

A

	Chromosomes with SPS	Chromosomes without SPS
Number with 0 CO	6	1
Number with 1 CO	139	142
Number with 2 CO	33	16
total	178	159
Mean number of COs	1.152	1.094

B

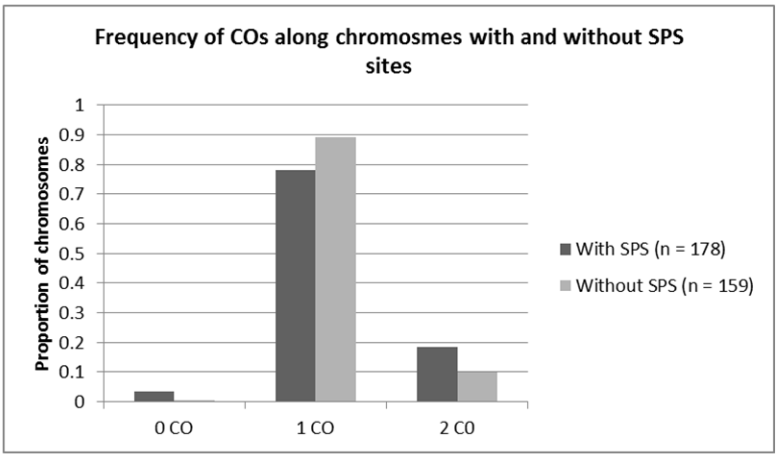

Figure 3.17. (A) Contingency table showing the frequencies of COs on chromosomes with or without an SPS site. (B) Histogram showing the relative frequencies of different CO numbers on chromosomes with or without an SPS site.

When visually inspecting the locations of MLH1 foci on synaptic multivalents with conformation B (figure 3.13), it was noticed that in a large number instances the two MLH1 foci appeared to be located at a similar position along both stretches of SC (*e.g.* in figure 3.12). In order to test this, the distance between the two MLH1 foci on separate paired SC stretches from synaptic multivalents with B conformations was measured and calculated as a proportion of total SC length from the chromosome end to the SPS site (figure 3.18, table S5). The relative frequency of these inter-foci distances were then plotted and compared to the expected relative frequency of inter-foci distances if foci were randomly paired (based on prior knowledge of CO positions from the chromosome end to SPS site region, figure 3.18C and table S6). It can be seen that the observed inter-foci distances are noticeably shifted to the left relative to the expected distances based on random pairing of foci. A one-tailed Kolmogorov-Smirnov test (F1(experimental) > F2(randomly paired)) was used to determine if the shift in continuous probability distribution between the two samples was significant (D= 0.155, p = 0.072) (table S7). The results show that we can reject the null hypothesis that the two samples follow the same distribution at a 10% significance level, indicating that MLH1 foci on neighbouring SC stretches attached by an SPS site are generally located at more similar positions than would be expected by chance, but not at the 5% level. The significance of this point will be covered in the discussion.

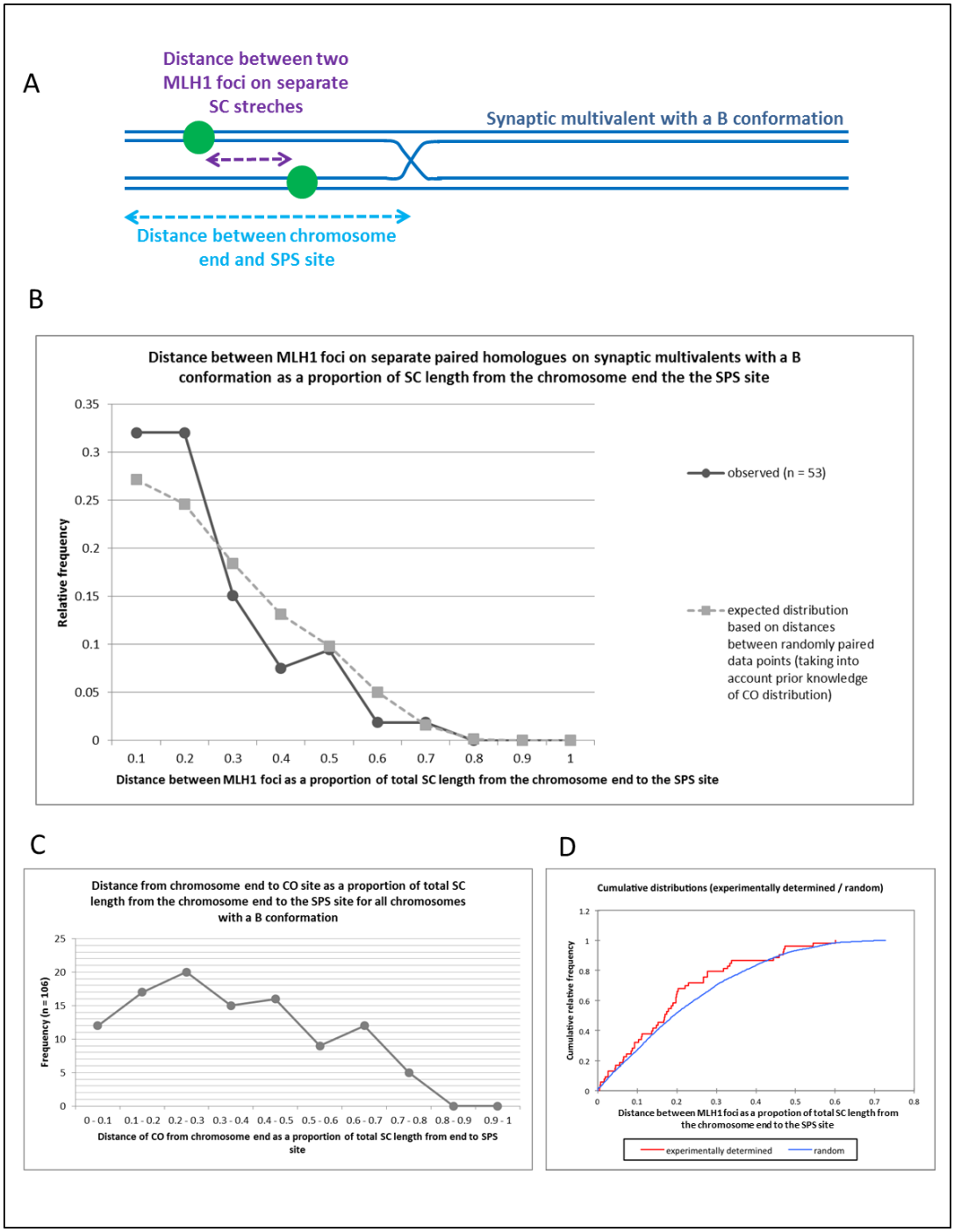

Figure 3.18. (A) Diagram showing the measurements taken to examine the relationship between the proximity of COs on synaptic multivalents with a B conformation. (B) Line plot showing the relative frequency of inter-MLH1 foci distances as a proportion of total SC length from the end of the chromosome to the SPS site. The expected relative frequency of inter-foci distances is also shown for a scenario where the two foci are completely randomly positioned along the chromosomes using distributions based on all known MLH1 positions in the region between the chromosome end and SPS sites (C). (C) Frequency distribution for CO position between the chromosome end and SPS site as a proportion of this total length. (D) Cumulative frequency distributions for the experimentally determined inter-MLH1 foci distances on B- conformation multivalents (red line) and for randomly paired MLH1 foci from all multivalents (blue line).

3.2.7 Dissecting pairing behaviour in aneuploid TBG *A. arenosa* using super-resolution microscopy

As mentioned in section 3.2.2, cytological analysis indicated that many plants present within the TBG *A. arenosa* population were, in fact, aneuploid. Again, pairing and synapsis during meiosis in aneuploids has been previously analysed using EM (Wallace and Hulten, 1983) and synapsis between an uneven number of chromosomes has also been cytologically investigated in a number of triploid species (*e.g.* Loidl and Jones 1986). We therefore set out to further dissect the behaviour of ZYP1 and ASY1 in an aneuploid context using super-resolution fluorescent microscopy.

Firstly, an aneuploid plant was identified via analysis of metaphase I DAPI spreads (figure 3.19A). Chromosome counts indicated that this plant was lacking a chromosome (n = 31) as many metaphase I cells contained 15 bivalents chromosomes and a single univalent. Pachytene spreads were then made using buds from this same aneuploid plant and immunostained for ASY1 and ZYP1 and viewed using SIM. In some cells it was apparent that an entire aneuploid chromosome remained completely asynapsed throughout pachytene (figure 3.19B) as indicated by the presence of a long-single axial element with a strong, linear ASY1 signal that did not appear to form SC with any of the other synapsed chromosomes. In other instances, large regions of asynapsis associated with a single chromosome were present at the pachytene stage but small regions of this chromosome also appeared to synapse with other axial elements at different regions within the cell. Synapsis still appeared to only occur in a pairwise manner, with no triple synapsed SC stretches observed. It is also not clear whether these regions of synapsis were between homologous or non-homologous chromosomes.

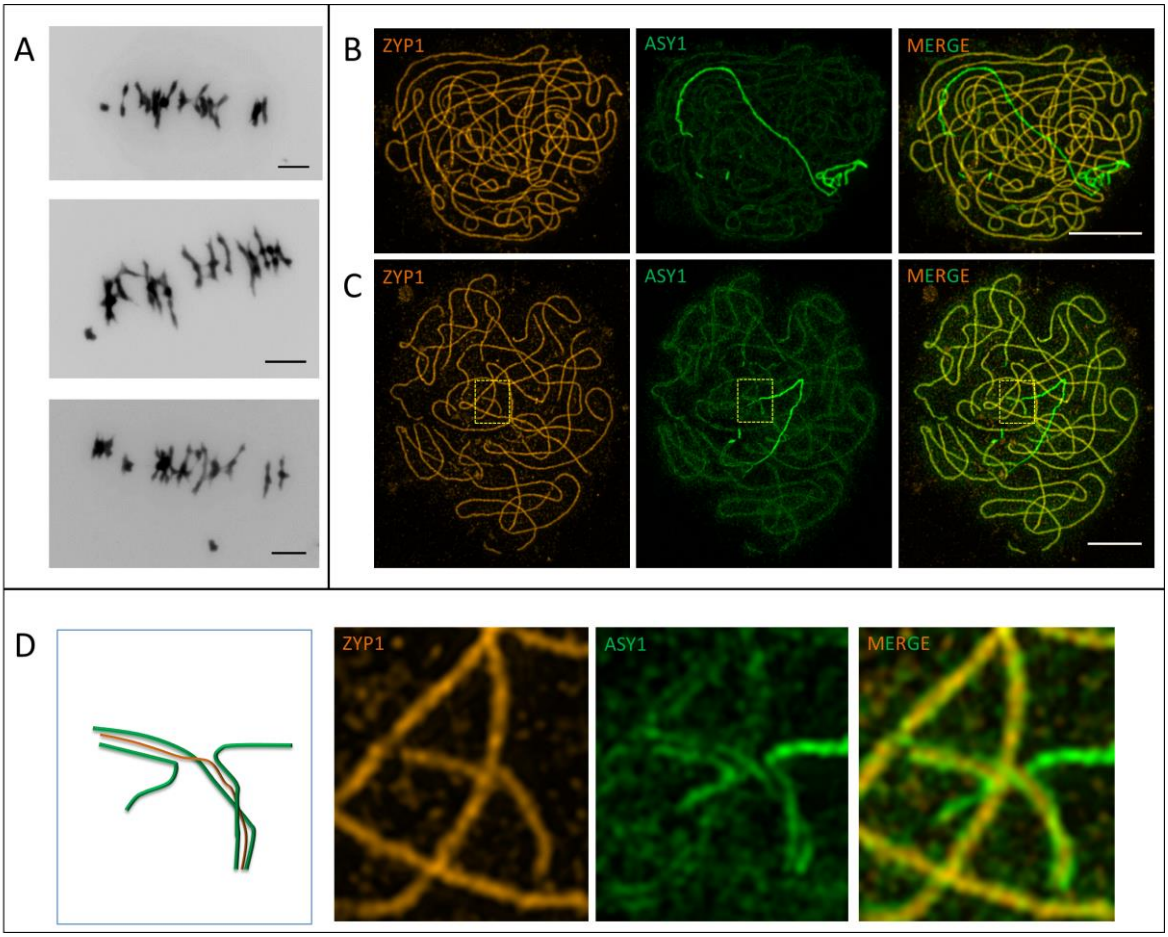

Figure 3.19. (A) DAPI stained metaphase I cells from an aneuploid TBG A. arenosa plant (n = 31). (B, C) Pachytene cells from aneuploid A. arenosa stained for ZYP1 (orange) and ASY1 (green). (D) A magnified section from 32C (yellow box) showing a region of synaptic exchange between an aneuploid chromosome and a separate region of synapsis. A cartoon representation is also shown for clarity. Scale bars = 5 µm.

3.3 Discussion

Here, we have presented the first detailed immunocytological analysis of pairing and CO formation in diploid and tetraploid *A. arenosa*. In doing so, we have shed light on many novel aspects of meiotic behaviour that occur within an autopolyploid context, some of which will now be discussed in more detail.

3.3.1 Fluorescence immunolocalisation microscopy is an effective technique for dissecting meiotic behaviour in *A. arenosa*

We have conclusively demonstrated that fluorescence immunolocalisation microscopy can be successfully applied to study many aspects of meiotic behaviour in *A. arenosa.* This includes the quantification of meiotic DSB levels and early recombination intermediates using RAD51, homologous pairing and synapsis using ASY1 and ZYP1 and class I CO formation using MLH1 antibodies. In the process, we have unearthed a number of intriguing similarities and differences in the meiotic behaviours of the diploid and tetraploid accessions of this recently established model organism.

Previous studies using chiasma counts from acid-fixed DAPI spreads have demonstrated that a significantly lower number of chiasma per bivalent are observed in the tetraploid TBG accession of *A. arenosa* compared to the diploid SN accession (Yant *et al.*, 2013). This reduction in chiasma frequency is hypothesised to stabilise tetraploid meiosis by reducing metaphase I multivalent frequency and it is also suggested that this reduction could be imposed by a relative increase in CO interference (Bomblies *et al.*, 2016). An alternative explanation is that a drop in meiotic DSB frequency earlier in prophase would lead to a reduction in precursor interactions which would, in turn, lead to a global reduction in CO

numbers. It is likely that this drop would have to be reasonably significant as CO homeostasis would counteract any minor changes in DSB numbers to maintain a constant number of COs. To test this alternative hypothesis, RAD51 foci counts were performed in both the diploid SN accession and tetraploid TBG accession. These counts indicated that there was no significant difference in meiotic DSB frequency per Mbp in the tetraploid relative to the diploid, indicating that this secondary explanation is unlikely to be valid and lending support to the interference based model of autotetraploid meiotic stabilisation.

3.3.2 Tetraploid TBG *A. arenosa* still encounters some meiotic challenges during prophase I

Tetraploid populations of *A. arenosa* arose 11,000 – 30,000 generations ago (Arnold *et al.*, 2015) and, since then, these polyploid accessions have evolved to exhibit a much higher degree of meiotic stability relative to neotetraploid plants by supressing multivalent formation and encouraging diploid-like bivalent pairing (Yant *et al.*, 2013). However, here we demonstrate that the journey to meiotic stabilisation in this species is far from complete, and that meiotic problems are still regularly encountered in the established tetraploid TBG population, albeit at a much lower frequency than in neotetraploid populations. For instance, we have shown that ring quadrivalents are still present in 11% of metaphase I cells and that many supposedly tetraploid TBG plants are in fact aneuploid, most likely as a consequence of the production of unbalanced gametes caused by missegregation at anaphase I.

For multivalent chromosomes to form at metaphase I, synaptic multivalents joined by SPS sites must also form during prophase I so that COs can occur between >2 homologues. Here, SPS sites have been visualised for the first time using super-resolution fluorescence immunolocalisation microscopy. At pachytene, small regions of asynapsis are associated with

the points of synaptic partner exchange, and ASY1 intensity is increased at these asynaptic regions relative to other synapsed chromosomal regions. As SPS sites are asynaptic, it would be reasonable to assume that no ZYP1 signal would be associated with these sites as the SC is only usually found in association with two synapsed lateral elements. On the contrary, linear ZYP1 signals appear to traverse some SPS sites in association with single lateral elements. Further super-resolution analysis utilising secondary antibodies that fluoresce at a shorter-wavelength, thus giving increased resolution, indicates that the ZYP1 signal associated with a single lateral elements appears to consist of two parallel transverse filaments, as we would expect to find at normally synapsed regions. Assuming that SC can only form between synapsed lateral elements, it is tempting to think that this unprecedented behaviour of the SC may support a model whereby SPS sites are resolved by 'peeling' previously formed SC from one pair of synapsed homologues and utilising the same SC to synapse one of the original homologues with a new homologous partner. By this method, SPS sites could be 'pushed off' the ends of synaptic multivalents to generate two wholly synapsed bivalents (figure 3.20A).

The persistence of many SPS sites into late pachytene does suggest, however, that not all SPS sites are resolved. Similar observations have been made previously in other autotetraploid species, such as the silk worm *Bombyx mori.* In *B. mori* the number of SPS sites per cell reduces going from zygotene through to pachytene, indicating that some form of resolution mechanism exists, but many SPS sites still remain at late pachytene (Rasmussen 1987). Rasmussen suggested it is likely that the formation of COs either side of these SPS sites prevents them from being resolved (figure 3.20B).

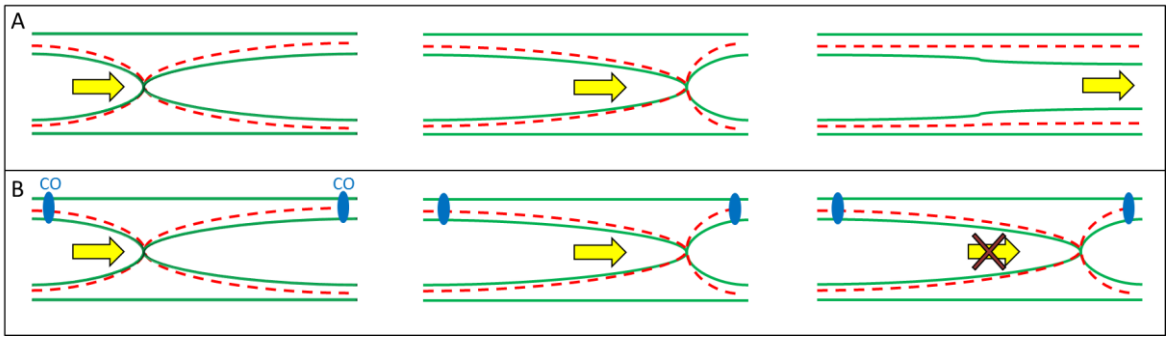

Figure 3.20. (A) Diagram showing a model for SPS site resolution whereby SC (red) is stripped from one lateral element (green) and replaced by the SC from a different lateral element as the SPS site migrates towards the end of the chromosome. Resolution is complete once the SPS site is pushed off the end of the chromosome to give two separately synapsed bivalents. (B) Rasmussen (1987) suggested that SPS sites might persist into late pachytene because the formation of COs either side of the SPS site would hold synapsed homologues in place, preventing SPS resolution.

We also used super-resolution microscopy to investigate how synapsis progresses in an aneuploid context. We observed that, in some instances a single fully asynaptic chromosome associated with strong linear ASY1 signal is present whilst in others partial synapsis of the aneuploid chromosome is observed. This is consistent with aneuploid pairing behaviour in other species, such as in trisomy 21 human oocytes (Robles *et al.*, 2007), however other species also often exhibit trivalent like SC pairing which was not observed in this instance (Rasmussen *et al.*, 1981).

3.3.3 Synaptic partner switch site persistence into pachytene can occur independently of class I CO formation

Using triple labelled immunofluorescence microscopy to simultaneously investigate the positions of SPS sites (ZYP1 and ASY1) and class I COs (MLH1) on pachytene chromosomes we have demonstrated that, in tetraploid *A. arenosa*, SPS sites can persist into late pachytene even in situations where their resolution is not inhibited by class I CO sites (as in figure 3.20B). We show that the most common form of synaptic multivalent (conformation B, figure 3.13) possesses two class I COs on the same side of the SPS site. These COs occur

between two completely separate pairs of homologues and would go on to generate two rod bivalents at metaphase I. It is possible that an undetectable class II CO event could be occurring on the other side of the SPS site, but this seems unlikely as this class of COs is comparatively rare (~1 per nucleus in *A. thaliana,* Higgins *et al.,* 2008) and would not be high enough to account for the 3-5 synaptic multivalents that can often be found in a single pachytene cell. The number of synaptic multivalents observed is also much higher than the number of metaphase I multivalents observed, indicating that most synaptic multivalents do not go on to form metaphase multivalents.

We have also shown that pachytene chromosomes that have an SPS site along them are on average significantly longer than those that don't. One explanation for the persistence of SPS sites into pachytene could therefore be that SPS site resolution takes more time for longer chromosomes. This would make sense if SPS sites must migrate towards the ends of the chromosomes to be resolved (figure 3.20). Therefore SPS sites on longer chromosomes may not have enough time to fully resolve by the time late pachytene is reached, whereas SPS sites on smaller chromosomes will.

3.3.4 Incorporating synaptic multivalents into a model for CO interference

Many models have been put forward in an effort to explain how CO interference is transmitted across meiotic chromosomes (reviewed in Zickler and Kleckner, 2015). However, all data gathered thus far to support these models has been performed exclusively within a diploid context. Here, we have collected immunocytological data that indicates the positions of class I, interference sensitive COs in a novel scenario when four homologous chromosomes are interacting with one another in a synaptic multivalent.

We firstly examined how frequently COs were found to occur either side of an SPS site and found that this was a relatively uncommon event with each homologue still only experiencing a single CO on one side of the SPS in the majority of cases. This suggests that CO interference is still operating across SPS sites such that, when one CO forms on one side it still inhibits the formation of another CO on the other side We also showed that there was no significant difference between inter-CO SC lengths running across SPS sites and for inter-CO SC lengths not running across SPS sites. Gamma distribution interference analysis of inter-foci distances also indicated that CO interference was operating across SPS sites and that the strength of interference across these sites was comparable with the strength of interference across normally synapsed regions. This indicates that the same strength of interference can be transmitted by a single axial element crossing an SPS site to pair with a separate homologue as is transmitted by both axial elements when COs occur between the same two homologues.

We have also shown that there is a general trend for MLH1 foci on separate pairs of SC stretches on the same side of an SPS site to be closer together than expected by random chance. A one-tailed Kolmogrov-Smirnov test only indicates that this trend was significant at the 10% level and therefore it will be worth collecting more data in the future to support this. This observation is particularly intriguing because it indicates that there may be some crosstalk between all four homologues involved in a synaptic multivalent that dictates the position of COs. We propose two models that could explain this phenomenon, a synaptic synchronisation model and an interference based model.

The first model is based on previously published observation that, in tetraploid *A. arenosa*, coalignment of all four homologues and pairwise synapsis can be observed in prophase I (Bomblies *et al.*, 2016). As homologous regions appear more likely to undergo synapsis at the

same time, this could promote COs to form in regions that synapse earlier which would be at similar positions across all four homologues (figure 3.21).

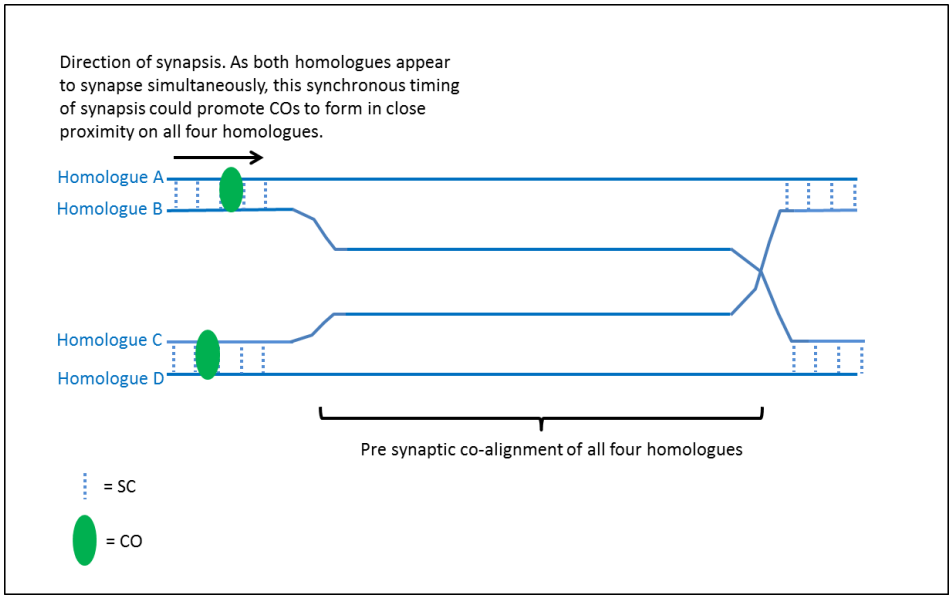

Figure 3.21. A synaptic synchronisation model to explain why COs on separate pairs of homologues are likely to occur in close proximity in a synaptic multivalent. As synapsis progresses simultaneously across all four homologues, COs may be more likely to form in regions that undergo synapsis earlier which will be at similar positions on all four homologues.

The second model involves CO interference 'backtracking' across homologues joined by an SPS site. We have already shown that interference can operate across an SPS site unidirectionally, such that a CO designation occurring between two homologues can affect the probability of CO designation occurring at regions downstream of an SPS site where those two homologues are synapsed and interacting with two separate homologues. An interesting question that also arises from this scenario, and again is inapplicable within a diploid context, is what affect this interference has on other regions upstream of the SPS site where CO designation has yet to occur? We suggest that this interference signal may somehow backtrack along the region upstream of the SPS site not directly involved in the initial CO designation to exert an effect on the position of the a second CO designation, such that it is more likely to occur at a similar position to the first (figure 3.22).

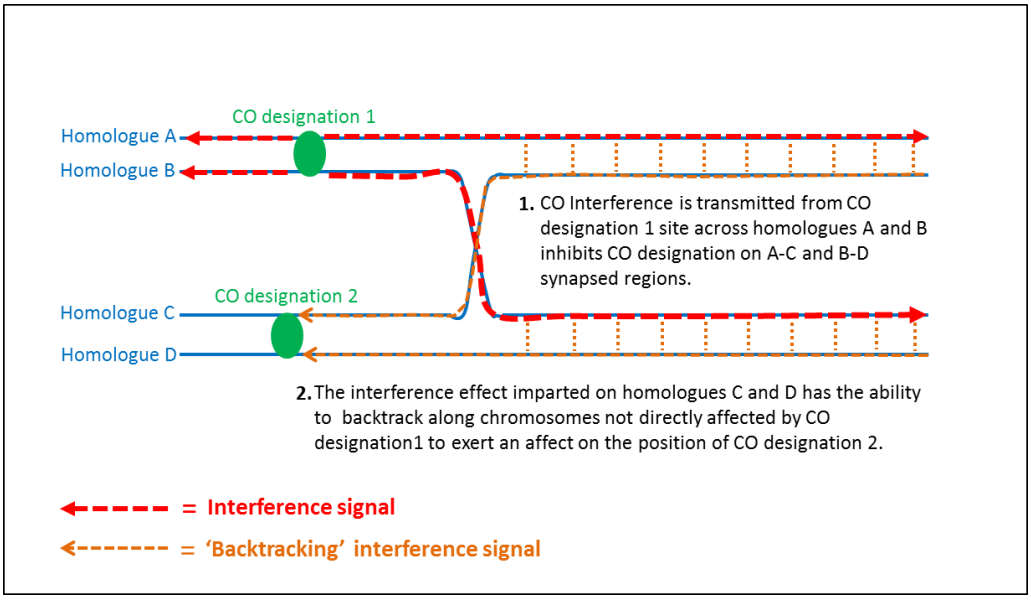

Figure 3.22. An interference based model to explain why COs on separate pairs of homologues are likely to occur in close proximity in a synaptic multivalent. Following CO designation between two homologues, interference spreads out across the SPS site to inhibit CO formation across all four homologues downstream of the SPS site. The interference signal being imposed on chromosomes C and D may then backtrack along the chromosomes to exert an effect on the position of the second CO designation, making it more likely to occur at a position similar to the first.

3.3.5 Summary

In summary, here we have used super-resolution microscopy to dissect how the early stages of meiosis progress and function in the model tetraploid species *A. arenosa*. Our observations have unearthed novel behaviours of the SC at SPS sites and posed new and interesting theories about how CO formation and interference may operate in an autotetraploid context. It is hoped that similar, future investigations in *A. arenosa* will be able to shed more light on many of the enigmatic, fundamental features of meiosis that are conserved across both polyploid and diploid species.

CHAPTER 4

EXPRESSING A DIPLOID ALLELE OF *ASY1* CAUSES A SHIFT IN CROSSOVER LOCALISATION IN AUTOTETRAPLOID *ARABIDOPSIS ARENOSA*

4. Expressing a diploid allele of *ASY1* causes a shift in crossover localisation in autotetraploid *Arabidopsis arenosa*

4.1 Introduction

The existence of extant diploid (2*n* = 2x = 16) and tetraploid (2*n* = 4x = 32) populations of *A. arenosa* has provided a valuable tool for researchers examining the evolutionary basis that lies behind autopolyloid meiotic stabilisation. In one of the first studies examining genetic adaptation associated with polyploidisation in *A. arenosa,* the genomes of 12 tetraploid individuals were sequenced and subsequently analysed for the presence of selective sweeps (Hollister *et al.,* 2012). Selective sweeps are found where standing sequence variation drops in regions linked to a recently fixed beneficial mutation (Nielsen *et al.,* 2005). Using this technique, Hollister and collaborators (2012) identified 192 genes in tetraploid *A. arenosa* that possessed strong signatures of selection and, amongst these, eight genes were identified as homologues of genes known to be required during meiosis. Included within these eight were the cohesin subunit *SMC3* (Lam *et al.,* 2005) and the *Hop1* homologue *ASY1* (Caryl *et al.,* 2000). A high-frequency derived single nucleotide polymorphism (SNP) was also identified in the conserved HORMA domain of the tetraploid *ASY1* allele. This tetraploid SNP causes an amino acid change to a positively charged glutamic acid residue from a negatively charged lysine. This particular amino acid change is unrepresented in any other sequenced vascular plant species but is present at a frequency of 90% and 4% in the tetraploid and diploid populations of *A. arenosa*, respectively (Hollister *et al.,* 2012).

In a second study, Yant and collaborators (2013) sequenced the whole-genomes of 8 diploid and 16 tetraploid *A. arenosa* individuals and used a genome scanning approach to compare the two ploidies. 44 genes were identified as being heavily differentiated between the diploid

and tetraploid and amongst these were 8 meiosis related genes. Again, these included *ASY1* and *SMC3* but also *ASY3, ZYP1a, ZYP1b, SYN1, PDS5* and *PRD3*. Apart from *PDS5*, which was recently shown to be dispensable for meiotic progression (Pradillo *et al,* 2015), all of these genes have been shown to have essential roles in meiotic prophase I in *A. thaliana* (Caryl *et al.,* 2000, Lam *et al.,* 2005, Ferdous *et al.,* 2012, Higgins *et al.,* 2005, Cai *et al.,* 2003, De Muyt *et al.,* 2009). The recurrence of *ASY1* between both of these studies suggests that the derived tetraploid allele of this gene may play an important role in helping to stabilise autopolyploid meiosis.

As previously mentioned in section 1.3.2, ASY1 is a homologue of the yeast Hop1 protein and is thought to play a role in ensuring IHR by stabilising the loading of AtDMC1 at DSB sites (Sanchez-Moran *et al.,* 2007). AtASY1 itself is a 596 amino-acid protein that contains a conserved HORMA domain (amino acids 15-228) as well as a chromatin binding SWIRM domain (amino acids 351-449) (Aravind and Iyre 2002). The HORMA domain is named after the three yeast proteins in which it was first identified: Hop1, Rev7 and Mad2. The domain itself consists of a 'core' region made up of three α-helices tightly packed with at least three β-sheets and a C-terminal 'safety belt' region that can exist in both an open and closed conformation (Rosenberg and Corbett, 2015). Structural studies in *C. elegans* indicate that the HORMA domains in meiotic proteins HIM-3, HTP-1, HTP-2 and HTP-3 bind short 'closure motifs' in their own disordered C-terminal tails to promote complex self-assembly (Kim *et al.,* 2014). This has led Rosenberg and Corbett (2015) to suggest a model for meiotic HORMA domain protein localisation whereby the HORMA domains bind closure motifs located on cohesins or cohesin associated axis-proteins to mediate initial axial recruitment which is then followed by head to tail self-assembly to form large HORMA domain protein containing complexes (figure 4.1).

Once the HORMA domain proteins Hop1 or ASY1 have been loaded onto the axis during leptotene, they then go on to become depleted from the meiotic axis at regions undergoing synapsis during the zygotene and pachytene substages. In both *S. cerevisiae* and *A. thaliana* this process is dependent on

the AAA+ ATPases Pch2 and PCH2, respectively. Other recent structural studies have also shown that the mouse Pch2 homologue, TRIP13, can disassemble complexes containing the HORMA domain protein MAD2 by manipulation of the 'safety belt' region (Ye *et al.*, 2015). It could be that PCH2's mechanism for ASY1 depletion works in a similar way by transiently unfolding the 'safety belt' region of the HORMA domain which would disrupt binding of the closure motif leading to ASY1 complex disassembly (Rosenberg and Corbett, 2015) (figure 4.1).

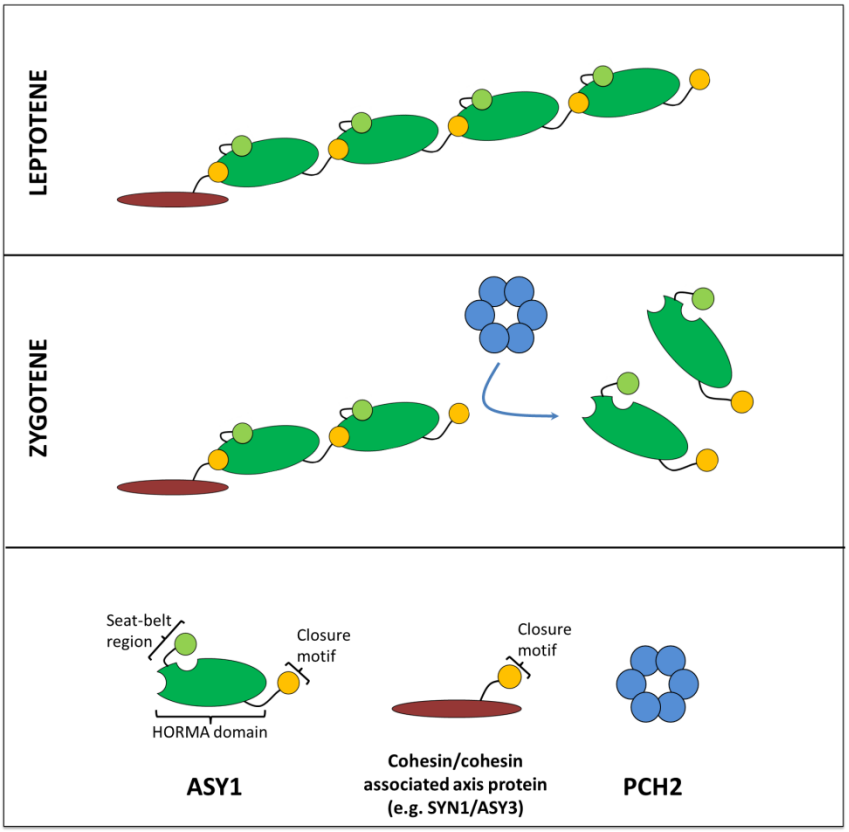

Figure 4.1. Model for ASY1 assembly/disassembly. During the leptotene stage ASY1 could be recruited to the axis by interaction of the HORMA domain with closure motifs on meiotic cohesin subunits (e.g. SYN1) or other core axis proteins (e.g. ASY3). ASY1 could then self-assemble into a complex by head to tail HORMA domain – closure motif interactions. During zygotene PCH2 is required for ASY1 removal from the axis. This could be achieved by PCH2 mediated destabilisation of the closure motif by transient unfolding of the HORMA's seatbelt region. Adapted from Rosenberg and Corbett (2015).

In this study we set out to determine what role the derived tetraploid *A. arenosa ASY1* allele has on stabilising autopolyploid meiosis. To accomplish this, we performed a large scale cytological analysis of tetraploid plants expressing either the diploid or tetraploid *ASY1*

alleles. As diploid and tetraploid *A. arenosa* plants populate different habitats in the wild it is also possible that any genetic differences could be the result of adaptive changes to new abiotic conditions (Wright *et al.*, 2014) rather than being due to changes in ploidy. Therefore, we also performed a temperature experiment to determine whether the different alleles resulted in altered meiotic behaviour at different temperatures.

4.2 Results

4.2.1 Tetraploid *A. arenosa* were generated that were homozygous for the diploid *ASY1* allele

As mentioned previously, a derived *ASY1* allele with a non-synonymous SNP occurs at high frequency (90%) in the tetraploid population. As well as a single, previously unrepresented amino-acid change in the protein's HORMA domain, a further five amino-acid changes are present in the tetraploid allele of *A.* arenosa that are not present in the diploid allele or in *ASY1* alleles from close relatives *A. thaliana* or *A. lyrata* (figure S1). As the diploid *ASY1* allele still occurs at low frequency (10%) within the tetraploid population (Hollister *et al.*, 2012), this allowed tetraploid TBG plants to be selected through conventional breeding that were homozygous for either the tetraploid *ASY1* allele (TBG *ASY1 TTTT*) or the diploid *ASY1* allele (TBG *ASY1 DDDD*) (K. Bomblies, K. Wright, personal communication). Plants with different genotypes can be identified using a restriction enzyme based-genotyping approach, with the diploid allele possessing an *XmnI* restriction site 623-632 bp upstream of the transcription start site that is not present in the tetraploid allele. Figure 4.2 shows the results of a genotyping experiment confirming TBG *ASY1 TTTT*, TBG *ASY1 DDDD* and TBG *ASY1 TxxD* (heterozygous for both alleles) lines had been successfully obtained.

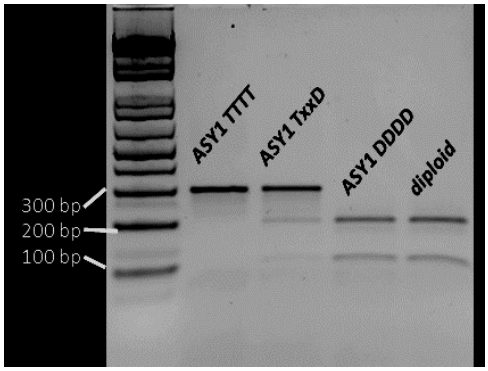

Figure 4.2. A restriction enzyme based genotyping method can distinguish between TBG A. arenosa plants possessing different ASY1 alleles. A diploid SN A. arenosa plant has also been genotyped for comparison.

4.2.2 *ASY1 DDDD* plants do not exhibit any severe meiotic defects

Neotetraploid *A. arenosa* lines generated by treating diploid *A. arenosa* accessions with colchicine exhibited severe multivalent formation at metaphase I and a significant reduction in fertility (Yant *et al.,* 2013). In order to test if a similar scenario occurred in *ASY1 DDDD* plants, DAPI stained acid-fixed meiotic cells were analysed for meiotic irregularities (figure 4.3). Visual inspection of the DAPI stained meiotic cells indicated that no severe defects similar to those observed in the neotetraploids could be detected. For instance, prophase I appeared to proceed in a conventional manner with *ASY1 DDDD* chromosomes condensing into long threads at the leptotene stage that appear to synapse in a pairwise fashion during the zygotene and pachytene substages. Also, at metaphase I homologues appeared to form mostly bivalents, with a low frequency of multivalents and univalents also being observed as would be expected during tetraploid meiosis in *A. arenosa* (section 3.2.2). Balanced homologue segregation was also observed at anaphase I.

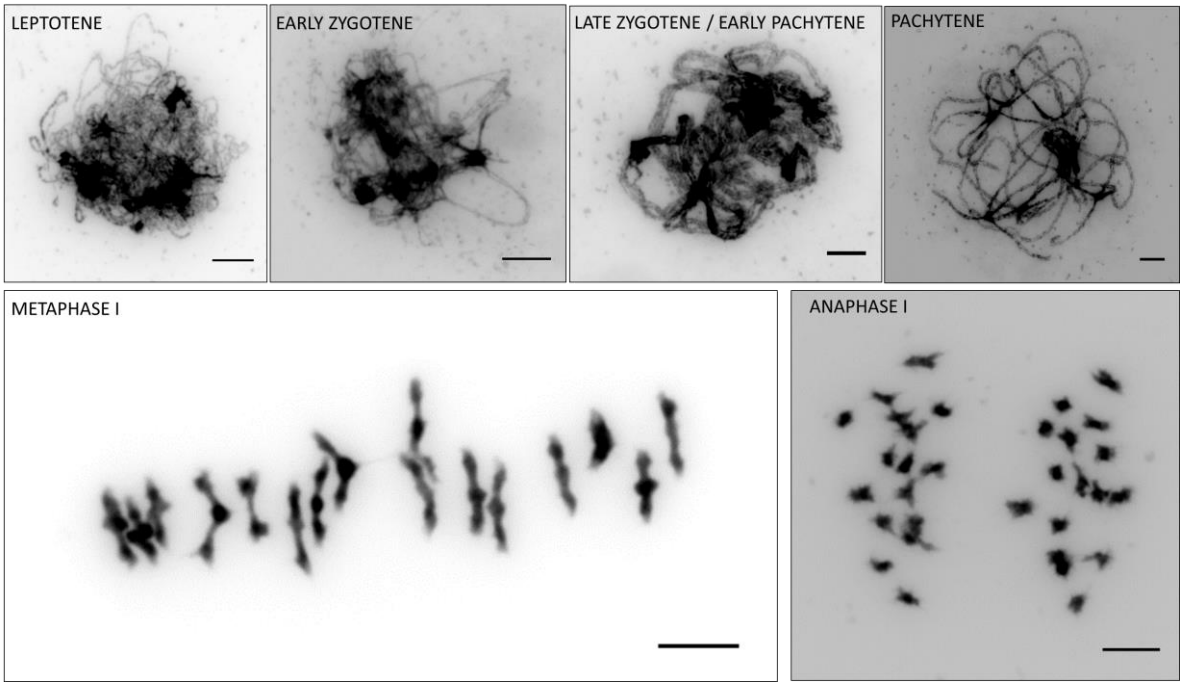

Figure 4.3. A partial meiotic atlas of DAPI stained acid-fixed meiocytes from TBG ASY1 DDDD A. arenosa. Scale bar = 5 µm.

Following on from the cytological analysis, male fertility of the *ASY1 DDDD* plants was also assessed by Alexander pollen staining (Alexander, 1969). This demonstrated that almost all pollen was non-aborted in *ASY1 DDDD* anthers, again indicating that no major disruptions to meiosis were present that would otherwise result in an increased frequency of aborted pollen grains (figure 4.4).

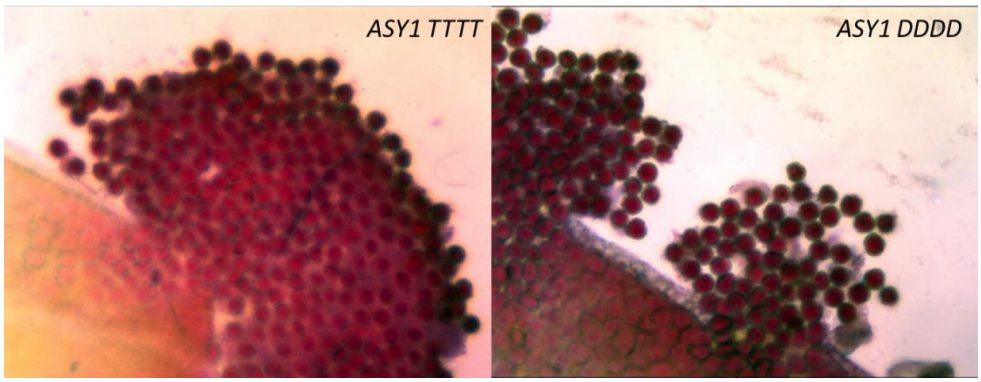

Figure 4.4. Alexander staining for pollen viability in ASY1 TTTT and ASY1 DDDD TBG A. arenosa. Viable pollen grains appear red and aborted pollen grains appear blue green. The vast majority of pollen grains are red in both genotypes indicating high levels of male fertility.

To investigate the localization and general behavior of ASY1 in both *ASY1 TTTT* and *ASY1 DDDD* plants, immunolocalised ASY1 protein was analysed at the leptotene stage of meiosis using SIM (figure 4.5). Close inspection of the protein in both lines showed that it formed a chromatin associated linear signal similar to that previously observed in *A. thaliana* using SIM microscopy (Lambing *et al*, 2015). Alternating regions of high and low intensity, indicative of a domain-like organization were also observed in *A. thaliana* but the distribution of intensity appeared much more uniform in both *A. arenosa* genotypes. This technique indicated that no significant global differences in ASY1 distribution or localization were observed between the two genotypes.

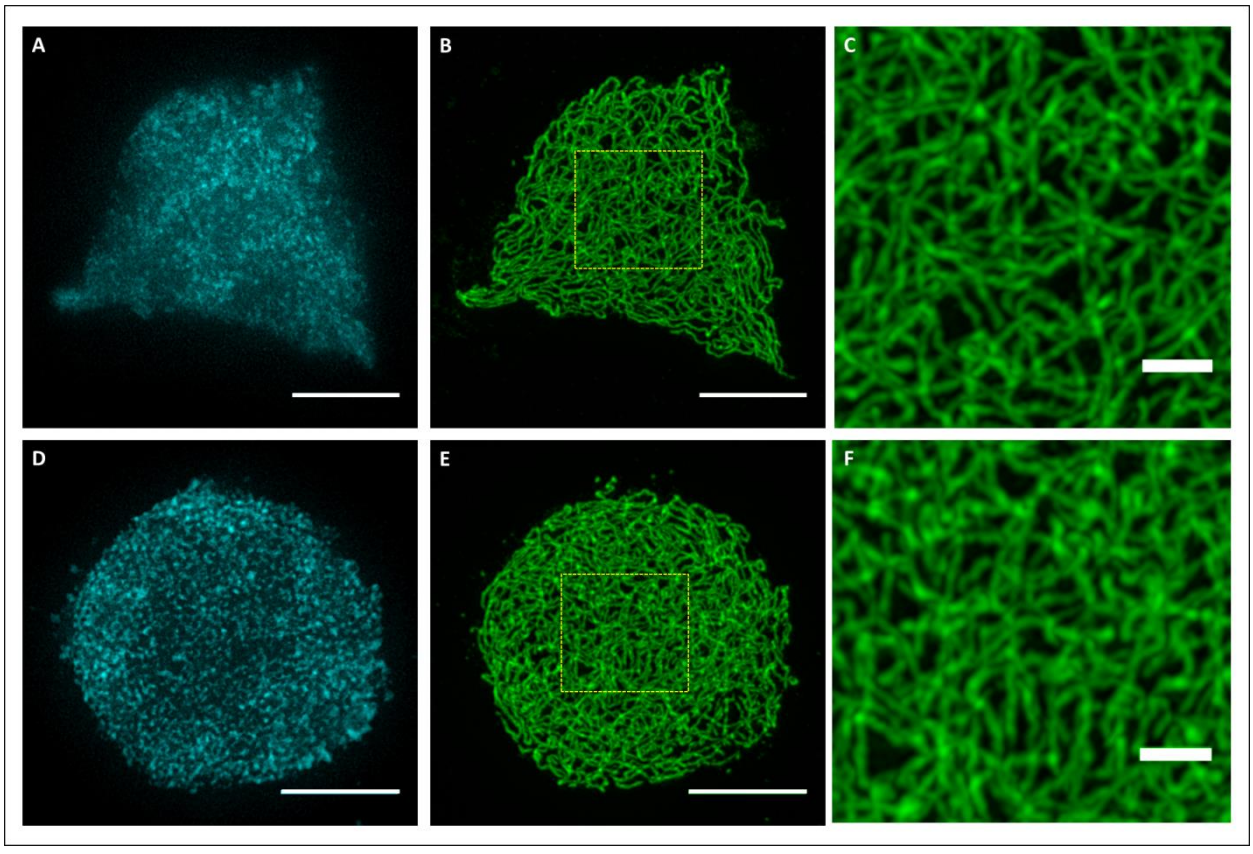

Figure 4.5. Leptotene spreads from ASY1 TTTT (A, B, C) and ASY1 DDDD (D, E, F) A. arenosa stained for DAPI (A,D) and ASY1 (B, E). Scale bar = 5 µm. A magnified image of ASY1 (yellow boxes B, E) is also shown (C, F). Scale bar = 1 µm.

4.2.3 Meiotic DSB and CO frequencies are similar between *ASY1 TTTT* and *ASY1 DDDD* TBG *A. arenosa*

To test if any more subtle meiotic differences could be detected between *ASY1 DDDD* and *ASY1 TTTT A. arenosa* lines, RAD51 foci counts and metaphase I chiasma counts were carried out to infer the number of meiotic DSBs and COs, respectively. A mean value of 395 RAD51 foci (n = 10, S.D = 54.1) were counted in *ASY1 TTTT* plants and 383 RAD51 foci (n = 10, S.D = 57.8) in *ASY1 DDDD* plants (figure 4.6), indicating that no major differences in meiotic DSB numbers could be detected between either genotype. This is perhaps not surprising as a reduction in meiotic DSB levels is also not detected in an *A. thaliana asy1* T-DNA insertion mutant (Sanchez-Moran *et al.,* 2007) so it is unlikely different *ASY1* alleles would have a major impact on this aspect of meiotic recombination.

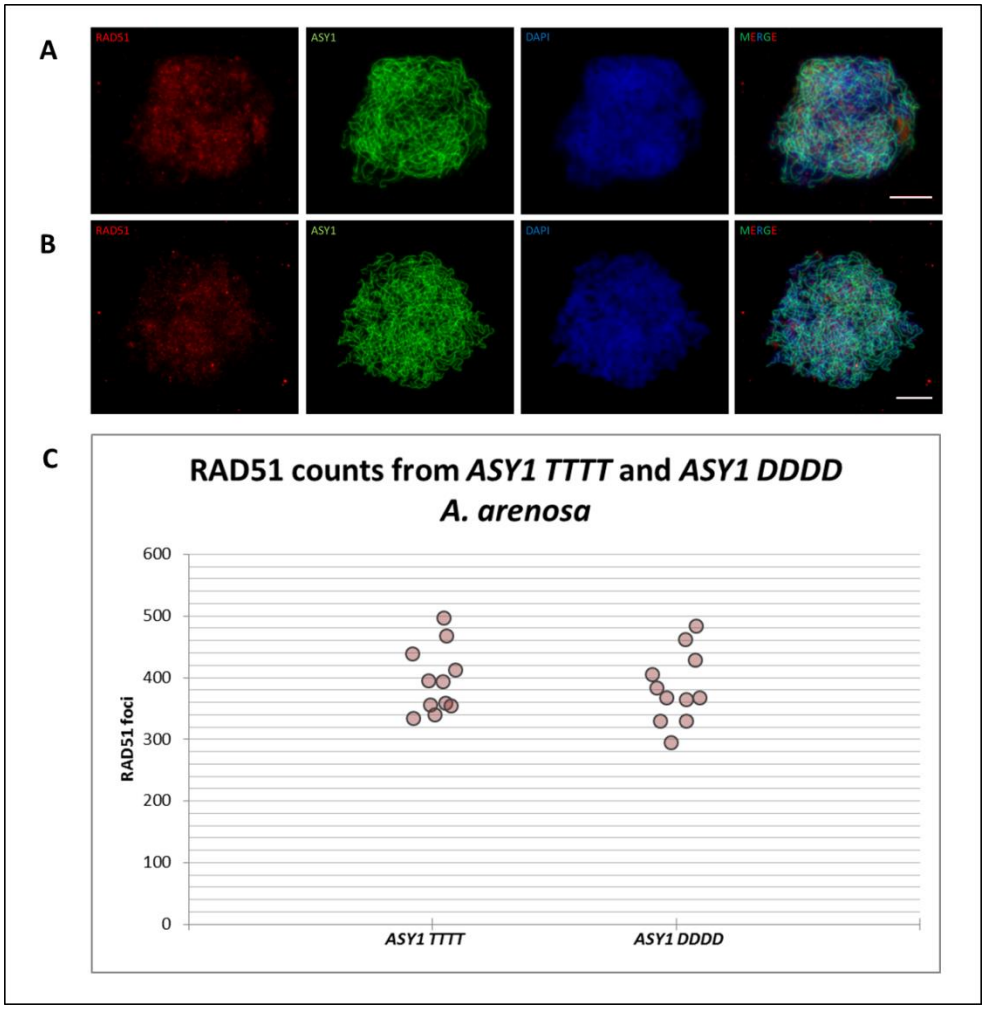

Figure 4.6. RAD51 (red), ASY1 (green) and DAPI (blue) signal on leptotene spreads from ASY1 TTTT (A) and ASY1 DDDD (B) A. arenosa. (C) Dot plot showing RAD51 foci counts from 10 ASY1 TTTT cells and 10 ASY1 DDDD cells.

asy1 T-DNA mutants in *A. thaliana* do, however, show a significant reduction in CO frequency as demonstrated by metaphase I chiasma counts (1.39 chiasma per cell, Sanchez-Moran *et al.*, 2001). Therefore, chiasma counts from metaphase I bivalents were also performed using *ASY1 TTTT* and *ASY1 DDDD* cells (figure 4.7). Bivalents were either categorized as rods (1 CO) or rings (2 COs) depending upon their appearance and multivalent and univalent chromosomes were also counted (figure 4.7A, table S8). In *A. thaliana* ring bivalents can sometimes contain >2 COs but, given that the CO frequency per chromosome in

A. arenosa is much lower, the assumption was made that any ring bivalents counted in this analysis were likely to only contain 2 COs. It is also worth noting that the large number of chromosomes coupled with the potential for overlapping or 'underspread' chromosomes to be identified as multivalents does mean that this technique has some potential drawbacks that could lead to inaccurate scoring of chiasma. Chiasma counts indicated that no difference in chiasma frequency could be detected between *ASY1 TTTT* (mean = 16.88 chiasma per cell, S.D = 1.13, n = 25) and *ASY1 DDDD A. arenosa* (mean = 16.96 chiasma per cell, S.D = 0.88, n = 23) (figure 4.7C, table S8). These numbers do, however, correlate closely with a previous study from Yant *et al.*, (2013) where 17.44 chiasma per cell were counted in tetraploid *A. arenosa*.

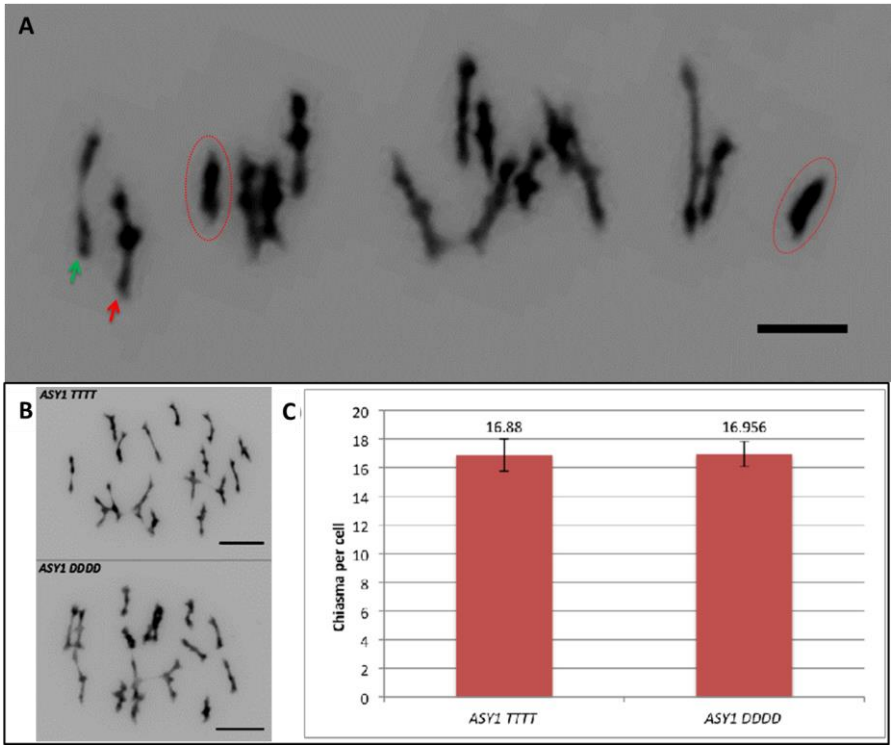

Figure 4.7. (A) A metaphase I cell from ASY1 DDDD A. arenosa. Ring bivalents are highlighted with red circles. The green arrow points to a rod bivalent with a distal (towards the end of the chromosome) CO and the red arrow points to a rod bivalent with a more interstitial (midway between the end of the chromosome and the centromere) CO as indicated by a more 'cruciform' like shape. (B) M1 cells from ASY1 TTTT and ASY1 DDDD A. Arenosa. (C) Bar chart showing the mean chiasma per cell for ASY1 TTTT and ASY1 DDDD A. arenosa (error bars indicate +/- S.D). Scale bar = 5 μm.

4.2.4 CO localization differs in *ASY1 DDDD* relative to *ASY1 TTTT*

It has also been observed in *asy1* mutants in *A. thaliana* that the few residual chiasma that remain tend to be associated with distal interhomologue connections, indicating a preponderance for COs being located near the ends of chromosomes (Sanchez-Moran *et al.*, 2001). We therefore set out to determine if a change in CO localization could be detected between *ASY1 TTTT* and *ASY1 DDDD* lines. In metaphase I spreads, bivalents with a single, more distal (towards the chromosome end) CO tend to have a more 'linear' rod conformation (figure 4.7A). Bivalents with a single interstitial (between the chromosome end and the centromere) CO tend to have a more 'cruciform-like' rod conformation, with the conformation becoming increasingly more 'cross-like' as the CO position becomes more proximal (towards the centromere). A large number of M1 cells from both *ASY1 DDDD* and *ASY1 TTTT* plants were therefore visually analysed and the number of bivalents of each conformation was counted. M1 cells from heterozygous *ASY1 TxxD* plants and diploid SN plants were also included in this analysis for comparison. To prevent the introduction of confirmation bias during data collection, images from different tetraploid genotypes were collected by the author and randomly assorted before being blindly assessed by our collaborator (K. Bomblies).

In total 124 diploid, 179 *ASY1 TTTT,* 63 *ASY1 TxxD* and 168 *ASY1 DDDD* M1 cells were analysed during this initial study. For each cell, the number of ring, 'cross-like' rod (proximal CO), 'cruciform-like' rod (interstitial CO) and 'linear' rod (distal CO) bivalents were counted and the proportion of each calculated relative to the total number of countable bivalents for that cell (in some cells not all bivalents were countable due to factors such as underspreading and multivalent formation) (figure 4.8A, table S9).

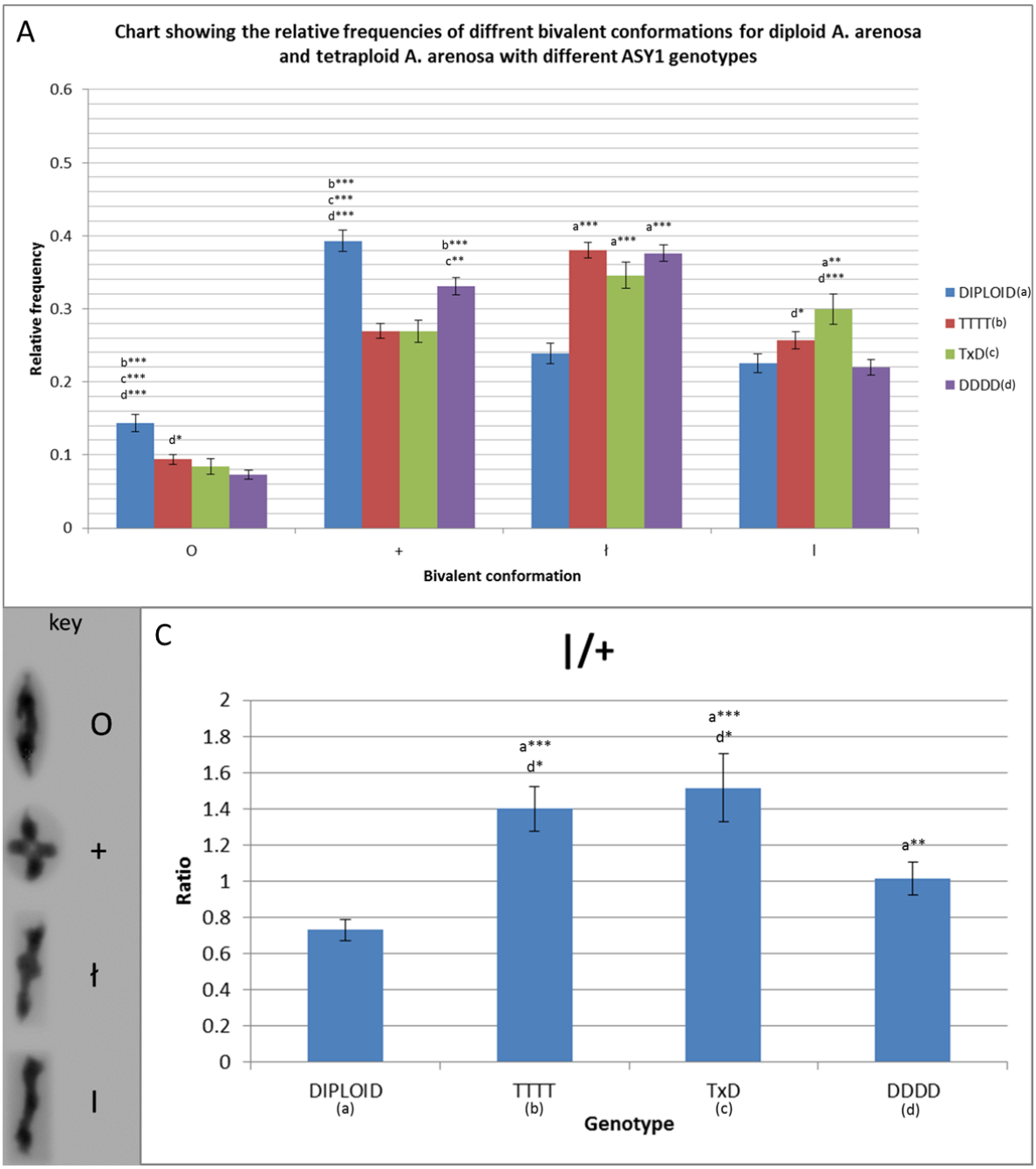

Figure 4.8. (A)Chart showing the relative frequencies of each bivalent conformation type in M1 cells from diploid, ASY1 TTTT, ASY1 TxxD and ASY1 DDDD lines. Values shown above the bars indicate if a conformation is significantly higher in one group than another (e.g. b* would indicate the relative frequency for a particular conformation is significantly higher than that found in ASY1 TTTT) calculated using an independent two-sample T.test. (p<0.001, **p<0.01, *p<0.05). (B) Key showing symbols used to represent different conformations and an examples of each, O = ring, + = 'cross-like', ł = "cruciform-like' and I = 'linear'. (C) Chart showing the ratio of 'linear' rods to 'cross-like' rods in each genotype. Between group significance values are displayed as in (A).***

Many interesting observations arise from this data. Firstly, it appears that the diploid has a significantly higher proportion of ring bivalents compared to any of the tetraploid genotypes. This is what would be expected based on previous observations that diploid *A. arenosa* has a higher frequency of COs per bivalent than the tetraploid (Yant *et al.,* 2013). The *ASY1 TTTT* line also has a significantly higher proportion of ring bivalents compared to the *ASY1 DDDD* line. It cannot be inferred from this that the total CO frequency is higher in one line than another though as COs involving multivalents were not included in this study. Diploids also have a significantly higher number of cross-like bivalents than any of the tetraploid genotypes and the *ASY1 DDDD* line has a significantly higher number of cross-like bivalents than the *ASY1 TTTT* or *ASY1 TxxD* lines. This indicates that, in general, COs are more likely to occur in proximal regions in the diploid and *ASY1 DDDD* lines compared to the *ASY1 TTTT* and *ASY1 TxxD* lines. In contrast to this, the *ASY1 TTTT* and *ASY1 TxxD* lines have a significantly higher proportion of linear rods compared to the *ASY1 DDDD* lines and the *ASY1 TxxD* line also has a significantly higher proportion of linear rods compared to the diploid. This indicates that COs in the *ASY1 TTTT* and *ASY1 TxD* lines tend to occur in more distal regions than in the *ASY1 DDDD* line. All tetraploid *ASY1* genotypes have a significantly greater proportion of cruciform-like bivalents than the diploid, indicating interstitial COs occur more frequently in these lines and there are no significant differences between the *ASY1 TTTT* and *ASY1 TxxD* lines for any bivalent conformations. The ratio of linear rods to cross-like bivalents was also calculated for each cell and the ratios were found to be significantly higher in the *ASY1 TTTT* and *ASY1 TxxD* lines than in the *ASY1 DDDD* and diploid lines. Taken together, this data suggests that the tetraploid *ASY1* allele exerts a dominant effect by shifting COs to more distal positions relative to the diploid allele.

In order to further test this hypothesis, class I CO positions were determined with a greater

degree of accuracy by measuring the position of MLH1 foci along the SC of chromosomes as a proportion of total SC length for *ASY1 TTTT* and *ASY1 DDDD A. arenosa* plants (figure 4.9). MLH1 foci measurements were taken from 151 *ASY1 TTTT* pachytene chromosomes and 142 *ASY1 DDDD* pachytene chromosomes with single MLH1 foci along their lengths. The proportional distance of the MLH1 foci from the middle of the chromosome was then calculated and the results were binned into five intervals of equal relative size from the middle of the chromosome to the chromosome end. It can be seen in figure 4.9C that the *ASY1 TTTT* line appears to have a much higher frequency of foci located near the chromosome end than *ASY1 DDDD*, which has a greater frequency of foci located towards the middle of the chromosome. A chi-squared test indicates that the shift in the distribution of foci in these five intervals between the two genotypes is significant (X^2 (4, N=142) = 12.7, p=0.013). A two-tailed Kolmogrov-Smirnov test (F1 (*TTTT*) ≠ F2 (*DDDD*)) using the unbinned continuous frequencies also demonstrated that there was a significant difference in the class I CO distributions between the two genotypes ((D= 0.172, p = 0.023) (figure 4.9D). This finding is in strong agreement with the previous observations using M1 data that the tetraploid allele of *ASY1* shifts CO position to a more distal position relative to the diploid *ASY1* allele.

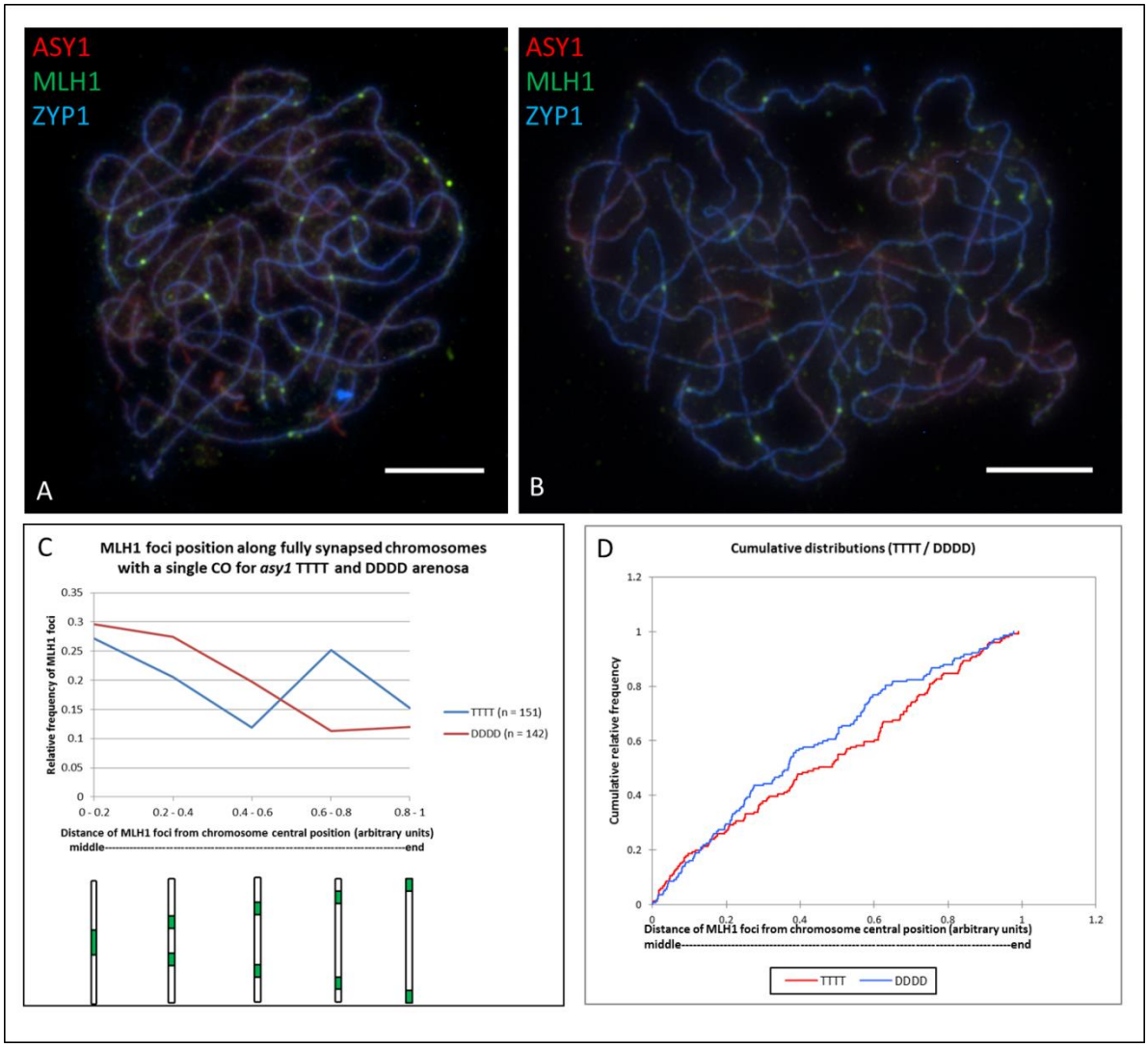

Figure 4.9. Pachytene chromosomes from ASY1 TTTT (A) and ASY1 DDDD (B) A. arenosa stained for ASY1 (red), MLH1 (green) and ZYP1 (blue). Scale bar = 5 µm. (C) Relative frequency distributions of MLH1 foci in five intervals from the middle of the chromosome to the chromosome end. (D) Cumulative frequency distributions for MLH1 foci on all chromosomes from ASY1 TTTT and ASY1 DDDD A. arenosa.

4.2.4 CO localization can also be assessed in transgenic *A. thaliana* expressing the diploid and tetraploid *ASY1* alleles from *A. arenosa*

To determine if the tetraploid allele of *ASY1* could have a similar effect on shifting CO distribution to a more distal position in other plant species, transgenic *A. thaliana* lines were generated that expressed either the diploid (SN) or tetraploid (HO) *ASY1* alleles from *A.*

arenosa. Transgenic lines were made by transforming *asy1* T-DNA insertion mutants with a binary vector containing the full genomic sequence and endogenous promoters and terminators for either the tetraploid allele from the HO accession of *A. arenosa* or the diploid allele from the SN accession of *A. arenosa* (K. Wright and K. Bomblies, personal communication) (Wright *et al.*, 2014). Transformants were selected by BASTA resistance and functional lines were selected that complemented the *asy1* T-DNA mutant by restoring fertility to wild type levels (K. Wright and K. Bomblies, personal communication). Segregating T2 lines were used for cytological analysis and the presence of the transgene was confirmed by genotyping. Analysis of DAPI stained M1 cells from acid-fixed meiocytes indicated that, as expected following the previous fertility screen, stable meiosis was observed in transgenic lines expressing both the diploid SN and tetraploid HO *ASY1* alleles. M1 cells in both lines consisted of five paired bivalents, as we would expect to see in Col-0 but not in the *asy1* mutant where a reduction in CO frequency means most cells experience only 1-4 bivalents with the remaining chromosomes forming univalents (Sanchez-Moran *et al.*, 2001) (figure 4.10). This indicates that, again, any changes caused by the tetraploid allele must be relatively subtle and don't appear to have a catastrophic effect on meiotic integrity.

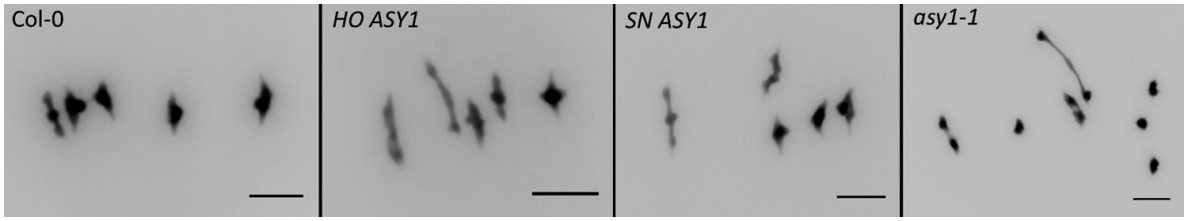

Figure 4.10. M1 cells from Col-O, HO ASY1 (tetraploid allele) transgenic lines, SN ASY1 (diploid allele) transgenic lines and an asy1-1 T-DNA insertion mutant. Scale bar = 5 µm.

To determine if a change in CO position could be detected between Col-0, HO *ASY1* or SN *ASY1* lines a blind analysis of bivalent conformations was conducted that was similar to that in section 4.2.3. Images from 66 Col-0, 77 HO *ASY1* and 35 SN *ASY1* M1 cells were collected

and analysed. For each cell the number of 'cruciform-like' rod bivalents, 'linear' rod bivalents and ring bivalents was counted by our collaborator (K. Bomblies) (figure 4.11, table S.10). Chi squared tests indicated that there was no significant difference between the frequency of 'cruciform-like' rods versus 'linear' rods or between rods versus rings for any of the lines. This may have been due to difficulties associated with collecting enough data in the *A. thaliana* background compared to the *A. arenosa* background. In *A. arenosa* a greater number of meiocytes per anther led to greater ease in collecting a large number of M1 cells and also a greater number of chromosomes coupled with a much higher frequency of rod bivalents made differences in single CO distributions easier to detect. However, it can be noted that there is a general, if not significant, trend within the data that the HO *ASY1* line does have a greater frequency of 'linear-like' rods compared to 'cruciform-like' rods than the Col-0 and SN *ASY1* lines and also a greater frequency of rings compared to rods, both of which are consistent with the findings from *A. arenosa* in section 4.2.3. In the future, it will be worthwhile gathering more, similar data from these lines to see if this difference becomes significant.

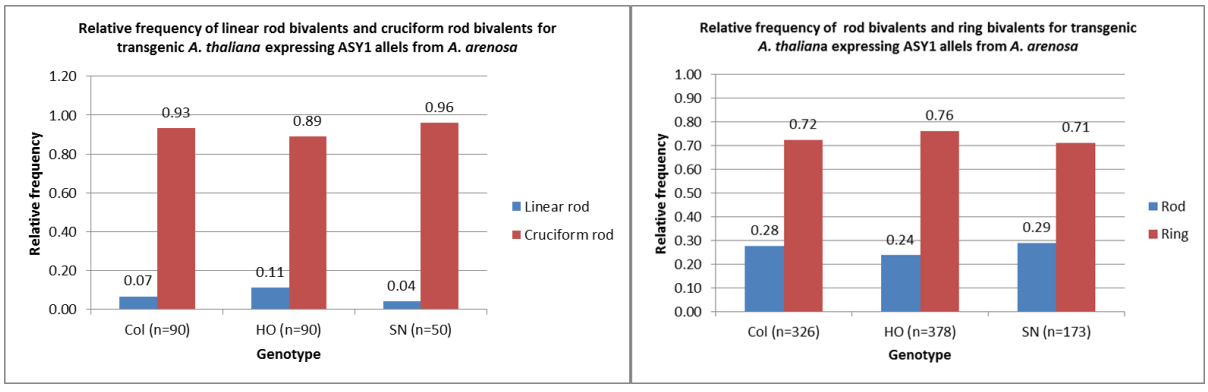

Figure 4.11. Bar charts showing the relative frequencies of 'cruciform-like' rods versus 'linear' rods and of rods versus rings in M1 cells from Col-0, HO ASY1 and SN ASY1 A. thaliana.

4.2.5 *A. arenosa* lines with different *ASY1* genotypes appear to exhibit differing levels of meiotic thermal tolerance

As well as exhibiting different ploidy levels, diploid and tetraploid populations of *A. arenosa* are also found in distinct biogeographic zones throughout Central and Eastern Europe (Wright *et al.,* 2014). Some diploid populations inhabit the Carpathian Mountains where temperatures are generally lower, whilst other diploid populations are located in the Pannonian basin of Slovakia and Hungary where temperatures are generally higher. Many tetraploid populations, on the other hand, are found along railway lines and experience a wider variation in the temperatures to which they are exposed (Wright *et al.,* 2014). It is worth noting, therefore, that changes in ploidy are not the only major selection pressures acting on the different *A. arenosa* populations and that other environmental factors such as temperature could be playing a role. Indeed, many previous studies have shown that meiotic stability can be highly sensitive to changes in ambient temperature (reviewed in Bomblies *et al.,* 2015).

To determine if the different *ASY1* alleles had differing effects on meiotic stability at high temperatures 2 *ASY1 TTTT (or TxxD)* plants, 2 *ASY1 TxD* plants and 2 *ASY1 DDDD A. arenosa* plants were exposed to 33 ^{o}C (>10 ^{o}C higher than the average summer temperatures experienced by all *A. arenosa* populations, Wright *et al.,* 2014) temperatures for 6 weeks (K. Bomblies and K. Wright, personal communication). Problems with genotyping meant that *ASY1 TTTT* plants could not be conclusively confirmed as such and so they could also have been *ASY1 TxxD.* Inflorescences from all plants were collected and fixed at 3 and 6 weeks (K. Bomblies and K. Wright, personal communication).

Tubes containing the fixed inflorescences were labelled with a random number so that DAPI slides could be made and cells could be analysed by the author whilst simultaneously being blind to the genotypes. Fixed material was also used to make immunolocalisation slides with

anti-ASY1 and anti-ZYP1 antibodies. Once DAPI and immunlocalisation slides had been made and images had been collected from each line, lines were classified as good, intermediate or bad depending on the severity of meiotic instability observed by cytological analysis. Summaries of the blind observations for each line and examples of some of the meiotic abnormalities observed at high temperature are shown in table 4.1 and figure 4.12. In a number of lines, severe meiotic defects were visible at various stages of meiosis and included problems such as fragmentation of chromosomes at prophase I, univalent formation at M1, missegregation at anaphase I giving unbalanced dyads and missegregation at anaphase II giving unbalanced tetrads. After unblinding it was clear that the two lines with the fewest meiotic defects after 3 or 6 weeks at 33^{o}C were both heterozygous *ASY1 TxxD* lines. Pollen fertility of these same lines had also been assayed by Alexander staining after 2 weeks at 33^{o}C and these results also showed that lines 1 and 5 has the highest fertility of all lines (94% and 78%, respectively). Fertility of lines 2, 3, 4 and 6 were 67%, 1%, 19% and 11% respectively (K. Bomblies and K. Wright, personal communication). It may, therefore, be the case that heterozygous *ASY1 TxxD* lines exhibit increased meiotic thermal tolerance relative to their homozygous counterparts. The potential significance of this will be covered in the discussion.

Plant	Observations of meiotic instability after examining DAPI stained cells and ASY1/ZYP1 stained cells after 3 or 6 weeks at 33°C	Genotype
1	Good - synapsis seems OK, no ZYP1 polycomplex formation, many M1 cells with 16 bivalents, some missegregation at anaphase II	*ASY1 TxxD*
2	Bad – many fragments observed at prophase I and M1, ZYP1 polycomplex formation, missegregation at anaphase I and II	*ASY1 DDDD*
3	Intermediate – some M1 cells with 16 bivalents but others with many univalents, some missegregation at anaphase I and II	*ASY1 TTTT (or TxxD)*
4	Bad – many fragments observed at prophase I and M1, ASY1 aggregates and small ZYP1 polycomplex formation, missegregation at anaphase I and II	*ASY1 DDDD*
5	Good – synapsis seems OK, no ZYP1 polycomplex formation, many M1 cells with 16 bivalents, some missegregation at anaphase II	*ASY1 TxxD*
6	Bad – many univalents and fragments observed in M1 cells, extensive ZYP1 polycomplex formation and ASY1 aggregate formation, missegregation at anaphase I and II	*ASY1 TTTT (or TxxD)*

Table 4.1. Blind observations of meiotic instability in different A. arenosa ASY1 genotypes following 3/6 weeks at 33°C.

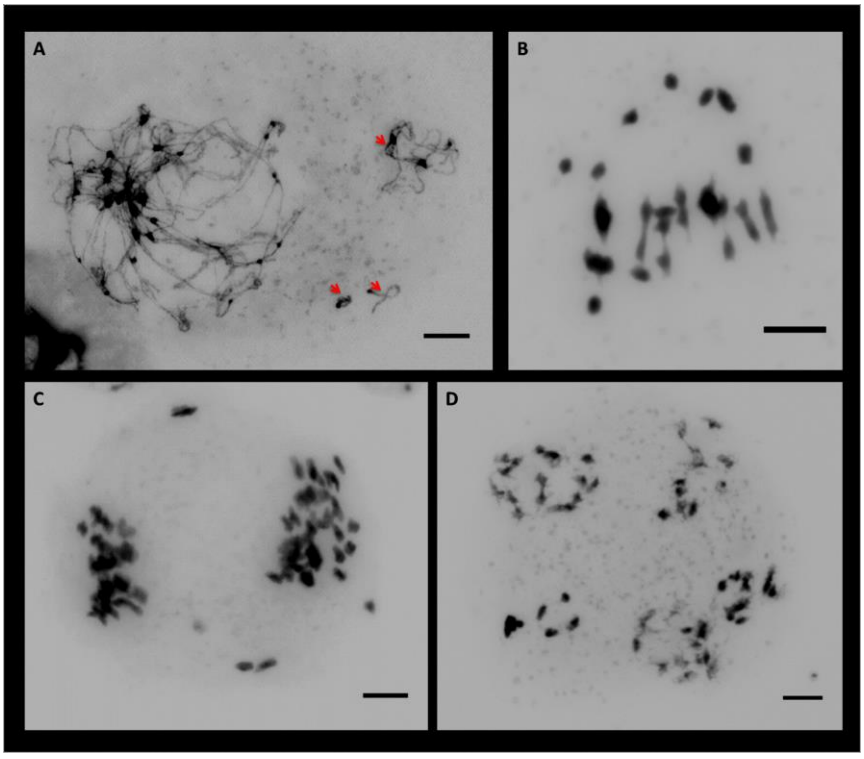

Figure 4.12. Meiotic abnormalities observed in DAPI stained meiotic cells from A. arenosa lines treated at 33°C for 3 or 6 weeks. (A) Prophase I cell from line 2 (ASY1 DDDD). Arrows point to chromosome fragments that are separate from the main nucleus. (B) M1 cell from line 3 (ASY1 TTTT/TxxD) showing extensive univalent formation. (C) Unbalanced dyad with a number of lone missegregated chromosomes that could go on to form micronuclei. (D) Tetrad with five unbalanced daughter nuclei caused by missegregation at anaphase II. Scale bars = 5 µm.

Meiotic abnormalities were also observed in the ASY1/ZYP1 immunolocalisation slides. One line in particular, line 6 (*ASY1 TTTT/TxxD*), showed a particularly striking meiotic phenotype with extensive ladder-like ZYP1 polycomplex formation and axis associated ASY1 aggregations (figure 4.13). EM studies in *Allium ursinum* treated at 35^{o}C for 30 hours showed very similar structures (Loidl, 1989). In some instances the ZYP1 polycomplexes can be seen extending from and between ASY1 aggregations (figure 4.13C, D).

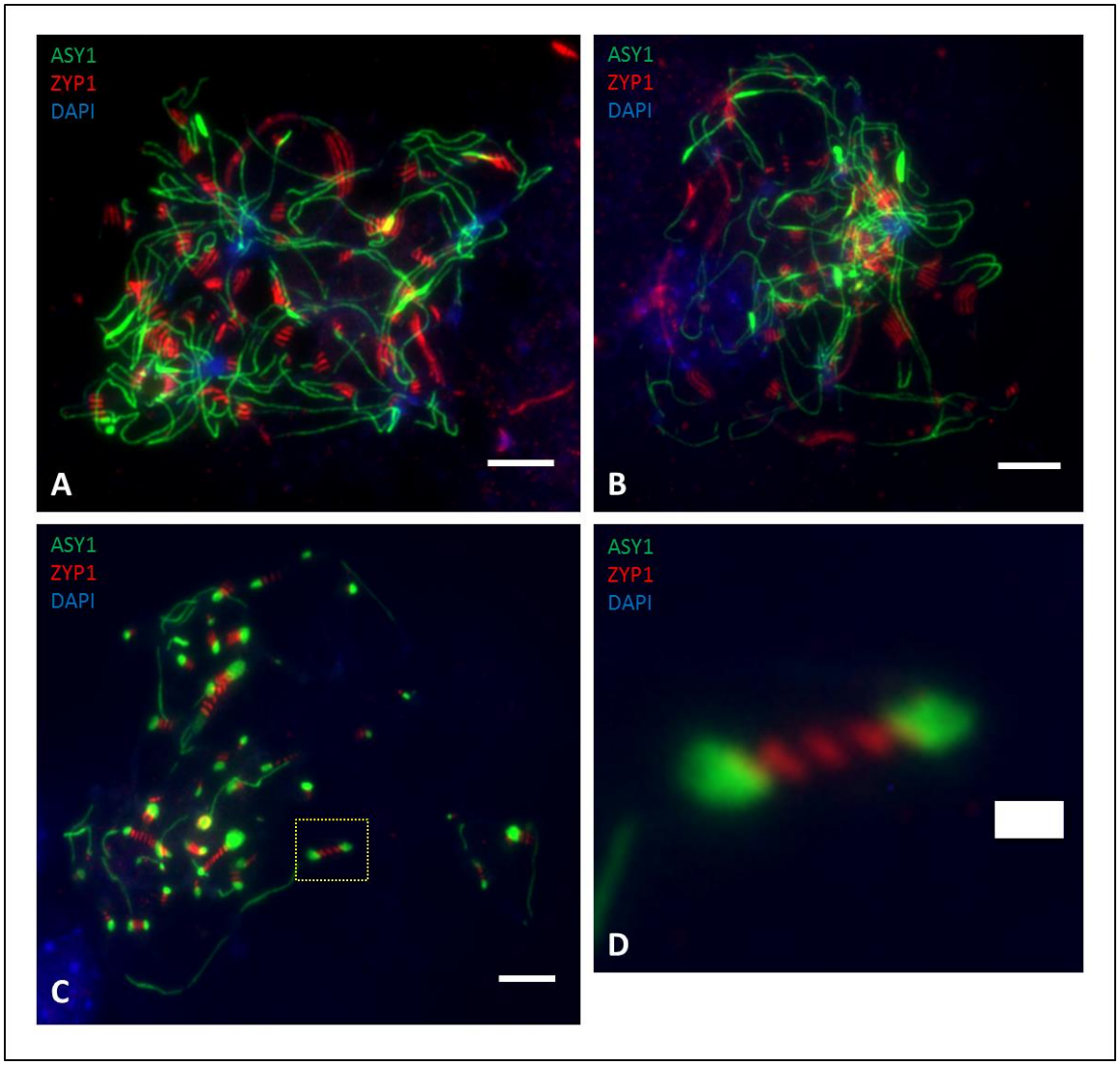

Figure 4.13. (A, B, C) Immunolocalisation of ASY1 (green) and ZYP1 (red) in fixed material from line 6 (ASY1 TTTT/TxxD) which had been at 33^{o}C for 6 weeks. DNA is stained with DAPI (blue). Ladder-like ZYP1 polycomplexes and bright ASY1 aggregates can be seen in all cells. Scale bars = 5 µm. (D) Close up of region in yellow box from C showing two ASY1 aggregates with a ZYP1 polycomplex extending between them. Scale bar = 1µm.

In some cells, enormous single polycomplexes can be observed that almost span the entire cell (fig 4.14). To determine the distances between the ZYP1 repeat units in the polycomplexes an intensity plot was measured along one of the larger polycomplexes and the mean interpeak distance was calculated as 0.46 µm. This is approximately double the width previously found to occur between the lateral elements of the SC (200-250 nm, section 3.2.4), suggesting these polycomplexes may assemble in a different manner to the conventional SC.

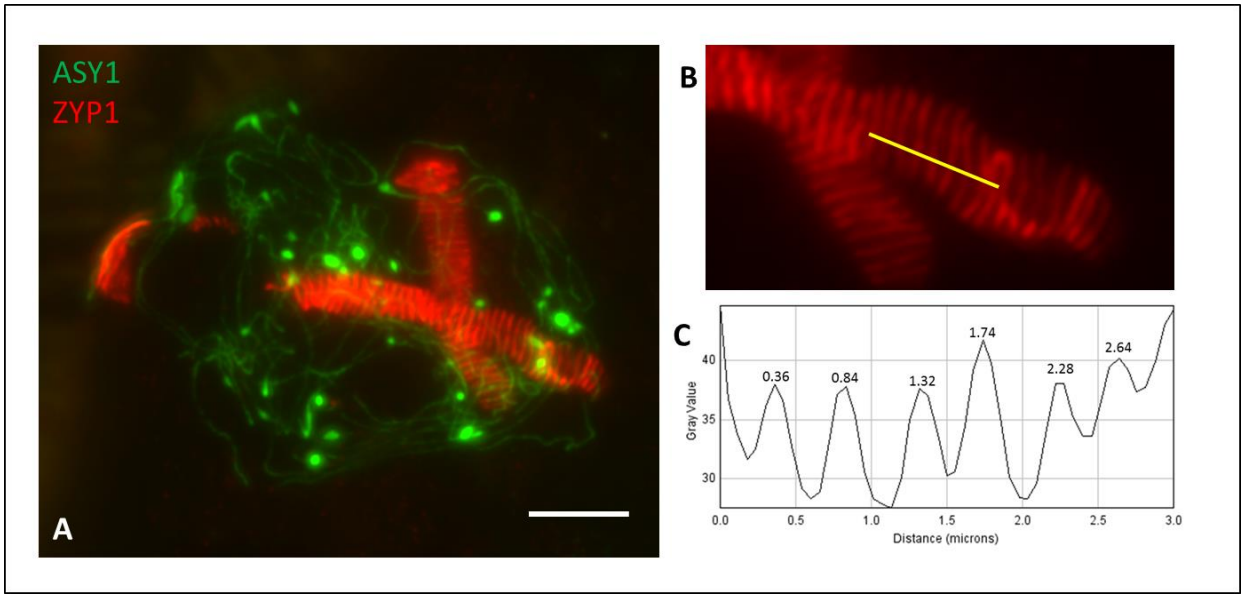

Figure 4.14. Immunolocalisation of ASY1 (green) and ZYP1 (red) in fixed material from line 6 (ASY1 TTTT/TxxD) which had been at 33°C for 6 weeks. (A) Very large ZYP1 polycomplexes span a cell which also contains numerous ASY1 aggregates. (B) Close up of a ZYP1 polycomplex with a yellow line indicating the position of the intensity line plot profile in (C). Scale bar = 5 µm.

Another interesting and novel observation was that, in instances where chromosomes have fragmented during prophase I, ZYP1 polycomplexes appear to be associated with all fragments, even the very small ones (figure 4.15). It is unclear, however, whether the polycomplexes have caused the fragmentations and, if they have, whether this could be an artefact of the chromosome spreading process such that chromosomal regions associates with bulky polycomplexes are more likely to break apart during spreading.

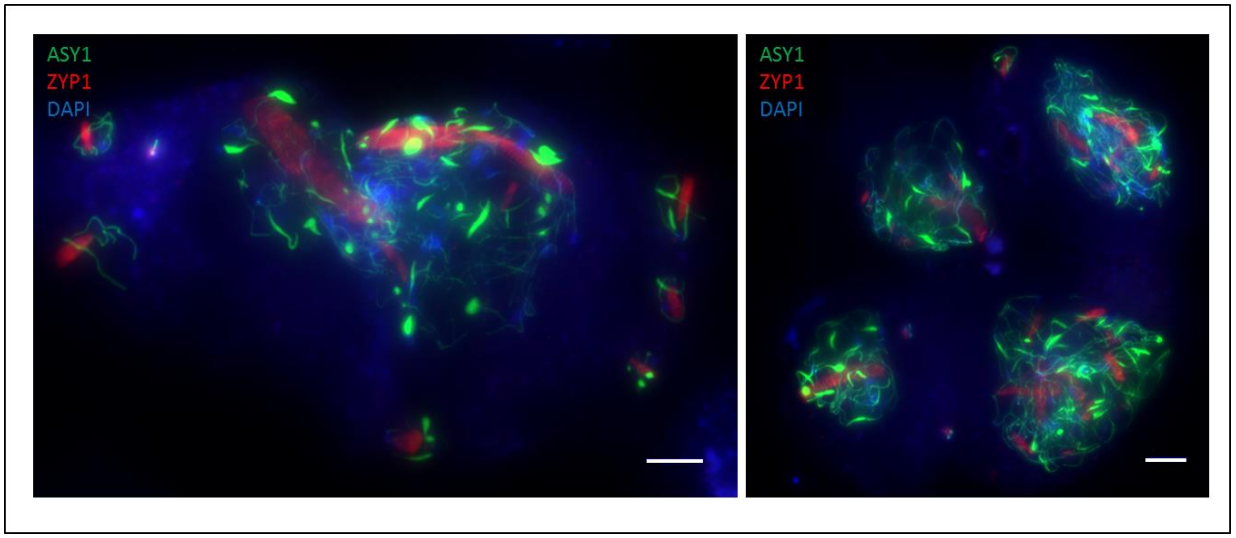

Figure 4.15. Immunolocalisation of ASY1 (green), ZYP1 (red) and DNA (blue) in fixed material from line 6 (ASY1 TTTT/TxxD) which had been at 33°C for 6 weeks. Fragmented prophase chromosomes are shown and in both instances all fragments are associated with ZYP1 polycomplexes. Scale bar = 5 µm.

4.3 Discussion

Here, we have demonstrated that two alleles of the same gene *ASY1*, the protein products of which only differ by 10 amino acids, appear to have separate, significant effects on meiotic CO localisation in the model tetraploid *A. arenosa*. We have also shown that both of these alleles are functional in the model organism *A. thaliana*, and may also contribute to meiotic thermal tolerance in *A. arenosa.*

4.3.1 The tetraploid allele of *ASY1* shifts CO localisation to a more distal position relative to the diploid allele

Initial analysis of tetraploid *A. arenosa* lines bred to be homozygous for the diploid *ASY1* allele (*ASY1 DDDD*) indicated that there were no major meiotic irregularities to be found within these lines when compared to the tetraploid lines homozygous for the tetraploid *ASY1* allele (*ASY1 TTTT*). This is at odds with the scenario in *A. arenosa* neotetraploids, which were also likely to be homozygous for the diploid allele, in which extensive multivalent formation

and fertility reduction were observed (Yant *et al.,* 2013). *ASY1* is, however, only one of eight meiotic genes identified as having undergone strong ploidy specific differentiation (Yant *et al.,* 2013) and therefore it may be likely that diploid alleles of all eight co-evolved meiotic proteins would need to be present to exert such a significant effect as that witnessed in the neotetraploid.

A much more subtle meiotic phenotype compared to that observed in the neotetraploid was, however, observed in *ASY1 DDDD* lines. Extensive cytological examination of *ASY1 TTTT* and *ASY1 DDDD* lines, as well as heterozygous *ASY1 TxxD* lines and diploid lines from the SN *A. arenosa* accession, indicated that the tetraploid *ASY1* allele appears to shift CO localisation to a more distal position relative to the diploid allele. This was confirmed by separate analyses examining differences in the distribution of chiasma at M1 and the distances of MLH1 foci from the chromosome ends in pachytene cells. Analysis of chiasma in diploid lines and *ASY1 TxxD* lines also showed that the CO localisation in *ASY1 DDDD* plants was most similar to that seen in the diploid lines, whilst the CO localisation witnessed in *ASY1 TxxD* plants was highly similar to that seen in *ASY1 TTTT* plants, suggesting that the tetraploid allele exerts a dominant effect on CO position.

The mechanism that lies behind this shift in CO localisation still remains somewhat mysterious. As mentioned in sections 1.2.2 and 1.3.2, ASY1 appears to play an important role in ensuring the correct timing of meiotic DSB formation and in establishing IHB (Sanchez-Moran *et al.,* 2007, Kurzbauer *et al.,* 2012). It could be the case that amino-acid changes in chromatin binding HORMA or SWIRM domains between the diploid and tetraploid versions of ASY1 cause a change in the dynamics of ASY1 loading onto the chromosomes, such that the tetraploid protein binds preferentially to more distal regions than the diploid protein. This could promote DSB formation/IHB in distal regions earlier than in

other regions which could, in turn, encourage CO designation to occur at distal positions first. It has also been shown that in *asy1* mutants in *A. thaliana* there is a large drop in chiasma frequency and the few chiasma that remain in these lines tend to be very distal (Sanchez-Moran *et al.,* 2001). It could therefore also be the case that amino-acid changes in the tetraploid *A. arenosa ASY1* allele cause the protein to function less effectively, leading chiasma distribution to shift to a more distal position as seen in the *A. thaliana* mutant.

One other major question that arises from this finding is, assuming the tetraploid *ASY1* allele has evolved to help stabilise polyploid meiosis, how and why might a more distal CO position be beneficial in this context? Previous studies have indicated that distal chiasma are positively correlated with balanced segregation of quadrivalent chromosomes (Hazarika and Rees, 1967). Therefore, by shifting COs to a more distal position, the tetraploid *ASY1* allele may help to neutralise any negative effects quadrivalent formation would have on homologue segregation, encouraging stable division at anaphase I even in situations when quadrivalents form. There may also be other effects that the tetraploid *ASY1* allele exerts on the cell, but perhaps these changes are only relevant in the context of the tetraploid alleles of some of the other meiotic genes that undergo selection, some of the protein products of which have previously been shown to interact directly with ASY1 (*e.g.* ASY3, Ferdous *et al.,* 2012). It will be interesting in the future to examine what contributions, if any, some of these other meiotic alleles have on stabilising polyploid meiosis in *A. arenosa.*

Transgenic lines of *A. thaliana* were also generated that expressed either the diploid (SN) or tetraploid (HO) allele of *A. arenosa* in an *asy1* mutant background. Both lines appeared to undergo stable meiosis, and although no significant shift in CO localisation could be detected between the two lines there was a trend in the data indicating the HO *ASY1* lines could be experiencing more distal chiasma. The higher frequency of COs per chromosome and lower

overall number of chromosomes in *A. thaliana* relative to *A. arenosa* made utilising the same analytical methods previously used in *A. arenosa* much more difficult in *A. thaliana*. An interesting experiment to carry out in the future will be to treat plants from both lines with colchicine to generate neotetraploids and to determine whether the HO *ASY1* line has increased fertility and meiotic stability relative to the SN *ASY1* line.

4.3.2 Heterozygous *ASY1 TxxD* tetraploid *A. arenosa* may exhibit increased meiotic thermal tolerance compared to its homozygous counterparts

As diploid and tetraploid populations of *A. arenosa* inhabit distinct biogeographic regions it is also possible that environmental factors such as climate could play a role in shaping the strong signatures of selection observed between diploid and tetraploid *A. arenosa* (Yant *et al.*, 2013, Wright *et al.*, 2015). A temperature experiment, where different genotypes were exposed to 33^{o}C for 3 or 6 weeks, indicated that the heterozygous *ASY1 TxxD* line may exhibit startlingly superior thermal tolerance relative to the homozygous genotypes. This may also help to explain why the diploid *ASY1* allele still persists at low frequencies within tetraploid populations. This interpretation comes with the significant caveat that, due to difficulties encountered with genotyping, the *ASY1 TTTT* lines used could have been *ASY1 TxxD* and also it is important to note that the sample size of this investigation is very small. In the future, therefore, it will be worth repeating this experiment with a larger sample size and with a clearer idea of the genotypes involved. It will also be worth trying this experiment with transgenic *A. thaliana* lines that are heterozygous for the diploid and tetraploid *A. arenosa ASY1* alleles. *A. thaliana* would also have the advantage that it is self-compatible and therefore seed set could be used as a clear demonstration of fertility. Even if *ASY1* turns out not to be a factor in dictating meiotic thermal tolerance it is clear from this experiment that

some *A. arenosa* plants tolerate higher temperatures much better than others and it will be interesting to find out what other factors might lie behind this thermotolerance.

If future investigations do indicate that the heterozygous lines tend to be more thermotolerant than homozygous lines it is interesting to consider why this may be the case. One potential explanation could be that ASY1 protein aggregation, which appears to be a significant feature of lines with low meiotic thermotolerance, is disrupted by the presence of both *ASY1* alleles and their protein counterparts. Similar examples of heterozygous inhibition of protein aggregation have been described by Kobayashi *et al.,* (2009) to explain why humans heterozygous for the human prion protein gene PRNP are resistant to sporadic Creutzfeldt–Jakob disease.

These temperature experiments have also unearthed some interesting observations relating to ASY1 and ZYP1 behaviour at high temperature, with ladder-like ZYP1 polycomplexes appearing to connect large axis associated ASY1 aggregates. Similar observations were made by Loidl, (1989) examining the impact of high temperature on meiosis in *Allium ursinum* although this investigation was carried out using EM of silver stained spreads and therefore the identities of the proteins involved could not be determined. ASY1 aggregates have also been observed in *A. thaliana* grown at 32^{o}C for 3 days, although ZYP1 polycomplexes were not observed in this instance (West, 2015). How this behaviour relates to how these proteins function at normal ambient temperatures is unclear, although the preponderance for ZYP1 polycomplex self-assembly to initiate at ASY1 aggregation sites may indicate that ASY1 plays some role in mediating synapsis initiation and SC assembly. It is also unclear whether the ASY1 aggregations consist solely of ASY1 protein or whether these structures in fact represent an aggregation of all underlying axis-associated proteins.

ZYP1 polycomplexes also appear to consist of repeat units that are separated by a distance of approximately 460 nm, which differs from the 200-250 nm distance measured between lateral elements using SIM. This observation is at odds with findings from a previous study examining polycomplex formation in yeast overexpressing Zip1 where the distance between repeat units was found to match that between synapsed lateral elements (Sym and Roeder 1995). This result indicates that ZYP1 polycomplex structure in plants may differ to that found in yeast, although it is worth noting that the SIM measurements of lateral element width were taken from slides made with fresh material whereas polycomplex measurements were taken from slides made using fixed material and the difference could be related to different slide preparation methods.

4.3.3 Summary

In summary, we have demonstrated that a derived, tetraploid allele of *ASY1* has the ability to shift CO localisation to a more distal position in the model organism *A. arenosa* and suggest that this leads to autopolyploid meiotic stabilisation by encouraging stable, balanced segregation of quadrivalents at MI. We have also proposed a model for how ASY1 heterozygosity could lead to meiotic thermotolerance. If these findings are recapitulated through further work, both of these potential discoveries could have significant impacts on agricultural improvement that will be covered in the general discussion.

CHAPTER 5

RNAi KNOCKDOWN OF MEIOTIC AXIS GENE EXPRESSION IN *ARABIDOPSIS THALIANA*

5. RNAi knockdown of meiotic axis gene expression in *Arabidopsis thaliana*

5.1 Introduction

As mentioned in sections 1.2.2 and 1.3.2, ASY1 and ASY3 are interacting proteins that are both associated with the meiotic axis during prophase I. Studies utilising immunocytochemistry have indicated that ASY1 appears to play a role in establishing IHR, whilst ASY3 is important for meiotic DSB formation and promoting ASY1 axial association (Sanchez-Moran *et al.,* 2007, Ferdous *et al.,* 2012). More recently, EM and SIM analysis of ASY1 behaviour in the leptotene substage of meiosis in *A. thaliana* has indicated that ASY1 may exhibit domain-like organisation along the axis (Lambing *et al.,* 2015, Ferdous *et al.,* 2012) and the hyper-abundant domains show close-association with both γH2AX and DMC1 foci (Ferdous *et al.,* 2012). Beyond these initial observations, relatively little is still known about how these two proteins mediate their functions in *A. thaliana* and what molecular mechanisms are involved. In chapter four we demonstrated that different alleles of *ASY1* affected CO distribution in the model tetraploid *A. arenosa*, and it is interesting to consider what other hidden functions might be unearthed following different perturbations to protein structure, function or expression.

One method that has previously been used extensively to alter levels of gene-expression in plants is RNA-interference (RNAi). RNAi was initially observed during the late 1980s when it was found that plants had an innate ability to silence the expression of T-DNA transgenes (Matske *et al.,* 1989). Since these initial discoveries, RNAi silencing using self-complimentary sense-antisense RNA transcripts has been used for a wide variety of reverse genetics studies and crop improvement strategies (reviewed in Eamens *et al.,* 2008). Sense-

antisense transcripts produce double stranded RNAs which are cleaved by Dicer-like proteins (DCL) to generate 21 or 24 nucleotide long short-interfering RNAs (siRNAs). siRNAs then combine with Argonaute proteins to generate an RNA-induced silencing complex (RISC) which mediates target mRNA cleavage and degradation (reviewed in Ghildyal & Zamore, 2009).

In this study we have utilised sense-antisense transcripts in transgenic *A. thaliana* lines to produce plants with knocked-down expression of *ASY1* and *ASY3*. By examining meiotic behaviour in plants with different levels of protein expression we aimed to uncover more information about how these proteins might function. We also generated colchicine induced neotetraploid lines from some of these RNAi lines, as well as from a *pch2-1* mutant, to determine what effect reduced chiasma formation might have on autotetraploid meiotic stabilisation.

5.2 Results

5.2.1 Binary vectors were constructed for targeted RNAi knockdown of genes *ASY1* and *ASY3* in *A. thaliana*

Sense-antisense RNAi constructs were designed to target the meiotic axis-associated proteins ASY1 and ASY3. Gene specific sequences of about 700bp were selected near to the 5' end of each of the target gene's coding sequences for the generation of each sense-antisense construct for efficient gene silencing using RNAi (Wesley *et al.*, 2001). These ~700bp target sequences were amplified from *A. thaliana* bud cDNA as described in the materials and methods, using primers containing restriction site adaptor sequences for cloning into the vector pHannibal. CaMV 35S- sense-intron-antisense-*OCS* terminator cassettes from pHannibal targeting *ASY1 and ASY3* were then cloned into pART27, a binary vector

containing the *NPTII* Kanamycin resistance gene, for plant transformation. ASY1 and ASY3 are both thought to fulfil meiosis-specific functions (Sanchez-Moran *et al.*, 2007; Ferdous *et al.*, 2012; Borner *et al.*, 2008) and, therefore, the constitutive CaMV 35S promoter was used to confer expression of the RNAi silencing gene products in all plant tissues, including those undergoing meiosis.

Previous work has demonstrated that the CaMV 35S promoter is less effective at producing severe gene knockdowns during meiosis (Stevens *et al.*, 2004) compared to the meiosis specific *DMC1* promoter. However, for the purposes of this investigation, where a partial gene knockdown, as opposed to a more severe 'knockout-like' knockdown, is required it was felt that the CaMV 35S was a suitable promoter. Cloning steps are summarised in figure 5.1.

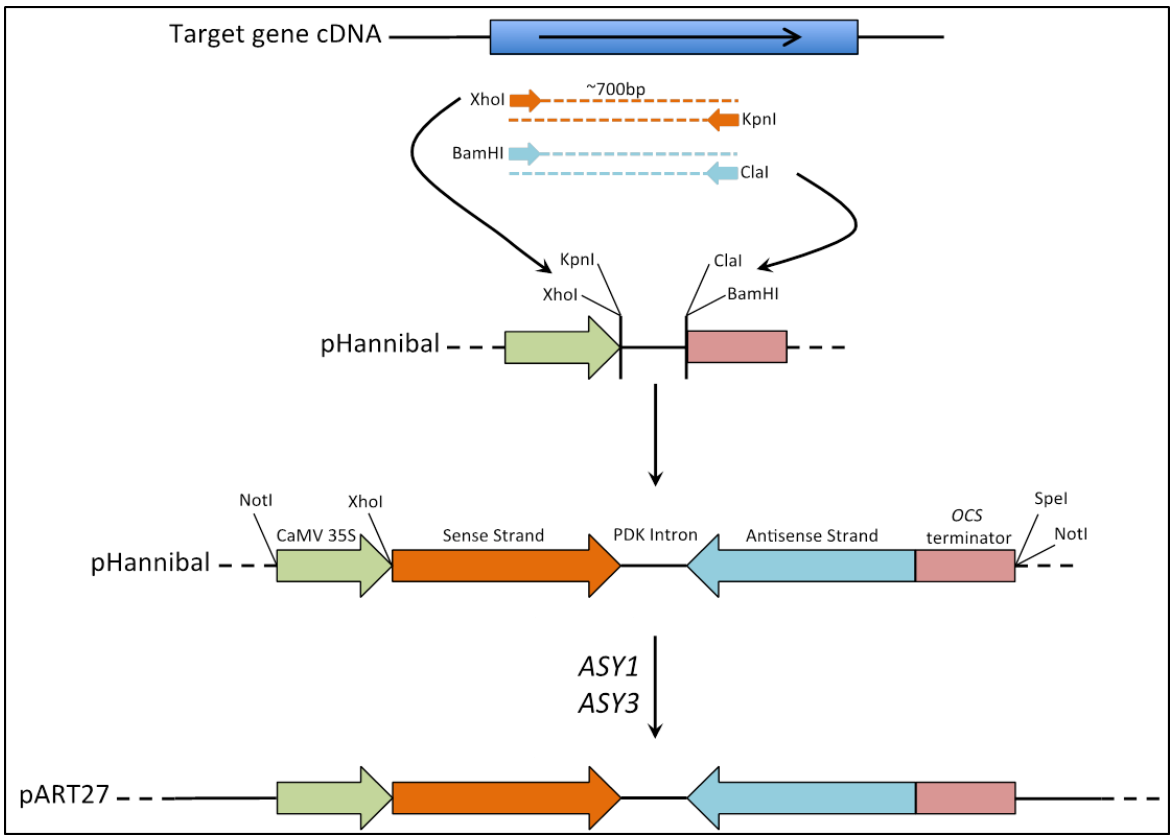

Figure 5.1. Strategy for cloning RNAi constructs. ~700bp sense and antisense strands were amplified from wild-type bud cDNA and cloned into binary vectors via restriction-ligation cloning. Modified from Wesley et al., 2001.

5.2.2 *ASY1* and *ASY3* RNAi lines exhibit a range of reduced fertility

Transgenic T1 plants were obtained containing the constructs pART27::*ASY1* RNAi and pART27::*ASY3* RNAi following transformation via *Agrobacterium* mediated floral dipping of Col-0 plants and kanamycin selection (figure 5.2A). Stable homozygous T3 populations were obtained for numerous lines exhibiting knocked-down expression of *ASY1* and *ASY3.*

The majority of *ASY1* RNAi plants were observed to have reduced silique length compared to wild-type Col-0 (figure 5.2B), a typical sign of reduced fertility in *A. thaliana.* Many *ASY3* RNAi plants were also observed to have slightly shorter silique lengths compared to wild-type.

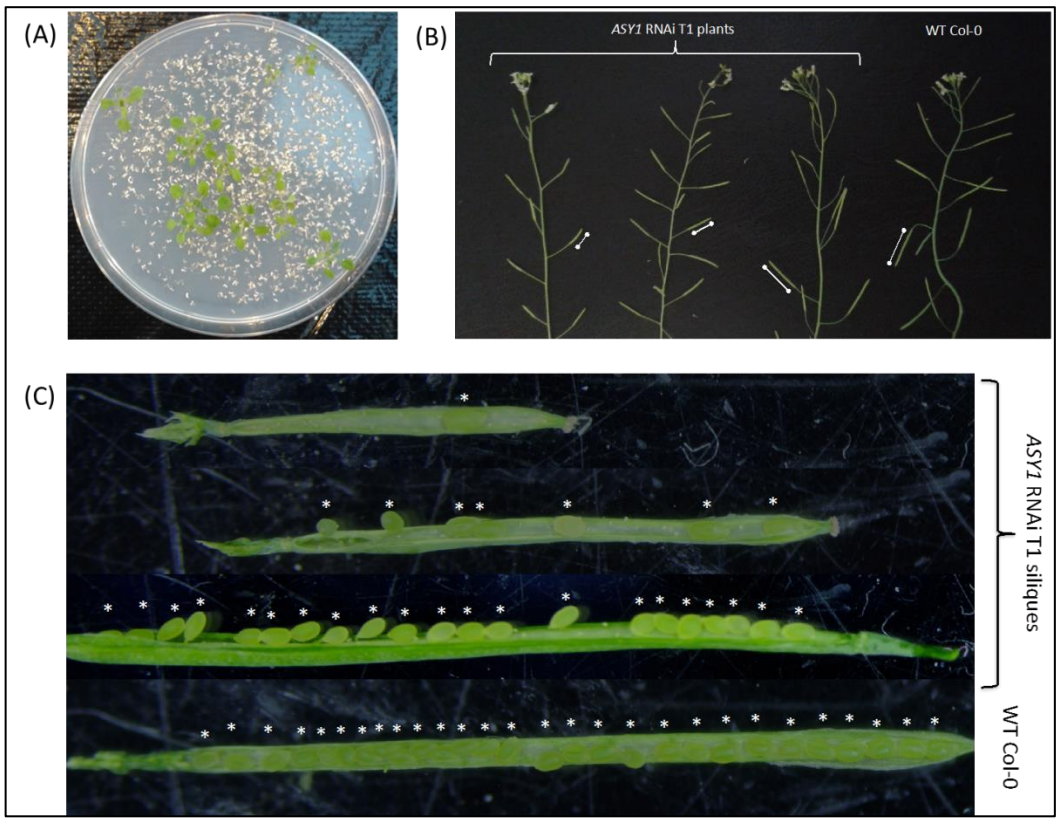

Figure 5.2. ASY1 RNAi lines have reduced fertility. Transgenic plants containing the pART27::ASY1 RNAi construct were selected by growth on kanamycin media (A). ASY1 RNAi T1 plants exhibited a range of reduced silique length (B) and seed set (C).

To determine a more quantitative measurement of fertility, the number of seeds found per silique was counted for a number of T3 plants from each line. Seed counts were also performed for wild type Col-0 and *asy1-1* and *asy3-1* T-DNA mutants for comparison (figure 5.3, table S11). The most likely explanation for a reduced number of seeds per silique in this instance would be due to problems encountered during female meiosis, such as chromosome missegregation, which could result in improper egg formation and aborted seed development leading to silique 'gaps'.

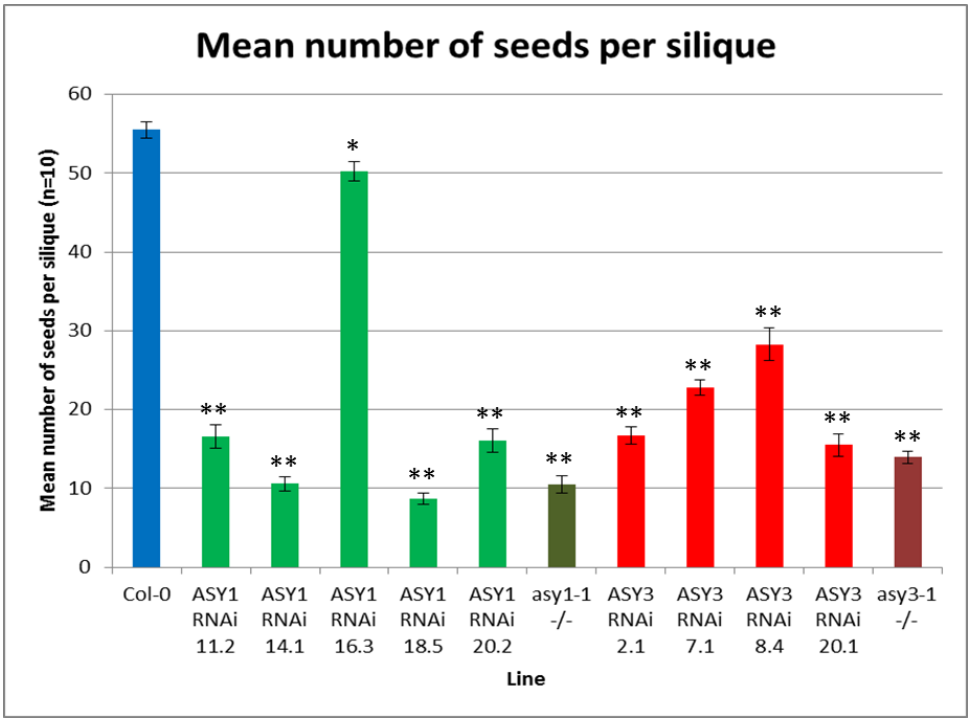

Figure 5.3. Seed counts from wild type Col-0, ASY1 RNAi and ASY3 RNAi homozygous T3 lines and asy1-1 and asy3-1 T-DNA mutants. Asterisks indicate a significant reduction in seed set compared to Col-0 calculated using an independent two-sample t.test (* p<0.01, **p<0.001). Error bars show +/- S.E.

Seed counts showed that all the RNAi lines experienced a significant reduction in seed set compared to wild-type Col-0 (p<0.01), with many lines exhibiting a highly significant reduction (p<0.001) calculated using an independent two-sample t.test. Some *ASY1* RNAi plants experienced less than 20% of the wild type level of fertility (e.g. line 18.5), which is

consistent with the level of fertility observed in *asy1-1* T-DNA knockout lines (Caryl *et al.*, 2000). Other lines showed an intermediate level of fertility, in between that of the *asy1* mutant and wild-type (e.g. line 11.2 had 30% and line 16.3 had 90% wild-type level of fertility). It is worth noting that, although *ASY1* RNAi line 16.3 did appear to have a significant reduction in seed set, siliques were still full of seeds (i.e. there were no gaps), which indicates that the reduction in seed number may not have reflected problems encountered in fertility.

Seed counts also demonstrated that many *ASY3* RNAi lines exhibited a reduction in fertility. Again, some *ASY3* RNAi lines experienced a 'knockout-like' reduction in fertility to about 28% of wild type levels and other lines had a more intermediate phenotype (e.g. line 8.4 had 50% wild type fertility).

5.2.3 *ASY1* and *ASY3* RNAi lines exhibit a range of reduction in meiotic CO number

In order to determine the number of meiotic COs occurring in each RNAi line, DAPI spreads of metaphase I (MI) chromosomes were generated and chiasma frequency was analysed. The number of COs can be inferred from the conformation of the *A. thaliana* MI bivalents, with rod shaped bivalents having a single CO and ring shaped bivalents having two or more COs (Sanchez-Moran *et al.*, 2001). The presence of univalents indicates a failure in CO assurance and a lack of COs between homologous chromosome pairs. The numbers of pairs of univalents per MI cell was recorded for each line (figure 5.4A, table S12).

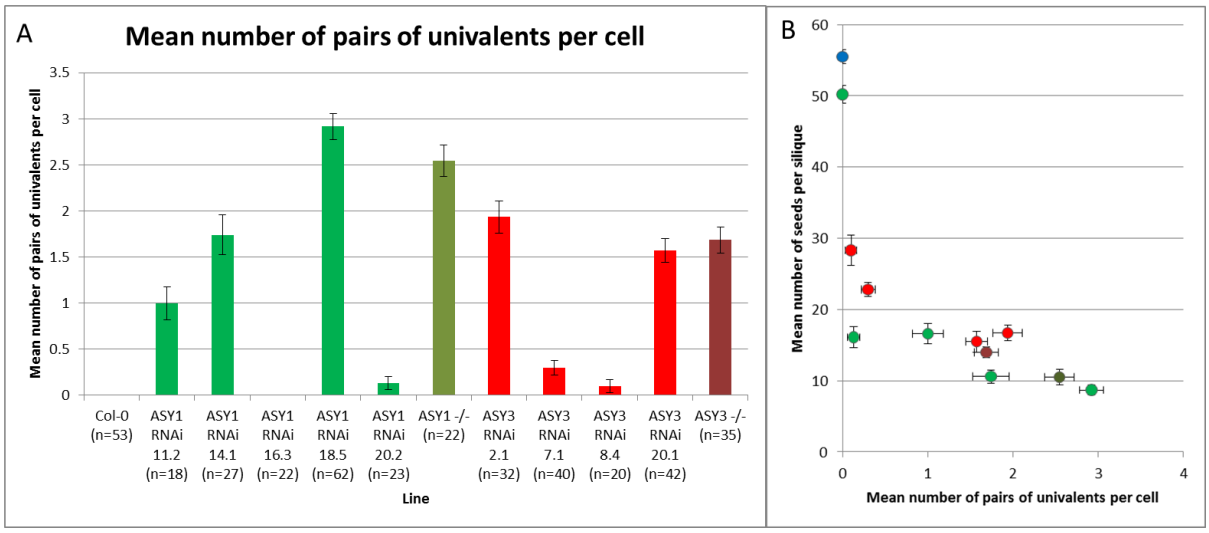

Figure 5.4. (A) Bar chart showing the mean number of pairs of univalents per M1 cell for Col-0, ASY1 RNAi, ASY3 RNAi, asy1-/- and asy3-/- lines. (B) Dot plot showing the relationship between the frequency of univalents and reductions in seed set for Col-0 (blue dot), ASY1 RNAi (bright green dots), ASY3 RNAi (bright red dots), asy1-/- (dark green dot) and asy3-/- (dark red dot) lines. Error bars = +/- S.E.

M1 chromosomes from *ASY1* RNAi lines are shown in figure 5.5. All lines apart from lines 16.3 appeared to show obvious meiotic defects as indicated by the presence of univalent chromosomes. However, the frequency of univalent formation, and hence total CO frequency, varied between different lines. Unsurprisingly, there appeared to be a correlation between a lower fertility and an increased frequency of univalent formation. This indicates that fertility in this context can be used as a reasonably reliable indication of meiotic stability, with lines experiencing decreased meiotic stability also exhibiting decreased fertility. For instance, line 18.5 appeared to have the lowest seed set of all the *ASY1* RNAi lines (16%) and had the highest frequency of univalent formation (an average of 2.9 pairs of univalents per cell), which an independent two-sample T.Test revealed was not significantly different from the *asy1-1* univalent frequency (2.5 pairs of univalents per cell, $p=0.098$) suggesting this line has a 'knockout' like phenotype. Interestingly, the relationship between increased univalent formation and reduced fertility did not appear to be entirely linear (figure 5.4B). For instance, in *ASY1* RNAi line 20.2 the mean number of pairs of univalents per cell was 0.13 (+/- 0.07),

which means only 13% of MI cells would contain univalents, and yet fertility in this line dropped by 70% compared to wild-type. As a similar pattern is observed for *ASY3* RNAi lines, this discrepancy could suggest that the 35S promoter used in this study is more active in female meiocytes than male meiocytes, which would result in a bigger reduction in *ASY1* or *ASY3* activity during female meiosis, causing a higher frequency of univalent formation and a proportional reduction in fertility. Another explanation is that chiasma frequency has previously been reported as being lower in female MI cells (8.5 chiasma per cell) compared to male MI cells (9.7 chiasma per cell) in *A. thaliana* (Armstrong and Jones 2000). Therefore, as there are fewer COs in female meiocytes in the first place an equal reduction in *ASY1* or *ASY3* expression could cause a similar reduction in CO numbers which would result in a greater frequency of univalents.

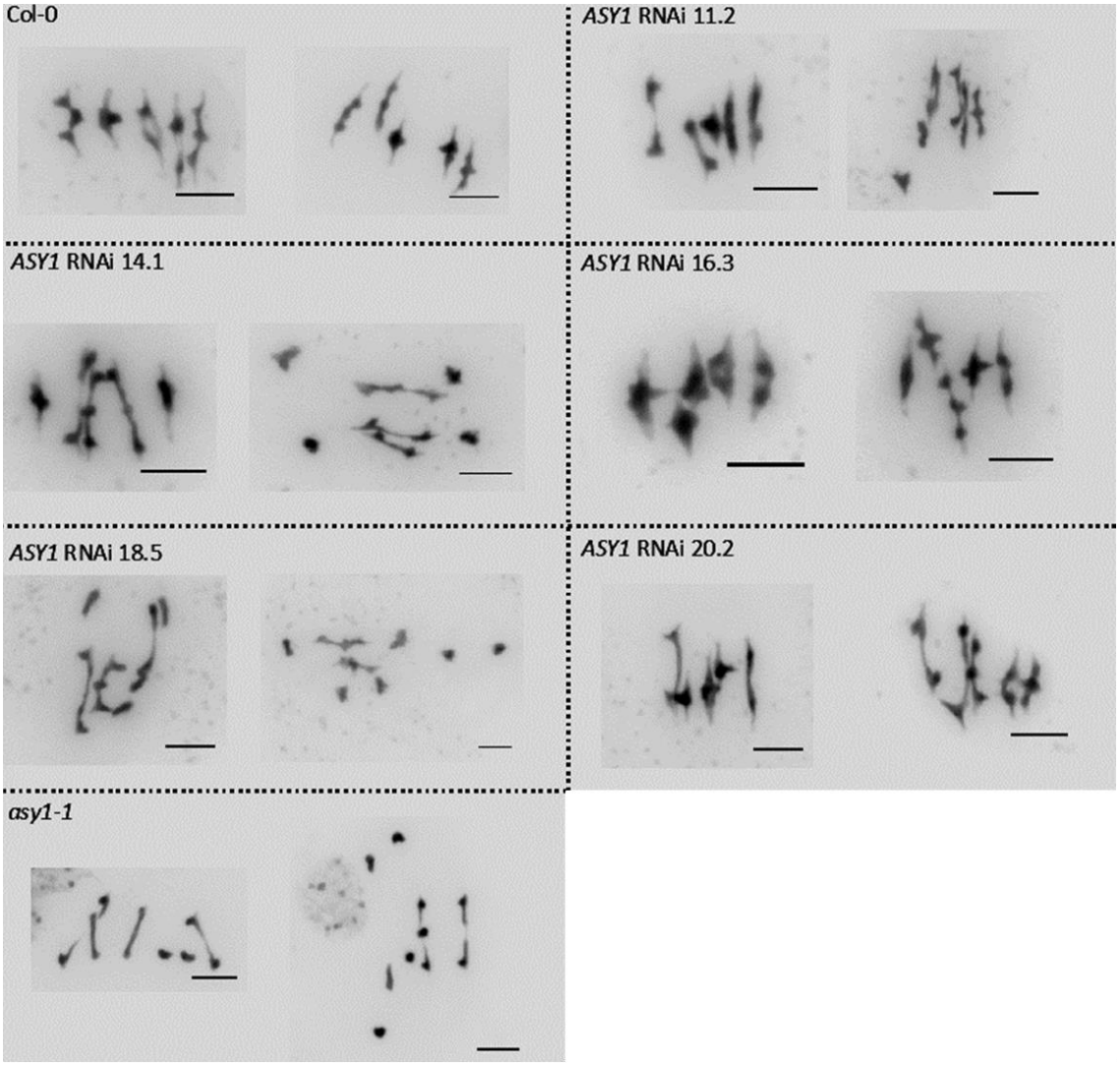

Figure 5.5. MI DAPI spreads from Col-0, different ASY1 RNAi lines and the asy1-1 T-DNA insertion mutant. Scale bars = 5 µm

A similar situation was observed in the *ASY3* RNAi lines, with MI cells from different lines displaying a range of reduced CO numbers with a non-linear correlation between an increase in univalent formation and a reduction in fertility (figure 5.6). For instance, line *ASY3* RNAi 2.1 experienced very low fertility (30%) and there was a high frequency of univalent formation observed in all MI spreads (1.9 pairs of univalents per cell) that did not statistically differ from the frequency of univalents in the *asy3-1* mutant as shown by an independent two-sample T.Test (1.7 pairs of univalent per cell, $p = 0.264$). This suggests line *ASY3* RNAi 2.1 had a 'knockout' like phenotype.

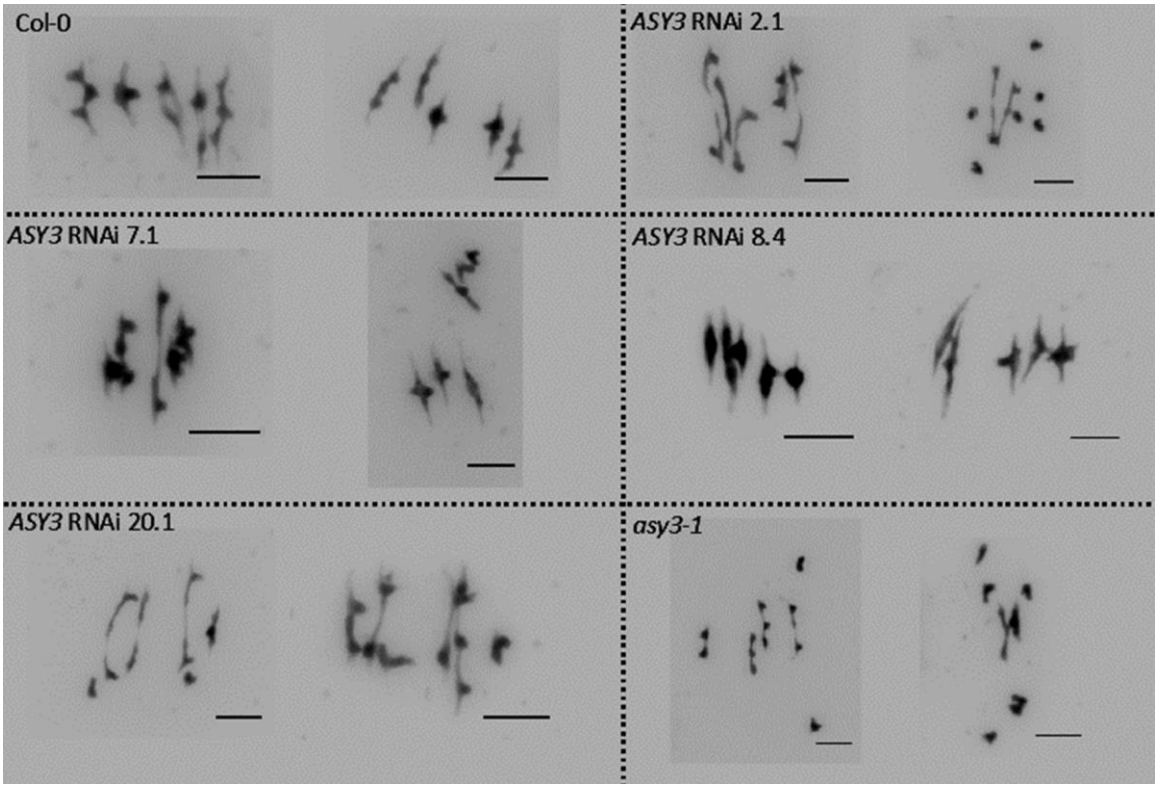

Figure 5.6. MI DAPI spreads from Col-0, different ASY3 RNAi lines and the asy3-1 T-DNA insertion mutant. Scale bars = 5 µm

5.3.4 *ASY1* and *ASY3* RNAi lines undergo differing levels of synapsis

In order to determine whether *ASY1* and *ASY3* RNAi lines underwent complete synapsis during prophase I of meiosis, immunolocalisation experiments were performed on fixed material using antibodies against the meiotic axis associated protein ASY1 and the SC lateral element protein ZYP1. In cells that undergo complete synapsis ZYP1 should form two parallel linear signals along the entire lengths of all chromosomes.

Different *ASY1* RNAi lines appeared to undergo differing levels of synapsis (figure 5.7). There appeared to be a correlation between higher fertility, higher CO number and an increased level of homologue synapsis. For instance, no cells were found to undergo complete synapsis from line 14.1 (Fertility = 19%), however one cell was found to be completely synapsed in line 11.2 (Fertility = 29%).

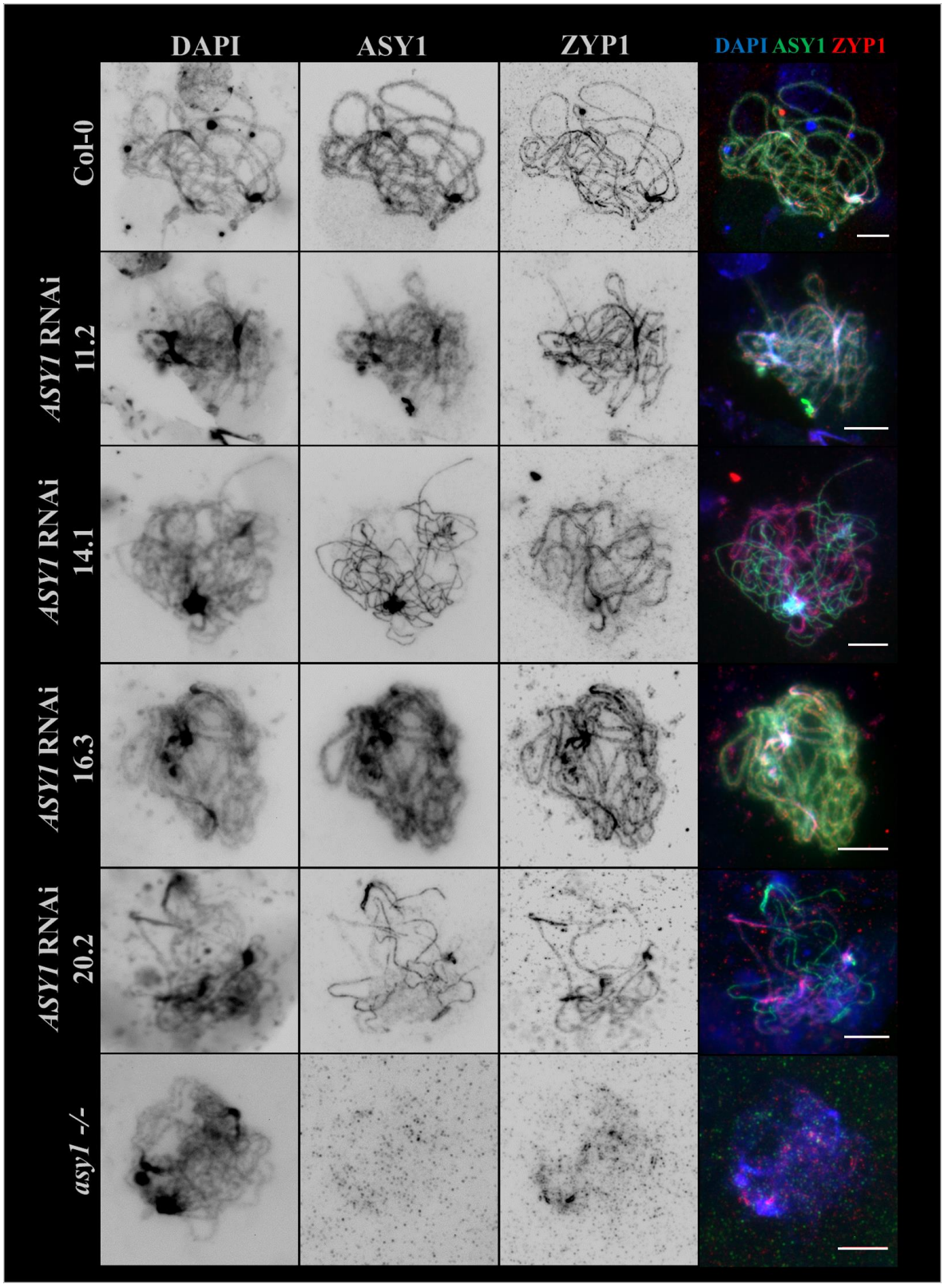

Figure 5.7. Immunolocalisation of ASY1 (green) and ZYP1 (red) in Col-0, ASY1 RNAi and asy1-1 prophase I nuclei. DNA is stained with DAPI (blue). Scale bars = 5 µm.

Interestingly, all *ASY1* RNAi lines appeared to exhibit a reasonable degree of axis associated ASY1 signal. No ASY1 signal, however, was observed in the *asy1-1* knockout mutant, although some very short stretches of synapsis were observed in the mutants as indicated by parallel linear ZYP1 signals. The detection of AtASY1 signal is all RNAi lines suggests that no lines experienced a complete knockout of *ASY1* expression, although immunolocalised prophase I cells from line 18.5, which had a similar fertility and univalent frequency to the *asy1-1* mutant, were not obtained. This indicates that axial localisation of ASY1 protein in itself is insufficient for ASY1 protein to mediate its function and that a sufficient level of ASY1 must be reached for ASY1 to carry out its role properly.

Different *ASY3* RNAi lines also appeared to undergo differing levels of synapsis (figure 5.8). Again, there was a correlation between increased fertility, increased CO number and increased synapsis. For example, line 2.1 (fertility = 30%) only had very short regions of synapsis, whilst line 7.1 (fertility = 41%) had very long regions of synapsis but did not undergo full synapsis and line 8.4 (Fertility = 50%) underwent full synapsis.

ASY1 localisation appears defective in the *asy3-1* mutant, with the protein appearing to form numerous diffuse axis associated foci in both synapsed and unsynapsed regions, as opposed to the normal linear signal found in the unsynapsed axis regions of wild-type plants. A similar phenotype was found in line 2.1, where ASY1 appeared as diffuse foci as opposed to a strong linear signal. In line 7.1, however, where synapsis was also defective, ASY1 localisation appeared normal, forming a linear signal on unsynapsed axial regions. It may be the case, however, that although there is axis associated ASY1 present in these cells, it is in insufficient quantity to carry out its function in a similar manner to the *ASY1* RNAi lines.

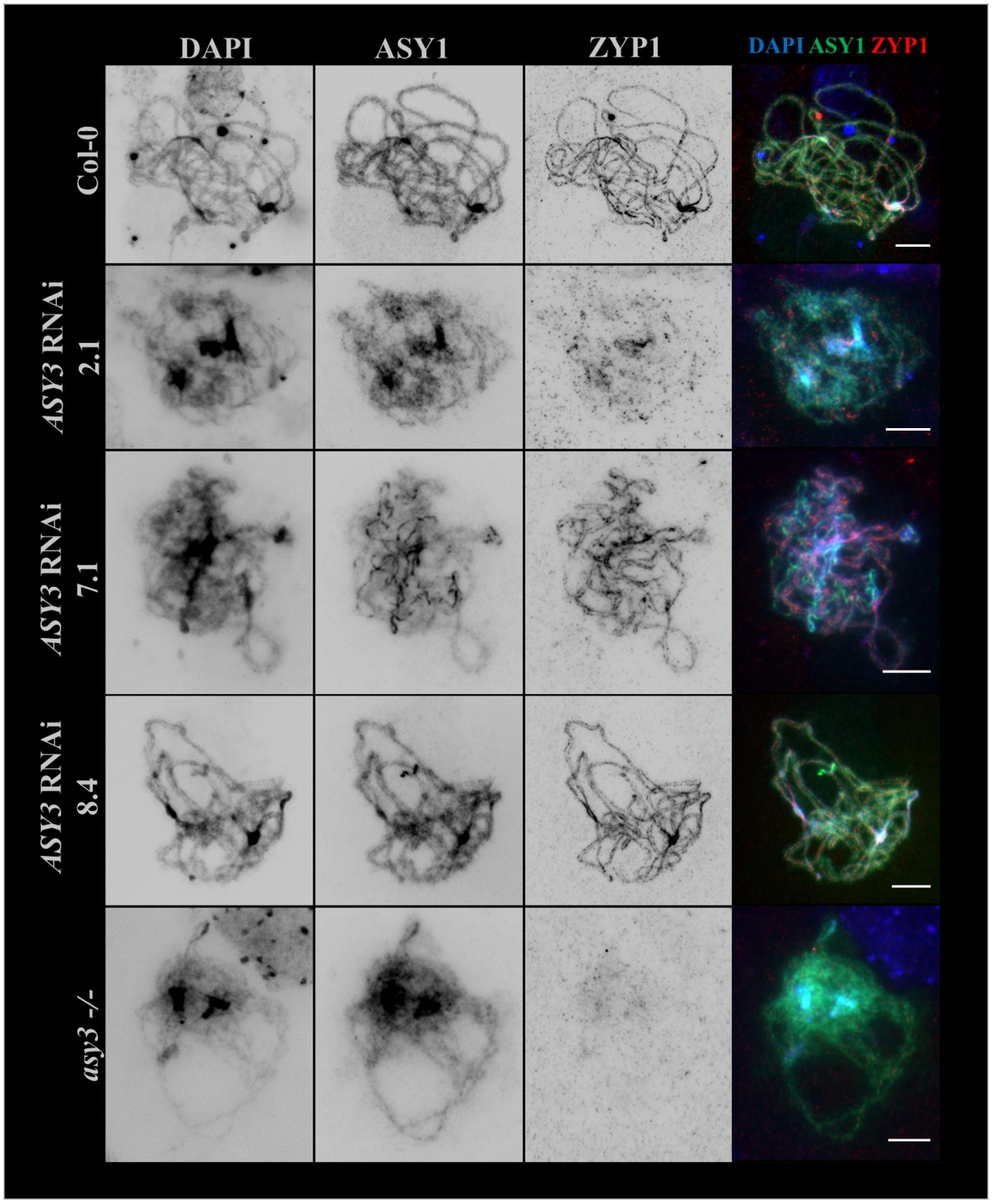

Figure 5.8. Immunolocalisation of ASY1 (Red) and ZYP1 (green) in Col-0, ASY3 RNAi and asy3-1 prophase I nuclei. DNA is stained with DAPI (blue). Scale bars = 5 µm.

5.2.5 Neotetraploid lines were generated from lines exhibiting reduced CO numbers

Previous work in *A. arenosa* has indicated that plants from an established autotetraploid population have a lower CO frequency relative to plants from the diploid population and that this may contribute to increased autopolyploid meiotic stabilisation (Yant *et al.,* 2013). It was therefore hypothesised that neotetraploids, generated via colchicine treatment, of *A. thaliana* lines experiencing a slightly reduced frequency of COs relative to wild-type Col-0 might also exhibit increased meiotic stability. As the RNAi lines generated during this study appeared to experience a range of reduction in CO numbers they stood-out as good candidates for generating neotetraploids to test this hypothesis. Another meiotic mutant that has a, comparatively, small reduction in meiotic CO numbers without simultaneously affecting vegetative growth is *pch2-1*. As mentioned in section 1.3.2, PCH2 is required for ASY1 removal from synapsed areas and in *pch2* mutants pairs of univalent chromosomes are observed in 10% of MI cells (Lambing *et al.,* 2015), which is equal to the number observed in line *ASY3* RNAi 8.4.

Col-0, *ASY1* RNAi, *ASY3* RNAi and *pch2* plants were therefore treated with colchicine as described in the materials and methods. From all the plants treated, neopolyploid lines were only obtained from Col-0, ASY3 RNAi 20.1 and *pch2-1* lines. The polyploid progeny from the lines treated with colchicine are referred to as the C1 generation. One reason that neopolyploids were only obtained from a relatively small number of lines may be that the colchicine concentration used in this study wasn't quite high enough to induce polyploidisation in all lines, or possibly that some plants were treated with colchicine at the incorrect developmental timepoint.

From the lines that successfully gave rise to polyploids, DAPI stained slides were made from

acid-fixed meiocytes from the C1 generation plants. It was noted that, due to meiotic errors encountered in the neotetraploids, coupled with these plants' ability to happily cope with single chromosome losses, many of the plants screened in this manner turned out to be aneuploid. Tetraploid plants were obtained for both the Col-0 and *pch2-1* lines, but only aneuploid lines were observed in the *ASY3* RNAi 20.1 C1 line. Figure 5.9 shows MI spreads from tetraploid Col-0 and *pch2-1* C1 lines (n=20) and from an aneuploid *ASY3* RNAi 20.1 C1 line (n=21).

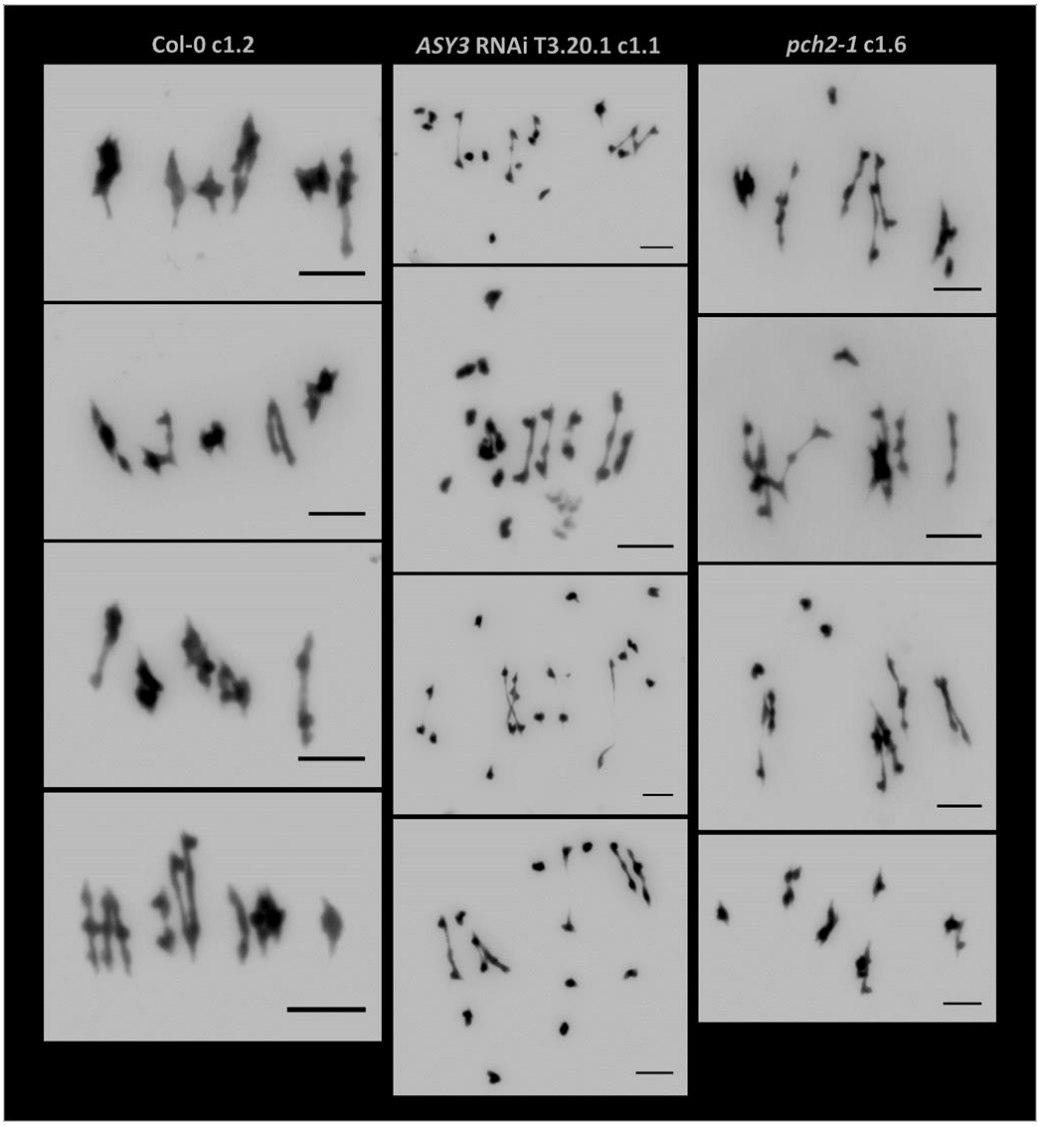

Figure 5.9. DAPI stained MI cells from Col-0 C1.2, ASY3 RNAi 20.1 C1.1 and pch2-1 C1.6 plants.

For each of the lines the number of univalent, bivalent, trivalent and quadrivalent chromosomal configurations per cell was counted and the number of seeds per silique was also counted for the neotetraploids and from diploid plants from each line (figure 5.10, table S13 and S14). Unsurprisingly there was a significant reduction in fertility between the diploid and neotetraploid Col-0 lines (independent two sample T.Test, p = 1.03961E-11), which correlated with an increase in univalent and multivalent frequency. Interestingly, there was a slight but not quite significant increase in fertility between the *ASY3* RNAi 20.1 diploid and tetraploid lines (two-sample T.Test p = 0.067). However, given that the expression of the RNAi cassette may vary in the neotetraploid relative to the diploid it cannot be confirmed whether this difference is solely due to the decrease in CO numbers or due to a weakened silencing of the *ASY3* gene. For the *pch2-1* mutant the fertility levels did not vary between the diploid and neotetraploid plants (two-sample T.Test p = 0.763), however the fertility of the neotetraploid *pch2-1* plant was still significantly lower than that of the neotetraploid Col-0 plant (independent two-sample T.Test, p = 0.011) indicating that the *pch2-1* C1 line does not exhibit increased meiotic stability relative to the Col-0 C1 line. The *pch2-1* mutant experiences an average reduction of 2.6 chiasma per cell compared to Col-0 (Lambing *et al.*, 2015), and thus it would appear a reduction in chiasma frequency of this magnitude is too large to confer meiotic stabilisation to neotetraploid lines. It will be interesting to try this experiment again if any meiotic T-DNA mutants are discovered in the future that exhibit a less severe reduction in chiasma frequency without an accompanying vegetative phenotype.

Another interesting observation that arises from this experiment is that the *pch2-1* C1.2 lines have a univalent frequency (mean = 2.5 univalents per cell) that is much greater than double the diploid *pch2-1* univalent frequency (mean = 0.2 univalents per cell, Lambing *et al.*, 2015). This increase is likely due to an increase in trivalent-univalent combinations that are present

in the neotetraploids that cannot form in the diploid lines. The higher frequency of COs in the Col-0 C1 line may prevent trivalent-univalent combinations from forming, which are thought to be more damaging to meiotic stability than quadrivalents (Bomblies *et al.*, 2016).

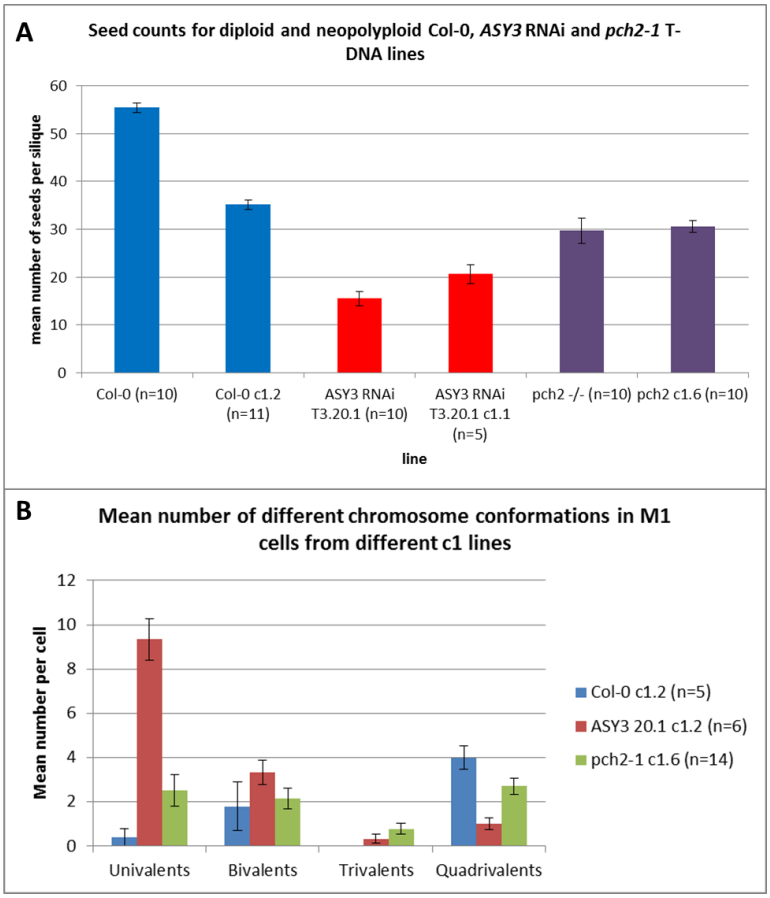

Figure 5.10. (A) Seed counts from diploid and tetraploid lines of Col-0, ASY3 RNAi 20.1 and pch2-1. (B) The mean number of different chromosomal conformations in M1 cells from different neopolyploid lines. Error bars = +/- S.E.

5.3 Discussion

Thus far, this study has demonstrated that stable homozygous T3 knockdown lines have been generated in the model plant *A. thaliana* targeting the genes *ASY1* and *ASY3.* All T3 plants analysed exhibited a decreased level of fertility, with many showing signatures of defective CO formation and synapsis during meiosis. We have also shown that a small but significant reduction in chiasma frequency in *A. thaliana* does not necessarily lead to any benefits in neotetraploid meiotic stabilisation.

5.3.1 *ASY1* and *ASY3* knockdown reveals that a reduction in CO formation and synapsis occurs in the presence of axis associated ASY1

ASY1 has previously been shown to be required for meiotic homologue synapsis and normal levels of CO formation in *A. thaliana.* Immunolocalisation experiments have also shown that the protein localises to unsynapsed regions of the meiotic axis as a linear signal consisting of alternating high and low intensity hyper-abundant domains (Sanchez-Moran *et al.,* 2007, Lambing *et al.,* 2015) and the protein is thought to play an essential role in promoting IHR over inter-sister repair, thereby encouraging CO formation. In *ASY1* RNAi knockdown lines, thought to reduce ASY1 protein expression, some lines appear to display normal localisation of ASY1 to the meiotic axis and yet CO formation and synapsis is still defective. ASY3 has also been shown to have an essential role in ASY1 localisation, with *asy3* mutants displaying defective ASY1 localisation. Here, we have shown that in some *ASY3* RNAi lines, where ASY1 appears to localise normally to unsynapsed regions, this localisation is not sufficient to ensure that CO formation and synapsis occur in a non-defective manner. It will be interesting to examine in the future how the localisation of ASY3 is affected in these RNAi lines.

In *S. cerevisiae,* the ASY1 homologue Hop1 has also been shown to localise to the meiotic

axis in hyperabundant domains (Borner *et al.,* 2008). Perhaps depletion of ASY1 effects this domain-like organisation, compromising ASY1's function in IHR imposition. Future work will include a deeper investigation into the effects of *ASY1* knockdown on the localisation of ASY1 to the axis, possibly via super-resolution microscopy. It will also be interesting to examine what other proteins co-localise with ASY1 or ASY3 in these knockdown lines to help further dissect what other proteins they might interact with, either directly or indirectly, *in vivo.*

It is also important to note that, in this study, a reduction in ASY1 and ASY3 protein expression has only been inferred from a reduced fertility phenotype and from immunolocalisation experiments and therefore, in the future, it will be important to carry out further experiments such as qPCR and western blotting to quantifiably demonstrate that gene and protein expression has been reduced in these lines.

5.3.2 A small but significant drop in chiasma frequency is insufficient to confer increased meiotic stabilisation to neotetraploid *A. thaliana*

In established, naturally evolved autotetraploid *A. arenosa* there is a reduced chiasma frequency relative to diploid *A. arenosa* (Yant *et al.,* 2013). It is hypothesised that this reduction in chiasma frequency stabilises autopolyploid meiosis by inhibiting multivalent frequency and promoting stable bivalent-like pairing. We therefore set out to determine if a small reduction in meiotic CO numbers in *A. thaliana* could increase meiotic stability, and hence fertility, in neotetraploids generated via colchicine treatment.

Neotetraploid lines were therefore generated from an *ASY3 RNAi* line and the *pch2-1* mutant, which has been shown to experience an average of 6.9 chiasma per cell as opposed to the 9.7 experienced in Col-0 (Lambing *et al.,* 2015). Interestingly, the relative chiasma frequency per

chromosome in the *pch2-1* mutant (1.38 chiasma per pair of chromosomes) is still greater than the chiasma frequency in tetraploid *A. arenosa* (~1.06 chiasma per pair of chromosomes, section 4.2.3 and Yant *et al.*, 2013) and yet the *pch2-1* neotetraploid has a significantly lower fertility than the Col-0 neotetraploid, indicating meiosis is less stable in the *pch2-1* neotetraploids. It is likely that this is due to an increase in trivalent-univalent combinations in the *pch2-1* neotetraploid compared to the Col-0 neotetraploid. This goes to show that a simple reduction in meiotic chiasma frequency is, in itself, insufficient to confer increased meiotic stabilisation in neotetraploids. It is therefore becoming increasingly apparent that a number of other factors, as well as reduced CO frequency, must be in place to ensure meiotic stabilisation. These factors most likely include an increase in the strength of CO interference (Bomblies et al., 2016) and an accompanying shift in CO localisation (section 4.2.4).

5.3.3 Summary

To summarise, we have generated *ASY1* and *ASY3* RNAi knockdown lines as well as neotetraploids exhibiting reduced chiasma frequencies in *A. thaliana.* The RNAi lines will provide a good foundation for further work examining the molecular behaviour of ASY1 and ASY3 using a combination of immunolocalisation and super-resolution microscopy. It will also be important to carry out experiments that will allow the level of knockdown to be quantified more accurately, for instance by utilising qPCR or western blotting. Although neotetraploid lines with a reduced chiasma frequency did not exhibit increased meiotic stabilisation, they have helped to emphasise that adaptation to autopolyploidisation most likely requires a number of complementary mechanisms, working together to prevent univalent formation, to minimise multivalent formation and to encourage stable segregation of multivalents as and when they do occur.

CHAPTER 6
GENERAL DISCUSSION

6. General discussion

6.1 Introduction

During this study we have described numerous experiments that were conducted within the model organisms *A. thaliana* and *A. arenosa*, which address the topics of autopolyploid meiotic stabilisation and meiotic axis protein function. We will now further discuss how all of these combined experiments have contributed to our knowledge within these key areas and, also, how these findings could impact upon efforts to facilitate crop improvement and advance current plant breeding technologies.

6.1.1 Autopolyploid meiotic stabilisation

Autopolyploids have been cytologically investigated in a variety of contexts during this study. Firstly, we have looked at the general meiotic behaviour of autotetraploid meiosis during both prophase I and metaphase I in the model species *A. arenosa*. Secondly, we have observed how meiosis differs in autotetraploid *A. arenosa* lines expressing different *ASY1* alleles. Thirdly, we have investigated how meiosis progresses and how fertility is affected in neopolyploid lines of *A. thaliana* exhibiting reduced chiasma frequencies.

The initial observations in autotetraploid *A. arenosa* have helped to shed light on some of the challenges that are faced during autopolyploid meiosis and also emphasise that, even in an established autotetraploid species like *A. arenosa*, meiotic problems are still encountered with a reasonable degree of frequency. For instance, we have shown that ring quadrivalents persist in 11% of autotetraploid *A. arenosa* metaphase I cells and that aneuploid *A. arenosa* lines still frequently arise from within the autotetraploid population. In addition to this, we used super-resolution microscopy to reveal that SPS sites are often present in pachytene cells from autotetraploid *A. arenosa* and that the SC transverse filament protein ZYP1 exhibits novel

behaviour at these SPS sites by appearing to form a bipartite SC structure associated with only a single lateral element.

However, alongside identifying the challenges encountered during autopolyploid meiosis, we have also gathered evidence that indicates how established autotetraploids might act to limit the effect that these challenges have on overall meiotic stability. For instance, it is hypothesised that the novel ZYP1 behaviour at SPS sites may represent an intermediate structure that is formed during the process of SPS resolution. We have also demonstrated that a tetraploid allele of the meiotic axis gene *ASY1,* that appears to have undergone strong ploidy specific differentiation, acts to shift CO localisation to a more distal position along the chromosomes relative to the diploid allele. It is suggested that this aids autotetraploid meiotic stabilisation by promoting balanced segregation of quadrivalent chromosomes which, as mentioned earlier, are still regularly observed in MI cells from autotetraploid *A. arenosa.* Previous studies have also indicated that autotetraploid *A. arenosa* experiences a reduction in chiasma frequency compared to diploid *A. arenosa* and it has been suggested that this helps to stabilise autotetraploid meiosis by preventing multivalent formation (Yant *et al.,* 2013). We therefore generated neotetraploids from Col-0, *pch2.1* and *asy3* RNAi lines in the more commonly used model plant *A. thaliana*. The *pch2.1* and *asy3* RNAi lines experienced mild and severe reductions in chiasma frequency, respectively. This experiment indicated that a mild or severe reduction in chiasma frequency is insufficient to stabilise polyploid meiosis, with both the *pch2.1* and *asy3* RNAi neotetraploids experiencing reduced fertility compared to the Col-0 neotetraploid. This does, however, lend support to the theory that a reduction in CO frequency must be imposed by an increase in CO interference in order to stabilise autotetraploid meiosis. This is because a reduction in CO frequency caused by a curtailment in CO precursor interactions or via a destabilisation of CO maturation (as would likely be the

case in the *asy3* RNAi and *pch2.1* neotetraploids, respectively) would lead to a loss of CO assurance and, hence, increased univalent formation (Bomblies *et al.,* 2015).

We have also shown that autotetraploids represent a useful system for investigating how some of the more fundamental aspects of meiosis might operate. This is because autotetraploids offer a novel scenario in which four homologues exist that are equally capable of pairing and recombining with one another, impeding the simple pairwise interactions would otherwise normally be found in diploid meiosis. For instance, immunocytogenetic analysis of pachytene cells in autotetraploid *A. arenosa* that were triple labelled with ASY1/ZYP1/MLH1 showed that CO interference appeared to operate as normal across chromosomal regions that spanned an SPS site, even though in these situations the interference signal would only be transmitted along one of the two homologues that were involved in the initial CO designation. More intriguingly still, perhaps, evidence is presented that seems to indicate that COs occurring on neighbouring stretches of SC on the same side of an SPS site appear to occur at more similar positions than might otherwise be expected by chance, albeit it with a low degree of significance. We have proposed two models to explain this phenomenon based upon the timing of pairwise synapsis or upon a CO interference backtracking mechanism, but appreciate other plausible explanations may also exist.

6.1.2 Meiotic axis protein function

Our experiments have also focused largely upon the enigmatic meiotic axis protein ASY1 and, to a smaller extent, the axis associated protein ASY3. Although ASY1 was identified as having a necessary role in meiosis 19 years ago (Ross *et al.,* 1997), little is known about how this protein functions beyond its requirement for establishing IHR during early prophase I (Sanchez-Moran *et al.,* 2007). In this study, we have examined how different *ASY1* alleles

affect meiotic CO position, how ASY1 localisation is altered at high temperatures and how a reduction in ASY1 expression disrupts meiotic progression.

As mentioned in the previous section, a derived tetraploid allele of *ASY1* has been shown to dominantly influence CO localisation by shifting COs to a more distal position along chromosomes. We have proposed two mechanisms by which the tetraploid allele might promote this shift, either by encouraging ASY1 to bind first at more distal positions along the chromosomes where it could encourage IHR and CO designation or by reducing the functional effectiveness of the protein such that chiasma shift to a more distal position as witnessed in the few remaining chiasma of an *asy1* mutant (Sanchez-Moran *et al.,* 2001).

Other experiments examining the effects of increased temperature on meiotic progression in *A. arenosa* have indicated that lines experiencing heterozygosity for different *ASY1* alleles may possess increased meiotic thermal tolerance relative to their homozygous counterparts, although the author concedes that due to potential genotyping errors and a low sample size further work will certainly be required to confirm this. It can be confirmed, however, that an increase in temperature to 33^{o}C in some lines leads to the formation of axis associated ASY1 aggregations that are often linked with ZYP1 polycomplexes. It is unclear whether these ASY1 aggregates consist solely of ASY1 or whether they are, in fact, aggregations of the entire underlying axis and all its associated proteins. The close association between these aggregates and the ZYP1 polycomplexes does, however, indicate that the axis may play an important role in promoting SC nucleation and synapsis initiation.

Previous studies have also demonstrated that ASY1 localises to the meiotic axis in *A. thaliana* in a series of hyper-abundant domains (Lambing *et al.,* 2015). Super-resolution analysis of ASY1 distribution in *A. arenosa*, however, has revealed that in this organism ASY1 appears

as a much more uniform linear signal during leptotene. In the future it will be interesting to investigate ASY1 behaviour using different super-resolution imaging techniques, other than SIM, such as stochastic optical reconstruction microscopy (STORM) which might be able to visualise ASY1 distribution at single-molecule resolution. It would also be useful to utilise this technique to determine how ASY1 localisation is affected in the *asy1* RNAi and *asy3* RNAi lines that were generated in *A. thaliana,* as in many of these lines ASY1 deposition along the axis appears normal and yet a decrease in meiotic chiasma frequency is observed. In these instances it may be that, although ASY1 is still localising to the axis, its domain-like distribution is compromised.

In summary, although we have identified a number of meiotic consequences that arise from altering ASY1 behaviour, either through the expression of different derived ASY1 alleles or via functional perturbation using RNAi or high-temperatures, the molecular mechanisms that lie behind these effects still remain elusive.

6.1.3 Potential benefits for agriculture and crop improvement

Earth's population is predicted to increase by more than 2.3 billion people by the year 2050, with over half of this substantial growth occurring within Africa (United Nations, 2015). In order to feed this growing number it is imperative that researchers develop new and innovative ways of sustainably intensifying the production of nutritious and high-quality food as part of a multi-focus approach encompassing other social, environmental and economic factors (Royal Society 2009). It is therefore both interesting and important to consider in what context the work presented during this study may possess a translational application for agricultural crop improvement.

It is well documented that, due to an increase in relative cell size, neoautopolyploid plants generated via colchicine treatment can often exhibit a corresponding increase in the size of leaves, roots, seeds and other organs compared to diploid varieties of the same species; a phenomena referred to as the 'gigas effect' (reviewed in Sattler *et al.,* 2015). Increasing the size of these organs in cultivated plants can lead to beneficial increases in yield, however the use of neoautopolyploids in plant breeding is often restricted to plants that are grown for their vegetative organs. This is because, as described in section 5.2.5, problems encountered during meiosis in neoautopolyploids can cause large reductions in fertility and viable seed production. This fertility barrier has prevented neoautopolyploids from being extensively used to generate new varieties of cereal crops (Sattler *et al.,* 2015). Understanding how established autopolyploid species have evolved to stabilise meiosis and overcome this fertility barrier may allow breeders and scientists to translate these findings into cereal crops, allowing neoautopolyploid varieties to be generated that could exhibit increased grain size without an accompanying reduction in fertility.

We have demonstrated that a derived tetraploid allele of the meiotic axis gene *ASY1,* found in the naturally evolved autotetraploid species *A. arenosa,* may help to stabilise autopolyploid meiosis by shifting COs to a more distal position. We have also shown that reducing overall CO number, in itself, is insufficient to impart enhanced meiotic stability in neoautopolyploid *A. thaliana.* In the future it will be important to build upon this work to identify what other molecular mechanisms are involved in autopolyploid meiotic stabilisation and to consider how these mechanisms could be translated into cereal crops.

It has also been noted that, in many major cereal crops and other members of the Poaceae, chiasma are preferentially located within the distal regions of chromosomes (Higgins *et al.,* 2014). This is known to restrict the potential variation that is available to plant breeders and

therefore it is desirable to find ways to manipulate CO localisation in these species to increase the frequency of COs occurring at more proximal and interstitial positions. In this study, we have shown that a derived tetraploid allele of *ASY1* shifts COs to a more distal position compared to the diploid allele in *A. arenosa*. This ability of different *ASY1* alleles to shift CO localisation has not been previously reported and it will be interesting in the future to determine why the diploid allele appears to encourage a higher frequency of proximal COs than the tetraploid allele as this could also help to facilitate the development of methods for shifting COs to more proximal positions in cereals.

Finally, there is growing evidence to suggest that global temperatures are rapidly increasing and that this increase in temperature could lead to accompanying reductions in the yields of many crops (Royal Society 2009). The cause of this reduced yield could, in many instances, be linked to the negative effects that increased temperature can have on meiotic stability, as shown in section 4.2.5. We have some evidence that indicates *A. arenosa* plants that are heterozygous for different *ASY1* alleles may have increased meiotic thermal tolerance compared to their homozygous counterparts and suggest this could be the result of heterozygous inhibition of protein aggregation. It will be worth pursuing this lead and performing more experiments to see if this result can be recapitulated with a greater sample size and in *A. thaliana* plants heterozygous for the transgenic alleles. If this observation persists following this further work then the co-expression of different *ASY1* alleles could offer a simple and elegant solution to meiotic problems associated with decreasing yields at higher temperatures.

6.1.4 Summary

In summary, we have presented a number of experiments that provide novel insights into the behaviour of autopolyploid meiosis and the roles of specific meiotic axis associated proteins. We have also put forward a number of models to help explain some of the molecular mechanisms that may underlie our observations. We hope that much of this work will be followed up with further experiments to help reinforce our findings and conclusions and that this study will provide fertile ground for future research.

CHAPTER 7

ENGAGING THE PUBLIC WITH RESEARCH IN PLANT REPRODUCTION

7. Engaging the public with research in plant reproduction

7.1 Introduction

Over the past two decades, funding bodies and policy makers within the UK have placed an increased emphasis upon the importance of engaging the public with scientific research (reviewed in Burchell 2015). This led to the establishment of a National Coordinating Centre for Public Engagement (NCCPE) in 2008 who define public engagement as:

"*The myriad ways in which the activity and benefits of higher education and research can be shared with the public. Engagement is by definition a two-way process, involving interaction and listening, with the goal of generating mutual benefit"* (NCCPE, 2015)

Examples of the sort of activities considered to fall under the public engagement umbrella term include, but are not limited to; delivering public lectures and talks, working with museums and running workshops in schools (Research Councils UK *et al.*, 2010). Notably, interactions with the media including television and radio appearances are often not considered to fall into the category of public engagement, perhaps because these forms of interaction are considered solely 'one-way' communication methods that are at odds with the 'two-way', mutually beneficial communication that appears as a prominent feature of contemporary definitions of public engagement (Burchell 2015). However, in contrast to this a 2014 survey by the Biotechnology and Biological Sciences Research Council (BBSRC) indicated that BBSRC funded principle investigators (PIs) perceived 'working with journalists' as being the most worthwhile public engagement or science communication activity available for them and the third most worthwhile activity for their audiences (BBSRC, 2014). This suggests a disconnection may exist between official definitions of public engagement and what scientific researchers perceive as public engagement.

The motivations and benefits for researchers taking part in public engagement activities are also well documented, and range from a desire to increase public understanding of science to simple personal enjoyment when delivering activities (Burchell, 2015). However, it has also been widely reported that the frequency of participation in public engagement activities is much lower within science, technology, engineering and mathematics (STEM) subjects than in the arts, humanities and social sciences (Vitae-CROS, 2015). A separate survey also revealed that the top three reasons for not participating in public engagement activities for both PIs and PhD students was a perceived lack of time, opportunities and training (BBSRC, 2014). Varner (2014) proposed a framework for effective public engagement that relies heavily on critically evaluating previously implemented public engagement activities before disseminating results to serve as case-studies and training tools. The aim of this chapter, therefore, is to describe the development, implementation and evaluation of a public engagement event that was organised by the author so that it may be used as a resource for STEM researchers planning future events.

7.2 Our public engagement activity

7.2.1 Development

Plant reproductive biology is an area of science that has received a reasonably substantial degree of attention from researchers over the past century and current and future research in this area will no doubt play a pivotal role in ensuring global food security. Yet, it is difficult to gauge how much the public knows about scientific advances that have been made within this field and whether they appreciate the potential positive impact this research could have on global society. Therefore, a public engagement activity was devised in order to help increase public awareness of the importance of research into plant reproductive biology and to help

researchers to understand to what extent the public already knows about this research and what their opinions and attitudes are towards it.

A collaboration with the Think Tank science museum in Birmingham was arranged and a Meet the Scientist event was organised to take place in the museum's Talking Point. This arrangement allowed researchers to gain access to a large, receptive audience that consisted mostly of primary and secondary school-aged children and their parents. Volunteers consisting of PIs, PhD students and undergraduates from the Franklin, Franklin-Tong and Sanchez-Moran labs also donated their free time to help run the event.

7.2.2 Implementation

The public engagement event was titled 'Flower Power: Feeding The World' and consisted of a series of interactive experiments and demonstrations complemented by five large descriptive posters, all centred around the theme of plant reproductive biology. There were three main experiments; strawberry DNA extraction and gel electrophoresis, microscopy of meiotic cells from grasshopper testis and stereomicroscopy of lily pollen tube growth and floral anatomy (figure 7.1). The experiments were designed to guide visitors on a journey from the smallest events of plant reproduction (DNA and meiosis) through to the bigger events (pollen tube growth and fertilisation). These experiments were mainly targeted at the children and, whilst the children were involved in these activities, other researchers were able to engage the parents in conversation to informally discuss the topic of plant reproductive biology at a more advanced level and to answer questions.

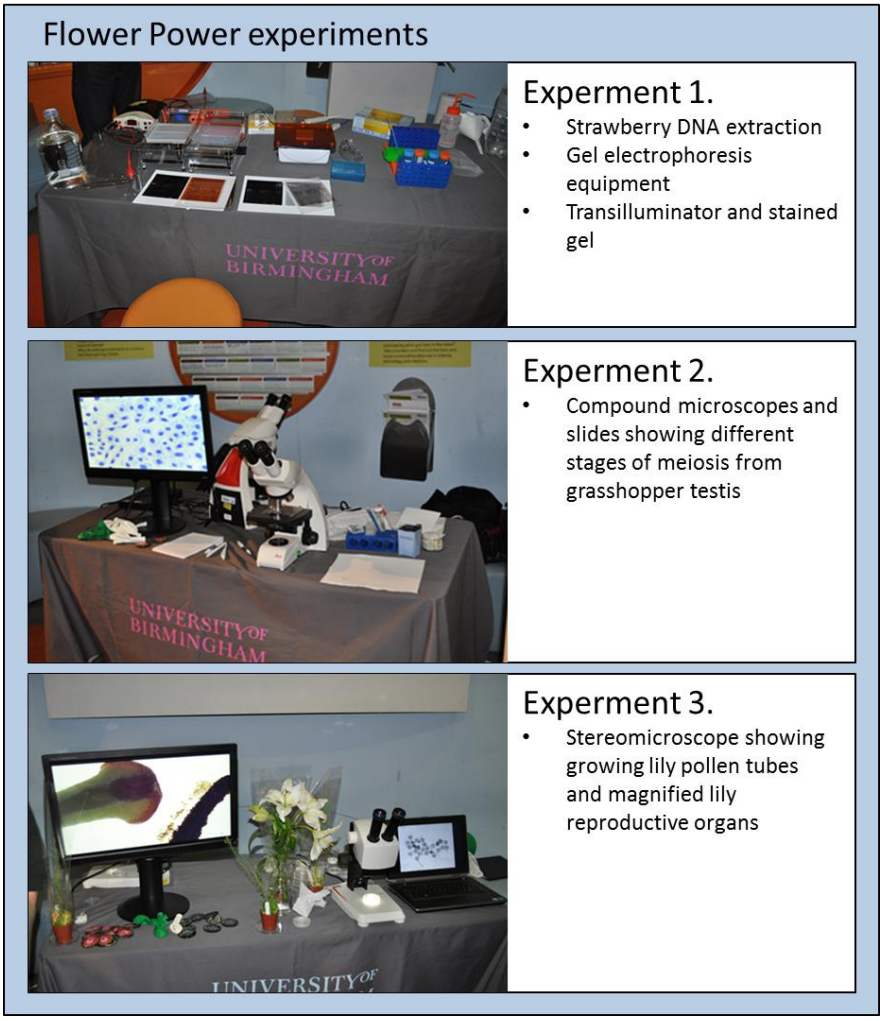

Figure 7.1. Images showing the interactive experiments from the Flower Power public engagement event.

The five posters presented were adapted from posters that had previously been designed by C. Franklin and N. Franklin-Tong (figure S2). Accompanying the posters was a 'Discovery Sheet' quiz (figure S3) that could be used to gauge interest and understanding in the topics being communicated. Badges and fridge magnets were also designed (figure S4) that were given as free gifts to visitors. These not only provided an incentive to guests walking past to come in and get involved with the activities but also served as a lasting physical memory from the event that would act as a constant reminder of the importance of plant reproduction and hopefully stimulate further conversations about the topic in the future.

7.2.3 Evaluation

Two questionnaires were constructed to help evaluate the success of Flower Power and to identify any particular strengths or weaknesses associated with the event. The first questionnaire was supplied to parents during the event itself and was designed to gauge whether the visitors enjoyed the activity and if they felt they had learned something about the subject (figure S5). Nine visitor questionnaires were received and the feedback is presented in figure 7.2. During the event these feedback forms were left on the side alongside a feedback box, but the low number of questionnaires received may reflect that a more regimented approach to collecting feedback, with volunteers directly asking parents to fill out the questionnaires, may have been more effective. The feedback that we did receive indicated that, in general, the visitors enjoyed the event, learned something and felt the information was communicated clearly and effectively. They also felt, in general, that plant science is important to produce enough food for the future but, interestingly, were mostly neutral towards the statement 'I did not know much about plant science before today', indicating that many of the visitors may have had a prior interest in the subject. The following comments were also received in the feedback:

"*Very informative and great with children."*

"Really interesting and explained at a level the children understood. Thanks."

"Thank you for putting this on. Great fun for the children. Good to discuss GM. I am for it, golden rice is the answer."

These comments all indicated that the level at which the event was aimed and the complexity of information communicated was suitable for the primary-target audience of children.

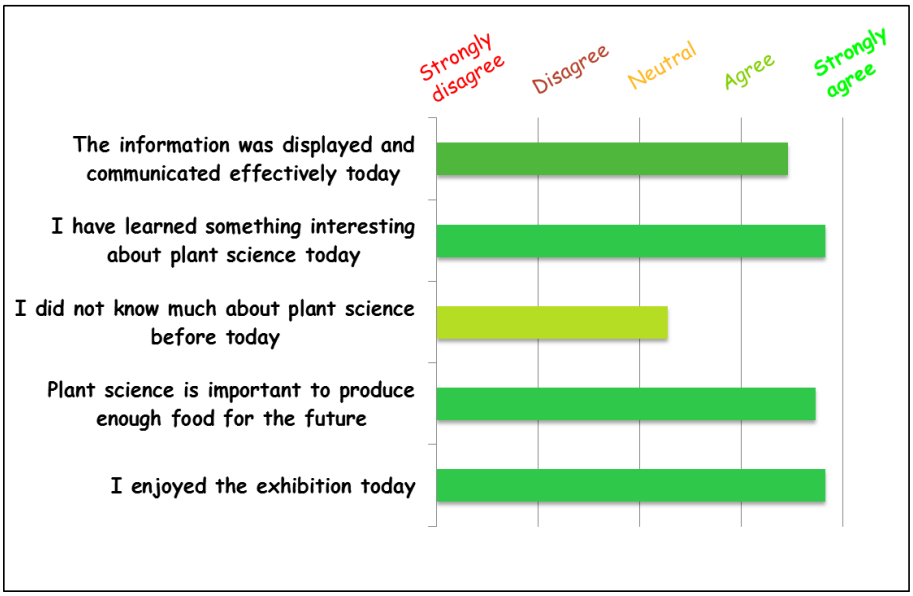

Figure 7.2. Summary of mean results from the visitor questionnaire feedback forms

A second questionnaire was also supplied to the volunteers that helped to deliver the Flower Power event once the event had been completed to evaluate their opinion of how successful the event was and to determine whether participating in the event had changed their attitudes towards public engagement and their own research (figure S6). The results from this questionnaire indicated that, in the opinion of the volunteers, the event successfully achieved its goal of communicating science to the general public and that the Think Tank was a good location for doing this (figure 7.3). The volunteers also generally strongly agreed that participating in this event had encouraged them to take part in more public engagement in the future and most also agreed that it had changed the way they think about or approach their own research. It was not made explicit, however, how or why the researchers felt participating in this event had changed their attitudes towards their own research and it may therefore have been useful to include a comments box at this section of the questionnaire to gather this information. Another section of the questionnaire asked which experiment the volunteers had

felt was most popular with the public and in all instances the number one choice was the strawberry DNA extraction experiment.

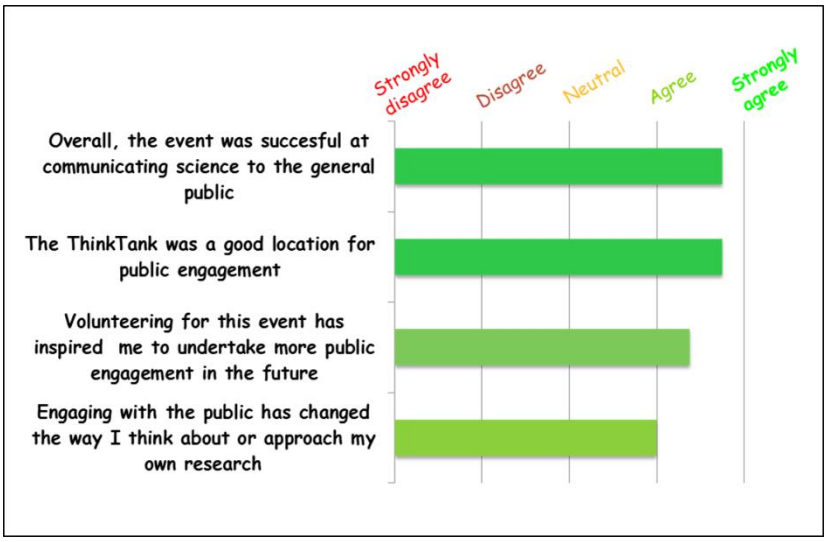

Figure 7.3. Summary of mean results from the volunteer questionnaire feedback forms

7.3 Discussion

Here we have presented a case-study of a public engagement event held at Birmingham's Think Tank Science museum. The aim of this event was to communicate information and engage in a two-way dialogue centring around plant reproduction with an audience consisting mostly of primary and secondary school-aged children and their parents. How this event was developed, implemented and evaluated is summarised in figure 7.4 following the model devised by Varner (2014).

Feedback from the event indicated that, in general, the event was a success and the original goals, which included disseminating information about plant reproduction in a fun and engaging way, had been met. One particular aspect of the feedback that was particularly insightful was that all volunteers felt that the strawberry DNA extraction had been the most successful experiment. Following on from this event, therefore, many other public

engagement events and activities participated in by the author also included strawberry DNA extractions. This experiment is useful because it links in to a number of key themes that run through plant meiosis research including plant genetics and polyploidy. A summary of some of the other public engagement events participated in by the author alongside short personal reflections are shown in table 7.1. It is hoped these will also serve as a resource of public engagement ideas that will be available to other researchers.

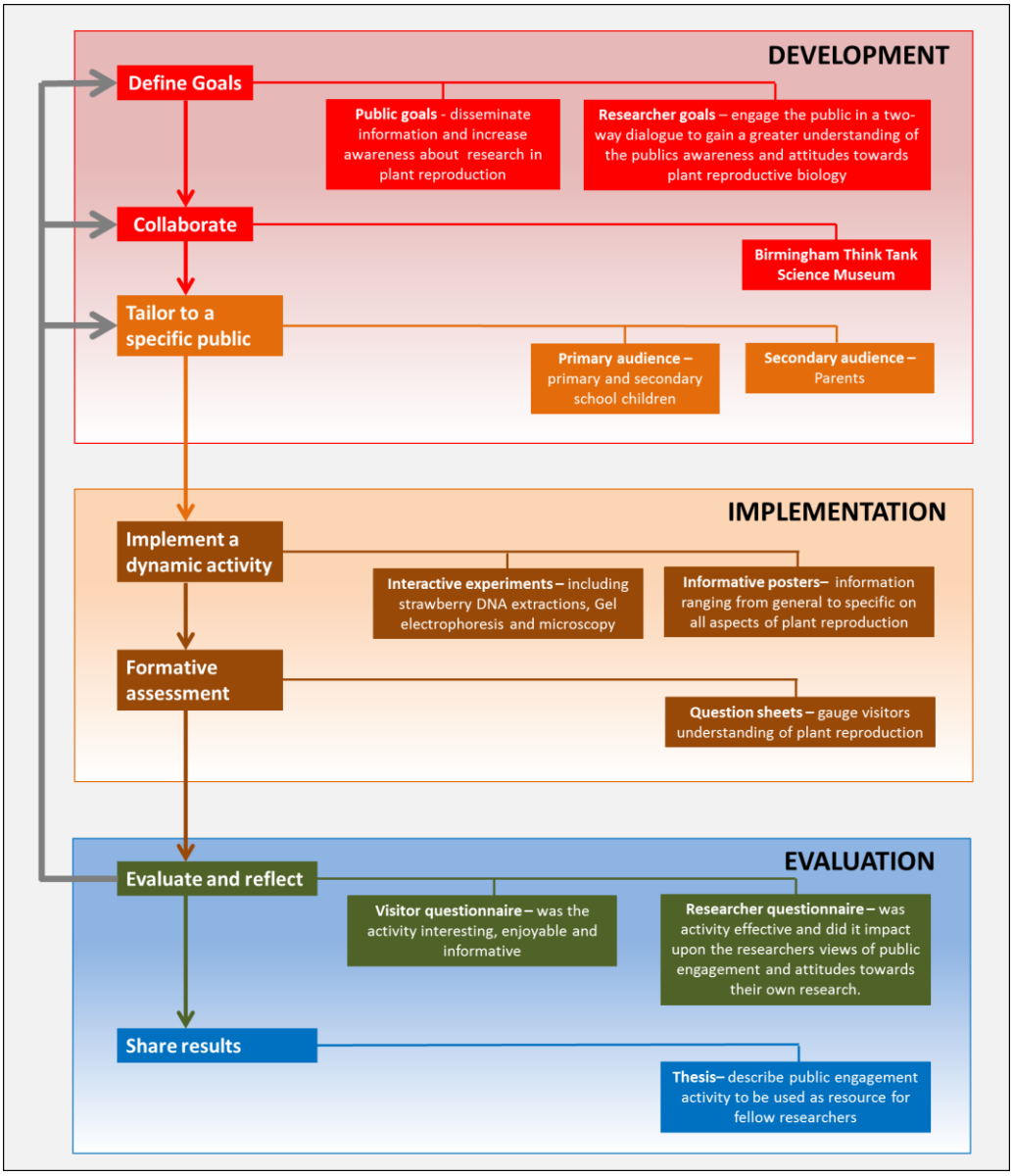

Figure 7.4. Model of how the Flower Power public engagement event was conceptualized following the framework set-out by Varner (2014).

Public engagement activity	Description	Reflection
Flower Power 2015	A similar Think Tank event to that described in the main text. This time the event was primarily organised by researchers from the COMREC doctoral training programme.	This iteration of Flower Power included more 'hands-on' games and activities which appealed greatly to the younger children and improved visitor participation and involvement.
Think Corner	A research themed pop-up shop in Birmingham's city centre. Strawberry DNA extractions experiments were performed alongside engaging the public in a two-way dialogue.	Very effective event at targeting a non-traditional audience from a very broad demographic of visitors.
UoB three minute thesis competition	A presentation to a non-specialist audience describing a doctoral research topic in only three minutes. http://tinyurl.com/gpekhrk	Very efficient way of communicating complex information in a short time. However, there was little opportunity for a two-way dialogue to be established.
University of Third Age public presentation	A presentation to an audience of retired and semi-retired individuals from a variety of backgrounds followed by an informal Q&A.	Effective two-way dialogue established during the Q&A leading to a beneficial and informative experience for both the presenter and audience.
Biochemical society science communication video competition	A video was made describing how CRISPR-Cas targeted mutagenesis works in plants, aimed at a non-specialist audience. http://tinyurl.com/zbytl7k	Efficient way of communicating complex information in a short amount of time with the potential to reach a large audience. Little opportunity for a two-way dialogue to be established.
UoB Less Talk More Action video competition	A video was made describing how why research in plant meiosis is important, aimed at a non-specialist audience. http://tinyurl.com/hmgbgpw	Efficient way of communicating complex information in a short amount of time with the potential to reach a large audience. Little opportunity for a two-way dialogue to be established.
UoB Images of Research competition	An image and short piece of text entitled 'Feeding the world with plant science' were displayed in a public gallery (figure S7).	Efficient way of communicating complex information in a short amount of time with the potential to reach a large audience. Little opportunity for a two-way dialogue to be established.
Brightclub	8 minute long science themed stand-up comedy at the REP theatre in Birmingham aimed at a non-specialist audience.	Efficient way of communicating complex information in an impactful, informal and memorable way. Little opportunity for a two-way dialogue to be established.

Table 7.1. A summary of other public engagement activities participated in by the author along with personal reflections of the merits and drawbacks of each activity.

In summary, the relative importance of public engagement in the minds of both funding bodies and higher education institutions appears greater now than ever before (Burchell 2015) and the call for all researchers to go out and engage the public in an effective two-way dialogue will undoubtedly only get stronger over the coming years. It therefore appears essential that extensive training opportunities and resources must be in place to facilitate this

and it is hoped that this case-study will contribute to the body of knowledge growing around this expanding subject.

References

Acquaviva, L., Drogat, J., Dehé, P.-M., La Roche Saint-André, de, C., and Géli, V. (2013). Spp1 at the crossroads of H3K4me3 regulation and meiotic recombination. Epigenetics **8**: 355–360.

Agarwal, S. and Roeder, G.S. (2000). Zip3 Provides a Link between Recombination Enzymes and Synaptonemal Complex Proteins. Cell **102**: 245-255.

Alberts, B., Bray, D., Lewis, J., Raff, M., Roberts K. and Watson, J.D. (1983). Molecular Biology of The Cell. London. Garland Publishing **1**

Alexander, M.P., (1969) Differential staining of aborted and nonaborted pollen. Stain Technol **44:** 117-122.

Aravind, L. and Iyer, L.M. (2002). The SWIRM domain: a conserved module found in chromosomal proteins points to novel chromatin-modifying activities. Genome Biol. **3**.

Armstrong, S.J. and Jones, G.H. (2001). Female meiosis in wild-type Arabidopsis thaliana and in two meiotic mutants. Sexual Plant Reproduction **13**: 177–183.

Armstrong, S.J., Caryl, A.P., Jones, G.H., and Franklin, F.C.H. (2002). Asy1, a protein required for meiotic chromosome synapsis, localizes to axis-associated chromatin in Arabidopsis and Brassica. J. Cell. Sci. **115**: 3645–3655.

Armstrong, S.J., Franklin, F.C.H., and Jones, G.H. (2003). A meiotic time-course for Arabidopsis thaliana. Sexual Plant Reproduction **16**: 141–149.

Arnold, B., Kim, S.-T., and Bomblies, K. (2015). Single Geographic Origin of a Widespread Autotetraploid Arabidopsis arenosa Lineage Followed by Interploidy Admixture. Mol. Biol. Evol. **32**: 1382–1395.

Baudat, F., Buard, J., Grey, C., Fledel-Alon, A., Ober, C., Przeworski, M., Coop, G., and de Massy, B. (2010). PRDM9 Is a Major Determinant of Meiotic Recombination Hotspots in Humans and Mice. Science **327**: 836–840.

BBSRC (2014) Public engagement and science communication survey, BBSRC External Communiations Unit. **http://www.bbsrc.ac.uk/web/FILES/Reviews/pe-and-science-comm-report.pdf**

Berchowitz, L.E., Hanlon, S.E., Lieb, J.D., and Copenhaver, G.P. (2009). A positive but complex association between meiotic double-strand break hotspots and open chromatin in Saccharomyces cerevisiae. Genome Research **19**: 2245–2257.

Bergerat, A., de Massy, B., Gadelle, D., Varoutas, P.C., Nicolas, A., and Forterre, P. (1997). An atypical topoisomerase II from Archaea with implications for meiotic recombination. Nature **386**: 414–417.

Bleuyard, J.-Y. and White, C.I. (2004). The Arabidopsis homologue of Xrcc3 plays an essential role in meiosis. The EMBO Journal **23**: 439–449.

Boden, S.A., Langridge, P., Spangenberg, G., and Able, J.A. (2009). TaASY1 promotes homologous chromosome interactions and is affected by deletion of Ph1. Plant J. **57**: 487–497.

Bomblies, K. and Madlung, A. (2014). Polyploidy in the Arabidopsis genus - Online First - Springer. Chromosome Research. **22**: 117-134.

Bomblies, K., Jones, G., Franklin, C., Zickler, D., and Kleckner, N. (2016). The challenge of evolving stable polyploidy: could an increase in "crossover interference distance" play a central role? Chromosoma **125**: 287–300.

Borde, V. (2000). Direct Coupling Between Meiotic DNA Replication and Recombination Initiation. Science **290**: 806–809.

Borde, V. and de Massy, B. (2013). Programmed induction of DNA double strand breaks during meiosis: setting up communication between DNA and the chromosome structure. Current Opinion in Genetics & Development **23**: 147–155.

Borde, V., Robine, N., Lin, W., Bonfils, S., Géli, V., and Nicolas, A. (2008). Histone H3 lysine 4 trimethylation marks meiotic recombination initiation sites. The EMBO Journal **28**:

99–111.

Börner, G.V., Barot, A., and Kleckner, N. (2008). Yeast Pch2 promotes domainal axis organization, timely recombination progression, and arrest of defective recombinosomes during meiosis. Proc. Natl. Acad. Sci. U.S.A. **105**: 3327–3332.

Börner, G.V., Kleckner, N., and Hunter, N. (2004). Crossover/noncrossover differentiation, synaptonemal complex formation, and regulatory surveillance at the leptotene/zygotene transition of meiosis. Cell **117**: 29–45.

Brick, K., Smagulova, F., Khil, P., Camerini-Otero, R.D., and Petukhova, G.V. (2012). Genetic recombination is directed away from functional genomic elements in mice. Nature **485**: 642–645.

Burchell, K. (2015). Factors affecting public engagement by researchers. Policy Studies Institute, London. **http://wellcome.ac.uk/sites/default/files/wtp060036.pdf**

Cai, X., Dong, F., Edelmann, R.E., and Makaroff, C.A. (2003). The Arabidopsis SYN1 cohesin protein is required for sister chromatid arm cohesion and homologous chromosome pairing. J. Cell. Sci. **116**: 2999–3007.

Carballo, J.A., Johnson, A.L., Sedgwick, S.G., and Cha, R.S. (2008). Phosphorylation of the Axial Element Protein Hop1 by Mec1/Tel1 Ensures Meiotic Interhomolog Recombination. Cell. **132**: 758-770

Carballo, J.A., Panizza, S., Serrentino, M.E., Johnson, A.L., Geymonat, M., Borde, V., Klein, F., and Cha, R.S. (2013). Budding Yeast ATM/ATR Control Meiotic Double-Strand Break (DSB) Levels by Down-Regulating Rec114, an Essential Component of the DSB-machinery. PLoS Genet. **9**: e1003545.

Carvalho, A., Delgado, M., Barao, A., Frescatada, M., Ribeiro, E., Pikaard, C.S., Viegas, W., and Neves, N. (2010). Chromosome and DNA methylation dynamics during meiosis in the autotetraploid Arabidopsis arenosa. Sexual Plant Reproduction **23**: 29–37.

Caryl, A.P., Armstrong, S.J., Jones, G.H., and Franklin, F.C. (2000). A homologue of the yeast HOP1 gene is inactivated in the Arabidopsis meiotic mutant asy1. Chromosoma **109**: 62–71.

Chelysheva, L., Gendrot, G., Vezon, D., Doutriaux, M.-P., Mercier, R., and Grelon, M. (2007). Zip4/Spo22 Is Required for Class I CO Formation but Not for Synapsis Completion in Arabidopsis thaliana. PLoS Genet. **3**: e83.

Chelysheva, L., Vezon, D., Chambon, A., Gendrot, G., Pereira, L., Lemhemdi, A., Vrielynck, N., Le Guin, S., Novatchkova, M., and Grelon, M. (2012). The Arabidopsis HEI10 Is a New ZMM Protein Related to Zip3. PLoS Genet. **8**.

Choi, K., Zhao, X., Kelly, K.A., Venn, O., Higgins, J.D., Yelina, N.E., Hardcastle, T.J., Ziolkowski, P.A., Copenhaver, G.P., Franklin, F.C.H., McVean, G., and Henderson, I.R. (2013). Arabidopsis meiotic crossover hot spots overlap with H2A.Z nucleosomes at gene promoters. Nature Publishing Group **45**: 1327–1336.

Chua, P.R. and Roeder, G.S. (1998). Zip2, a Meiosis-Specific Protein Required for the Initiation of Chromosome Synapsis. Cell **93**: 349–359.

Cifuentes, M., Grandont, L., Moore, G., Chèvre, A.M., and Jenczewski, E. (2010). Genetic regulation of meiosis in polyploid species: new insights into an old question. New Phytol. **186**: 29–36.

Clough, S.J. and Bent, A.F. (1998). Floral dip: a simplified method for Agrobacterium-mediated transformation of Arabidopsis thaliana. Plant J. **16**: 735–743.

Comai, L., Tyagi, A.P., and Lysak, M.A. (2003). FISH analysis of meiosis in Arabidopsis allopolyploids. Chromosome Res. **11**: 217–226.

Corbett, K.D. and Berger, J.M. (2004). Structure, Molecular Mechanisms, and Evolutionary Relationships in DNA Topoisomerases. Annu. Rev. Biophys. Biomol. Struct. **33**: 95–118.

Crismani, W., Girard, C., Froger, N., Pradillo, M., Santos, J.L., Chelysheva, L., Copenhaver, G.P., Horlow, C., and Mercier, R. (2012). FANCM Limits Meiotic

Crossovers. Science **336**: 1588–1590.

Crow, K.D. (2006). What Is the Role of Genome Duplication in the Evolution of Complexity and Diversity? Mol. Biol. Evol. **23**: 887–892.

Davies, A., Jenkins, G., and Reed, H. (1990). Diploidisation of Lotus corniculatus L. (Fabaceae) by elimination of multivalents. Chromosoma **99**: 289-295.

de Boer, E., Stam, P., Dietrich, A., Pastink, A., and Heyting, C. (2006). Two levels of interference in mouse meiotic recombination. Proc. Natl. Acad. Sci. U.S.A. **103**: 9607–9612.

de los Santos, T., Hunter, N., Lee, C., Larkin, B., Loidl, J., and Hollingsworth, N.M. (2003). The Mus81/Mms4 Endonuclease Acts Independently of Double-Holliday Junction Resolution to Promote a Distinct Subset of Crossovers During Meiosis in Budding Yeast. Genetics **164**: 81-94

De Muyt, A., Jessop, L., Kolar, E., Sourirajan, A., Chen, J., Dayani, Y., and Lichten, M. (2012). BLM helicase ortholog Sgs1 is a central regulator of meiotic recombination intermediate metabolism. Molecular Cell **46**: 43–53.

De Muyt, A., Pereira, L., Vezon, D., Chelysheva, L., Gendrot, G., Chambon, A., Lainé-Choinard, S., Pelletier, G., Mercier, R., Nogué, F., and Grelon, M. (2009). A high throughput genetic screen identifies new early meiotic recombination functions in Arabidopsis thaliana. PLoS Genet. **5**: e1000654.

De Muyt, A., Vezon, D., Gendrot, G., Gallois, J.-L., Stevens, R., and Grelon, M. (2007). AtPRD1 is required for meiotic double strand break formation in Arabidopsis thaliana. The EMBO Journal **26**: 4126–4137.

Doutriaux, M.P., Couteau, F., Bergounioux, C.,and White, C. (1998) Isolation and characterization of the RAD51 and DMC1 homologs from Arabidopsis thaliana. Mol Gen Genet **257**: 283-291.

Eamens, A., Wang, M.-B., Smith, N.A., and Waterhouse, P.M. (2008). RNA silencing in plants: yesterday, today, and tomorrow. Plant Physiol. **147**: 456–468.

Ferdous, M., Higgins, J.D., Osman, K., Lambing, C., Roitinger, E., Mechtler, K., Armstrong, S.J., Perry, R., Pradillo, M., Cuñado, N., and Franklin, F.C.H. (2012). Inter-homolog crossing-over and synapsis in Arabidopsis meiosis are dependent on the chromosome axis protein AtASY3. PLoS Genet. **8**: e1002507.

Foss, E., Lande, R., Stahl, F.W., and Steinberg, C.M. (1993). Chiasma Interference as a Function of Genetic-Distance. Genetics **133**: 681–691.

Fung, J.C., Rockmill, B., Odell, M., and Roeder, G.S. (2004). Imposition of Crossover Interference through the Nonrandom Distribution of Synapsis Initiation Complexes. Cell. **116**: 795-802

Gasior, S.L., Wong, A.K., Kora, Y., Shinohara, A., and Bishop, D.K. (1998). Rad52 associates with RPA and functions with Rad55 and Rad57 to assemble meiotic recombination complexes. Genes Dev. **12**: 2208–2221.

Genetic Adaptation Associated with Genome-Doubling in Autotetraploid Arabidopsis arenosa (2012). Genetic Adaptation Associated with Genome-Doubling in Autotetraploid Arabidopsis arenosa.: 1–10.

Ghildiyal, M. and Zamore, P.D. (2009). Small silencing RNAs: an expanding universe. Nat Rev Genet **10**: 94–108.

Girard, C., Chelysheva, L., Choinard, S., Froger, N., Macaisne, N., Lehmemdi, A., Mazel, J., Crismani, W., and Mercier, R. (2015). AAA-ATPase FIDGETIN-LIKE 1 and Helicase FANCM Antagonize Meiotic Crossovers by Distinct Mechanisms. PLoS Genet. **11**: e1005369.

Girard, C., Crismani, W., Froger, N., Mazel, J., Lemhemdi, A., Horlow, C., and Mercier, R. (2014). FANCM-associated proteins MHF1 and MHF2, but not the other Fanconi anemia factors, limit meiotic crossovers. Nucleic Acids Res. **42**: 9087–9095.

Giraut, L., Falque, M., Drouaud, J., Pereira, L., Martin, O.C., and Mézard, C. (2011). Genome-wide crossover distribution in Arabidopsis thaliana meiosis reveals sex-specific patterns along chromosomes. PLoS Genet. **7**: e1002354.

Greer, E., Martín, A.C., Pendle, A., Colas, I., Jones, A.M.E., Moore, G., and Shaw, P. (2012). The Ph1 Locus Suppresses Cdk2-Type Activity during Premeiosis and Meiosis in Wheat. The Plant ….

Grelon, M. (2001). AtSPO11-1 is necessary for efficient meiotic recombination in plants. The EMBO Journal **20**: 589–600.

Griffiths, S., Sharp, R., Foote, T.N., Bertin, I., Wanous, M., Reader, S., Colas, I., and Moore, G. (2006). Molecular characterization of Ph1 as a major chromosome pairing locus in polyploid wheat. Nature **439**: 749–752

.

Gustafsson, M. (2000). Surpassing the lateral resolution limit by a factor of two using structured illumination microscopy. J Microsc **198**: 82–87.

Hartung, F. and Puchta, H. (2000). Molecular characterisation of two paralogous SPO11 homologues in Arabidopsis thaliana. Nucleic Acids Res.

Hazarika, M.H. and Rees, H. (1967). Heredity - Abstract of article: Genotypic control of chromosome behaviour in rye X. Chromosome pairing and fertility in autotetraploids (Heredity).

Henderson, K.A., Kee, K., Maleki, S., Santini, P.A., and Keeney, S. (2006). Cyclin-Dependent Kinase Directly Regulates Initiation of Meiotic Recombination. Cell **125**: 1321–1332.

Henry, I.M., Dilkes, B.P., Tyagi, A., Gao, J., Christensen, B., and Comai, L. (2014). The BOY NAMED SUE quantitative trait locus confers increased meiotic stability to an adapted natural allopolyploid of Arabidopsis. Plant Cell **26**: 181–194.

Higgins, J.D., Armstrong, S.J., Franklin, F.C.H., and Jones, G.H. (2004). The Arabidopsis MutS homolog AtMSH4 functions at an early step in recombination: evidence for two classes

of recombination in Arabidopsis. Genes Dev. **18**: 2557–2570.

Higgins, J.D., Sanchez-Moran, E., Armstrong, S.J., Jones, G.H., and Franklin, F.C. (2005). The Arabidopsis synaptonemal complex protein ZYP1 is requiredfor chromosome synapsis and normal fidelity of crossing over. Genes Dev **19**: 2488-2500.

Higgins, J.D., Buckling, E.F., Franklin, F.C.H., and Jones, G.H. (2008a). Expression and functional analysis of AtMUS81 in Arabidopsis meiosis reveals a role in the second pathway of crossing-over. Plant J. **54**: 152–162.

Higgins, J.D., Perry, R.M., Barakate, A., Ramsay, L., Waugh, R., Halpin, C., Armstrong, S.J., and Franklin, F.C.H. (2012). Spatiotemporal asymmetry of the meiotic program underlies the predominantly distal distribution of meiotic crossovers in barley. Plant Cell **24**: 4096–4109.

Higgins, J.D., Vignard, J., Mercier, R., Pugh, A.G., Franklin, F.C.H., and Jones, G.H. (2008b). AtMSH5 partners AtMSH4 in the class I meiotic crossover pathway in Arabidopsis thaliana, but is not required for synapsis. The Plant Journal **55**: 28–39.

Higgins, J.D., Wright, K.M., Bomblies, K., and Franklin, F.C.H. (2014). Cytological techniques to analyze meiosis in Arabidopsis arenosa for investigating adaptation to polyploidy. Front Plant Sci **4**: 546.

Ho, H.C., and Burgess, S.M. (2011). Pch2 acts through Xrs2 and Tel1/ATM to modulate interhomolog bias and checkpoint function during meiosis. PLoS Genet. **7**: e1002351.

Hobolth, P. (1981). Chromosome pairing in allohexaploid wheat var. Chinese Spring. Transformation of multivalents into bivalents, a mechanism for exclusive bivalent formation. Carlsberg Res. Commun. **46**: 129–173.

Hollingsworth, N.M., Goetsch, L., and Byers, B. (1990). The HOP1 gene encodes a meiosis-specific component of yeast chromosomes. Cell **61**: 73–84.

Hollingsworth, N.M., Ponte, L., and Halsey, C. (1995). MSH5, a novel MutS homolog, facilitates meiotic reciprocal recombination between homologs in Saccharomyces cerevisiae

but not mismatch repair. Genes Dev.

Hollister, J.D., Arnold, B.J., Svedin, E., Xue, K.S., Dilkes, B.P., and Bomblies, K. (2012). Genetic Adaptation Associated with Genome-Doubling in Autotetraploid Arabidopsis arenosa. PLoS Genet. **8** e1003093.

Holm, P.B. (1986). Chromosome pairing and chiasma formation in allohexaploid wheat, Triticum aestivum analyzed by spreading of meiotic nuclei. Carlsberg Res. Commun. **51**: 239–294.

Hyppa, R.W. and Smith, G.R. (2010). Crossover Invariance Determined by Partner Choice for Meiotic DNA Break Repair. Cell. **142**: 243-255

Jang, J.K., Sherizen, D.E., Bhagat, R., Manheim, E.A., and McKim, K.S. (2003). Relationship of DNA double-strand breaks to synapsis in Drosophila. J. Cell. Sci. **116**: 3069–3077.

Jenczewski, E., Eber, F., Grimaud, A., Huet, S., Lucas, M.O., Monod, H., and Chèvre, A.M. (2003). PrBn, a Major Gene Controlling Homeologous Pairing in Oilseed Rape (Brassica napus) Haploids. Genetics **164**: 645–653.

Johnston, J.S., Pepper, A.E., Hall, A.E., Chen, Z.J., Hodnett, G., Drabek, J., Lopez, R., and Price, H.J. (2005). Evolution of genome size in Brassicaceae. Annals of Botany **95**: 229–235.

Jones, G.H. (1994). Meiosis in Autopolyploid Crepis-Capillaris .3. Comparison of Triploids and Tetraploids - Evidence for Nonindependence of Autonomous Pairing Sites. Heredity **73**: 215–219.

Jones, G.H. and Franklin, F.C.H. (2006). Meiotic crossing-over: obligation and interference. Cell **126**: 246–248.

Jones, G.H. and Vincent, J.E. (1994) Meiosis in allopolyploid Crepis capillaris. II. Autotetraploids. Genome **37**: 497-505.

Joyce, E.F., Pedersen, M., Tiong, S., White-Brown, S.K., Paul, A., Campbell, S.D., and McKim, K.S. (2011). Drosophila ATM and ATR have distinct activities in the regulation of meiotic DNA damage and repair. J. Cell Biol. **195**: 359–367.

Kauppi, L., Barchi, M., Lange, J., Baudat, F., Jasin, M., and Keeney, S. (2013). Numerical constraints and feedback control of double-strand breaks in mouse meiosis. Genes & Dev. **27**: 873-886.

Kaur, H., De Muyt, A., and Lichten, M. (2015). Top3-rmi1 DNA single-strand decatenase is integral to the formation and resolution of meiotic recombination intermediates. Molecular Cell **57**: 583–594.

Keeney, S., Giroux, C.N., and Kleckner, N. (1997). Meiosis-specific DNA double-strand breaks are catalyzed by Spo11, a member of a widely conserved protein family. Cell **88**: 375–384.

Kim, Y., Rosenberg, S.C., Kugel, C.L., Kostow, N., Rog, O., Davydov, V., Su, T.Y., Dernburg, A.F., and Corbett, K.D. (2014). The Chromosome Axis Controls Meiotic Events through a Hierarchical Assembly of HORMA Domain Proteins. Dev. Cell **31**: 487–502.

King, J.S. and Mortimer, R.K. (1990). A polymerization model of chiasma interference and corresponding computer simulation. Genetics **126**: 1127–1138.

Kleckner, N. (2006). Chiasma formation: chromatin/axis interplay and the role(s) of the synaptonemal complex. Chromosoma **115**: 175–194.

Kleckner, N., Zickler, D., Jones, G.H., Dekker, J., Padmore, R., Henle, J., and Hutchinson, J. (2004). A mechanical basis for chromosome function. Proc Natl Acad Sci USA **101**: 12592-12597

Klein, F., Mahr, P., Galova, M., Buonomo, S.B.C., Michaelis, C., Nairz, K., and Nasmyth, K. (1999). A Central Role for Cohesins in Sister Chromatid Cohesion, Formation of Axial Elements, and Recombination during Yeast Meiosis. Cell **98**: 91–103.

Kobayashi, A., Hizume, M., Teruya, K., Mohri, S., and Kitamoto, T. (2009). Heterozygous inhibition in prion infection The stone fence model. Prion **3**: 27–30.

Kumar, R., Bourbon, H.M., and de Massy, B. (2010). Functional conservation of Mei4 for meiotic DNA double-strand break formation from yeasts to mice. Genes Dev. **24**: 1266–1280.

Kurzbauer, M.-T., Uanschou, C., Chen, D., and Schlögelhofer, P. (2012). The recombinases DMC1 and RAD51 are functionally and spatially separated during meiosis in Arabidopsis. Plant Cell **24**: 2058–2070.

Lam, W.S., Yang, X.H., and Makaroff, C.A. (2005). Characterization of Arabidopsis thaliana SMC1 and SMC3: evidence that AtSMC3 may function beyond chromosome cohesion. J. Cell. Sci. **118**: 3037–3048.

Lambing, C., Osman, K., Nuntasoontorn, K., West, A., Higgins, J.D., Copenhaver, G.P., Yang, J., Armstrong, S.J., Mechtler, K., Roitinger, E., and Franklin, F.C.H. (2015). Arabidopsis PCH2 Mediates Meiotic Chromosome Remodeling and Maturation of Crossovers. PLoS Genet. **11**: e1005372.

Lange, J., Pan, J., Cole, F., Thelen, M.P., Jasin, M., and Keeney, S. (2011). ATM controls meiotic double-strand-break formation. Nature **479**: 237–240.

Le Comber, S.C., Ainouche, M.L., Kovarik, A., and Leitch, A.R. (2010). Making a functional diploid: from polysomic to disomic inheritance. New Phytol. **186**: 113–122.

Lhuissier, F.G.P., Offenberg, H.H., Wittich, P.E., Vischer, N.O.E., and Heyting, C. (2007). The mismatch repair protein MLH1 marks a subset of strongly interfering crossovers in tomato. Plant Cell **19**: 862–876.

Li, J., Hooker, G.W., and Roeder, G.S. (2006). Saccharomyces cerevisiae Mer2, Mei4 and Rec114 form a complex required for meiotic double-strand break formation. Genetics **173**: 1969–1981.

Libuda, D.E., Uzawa, S., Meyer, B.J., and Villeneuve, A.M. (2013). Meiotic chromosome structures constrain and respond to designation of crossover sites. Nature **502**: 703-706

Lloyd, A. and Bomblies, K. (2016). Meiosis in autopolyploid and allopolyploid Arabidopsis. Curr. Opin. Plant Biol. **30**: 116–122.

Lo, Y.H., Chuang, C.N., and Wang, T.F. (2014). PLOS ONE: Pch2 Prevents Mec1/Tel1-Mediated Hop1 Phosphorylation Occurring Independently of Red1 in Budding Yeast Meiosis. PLoS ONE. **9**: e85687

Loidl, J. (1989) Effects of elevated temperature on meiotic chromosome synapsis in Allium ursinum. Chromosoma **97**: 449-458.

Loidl, J. and Jones, G.H. (1986) Synaptonemal complex spreading in Allium. Chromosoma **93**: 420-428.

Matzke, M.A., Primig, M., Trnovsky, J., and Matske, A.J.M. (1989). Reversible methylation and inactivation of marker genes in sequentially transformed tobacco plants. The EMBO Journal **8**: 643-649.

Macaisne, N., Novatchkova, M., Peirera, L., Vezon, D., Jolivet, S., Froger, N., Chelysheva, L., Grelon, M., and Mercier, R. (2008). SHOC1, an XPF endonuclease-related protein, is essential for the formation of class I meiotic crossovers. Current Biology **18**: 1432–1437.

Macaisne, N., Vignard, J., and Mercier, R. (2011). SHOC1 and PTD form an XPF-ERCC1-like complex that is required for formation of class I crossovers. J. Cell. Sci. **124**: 2687–2691.

Maluszynska,J., Maluszynski, M., Rebes, O., and Wietrzyk, E. (1990). Induced polyploids of *Arabidopsis thaliana*. IV International Conference on *Arabidopsis* Res., Vienna, Austria, p4.

Martini, E., Diaz, R.L., Hunter, N., and Keeney, S. (2006). Crossover homeostasis in yeast meiosis. Cell **126**: 285–295.

Martín, A.C., Shaw, P., Phillips, D., Reader, S., and Moore, G. (2014). Licensing MLH1 sites for crossover during meiosis. Nat Comms **5**: 4580

Mazina, O.M., Mazin, A.V., Nakagawa, T., and Kolodner, R.D. (2004). Saccharomyces cerevisiae Mer3 Helicase Stimulates 3′–5′ Heteroduplex Extension by Rad51: Implications for Crossover Control in Meiotic Recombination. Cell **117**: 47-56.

Mccollum, G.D. (1957) Comparitive studies of chromosome pairing in natural and induced tetraploid dactylis. Chromosoma **9**: 571-605.

Mercier, R. (2001). SWITCH1 (SWI1): a novel protein required for the establishment of sister chromatid cohesion and for bivalent formation at meiosis. Genes Dev. **15**: 1859–1871.

Mercier, R., Jolivet, S., Vezon, D., Huppe, E., Chelysheva, L., Giovanni, M., Nogué, F., Doutriaux, M.-P., Horlow, C., Grelon, M., and Mézard, C. (2005). Two Meiotic Crossover Classes Cohabit in Arabidopsis. Current Biology **15**: 692–701.

Mets, D.G. and Meyer, B.J. (2009). Condensins Regulate Meiotic DNA Break Distribution, thus Crossover Frequency, by Controlling Chromosome Structure. Cell **139**: 73–86.

Meuwissen, R.L., Offenberg, H.H., Dietrich, A.J., Riesewijk, A., Van Iersel, M., and Heyting, C. (1992). A coiled-coil related protein specific for synapsed regions of meiotic prophase chromosomes. EMBO J **11**: 5091-5100

Mimitou, E.P. and Symington, L.S. (2009). Nucleases and helicases take center stage in homologous recombination. Trends in biochemical sciences. **34**: 264-272

Mulligan, G.A. (1967) Diploid and autotetraploid Physaria vitulifera (cruciferae). Canadian Journal of Botany **45**: 183-188.

Murakami, H. and Keeney, S. (2014). Temporospatial Coordination of Meiotic DNA Replication and Recombination via DDK Recruitment to Replisomes. Cell **158**: 861-873.

Murashige, T., and Skoog, F. (1962) A revised medium for rapid growth and bio assays with tobacco tissue cultures. Physiologia Plantarum **15** 473.

NCCPE (2015) **http://www.publicengagement.ac.uk/**

Neale, M.J., Pan, J., and Keeney, S. (2005). Endonucleolytic processing of covalent protein-linked DNA double-strand breaks. Nature **436**: 1053–1057.

Nielsen, R., Williamson, S., Kim, Y., Hubisz, M.J., Clark, A.G., and Bustamante, C. (2005). Genomic scans for selective sweeps using SNP data. Genome Research **15**: 1566–1575.

Niu, H., Wan, L., Busygina, V., Kwon, Y., Allen, J.A., Li, X., Kunz, R.C., Kubota, K., Wang, B., Sung, P., Shokat, K.M, Gygi, S.P., and Hollingsworth, N.M. (2009). Regulation of meiotic recombination via Mek1-mediated Rad54 phosphorylation. Molecular Cell **36**: 393–404.

Niu, H., Wan, L., Baumgartner, B., Schaefer, D., Loidl, J., and Hollingsworth, N.M. (2005). Partner Choice during Meiosis Is Regulated by Hop1-promoted Dimerization of Mek1. Molecular biology of the cell **16**: 5804-5818.

Nonomura, K.-I., Nakano, M., Fukuda, T., Eiguchi, M., Miyao, A., Hirochika, H., and Kurata, N. (2004). The Novel Gene HOMOLOGOUS PAIRING ABERRATION IN RICE MEIOSIS1 of Rice Encodes a Putative Coiled-Coil Protein Required for Homologous Chromosome Pairing in Meiosis. The Plant Cell **16**: 1008-1020.

Osman, K., Higgins, J.D., Sanchez-Moran, E., Armstrong, S.J., and Franklin, F.C.H. (2011). Pathways to meiotic recombination in Arabidopsis thaliana. New Phytol. **190**: 523–544.

Page, S.L. and Hawley, R.S. (2004). The genetics and molecular biology of the synaptonemal complex. Annu. Rev. Cell Dev. Biol. **20**: 525–558.

Pan, J., Sasaki, M., Kniewel, R., Murakami, H., Blitzblau, H.G., Tischfield, S.E., Zhu, X., Neale, M.J., Jasin, M., Socci, N.D., Hochwagen, A., and Keeney, S. (2011). A hierarchical combination of factors shapes the genome-wide topography of yeast meiotic recombination initiation. Cell **144**: 719–731.

Panizza, S., Mendoza, M.A., Berlinger, M., Huang, L., Nicolas, A., Shirahige, K., and Klein, F. (2011). Spo11-accessory proteins link double-strand break sites to the chromosome axis in early meiotic recombination. Cell **146**: 372–383.

Panoli, A.P., Ravi, M., Sebastian, J., and Nishal, B. (2006) AtMND1 is required for homologous pairing during meiosis in Arabidopsis. BMC molecular biology **7**: 24

Pâques, F. and Haber, J.E. (1999). Multiple Pathways of Recombination Induced by Double-Strand Breaks in Saccharomyces cerevisiae. Microbiology and molecular biology reviews. **63**: 349-404.

Pezza, R.J., Voloshin, O.N., Vanevski, F., and Camerini-Otero, R.D. (2007). Hop2/Mnd1 acts on two critical steps in Dmc1-promoted homologous pairing. Genes Dev. **21**: 1758–1766.

Phillips, D., Nibau, C., Wnetrzak, J., and Jenkins, G. (2012). High resolution analysis of meiotic chromosome structure and behaviour in barley (Hordeum vulgare L.). PLoS ONE **7**: e39539.

Pradillo, M., Knoll, A., Oliver, C., Varas, J., Corredor, E., Puchta, H., and Santos, J.L. (2015). Involvement of the Cohesin Cofactor PDS5 (SP076) During Meiosis and DNA Repair in Arabidopsis thaliana. Front Plant Sci **6**.

Pratto, F., Brick, K., Khil, P., Smagulova, F., Petukhova, G.V., and Camerini-Otero, R.D. (2014). Recombination initiation maps of individual human genomes. Science **346**: 1256442–1256442.

Puizina, J., Siroky, J., Mokros, P., Schweizer, D., and Riha, K. (2004). Mre11 Deficiency in Arabidopsis Is Associated with Chromosomal Instability in Somatic Cells and Spo11-Dependent Genome Fragmentation during Meiosis. Plant Cell **16**: 1968-1978.

Ramsey, J. and Schemske, D.W. (1998). Pathways, Mechanisms, and Rates of Polyploid Formation in Flowering Plants. Annual Review of Ecology and Systematics. **29**: 467-501.

Rasmussen, S.W. (1987). Chromosome-Pairing in Autotetraploid Bombyx Males - Inhibition of Multivalent Correction by Crossing Over. Carlsberg Res. Commun. **52**: 211–242.

Rasmussen, S.W., Holm, P.B., Lu, B.C., Zickler, D., and Sage, J. (1981). Synaptonemal complex formation and distribution of recombination nodules in pachytene trivalents of triploid Coprinus cinereus. Carlsberg Res. Commun. **46**: 347–360.

Research Councils UK *et al.*, (2010) Concordat for engaging the public with research: a set of principles drawn up by the funders of research in the UK. **http://www.rcuk.ac.uk/per/Pages/Concordat.aspx**

Riley, R. and Chapman, V. (1958) Genetic control of the cytologically diploid behavior of hexaploid wheat. Nature **182**: 713-715.

Robert, T., Nore, A., Brun, C., Maffre, C., Crimi, B., Bourbon, H.M., and de Massy, B. (2016). The TopoVIB-Like protein family is required for meiotic DNA double-strand break formation. Science **351**: 943–949.

Robles, P., Roig, I., Garcia, R., Ortega, A., Egozcue, J., Cabero, L.L., and Garcia, M. (2007). Pairing and synapsis in oocytes from female fetuses with euploid and aneuploid chromosome complements. Reproduction **133**: 899–907.

Rockmill, B. and Roeder, G.S. (1991). A meiosis-specific protein kinase homolog required for chromosome synapsis and recombination. Genes Dev. **5**: 2392–2404.

Rosenberg, S.C. and Corbett, K.D. (2015). The multifaceted roles of the HORMA domain in cellular signaling. J. Cell Biol. **211**: 745–755.

Royal Society (2009) Reaping the benefits: science and sustainable intensification of global agriculture. **http://royalsociety .org/~/media/Royal_Society_Content/policy/publications/2009/4294967719.pdf**

Sanchez-Moran, E. and Armstrong, S.J. (2014). Meiotic chromosome synapsis and recombination in Arabidopsis thaliana: new ways of integrating cytological and molecular approaches. Chromosome Res. **22**: 179–190.

Sanchez-Moran, E., Armstrong, S.J., Santos, J.L., Franklin, F.C., and Jones, G.H. (2001). Chiasma formation in Arabidopsis thaliana accession Wassileskija and in two meiotic mutants. Chromosome Res. **9**: 121–128.

Sanchez-Moran, E., Santos, J.-L., Jones, G.H., and Franklin, F.C.H. (2007). ASY1 mediates AtDMC1-dependent interhomolog recombination during meiosis in Arabidopsis. Genes Dev. **21**: 2220–2233.

Santos, J.L., Alfaro, D., Sanchez-Moran, E., Armstrong, S.J., Franklin, F.C.H., and Jones, G.H. (2003). Partial diploidization of meiosis in autotetraploid Arabidopsis thaliana. Genetics **165**: 1533–1540.

Sasanuma, H., Murakami, H., Fukuda, T., Shibata, T., Nicolas, A., and Ohta, K. (2007). Meiotic association between Spo11 regulated by Rec102, Rec104 and Rec114. Nucleic Acids Res. **35**: 1119–1133.

Sattler, M.C., Carvalho, C.R., and Clarindo, W.R. (2016). The polyploidy and its key role in plant breeding. Planta **243**: 281–296.

Schmickl, R., Paule, J., Klein, J., Marhold, K., and Koch, M.A. (2012). The evolutionary history of the Arabidopsis arenosa complex: diverse tetraploids mask the Western Carpathian center of species and genetic diversity. PLoS ONE **7**: e42691.

Schommer, C., Beven, A., Lawrenson, T., Shaw, P., and Sablowski, R. (2003). AHP2 is required for bivalent formation and for segregation of homologous chromosomes in Arabidopsis meiosis. The Plant Journal **36**: 1–11.

Schücker, K., Holm, T., Franke, C., Sauer, M., and Benavente, R. (2015). Elucidation of synaptonemal complex organization by super-resolution imaging with isotropic resolution. Proc. Natl. Acad. Sci. U.S.A. **112**: 2029–2033.

Schwacha, A. and Kleckner, N. (1997). Interhomolog Bias during Meiotic Recombination: Meiotic Functions Promote a Highly Differentiated Interhomolog-Only Pathway. Cell. **90**: 1123-1135.

Serrentino, M.E., Chaplais, E., Sommermeyer, V., and Borde, V. (2013). Differential Association of the Conserved SUMO Ligase Zip3 with Meiotic Double-Strand Break Sites Reveals Regional Variations in the Outcome of Meiotic Recombination. PLoS Genet. **9**: e1003416.

Séguéla-Arnaud, M., Crismani, W., Larcheveque, C., Mazel, J., Froger, N., Choinard, S., Lemhemdi, A., Macaisne, N., Van Leene, J., Gevaert, K., De Jaeger, G., Chelysheva, L., and Mercier, R. (2015). Multiple mechanisms limit meiotic crossovers: TOP3α and two BLM homologs antagonize crossovers in parallel to FANCM. Proc. Natl. Acad. Sci. U.S.A. **112**: 4713–4718.

Shimizu, K.K., Fujii, S., Marhold, K., Watanabe, K., and Kudoh, H. (2005). Arabidopsis kamchatica (Fisch. ex DC.) K. Shimizu & Kudoh and A. kamchatica subsp. kawasakiana (Makino) K. Shimizu & Kudoh, New Combinations. APG : Acta phytotaxonomica et geobotanica **56**: 163–172.

Siaud, N., Dray, E., Gy, I., Gérard, E., Takvorian, N., and Doutriaux, M.-P. (2004). Brca2 is involved in meiosis in Arabidopsis thaliana as suggested by its interaction with Dmc1. The EMBO Journal **23**: 1392–1401.

Smagulova, F., Gregoretti, I.V., Brick, K., Khil, P., Camerini-Otero, R.D., and Petukhova, G.V. (2011). Genome-wide analysis reveals novel molecular features of mouse recombination hotspots. Nature **472**: 375–378.

Smith, A.V. and Roeder, G.S. (1997). The yeast Red1 protein localizes to the cores of meiotic chromosomes. J. Cell Biol. **136**: 957–967.

Snowden, T., Acharya, S., Butz, C., Berardini, M., and Fishel, R. (2004). hMSH4-hMSH5 Recognizes Holliday Junctions and Forms a Meiosis-Specific Sliding Clamp that Embraces Homologous Chromosomes. Molecular Cell **15**: 437–451.

Sommermeyer, V., Béneut, C., Chaplais, E., Serrentino, M.E., and Borde, V. (2013). Spp1, a member of the Set1 Complex, promotes meiotic DSB formation in promoters by tethering histone H3K4 methylation sites to chromosome axes. Molecular Cell **49**: 43–54.

Stacey, N.J., Kuromori, T., Azumi, Y., Roberts, G., Breuer, C., Wada, T., Maxwell, A., Roberts, K., and Sugimoto-Shirasu, K. (2006). Arabidopsis SPO11-2 functions with SPO11-1 in meiotic recombination. The Plant Journal **48**: 206-216.

Stevens, R., Grelon, M., Vezon, D., Oh, J., Meyer, P., Perennes, C., Domenichini, S., and Bergounioux, C. (2004). A CDC45 homolog in Arabidopsis is essential for meiosis, as shown by RNA interference-induced gene silencing. Plant Cell **16**: 99–113.

Storlazzi, A., Tesse, S., Ruprich-Robert, G., Gargano, S., Pöggeler, S., Kleckner, N., and Zickler, D. (2008). Coupling meiotic chromosome axis integrity to recombination. Genes Dev. **22**: 796–809.

Sturtevant, A.H. (1915) The behavior of the chromosomes as studied through linkage. Z induct Abstamm-u VererbLehre **13**: 234-287.

Subramanian, V.V., MacQueen, A.J., Vader, G., Shinohara, M., Sanchez, A., Borde, V., Shinohara, A., and Hochwagen, A. (2016). Chromosome Synapsis Alleviates Mek1-Dependent Suppression of Meiotic DNA Repair. PLOS Biol **14**: e1002369.

Sun, X., Huang, L., Markowitz, T.E., Blitzblau, H.G., Chen, D., Klein, F., and Hochwagen, A. (2015). Transcription dynamically patterns the meiotic chromosome-axis interface. Elife **4**.

Sym, M. and Roeder, G.S. (1995). Zip1-induced changes in synaptonemal complex structure and polycomplex assembly. J. Cell Biol. **128**: 455–466.

Tang, S., Wu, M.K.Y., Zhang, R., and Hunter, N. (2015). Pervasive and essential roles of the top3-rmi1 decatenase orchestrate recombination and facilitate chromosome segregation in meiosis. Molecular Cell **57**: 607–621.

Tsubouchi, T., Zhao, H., and Roeder, G.S. (2006). The Meiosis-Specific Zip4 Protein Regulates Crossover Distribution by Promoting Synaptonemal Complex Formation Together with Zip2. Dev. Cell **10**: 809–819.

Uanschou, C., Siwiec, T., Pedrosa-Harand, A., Kerzendorfer, C., Sanchez-Moran, E., Novatchkova, M., Akimcheva, S., Woglar, A., Klein, F., and Schlögelhofer, P. (2007). A novel plant gene essential for meiosis is related to the human CtIP and the yeast COM1/SAE2 gene. The EMBO Journal **26**: 5061–5070.

United Nations (2015) World Population Prospects. **http://esa.un.org/unpd/wpp/Publications/Files/WPP2015_DataBooklet.pdf**

Vader, G. (2015). Pch2(TRIP13): controlling cell division through regulation of HORMA domains. Chromosoma **124**: 333–339.

Varner, J. (2014). Scientific Outreach: Toward Effective Public Engagement with Biological Science. BioScience **64**: 333–340.

Vignard, J., Siwiec, T., Chelysheva, L., Vrielynck, N., Gonord, F., Armstrong, S.J., Schlögelhofer, P., and Mercier, R. (2007). The interplay of RecA-related proteins and the MND1-HOP2 complex during meiosis in Arabidopsis thaliana. PLoS Genet. **3**: 1894–1906.

Vitae-CROS (2015) Vitae Careers in Research Online Survey (CROS): 2015 UK aggregated results. **http://www.vitae.ac.uk/vitae-publications/reports/cros-report-vitae-2015.pdf/view**

Vrielynck, N., Chambon, A., Vezon, D., Pereira, L., Chelysheva, L., De Muyt, A., Mézard, C., Mayer, C., and Grelon, M. (2016). A DNA topoisomerase VI-like complex initiates meiotic recombination. Science **351**: 939–943.

Wallace, B.M. and Hulten, M.A. (1983) Triple chromosome synapsis in oocytes from a human foetus with trisomy 21. Ann Hum Genet. **47**: 271-276.

Wan, L., Niu, H., Futcher, B., Zhang, C., Shokat, K.M., Boulton, S.J., and Hollingsworth, N.M. (2008). Cdc28–Clb5 (CDK-S) and Cdc7–Dbf4 (DDK) collaborate to initiate meiotic recombination in yeast. Genes Dev **22**: 386-397.

Waterworth, W.M., Altun, C., Armstrong, S.J., Roberts, N., Dean, P.J., Young, K., Weil, C.F., Bray, C.M., and West, C.E. (2007). NBS1 is involved in DNA repair and plays a synergistic role with ATM in mediating meiotic homologous recombination in plants. The Plant Journal **52**: 41–52.

Weiss, H. and Maluszynska, J. (2000). Chromosomal rearrangement in autotetraploid plants of Arabidopsis thaliana. Hereditas **133**: 255–261.

Wesley, S.V., Helliwell, C.A., Smith, N.A., Wang, M.B., Rouse, D.t., Liu, Q., Gooding, P.S., Singh, S.P., Abbot, D., Stoutjesdijk, P.A., Robinson, S.P., Gleave, A.P., Green, A.G., and Waterhouse, P.M. (2001). Construct design for efficient, effective and high-throughput gene silencing in plants. The Plant Journal **27**: 581-590.

West, A. (2015) Investigating the links between meiotic chromosome structure and homologous recombination in Arabidopsis thaliana. PhD Thesis, University of Birmingham.

Woltering, D., Baumgartner, B., Bagchi, S., Larkin, B., Loidl, J., de los Santos, T., and Hollingsworth, N.M. (2000). Meiotic segregation, synapsis, and recombination checkpoint functions require physical interaction between the chromosomal proteins Red1p and Hop1p. Mol. Cell. Biol. **20**: 6646–6658.

Wright, K.M., Arnold, B., Xue, K., Šurinová, M., O'Connell, J., and Bomblies, K. (2014). Selection on meiosis genes in diploid and tetraploid Arabidopsis arenosa. Mol. Biol. Evol. **32**: 944-955.

Yant, L., Hollister, J.D., Wright, K.M., Arnold, B.J., Higgins, J.D., Franklin, F.C.H., and Bomblies, K. (2013). Meiotic Adaptation to Genome Duplication in Arabidopsis arenosa. Current Biology **23**: 2151-2156.

Ye, Q., Rosenberg, S.C., Moeller, A., Speir, J.A., Su, T.Y., and Corbett, K.D. (2015). TRIP13 is a protein-remodeling AAA plus ATPase that catalyzes MAD2 conformation switching. Elife **4**.

Yelina, N.E., Choi, K., Chelysheva, L., Macaulay, M., de Snoo, B., Wijnker, E., Miller, N., Droudaud, J., Grelon, M., Copenhaver, G.P., Mezard, C., Kelly, K.A., and Henderson, I.R. (2012). Epigenetic Remodeling of Meiotic Crossover Frequency in Arabidopsis thaliana DNA Methyltransferase Mutants. PLoS Genet. **8**: e1002844

Zakharyevich, K., Tang, S., Ma, Y., and Hunter, N. (2012). Delineation of Joint Molecule Resolution Pathways in Meiosis Identifies a Crossover-Specific Resolvase. Cell **149**: 334–347.

Zanders, S. and Alani, E. (2009). The pch2Delta mutation in baker's yeast alters meiotic crossover levels and confers a defect in crossover interference. PLoS Genet. **5**: e1000571.

Zanders, S., Sonntag Brown, M., Chen, C., and Alani, E. (2011). Pch2 modulates chromatid partner choice during meiotic double-strand break repair in Saccharomyces cerevisiae. Genetics **188**: 511–521.

Zhang, C., Song, Y., Cheng, Z.-H., Wang, Y.-X., Zhu, J., Ma, H., Xu, L., and Yang, Z.-N. (2012). The Arabidopsis thaliana DSB formation (AtDFO) gene is required for meiotic double-strand break formation. Plant J. **72**: 271–281.

Zhang, L., Kim, K.P., Kleckner, N.E., and Storlazzi, A. (2011). Meiotic double-strand breaks occur once per pair of (sister) chromatids and, via Mec1/ATR and Tel1/ATM, once per quartet of chromatids. Proc Natl Acad Sci USA **108**: 20036-20041.

Zhang, L., Liang, Z., Hutchinson, J., and Kleckner, N. (2014a). Crossover patterning by the beam-film model: analysis and implications. PLoS Genet. **10**: e1004042.

Zhang, L., Wang, S., Yin, S., Hong, S., Kim, K.P., and Kleckner, N. (2014b). Topoisomerase II mediates meiotic crossover interference. Nature **511**: 551

Zickler, D. and Kleckner, N. (2016). A few of our favorite things: Pairing, the bouquet, crossover interference and evolution of meiosis. Semin. Cell Dev. Biol. **54**: 135–148.

Appendix

Table S1. Measurements from pachytene synaptic multivalent chromosomes from TBG A. arenosa triple labelled for ASY1/ZYP1/MLH1. Distances from chromosome ends to MLH1 foci and between foci (CO-CO distance) and distances from chromosome ends to SPS site and between SPS site (SPS-SPS distance) were measured for each chromosome. Images with names that have the same first four digits (e.g. 1058.11) come from the same pachytene cell and images with the same fifth digit (e.g. 1058.11) come from the same synaptic multivalent.

Image	CO - CO distance (uM)			SPS - SPS distance (uM)		
1058.11	25.14	7.95		12.13	20.87	
1058.12	25.21	5.72		10.06	20.6	
1058.21	12.55	12.55		6.24	19.23	
1058.22	11.01	14.61		5.76	19.73	
1059.11	20.93	5.16		8.46	17.8	
1059.12	15.68	8.42		6.12	17.7	
1060.11	11.08	11.08		4.7	17.28	
1060.12	14.56	9.94	0.71	6.1	19.45	
1061.11	23.24			6.21	16.46	
1061.12	3.02	8.31	12.83	6.36	18.17	
1061.21	16.89	6.34		3.76	19.34	
1061.22	12.02	8.14		3.2	17.09	
1061.31	13.54	12.52		2.62	23.46	
1061.32	14.76	11.15		2.76	23.29	
1062.11	16.21	7.52		11.86	11.9	
1062.12	23.48	2.12		12.03	13.12	
1066.11	24.49	2.93		6.74	4.45	15.62
1066.12	16.97	7.88		6.51	3.33	14.43
1066.21	13.65	10.56		8.59	15.05	
1066.22	1.53	15.76	10.08	12.21	15.27	
1067.11	0.44	21.73		10.37	4.59	6.85
1067.12	2.77	9.17	9.31	10.46	4.99	6.05
1067.21	21.06	4.01		6.81	17.94	
1067.22	20.03	4.23		6.51	17.64	
1068.11	14.44	10.81	0.92	4.26	15.25	5.89
1068.12	15.15	7.33	1.68	4.25	14.27	5.89
1069.11	39.36	1.16		18.47	7.73	13.67
1069.12	20.86	21.78		15	8.83	17.79
1070.11	27.27	1.18		10.13	18.03	

1070.12	26.85	1.5		11.3	16.36	
1070.21	11.86	16.32		5.08	22.69	
1070.22	26.53	2.6		6.94	21.96	
1072.11	11.57	6.61	6.09	3.23	21.46	
1072.12	12.69	9.49		2.52	19.53	
1072.21	14.05	2.68		4.65	12.07	
1072.22	12.83	5.97		5.72	13.23	
1074.11	19.56	8		2.74	24.93	
1074.12	14.07	11.23		3.71	21.62	
1076.11	17.06	5.13		2.22	19.87	
1076.12	20.67	2.16		2.42	20.44	
1087.11	18.48	13.15		3.43	28.1	
1087.12	23.13	7.28		3.45	26.87	
1087.21	17.18	2.55		6.51	13.24	
1087.22	16.14	2.14		5.44	12.92	
1088.11	18.38	0.41		7.1	11.12	
1088.12	20.06	2.42		8.81	13.75	
1088.21	14.44	4.2		4.56	14.03	
1088.22	19.02	2.18		4.54	16.52	
1093.11	19.83	0.42		6.2	14.04	
1093.12	2.57	6.6	9.86	5.22	14.25	
1098.11	15.47	6.2		1.53	19.97	
1098.12	15.48	7.94		1.77	21.23	
1104.11	18.12	11.95		10.68	19.17	
1104.12	24.24	3.59		7.69	19.98	
1104.21	21.76	3.2		4.32	20.66	
1104.22	11.09	11.09		4.42	17.65	
1104.31	11.23	19.9	1.14	5.91	26.51	
1104.32	17.01	12.31	4.88	6.08	28.14	
1105.11	11.79	4.38		3.72	12.52	
1105.12	14.77	3.46		4.6	13.45	
1105.21	4.83	28.22	1.51	20.21	14.71	
1105.22	2.72	31.15	1.59	19.08	16.66	
1106.11	11.36	11.15		5.12	17.4	
1106.12	10.97	11.64		6.6	15.87	
1106.21	17.74	0.82		7.83	10.75	
1106.22	15.55	3.6		8.68	10.47	
1106.31	2.17	13.86	5.069	5.33	16	
1106.32	17.11	5.63		5.64	17.18	
1108.11	26.51			10.88	11.52	3.18
1108.12	3.51	11.21	7.17	8.55	11.11	2.17
1108.21	30.71	1.98		6.49	13.08	12.34
1108.22	32.6	2.87		7.14	11.37	16.94

1119.11	17.96			7.73	9.65	
1119.12	15.73	3.45		8.24	10.73	
1122.11	27.48	1.47		7.81	20.24	
1122.12	3.6	25.59	0.51	7.86	22.19	
1125.11	16.95	9.33		5.71	20.51	
1125.12	13.86	14.74		5.76	22.6	
1125.21	29.68	0.24		3.24	10.3	15.35
1125.22	25.79	1.3		3.33	9.33	14.14
1125.31	24.35	0.98		4.56	20.44	
1125.32	23.85	0.84		4.79	19.63	
1126.11	25.2	2.57		17.2	10.52	
1126.12	7.15	21.55		14.9	13.7	
1126.21	18.65	11.83		3.11	27.14	
1126.22	17.15	14.99		3.17	28.78	
1129.11	22.71	3.2		13.09	12.93	
1129.12	0.84	26.88	1.83	15.2	14.14	
1130.11	14.22	10.71		4.49	20.49	
1130.12	11.7	13.36		3.89	21.08	
1132.11	19.78	8.67		8.04	20.19	
1132.12	2.23	25.66	1.61	8.9	20.71	
1133.11	0.45	21.65	0.51	8.66	14.15	
1133.12	22.46	3.57		9.92	16.41	
1133.21	16.84	13.64		4.38	26.25	
1133.22	23.51	6.48		4.66	25.7	
1133.31	0.53	22.79	1.9	13.01	12.54	
1133.32	3.81	19.21	3.81	12.84	12.14	
1138.11	13.36	10.4		6.16	17.49	
1138.12	10.76	13.99		6.12	18.29	
1138.21	22.52			5.96	9.71	5.8
1138.22	14.62	7.5		6.92	9.44	5.39
1138.31	13.02	6.39		1.07	18.41	
1138.32	14.18	4.08		1.38	17.36	
1140.11	13.71	9.71		4.13	19.47	
1140.12	19.06	4.27		4.22	19.3	
1140.21	16.92	9.25		3.51	22.46	
1140.22	25.73	1.78		3.71	24.12	
1141.11	22.41	3.48		8.34	17.59	
1141.12	17.53	6.36		7.85	15.85	
1143.11	15.36	6.57		1.57	20.13	
1143.12	13.23	10.17		1.65	21.93	
1146.11	20.35	19.11		10.24	29.19	
1146.12	21.92	18.13		12.09	28.03	
1154.11	12.12	6.64	3.59	5.55	17.11	

1154.12	15.8	4.55		4.64	15.74	
1154.21	1.52	27.13		15.73	12.75	
1154.22	1.11	27.44	1.5	17.89	12.14	
1154.31	8.79	15.56	0.86	3.39	21.35	
1154.32	11.11	17.51	1.05	3.85	26.05	
1154.41	27.32	0.71		15.14	12.69	
1154.42	3.96	17.12	3.67	15.77	9.87	
1154.51	26.09	1.74		14.88	12.97	
1154.52	2.88	12.91	11.02	13.3	14.06	
1155.11	20.64	0.74		8.52	12.75	
1155.12	21	1.53		10.38	12.4	
1155.21	16.82	2.54		3.25	15.96	
1155.22	13.7	7.33		4.18	16.78	
1155.31	17.73	11.53		9.26	19.98	
1155.32	25.93	5.62		9.14	22.58	
1155.41	19.41	6.14		4.14	21.7	
1155.42	16.87	6.84		4.33	19.19	
1158.11	16.76	17.37		6.68	27.09	
1158.12	31.87	5.5		5.86	31.79	
1158.21	17.51	3.31		6.12	14.75	
1158.22	18.07	2.93		4.99	16.23	
1161.11	27.18	6.17		5.81	27.13	
1161.12	15.65	14.69	2.82	4.93	28.28	
1161.21	17.31	13.4		8.94	21.55	
1161.22	26.58	1.53		8.45	19.58	
1164.11	9.57	14.14	3.93	14.03	13.93	
1164.12	0.82	22.39	1.74	12.37	13.05	
1164.21	25.31			8.15	17.08	
1164.22	18.45	3.21		8.4	13.28	
1167.11	12.06	7.63		4.09	15.37	
1167.12	20.47	0.64		3.96	17.07	
1167.21	16.81	9.47		6.66	19.57	
1167.22	13.68	15.95		6.82	22.64	
1167.31	16.57			5.31	10.73	
1167.32	13.85	1.99		3.11	13.04	
1171.11	16.39	7.87		4.2	19.43	
1171.12	15.95	10.43		3.03	23.18	
1171.21	23.57	5.89		8.05	21.32	
1171.22	15.91	12.68		7.97	20.78	
1171.31	25.32	0.5		11.88	14.07	
1171.32	5.49	10.73	6.76	11.53	11.83	
1172.11	20.7	0.96		6.22	14.83	
1172.12	17.36	4.18		5.19	16.36	

1172.21	26.44	5.2		3.74	27.37	
1172.22	17.86	14.3		3.39	28.14	
1172.31	17.91	5.3		8.46	14.53	
1172.32	18.52	2.35		8.58	12.31	
1172.41	14.18	5.19		3.93	15.49	
1172.42	11.9	8.27		4.5	15.43	
1172.51	13.87	13.06		4.55	18.09	4
1172.52	14.79	11.84		3.96	16.85	5.68
1173.11	2.23	21.88	0.36	14.59	9.94	
1173.12	4.79	18.6	0.44	14.48	9.24	
1173.21	19.14	1.65		3.83	16.93	
1173.22	14.14	4.23		3.46	15.28	
1173.31	20.9	2.24		7.74	15.48	
1173.32	19.68	5.47		7.87	17.46	
1173.41	19.55	11.51		7.4	23.8	
1173.42	12.98	10.79	5.11	5.19	23.96	
1127.11	18.75	4.39		3.84	19.48	
1127.12	20.58	4.47		4.75	20.4	
1127.21	20.03	7.34		6.52	20.69	
1127.22	20.58	6.93		6.59	20.64	

Table S2. Measurements from pachytene bivalent chromosomes from TBG A. arenosa triple labelled for ASY1/ZYP1/MLH1. Distances from chromosome ends to MLH1 foci and between foci (CO-CO distance) were measured.

chromosomes without SPS co-co distances (uM)			total length (uM)
1.14	23.86		25
18.52	7.25		25.77
3.82	18.72	0.2	22.74
13.63	8.57		22.2
2.45	20.73	1.67	24.85
11.57	12.32		23.89
0.82	18.46	0.91	20.19
14.99	6.9		21.89
25.41	0.44		25.85
14.2	8.15		22.35
18.89	0.74		19.63
12.96	5.96		18.92
10.61	12.69		23.3
1.39	18.97		20.36
16.53	2.53		19.06
5.25	18.3		23.55
14.22	4.68		18.9
3.31	14.56		17.87
11.08	16.56		27.64
12.34	4.17		16.51
16.45	2.35		18.8
11.22	15.5		26.72
6.79	10.1		16.89
4.87	18.69		23.56
9.33	16.32		25.65
9.49	26.61		36.1
3.14	18.39	1.94	23.47
7.17	8.63	12.57	28.37
25.76	3.95		29.71
4.27	16.08		20.35
11.78	20.23		32.01
18.12	10.73		28.85

12.49	7.5		19.99
1.84	21.59		23.43
18.33	8.97		27.3
6.89	14.85		21.74
10.94	16.24		27.18
22.28	11.2		33.48
14.49	6.93		21.42
11.16	13.37		24.53
7.87	8.1		15.97
0.47	15.64		16.11
2.5	17.84		20.34
17.75	1.61		19.36
0.98	21.86		22.84
5.03	6.63		11.66
6.92	21.49		28.41
11.17	5.07		16.24
18.99	4.06		23.05
16.68	4.91		21.59
14.9	7.14		22.04
14.98	18.29		33.27
17.08	9.72		26.8
12.61	12.87		25.48
13.84	6.18		20.02
11.42	16.27		27.69
10	8.55		18.55
8	13.35		21.35
10.1	9.52		19.62
16.5	4.46		20.96
18.43	1.12		19.55
16.04	1.66		17.7
4.93	14.98		19.91
10.86	2.54		13.4
7.37	9.29		16.66
3.52	17.06	1.06	21.64
7.66	11.75		19.41
10.92	8.4		19.32
8.49	14.08		22.57
14.35	3.94		18.29
15.47	12		27.47
6.43	14.04		20.47

8.61	16.98		25.59
12.81	9.15		21.96
9.28	10.04		19.32
13.76	12		25.76
17.4	12.94		30.34
10.54	13.23		23.77
19.88	13	0.59	33.47
31.94	1.6		33.54
7.61	12.69		20.3
16.97	4.01		20.98
5.28	15.85		21.13
7.65	14.21		21.86
14.78	4.13		18.91
9.65	13.2		22.85
18.55	8.29		26.84
1.08	17.8	5.53	24.41
15.12	7.7		22.82
10.52	10.49		21.01
29.52	0.76		30.28
15.45	7.34		22.79
10.99	11.96		22.95
12.22	7.86		20.08
19.66	0.23		19.89
20.37			20.37
15.74	2.34		18.08
3.69	20.03		23.72
14.71	9.51		24.22
13.41	8.75		22.16
8.99	19.75		28.74
12.72	6.98	3.52	23.22
14.65	5.59		20.24
4.43	15.88		20.31
10.62	9.44		20.06
9.92	17.05		26.97
3.18	14.58	14.52	32.28
7.95	7.31		15.26
2.45	18.91	1.92	23.28
15.74	5.8		21.54
20.09	5.2		25.29
21.92	6.42		28.34

14.26	9.95		24.21
22.9	2.37		25.27
4.45	7.98	0.5	12.93
14.6	1.75		16.35
7.92	12.96		20.88
6.66	9.21		15.87
12.4	0.77		13.17
7.8	13.47		21.27
10.76	10.05		20.81
20.02	0.84		20.86
15.23	3.45		18.68
2.68	18.89		21.57
10.47	8.91		19.38
17.26	10.64		27.9
17.66	2.21		19.87
12.47	3.16		15.63
13.25	8.39		21.64
10.43	14.54		24.97
2.76	21.31	1.4	25.47
13.5	6.19		19.69
9.46	10.34		19.8
4.61	17.06		21.67
10.96	10.6		21.56
10.88	9.57		20.45
13.7	2.91		16.61
10.06	6.87	0.14	17.07
4.41	10.46		14.87
5.62	19.78	5.68	31.08
26.1	6.29		32.39
1.11	16.51	1.36	18.98
1.93	19.13		21.06
12.1	4		16.1
10.67	8.2		18.87
4.99	19.08		24.07
17.61	5.89		23.5
12.83	10.91		23.74
17.65	7.61		25.26
21.03	6.06		27.09
10.08	12.74		22.82
9.85	11.39		21.24

15.23	12.92		28.15
5.59	20.57		26.16
12.02	12.38		24.4
11.73	14.63		26.36
22.94	6.92		29.86
17.04	10.99		28.03
8.88	20.18		29.06

Table S3. Distances between MLH1 foci going across SPS sites and not going across PPS sites

	distance between 2 COs (across PPS) (uM)	total chromosome length (uM)	inter-focus distances as percentage of total length	distance between 2 COs (not across PPS) (uM)	total chromosome length (uM)	inter-focus distances as a percentage of total length
	8.31	24.16	34.39569536	9.94	25.21	39.4287981
	15.76	27.37	57.58129339	6.61	24.27	27.23526988
	9.17	21.25	43.15294118	19.9	32.27	61.66718314
	10.81	26.17	41.30683989	12.31	34.2	35.99415205
	7.33	24.16	30.33940397	6.64	22.35	29.70917226
	6.6	19.03	34.68208092	15.56	25.21	61.72153907
	28.22	34.56	81.65509259	17.51	29.67	59.01584092
	31.15	35.46	87.84545967	14.69	33.16	44.30036188
	13.86	21.099	65.69031708	10.79	28.88	37.36149584
	11.21	21.89	51.21059845	18.72	22.74	82.32189974
	25.59	29.7	86.16161616	20.73	24.85	83.42052314
	26.88	29.55	90.96446701	18.46	20.19	91.43140168
	25.66	29.5	86.98305085	18.39	23.47	78.35534725
	21.65	22.61	95.75409111	8.63	28.37	30.41945717
	22.79	25.22	90.36478985	17.06	21.64	78.83548983
	19.21	26.83	71.59895639	13	33.47	38.84075291
	27.44	30.05	91.31447587	17.8	24.41	72.92093404
	17.12	24.75	69.17171717	6.98	23.22	30.06029285
	12.91	26.81	48.153674	14.58	32.28	45.16728625
	14.14	27.64	51.1577424	18.91	23.28	81.22852234
	22.39	24.95	89.73947896	7.98	12.93	61.71693735
	10.73	22.98	46.69277633	21.31	25.47	83.66705929
	21.88	24.47	89.41561095	6.87	17.07	40.24604569
	18.6	23.83	78.05287453	19.78	31.08	63.64221364
				16.51	18.98	86.98630137
	distance between 2 COs (across PPS)			distance between 2 COs (not across PPS)		
mean	17.89208333	26.001625	67.22437684	14.3864	25.5468	57.82777111
stdev	7.412758085	4.02930967	22.02661327	4.996060848	5.429763439	21.52150197

Table S4. Summary statistics for gamma distribution fitting to inter-MLH1 foci distances either going across an SPS site or not across an SPS site.

Summary statistics:

Variable	Observations	Obs. with missing data	Obs. without missing data	Minimum	Maximum	Mean	Std. deviation
inter-MLH1-foci distance across SPS site (% total SC length)	24	0	24	30.339	95.754	67.224	22.027

Estimated parameters:

Parameter	Value	Standard error
k	8.514	2.455
beta	7.895	2.342

Statistics estimated on the input data and computed using the estimated parameters of the Gamma (2) distribution:

Statistic	Data	Parameters
Mean	67.224	67.219
Variance	485.172	530.717
Skewness (Pearson)	-0.246	0.685
Kurtosis (Pearson)	-1.585	0.705

Chi-square test:

Chi-square (Observed value)	10.148
Chi-square (Critical value)	5.991
DF	2
p-value	0.006
alpha	0.05

Summary statistics:

Variable	Observations	Obs. with missing data	Obs. without missing data	Minimum	Maximum	Mean	Std. deviation
inter-MLH1-foci distance not across SPS site (% total SC length)	25	0	25	27.235	91.431	57.828	21.522

Estimated parameters:

Parameter	Value	Standard error
k	6.987	1.975
beta	8.276	2.421

Statistics estimated on the input data and computed using the estimated parameters of the Gamma (2) distribution:

Statistic	Data	Parameters
Mean	57.828	57.825
Variance	463.175	478.565
Skewness (Pearson)	0.045	0.757
Kurtosis (Pearson)	-1.616	0.859

Chi-square test:

Chi-square (Observed value)	9.086
Chi-square (Critical value)	5.991
DF	2
p-value	0.011
alpha	0.05

Table S5. Measurements of difference in inter-MLH1 foci distances as a proportion of SC length from the chromosome end to the SPS site for both MLH1 foci on the same side of a synaptic multivalent with a B conformation.

Distances of MLH1 foci from chromosome end (uM) on both SC streches on the same side of an SPS in a synaptic multivalent with a B conformation as a proportion of SC length from the chromosome end to the SPS site		Difference between the two distances	Absolute value of difference between the two distances
0.380929564	0.277669903	0.1032597	0.103259661
0.652626105	0.740496706	-0.087871	0.0878706
0.28988764	0.475706215	-0.185819	0.185818574
0.327817994	0.476301931	-0.148484	0.148483937
0.533674339	0.478746243	0.0549281	0.054928096
0.631932773	0.161585366	0.4703474	0.470347407
0.223522854	0.239795918	-0.016273	0.016273064
0.065446478	0.091687042	-0.026241	0.026240563
0.719259586	0.118397086	0.6008625	0.6008625
0.222038111	0.451247166	-0.229209	0.229209055
0.320898516	0.519426457	-0.198528	0.198527941
0.258178158	0.105675147	0.152503	0.152503011
0.46797153	0.270934127	0.1970374	0.197037403
0.192598187	0.165634675	0.0269635	0.026963512
0.036870504	0.176	-0.139129	0.139129496
0.299358517	0.131961259	0.1673973	0.167397258
0.310465699	0.373999058	-0.063533	0.063533359
0.623369849	0.17967968	0.4436902	0.443690169
0.154888674	0.628328612	-0.47344	0.473439938
0.349840256	0.257249071	0.0925912	0.092591185
0.640804598	0.733459357	-0.092655	0.09265476
0.07627907	0.343839542	-0.26756	0.267560472
0.454900049	0.652212389	-0.197312	0.197312341
0.047945205	0.042791645	0.0051536	0.00515356
0.435887988	0.520847811	-0.08496	0.084959823
0.522693997	0.633776091	-0.111082	0.111082094
0.519619048	0.252140078	0.267479	0.26747897
0.5946255	0.764898852	-0.170273	0.170273352
0.347093971	0.235023041	0.1120709	0.112070929
0.498715973	0.221243523	0.2774724	0.27747245
0.411843277	0.073797678	0.3380456	0.338045599
0.197839682	0.40126183	-0.203422	0.203422148
0.326378539	0.46374829	-0.13737	0.137369751
0.654676259	0.646806993	0.0078693	0.007869266
0.058039216	0.123387097	-0.065348	0.065347881
0.15914787	0.436829559	-0.277682	0.277681689
0.577077077	0.248892826	0.3281843	0.328184252
0.282949309	0.356435644	-0.073486	0.073486335
0.641196013	0.173010381	0.4681856	0.468185633
0.22440678	0.180529883	0.0438769	0.043876897
0.621809745	0.07814096	0.5436688	0.543668785
0.496421601	0.037492677	0.4589289	0.458928923
0.483903935	0.7045053	-0.220601	0.220601366
0.405043747	0.449956859	-0.044913	0.044913113
0.276266417	0.610202117	-0.333936	0.333935701
0.064733648	0.255501222	-0.190768	0.190767574
0.189989039	0.508173419	-0.318184	0.31818438
0.36476256	0.190901706	0.1738609	0.173860854
0.335054874	0.535968892	-0.200914	0.200914018
0.09746013	0.276832461	-0.179372	0.179372331
0.144702842	0.313287514	-0.168585	0.168584672
0.225359343	0.219117647	0.0062417	0.006241696
0.354760754	0.335755814	0.0190049	0.01900494
		mean	0.19370893
		st.dev	0.14966631

Table S6. Example of how Random CO-CO distances were calculated for all synaptic multivalents with a B conformation (only 10 measurements shown). The distance between all MLH1 foci was calculated by subtracting the distances from the chromosome ends of one MLH1 focus from another (red boxes). This was repeated for all 106 distance measurements (rather than just the 10 shown here) to give 11236 random inter-foci distances from which the distribution frequency of random interactions could be calculated.

distance from end to CO (% SC to SPS)	0.626294	0.786196	0.114238	0.516312	0.747171	0.421083	0.912374	0.940578	0.782423	0.653512
0.626293847	0	0.159903	0.512056	0.109982	0.120877	0.205211	0.28608	0.314284	0.156129	0.027218
0.786196461	0.159903	0	0.671959	0.269885	0.039026	0.365113	0.126177	0.154382	0.003773	0.132685
0.114237847	0.512056	0.671959	0	0.402074	0.632933	0.306845	0.798136	0.82634	0.668185	0.539274
0.516311534	0.109982	0.269885	0.402074	0	0.230859	0.095229	0.396062	0.424266	0.266112	0.1372
0.747170698	0.120877	0.039026	0.632933	0.230859	0	0.326088	0.165203	0.193407	0.035253	0.093659
0.421083028	0.205211	0.365113	0.306845	0.095229	0.326088	0	0.491291	0.519495	0.36134	0.232429
0.912373685	0.28608	0.126177	0.798136	0.396062	0.165203	0.491291	0	0.028204	0.12995	0.258862
0.94057798	0.314284	0.154382	0.82634	0.424266	0.193407	0.519495	0.028204	0	0.158155	0.287066
0.782423325	0.156129	0.003773	0.668185	0.266112	0.035253	0.36134	0.12995	0.158155	0	0.128911
0.653511954	0.027218	0.132685	0.539274	0.1372	0.093659	0.232429	0.258862	0.287066	0.128911	0

Table S7. Summary statistics for Kolmogorov-Smirnov test analysing the difference between observed inter-foci distances on different SC stretches on synaptic multivalents with a B conformation versus distances between randomly paired MLH1 foci from all bivalents.

Summary statistics:

Variable	Observations	Obs. with missing data	Obs. without missing data	Minimum	Maximum	Mean	Std. deviation
experiment	53	0	53	0.005	0.601	0.194	0.150
random	11236	0	11236	0.000	0.728	0.224	0.162

Two-sample Kolmogorov-Smirnov test / Upper-tailed test:

D	0.155
p-value	0.072

Table S8. Rod/Ring/Multivalent/Univalent counts from ASY1 TTTT and ASY1 DDDD metaphase I cells. Due to the difficulty in interpreting multivalent chiasma conformations, total chiasma numbers were not included for cells containing multivalent chromosomes.

Line	Rod	Ring	Multi	Uni	Total Chiasma	Chiasma per pair
ASY1 TTTT	13	3	0	0	19	1.1875
ASY1 TTTT	16	0	0	0	16	1
ASY1 TTTT	16	0	0	0	16	1
ASY1 TTTT	9	0	2	0		
ASY1 TTTT	16	0	0	0	16	1
ASY1 TTTT	16	0	0	0	16	1
ASY1 TTTT	13	1	1	0		
ASY1 TTTT	14	2	0	0	18	1.125
ASY1 TTTT	16	0	0	0	16	1
ASY1 TTTT	16	0	0	0	16	1
ASY1 TTTT	16	0	0	0	16	1
ASY1 TTTT	15	1	0	0	17	1.0625
ASY1 TTTT	13	3	0	0	19	1.1875
ASY1 TTTT	16	0	0	0	16	1
ASY1 TTTT	15	1	0	0	17	1.0625
ASY1 TTTT	13	1	1	0		
ASY1 TTTT	15	1	0	0	17	1.0625
ASY1 TTTT	14	2	0	0	18	1.125
ASY1 TTTT	16	0	0	0	16	1
ASY1 TTTT	16	0	0	0	16	1
ASY1 TTTT	13	3	0	0	19	1.1875
ASY1 TTTT	15	0	0	2	15	0.9375
ASY1 TTTT	14	2	0	0	18	1.125
ASY1 TTTT	14	0	1	0		
ASY1 TTTT	16	0	0	0	16	1
ASY1 TTTT	13	2	0	2	17	1.0625
ASY1 TTTT	14	2	0	0	18	1.125
ASY1 TTTT	13	1	1	0		
ASY1 TTTT	15	1	0	0	17	1.0625
ASY1 TTTT	15	1	0	0	17	1.0625
ASY1 DDDD	15	1	0	0	17	1.0625
ASY1 DDDD	14	0	1	0		
ASY1 DDDD	14	0	1	0		
ASY1 DDDD	14	0	1	0		
ASY1 DDDD	15	1	0	0	17	1.0625
ASY1 DDDD	15	1	0	0	17	1.0625
ASY1 DDDD	14	1	1	0		
ASY1 DDDD	15	1	0	0	17	1.0625
ASY1 DDDD	15	1	0	0	17	1.0625
ASY1 DDDD	15	1	0	0	17	1.0625
ASY1 DDDD	16	0	0	0	16	1
ASY1 DDDD	16	0	0	0	16	1
ASY1 DDDD	11	3	1	0		
ASY1 DDDD	16	0	0	0	16	1
ASY1 DDDD	16	0	0	0	16	1
ASY1 DDDD	16	0	0	0	16	1
ASY1 DDDD	16	0	0	0	16	1
ASY1 DDDD	14	2	0	0	18	1.125
ASY1 DDDD	14	2	0	0	18	1.125
ASY1 DDDD	14	2	0	0	18	1.125
ASY1 DDDD	15	1	0	0	17	1.0625
ASY1 DDDD	15	1	0	0	17	1.0625
ASY1 DDDD	14	0	1	0		
ASY1 DDDD	16	0	0	0	16	1
ASY1 DDDD	14	2	0	0	18	1.125
ASY1 DDDD	11	3	1	0		
ASY1 DDDD	14	2	0	0	18	1.125
ASY1 DDDD	13	3	0	0	19	1.1875
ASY1 DDDD	16	0	0	0	16	1
ASY1 DDDD	15	1	0	0	17	1.0625
					mean chiasma per cell	**S.D**
				ASY1 TTTT	16.88	1.12989675
				ASY1 DDDD	16.95652174	0.87792425

Table S9. Counts of different bivalent conformations per cell and as a proportion of total bivalents from diploid SN A. arenosa and tetraploid arenosa with different ASY1 genotypes

Mean number per cell	O	+	ł	I
DIPLOID (n=123)	1.438202	2.846774	1.990741	1.837838
2X diploid	2.876404	5.693548	3.981481	3.675676
TTTT (n=178)	1.378882	3.642045	5.151685	3.549133
TxD (n=63)	1.190476	3.746032	4.825397	4.111111
DDDD (n=167)	1.134752	4.39521	4.994048	3.165605
Counts from individual tetraploid plants				
TBG ♯2 (TTTT)	1.222222	2.454545	4.636364	5.441176
TBG ♯4(TTTT)	1.410448	3.916084	5.268966	3.086331
TBG.5Bx3B ♯2 (DDDD)	1.134021	4.403361	4.915966	3.327434
TBG.5Bx3B ♯4 (DDDD)	1.272727	4.692308	4.153846	2.666667
TBG.5Bx3B ♯6 (DDDD)	1.129032	4.1875	5.545455	2.78125

Proportions of total countable bivalents	O	+	ł	I	|/+
DIPLOID	0.143346774	0.39281874	0.238844086	0.224990399	0.733198925
TTTT	0.093840959	0.26959007	0.380228981	0.25633999	1.401343637
TxD	0.084390675	0.269403581	0.345496458	0.299575498	1.518682796
DDDD	0.073102613	0.330741857	0.375981312	0.219716342	1.017571999
TBG ♯2 (TTTT)	0.075861924	0.177003103	0.332159466	0.414975507	
TBG ♯4(TTTT)	0.098056733	0.291300118	0.391500454	0.219142696	
TBG.5Bx3B ♯2 (DDDD)	0.067985236	0.329103926	0.369835253	0.232429172	
TBG.5Bx3B ♯4 (DDDD)	0.113764868	0.414822784	0.334053553	0.137358795	
TBG.5Bx3B ♯6 (DDDD)	0.080289474	0.301735957	0.409602949	0.208371619	

T.Test on +	T4	D2	D4	D6
TBG ♯2 (TTTT)	3.24E-05	2.23E-07	0.000588	0.000889
TBG ♯4(TTTT)		0.026812	0.035805	0.006776
TBG.5Bx3B ♯2 (DDDD)			0.130147	0.272741
TBG.5Bx3B ♯4 (DDDD)				0.30261
TBG.5Bx3B ♯6 (DDDD)				

Conclusions:

None of the DDDD plants differ from one another statisitcally

The two TTTT lines do, but both are lower than DDDD

T.TEST O	DIPLOID	TTTT	TxD
DIPLOID			
TTTT	0.000243		
TxD	0.000217	0.442712	
DDDD	3.29E-07	0.023845	0.361319

T.TEST +	DIPLOID	TTTT	TxD
DIPLOID			
TTTT	3.53E-11		
TxD	2.23E-08	0.992005792	
DDDD	0.000823	0.00010511	0.001677757

T.TEST ł	DIPLOID	TTTT	TxD
DIPLOID			
TTTT	4.25133E-14		
TxD	6.22458E-06	0.0985701	
DDDD	5.86041E-13	0.787092247	0.15326323

T.TEST I	DIPLOID	TTTT	TxD
DIPLOID			
TTTT	0.073105		
TxD	0.002615	0.070931	
DDDD	0.751506	0.021587	0.000823

T.TEST |/+	DIPLOID	TTTT	TxD
DIPLOID			
TTTT	3.71E-06		
TxD	0.000173	0.609285948	
DDDD	0.009684	0.015816849	0.019586504

Table S.10. Rod/ring bivalent counts and associated statistical analysis from Col-0, HO ASY1 and SN ASY1 lines

Line	Linear rods	Cruciform rods	All rods	All rings
Col	1	0	1	4
Col	1	0	1	4
Col	2	0	2	3
Col	0	2	2	3
Col	0	2	2	3
Col	0	2	2	3
Col	0	2	2	3
Col	0	2	2	3
Col	0	3	3	2
Col	0	3	3	2
Col	0	3	3	2
Col	0	1	1	4
Col	0	1	1	4
Col	0	1	1	4
Col	0	1	1	4
Col	0	1	1	4
Col	0	1	1	4
Col	0	1	1	4
Col	0	1	1	4
Col	0	1	1	4
Col	0	1	1	4
Col	0	1	1	4
Col	0	1	1	4
Col	0	1	1	4
Col	0	1	1	4
Col	0	1	1	4
Col	1	1	2	3
Col	0	3	3	2
Col	0	3	3	2
Col	0	3	3	2
Col	0	2	2	3
Col	0	2	2	3
Col	0	2	2	3
Col	0	2	2	4
Col	0	2	2	3
Col	0	2	2	3
Col	0	2	2	3
Col	0	2	2	3
Col	0	2	2	3
Col	0	2	2	3
Col	0	2	2	3
Col	0	2	2	3
Col	1	2	3	2
Col	0	3	3	2
Col	0	4	4	1
Col	0	1	1	4
Col	0	1	1	4
Col	0	1	1	4
Col	0	1	1	4
Col	0	1	1	4
Col	0	2	2	3
Col	0	0	0	5
Col	0	0	0	5
Col	0	0	0	5
Col	0	0	0	5
Col	0	0	0	5
Col	0	0	0	5
Col	0	0	0	5
Col	0	0	0	5
Col	0	0	0	5
Col	0	0	0	5
Col	0	0	0	0
Col	0	0	0	5
Col	0	0	0	5
Col	0	0	0	5
Col	0	0	0	5
HO-07	1	0	1	4
HO-07	0	2	2	3
HO-07	0	2	2	3
HO-07	0	2	2	3
HO-07	1	2	3	2
HO-07	0	1	1	4
HO-07	0	1	1	5
HO-07	0	1	1	4
HO-07	0	1	1	4
HO-07	0	1	1	4
HO-07	0	1	1	4
HO-07	0	1	1	4
HO-07	0	1	1	4
HO-07	0	1	1	4
HO-07	0	1	1	4
HO-07	0	1	1	4
HO-07	0	3	3	2
HO-07	0	2	2	3
HO-07	0	2	2	3
HO-07	0	2	2	3
HO-07	0	2	2	3
HO-07	0	2	2	3
HO-07	0	2	2	3
HO-07	1	2	3	2
HO-07	0	3	3	2
HO-07	0	1	1	3
HO-07	1	1	2	3
HO-07	1	1	2	3
HO-07	0	0	0	5
HO-07	0	0	0	5
HO-07	0	0	0	5
HO-07	0	0	0	5
HO-07	0	0	0	5
HO-07	0	0	0	5
HO-07	0	0	0	5
HO-07	0	0	0	5
HO-104	1	0	1	4
HO-104	1	0	1	4
HO-104	0	2	2	3
HO-104	1	2	3	2
HO-104	1	2	3	2
HO-104	0	3	3	2
HO-104	0	1	1	4
HO-104	0	1	1	4
HO-104	0	1	1	4
HO-104	0	1	1	4
HO-104	0	1	1	4
HO-104	0	1	1	4
HO-104	0	1	1	4
HO-104	0	1	1	4
HO-104	0	1	1	4
HO-104	0	1	1	4
HO-104	0	1	1	4
HO-104	1	1	2	1
HO-104	0	2	2	3
HO-104	0	2	2	3
HO-104	0	2	2	3
HO-104	0	2	2	3
HO-104	0	2	2	3
HO-104	0	2	2	3
HO-104	0	1	1	4
HO-104	0	1	1	4
HO-104	0	1	1	4
HO-104	0	1	1	4
HO-104	0	1	1	4
HO-104	0	0	0	5
HO-104	0	0	0	5
HO-104	0	0	0	5
HO-104	0	0	0	5
HO-104	0	0	0	5
HO-104	0	0	0	5
HO-104	0	0	0	5
HO-104	0	0	0	5
HO-104	0	0	0	5
HO-104	0	0	0	5
HO-104	0	0	0	5
HO-104	0	0	0	0
SN-102	0	3	3	1
SN-102	0	1	1	3
SN-102	0	0	0	5
SN-104	1	0	1	4
SN-12	0	0	0	5
SN-12	0	0	0	5
SN-12	0	2	2	3
SN-12	0	2	2	3
SN-12	0	2	2	3
SN-12	0	2	2	3
SN-12	1	2	3	2
SN-12	0	3	3	2
SN-12	0	4	4	1
SN-12	0	3	3	2
SN-12	0	1	1	4
SN-7	0	0	0	5
SN-7	0	0	0	5
SN-7	0	0	0	5
SN-7	0	0	0	5
SN-7	0	0	0	5
SN-7	0	0	0	5
SN-7	0	2	2	3
SN-7	0	2	2	3
SN-7	0	2	2	3
SN-7	0	2	2	3
SN-7	0	1	1	4
SN-7	0	1	1	4
SN-7	0	1	1	4
SN-7	0	1	1	4
SN-7	0	2	2	3
SN-7	0	3	3	2
SN-7	0	3	3	2
SN-7	0	1	1	4
SN-7	0	1	1	4
SN-7	0	1	1	4

Mean	**Linear rods**	**Cruciform rods**	**All rods**	**All rings**
Col	0.0909091	1.272727273	1.363636	3.575758
HO	0.1298701	1.038961039	1.168831	3.74026
SN	0.0526316	1.263157895	1.315789	3.236842
HO-07				
HO-104				
Inter-group T.TESTs (p-values)				
Col vs HO	0.4937956	0.145580084	0.235798	0.367081
Col vs SN	0.5594352	0.670220649	0.779103	0.801298
HO vs SN	0.1927095	0.129195409	0.243453	0.342595

Contingency tables for Chi-squared tests

		Rod true	Rod other	total		Rod	Ring	total
observed		Rod true	Rod other	total		Rod	Ring	total
	Col	6	84	90	Col	90	236	326
	HO	10	80	90	HO	90	288	378
	SN	2	48	50	SN	50	123	173
	total	18	212	230	total	230	647	877
expected		Rod true	Rod other	total		Rod	Ring	total
	Col	7.043478261	82.95652	90	Col	85.49601	240.504	326
	HO	7.043478261	82.95652	90	HO	99.13341	278.8666	378
	SN	3.913043478	46.08696	50	SN	45.37058	127.6294	173
	total	18	212	230	total	230	647	877
Chi.squared *p* values		0.282413243				0.349496		

Table S11. Seed counts from ASY1 and ASY3 RNAi lines

Line	Silique 1	Silique 2	Silique 3	Silique 4	Silique 5	Silique 6	Silique 7	Silique 8	Silique 9	Silique 10	Mean number of seeds per silique (n=10)	s.d	P value (two sample t test vs. Col-o)	% fertility
Col-0	55	54	59	59	54	53	50	60	57	54	55.5	3.17105		
ASY1 RNAi 11.2	26	10	14	18	21	12	16	15	19	15	16.6	4.623611	1.93566E-14	29.90991
ASY1 RNAi 14.1	6	14	13	11	7	9	10	15	12	9	10.6	2.951459	1.67522E-17	19.0991
ASY1 RNAi 16.3	53	49	50	53	50	54	55	45	50	43	50.2	3.852849	0.003496694	90.45045
ASY1 RNAi 18.5	9	12	6	13	7	7	8	10	7	8	8.7	2.311805	1.38767E-18	15.67568
ASY1 RNAi 20.2	7	18	21	17	16	21	22	11	14	14	16.1	4.771443	2.25736E-14	29.00901
asy1-1 -/-	12	11	7	8	14	9	7	14	16	7	10.5	3.374743	5.24346E-17	18.91892
ASY3 RNAi 2.1	18	16	20	20	21	14	16	19	12	11	16.7	3.497618	1.00435E-15	30.09009
ASY3 RNAi 7.1	19	22	28	20	22	25	20	26	21	25	22.8	3.011091	5.24882E-15	41.08108
ASY3 RNAi 8.4	41	32	21	34	26	33	26	20	22	28	28.3	6.684144	8.38332E-10	50.99099
ASY3 RNAi 18.4	16	17	18	19	13	12	14	14	24	17	16.4	3.50238	8.88888E-16	29.54955
ASY3 RNAi 20.1	14	22	16	25	12	16	12	15	10	13	15.5	4.672615	1.35056E-14	27.92793
asy3-1 -/-	17	13	13	15	18	14	16	11	11	12	14	2.44949	1.69705E-17	25.22523

Table S12. Univalent counts from ASY1 and ASY3 RNAi lines

Line	Mean number of univalents	S.D	S.E
Col-0 (n=53)	0	0	0
ASY1 RNAi 11.2 (n=18)	1	0.766965	0.180775
ASY1 RNAi 14.1 (n=27)	1.740740741	1.129758	0.217422
ASY1 RNAi 16.3 (n=22)	0	0	0
ASY1 RNAi 18.5 (n=62)	2.919354839	1.120573	0.142313
ASY1 RNAi 20.2 (n=23)	0.130434783	0.34435	0.071802
ASY1 -/- (n=22)	2.545454545	0.800433	0.170653
ASY3 RNAi 2.1 (n=32)	1.9375	0.981687	0.173539
ASY3 RNAi 7.1 (n=40)	0.3	0.516398	0.08165
ASY3 RNAi 8.4 (n=20)	0.1	0.307794	0.068825
ASY3 RNAi 20.1 (n=42)	1.571428571	0.830599	0.128164
ASY3 -/- (n=35)	1.685714286	0.832128	0.140655

Table S13. Seed counts from diploid and neopolyploid Col-0, ASY3 RNAi 20.1 and pch2-1 lines

line	Col-0 (n=10)	Col-0 c1.2 (n=11)	ASY3 RNAi T3.20.1 (n=10)	ASY3 RNAi T3.20.1 c1.1 (n=5)	pch2 -/- (n=10)	pch2 c1.6 (n=10)
number of seeds per silique	55	35	14	26	42	36
	54	34	22	16	29	32
	59	36	16	17	31	33
	59	36	25	24	39	27
	54	38	12	20	29	34
	53	41	16		21	27
	50	30	12		38	36
	60	37	15		30	29
	57	36	10		20	25
	54	34	13		18	27
		30				
mean	55.5	35.18181818	15.5	20.6	29.7	30.6
s.d	3.171049598	3.21926022	4.672615256	4.335896678	8.273787256	4.087922591
s.e	1.00277393	0.970643477	1.477610684	1.939071943	2.61640126	1.292714629

t.tests n *p* values					
	Col-0	Col-0 C1.2	ASY3 RNAi T3.20.1	ASY3 RNAi T3.2(	pch2 -/-
Col-0					
Col-0 C1.2	1.03961E-11				
ASY3 RNAi T3	2.03661E-13	6.93826E-09			
ASY3 RNAi T3	2.7263E-06	0.000489973	0.067058239		
pch2 -/-	1.13225E-06	0.074219931	0.000312295	0.015319001	
pch2 c1.6	2.56707E-11	0.011393222	4.79322E-07	0.002917135	0.762613761

Table S14. Univalent, bivalent, trivalent and quadrivalent counts from M1 cells from neopolyploid Col-0, ASY3 RNAi 20.1 and pch2-1 lines

Line	Image	Univalents	Bivalents	Trivalents	Quadrivalents	Total number of chromosomes
Col-0	11724	0	2	0	4	20
Col-0	11723	2	1	0	4	20
Col-0	11722	0	6	0	2	20
Col-0	11721	0	0	0	5	20
Col-0	11714	0	0	0	5	20
ASY3 20.1 c1.2	11725	8	3	1	1	21
ASY3 20.1 c1.2	11734	13	4	0	0	21
ASY3 20.1 c1.2	11735	7	5	0	1	21
ASY3 20.1 c1.2	11736	8	1	1	2	21
ASY3 20.1 c1.2	11737	9	4	0	1	21
ASY3 20.1 c1.2	11738	11	3	0	1	21
pch2-1 c1.6	878	2	7	0	1	20
pch2-1 c1.6	879	0	2	0	4	20
pch2-1 c1.6	883	0	2	0	4	20
pch2-1 c1.6	884	2	3	0	3	20
pch2-1 c1.6	885	3	2	3	1	20
pch2-1 c1.6	886	1	2	1	3	20
pch2-1 c1.6	889	1	2	1	3	20
pch2-1 c1.6	890	2	0	2	3	20
pch2-1 c1.6	891	1	0	1	4	20
pch2-1 c1.6	896	10	2	2	0	20
pch2-1 c1.6	899	5	2	1	2	20
pch2-1 c1.6	900	4	4	0	2	20
pch2-1 c1.6	906	4	2	0	3	20
pch2-1 c1.6	907	0	0	0	5	20

Mean	Univalents	Bivalents	Trivalents	Quadrivalents
Col-0 c1.2 (n=5)	0.4	1.8	0	4
ASY3 20.1 c1.2 (n=6)	9.333333333	3.333333333	0.333333333	1
pch2-1 c1.6 (n=14)	2.5	2.142857143	0.785714286	2.714285714

Figure S1. Protein sequence alignment for ASY1 proteins from A. thaliana, A. lyrata, diploid A. arenosa and tetraploid A. arenosa.

```
CLUSTAL 2.1 Multiple Sequence Alignments


Sequence type explicitly set to Protein
Sequence format is Pearson
Sequence 1: Athaliana_ASY1             596 aa
Sequence 2: ALyrata_ASY1               596 aa
Sequence 3: Aarenosa_Diploid_ASY1      594 aa
Sequence 4: Aarenosa_Tetraploid_ASY1   596 aa

Sequences (1:2) Aligned. Score: 94.9664
Sequences (1:3) Aligned. Score: 91.0774
Sequences (1:4) Aligned. Score: 91.443
Sequences (2:3) Aligned. Score: 92.4242
Sequences (2:4) Aligned. Score: 92.6174
Sequences (3:4) Aligned. Score: 97.3064

Aarenosa_Diploid_ASY1         MAQKLKEAEITEQDSLLLTRNLLRIAIFNISYIRGLFPEKYFNDKSVPAL
Aarenosa_Tetraploid_ASY1      MAQKLKEAEITEQDSLLLTRNLLRIAIFNISYIRGLFPEEYFNDKSVPAL
Athaliana_ASY1                MAQKLKEAEITEQDSLLLTRNLLRIAIFNISYIRGLFPEKYFNDKSVPAL
ALyrata_ASY1                  MAQKLKEAEITEQDSLLLTRNLLRIAIFNISYIRGLFPEKYFNDKSVPAL
                              ************************************:**********

Aarenosa_Diploid_ASY1         DMKIKKLMPMDAESRRLIDWMEKGVYDALQRKYLKTLMFCICETVDGPMI
Aarenosa_Tetraploid_ASY1      DMKIKKLMPMDAESRRLIDWMEKGVYDALQRKYLKTLMFCICETVDGPMI
Athaliana_ASY1                DMKIKKLMPMDAESRRLIDWMEKGVYDALQRKYLKTLMFSICETVDGPMI
ALyrata_ASY1                  DMKIKKLMPMDAESRRLIDWMEKGVYDALQRKYLKTLMFCICETVDGPMI
                              ************************************.**********

Aarenosa_Diploid_ASY1         EEYAFSFSYSDSDSQDVMMNINRTGNKKNGGTFNSTADITPNQIRSSACK
Aarenosa_Tetraploid_ASY1      EEYAFSFSYSDSDSQDVMMNINRTGNKKNGGTFNSTADITPNQIRSSACK
Athaliana_ASY1                EEYSFSFSYSDSDSQDVMMNINRTGNKKNGGIFNSTADITPNQMRSSACK
ALyrata_ASY1                  EEYAFSFSYSDSDSQDVMMNINRTGNKKNGGTFNSTADITPNQMRSSACK
                              ***:************************** ***********:******

Aarenosa_Diploid_ASY1         MVRTLVQLMRTLDKMPDERTIVMKLLYYDDVTPPDYEPPFFRGCTEDEAQ
Aarenosa_Tetraploid_ASY1      MVRTLVQLMRTLDKMPDERTIVMKLLYYDDVTPPDYEPPFFRGCTEDEAQ
Athaliana_ASY1                MVRTLVQLMRTLDKMPDERTIVMKLLYYDDVTPPDYEPPFFRGCTEDEAQ
ALyrata_ASY1                  MVRTLVQLMRTLDKMPDERTIVMKLLYYDDVTPPDYEPPFFRGCTEDEAQ
                              **************************************************

Aarenosa_Diploid_ASY1         YVWTKNPLRMEIGNVNSKHLVLTLKVKSVLDPCEDENDDMQDDGKSIGPD
Aarenosa_Tetraploid_ASY1      YVWTKNPLRMEIGNVNSKHLVLTLKVKSVLDPCEDENDDMQDDGKSIGPD
Athaliana_ASY1                YVWTKNPLRMEIGNVNSKHLVLTLKVKSVLDPCEDENDDMQDDGKSIGPD
ALyrata_ASY1                  YVWTKNPLRMEIGNVNSKHLVLTLKVKSVLDPCEDENDDMQNDGKSIGPD
                              ****************************************:********

Aarenosa_Diploid_ASY1         SVHDDQPSDSDSEISQTQENQFIVAPVEKQDDDDGEVDEDDNTQDPVENE
Aarenosa_Tetraploid_ASY1      SVHDDQPSDSDSEISQTQENQSIVAPVEKQDDDDGEVDEDDNTQDPVENE
Athaliana_ASY1                SVHDDQPSDSDSEISQTQENQFIVAPVEKQDDDDGEVDEDDNTQDPAENE
ALyrata_ASY1                  SVHDDQPSDSDSEISQTQENQFIVAPVEKQDDDDGEVDEDDNTQDPVENE
                              ******************** ************************.***

Aarenosa_Diploid_ASY1         QQLARVKDWINSRHLDTLELTDILANFPDISIVLSEEIMDQLVTEGVLSK
Aarenosa_Tetraploid_ASY1      QQLARVKDWINSHHLDTLELTDILANFPDISIVLSEEIMDQLVTEGVLSK
Athaliana_ASY1                QQLARVKDWINSRHLDTLELTDILANFPDISIVLSEEIMDQLVTEGVLSK
ALyrata_ASY1                  QQLARVKDWINSRHLDTLELTDILANFPDISIVLSEEIMDQLVTEGVLSK
                              ************:************************************

Aarenosa_Diploid_ASY1         TG-KTYIKKRDKTPESEFTFVKEEADGQTAPKDGKPVAPEDYLYMKALYH
Aarenosa_Tetraploid_ASY1      TGKDTYIKKRDKTPVSEFTFVKEEADGQTAPKDGKPVAPEDYLYMKALYH
Athaliana_ASY1                TGKDMYIKKRDKTPESEFTFVKEEADGQISP--GKSVAPEDYLYMKALYH
ALyrata_ASY1                  TGKDTYIKKRDKTPESEFTFVKDEADVQTVPKDGKPVAPEDYLYMKALYH
                              ** . ********* *******:*** *  *  **.**************

Aarenosa_Diploid_ASY1         SLPMNYVTITKLHNMLDGEANQTAVRKLMDRMTQEGYVEASSNRRLGKRV
Aarenosa_Tetraploid_ASY1      SLPMKYVTITKLHNMLDGEANQTAVRKLMDRMTQEGYVEASSNRRLGKRV
Athaliana_ASY1                SLPMKYVTITKLHNMLDGEANQTAVRKLMDRMTQEGYVEASSNRRLGKRV
```

```
ALyrata_ASY1                SLPMKYVTITKLHNMLDGEANQTAVRKLMDRMTQEGYVEASSNRRLGKRV
                            ****:*******************************************

Aarenosa_Diploid_ASY1       IHSSLTERKLNEVRKVLDPDDMDVDVNEANKTNG---LEAKVTADVSTCG
Aarenosa_Tetraploid_ASY1    IHSSLTERKLNEVRKVLDTDDMDVDVNEAINKTNG--LEAKVTADVSTCG
Athaliana_ASY1              IHSSLTEKKLNEVRKVLATDDMDVDVTETINKTNGPDADAKVTADVSTCG
ALyrata_ASY1                IHSSLTERKLNEVRKVLATDDMDVDVNEAANKTNG--LEGKVTADVSTCG
                            *******:********* .*******.*: :...    :.**********

Aarenosa_Diploid_ASY1       GIHSIGSDFTRTKGRSGGMQQNGSVLSEQTISKAGNTPISNKAQPAASRE
Aarenosa_Tetraploid_ASY1    GIHSIGSDFTRMKGRSGGMQQNGSVLSEQTISKAGNTPISNKAQPAASRE
Athaliana_ASY1              GIHSIGSDFTRTKGRSGGMQQNGSVLSEQTISKAGNTPISNKAQPAASRE
ALyrata_ASY1                GIHSIGSDFTRTKGRSGGMQQNGSVLSEQTISKAGNTPISNKAQPAASRE
                            ********** ************************************

Aarenosa_Diploid_ASY1       SFAVHG-TAKEAETVNCSQASQDRRAGKPAWETQFCSTRSVRNLKLI-
Aarenosa_Tetraploid_ASY1    SFAVHG-TAKEAETVNCSRASQDRRAGKPAWETQFCSTRSVRNLKLI-
Athaliana_ASY1              SFAVHGGAVKEAETVNCSQASQDRRGRKTSMVREPILQYSKRQKSQAN
ALyrata_ASY1                SFAVNGGAAKEVETVNCSQASQDRRCRKTSMVREPILQYSKRQKSQAN
                            ****:* :.**.******:******  *.:   :     * *: .
```

An * (asterisk) indicates positions which have a single, fully conserved residue.

A : (colon) indicates conservation between groups of strongly similar properties - scoring > 0.5 in the Gonnet PAM 250 matrix.

A . (period) indicates conservation between groups of weakly similar properties - scoring =< 0.5 in the Gonnet PAM 250 matrix.

HORMA domain

SWIRM domain

Amino-acids that differ from A. thaliana